iSCAPE

Detailed report based on numerical simulations of the effect of PCSs at the urban level

D6.3

February 2019

Project Acronym and Name	iSCAPE - Improving the Smart Control of Air Pollution in Europe	
Grant Agreement Number	689954	
Document Type	Report	
Document version & WP No.	V. 0.2	WP6
Document Title	Detailed report based on numerical simulations of the effect of PCSs at the urban level	
Main authors	Felix Othmer (TUDO), Jörg Peter Schmitt (TUDO), Silvana Di Sabatino (UNIBO), Erika Brattich (UNIBO), Francesca Di Nicola (UNIBO), Francesco Barbano (UNIBO), Bidroha Basu (UCD), Achim Drebs (FMI), Arvind Tiwari (UoS), Gopinath Kalaiarasan (UoS), Prashant Kumar (UoS), Sachit Mahajan (UoS)	
Partner in charge	TUDO	
Contributing partners	FMI, UCD, UNIBO, UoS	
Release date	February 2019	

The publication reflects the author's views. The European Commission is not liable for any use that may be made of the information contained therein.

Document Control Page	
Short Description	*This report is the output of the work carried out in Task 6.3 of the iSCAPE project, which takes outcome from previous Task 6.2 on infrastructure interventions at neighbourhood level further by investigating the effect of proposed infrastructural solution at city scale on both air quality and urban heat island (UHI). The work is grounded from recent research showing that separating areas of densely built-up neighbourhoods with vegetation or barriers from outskirts with low density and low height buildings will improve ventilation and therefore reduce concentration of airborne pollutants and UHI. In this task this is done in each neighbourhood selected representing different morphology and microclimate therefore of*

	use in other cities in Europe. As such, this document reports the results of numerical simulations carried out in selected iSCAPE cities to document and analyse the effectiveness of various PCSs in reducing air pollution and improving urban thermal comfort.		
Review status	**Action**	**Person**	**Date**
	Quality Check	*Coordination Team*	
	Internal Review	*Achim Drebs (FMI)* *Salem Gharbia (UCD)*	08.02.2019
Distribution	Public		

Revision history			
Version	**Date**	**Modified by**	**Comments**
V0.1	08 Feb. 2019	Felix Othmer, Jörg Peter Schmitt, Silvana Di Sabatino, Erika Brattich, Francesca Di Nicola, Francesco Barbano, Bidroha Basu, Achim Drebs, Arvind Tiwari, Gopinath Kalaiarasan, Sachit, Mahajan, Prashant Kumar	First draft for internal revision; missing part of contribution from Guildford; missing conclusions.
V0.2	20 Feb. 2019	Felix Othmer, Jörg Peter Schmitt	General revision and inclusion of internal reviews. Including the conclusion. Annex added.
V0.3	26. Feb. 2019	Felix Othmer, , Jörg Peter Schmitt, Silvana Di Sabatino, Erika Brattich, Francesca Di Nicola, Francesco Barbano, Bidroha Basu, Achim Drebs, Arvind Tiwari, Gopinath Kalaiarasan, Sachit, Mahajan, Prashant Kumar	Changes and additions to address the comments raised by the internal reviewers and the WP leader.
V0.4	26 Feb 2019	Silvana Di Sabatino, Erika Brattich	Final edit from the WP leader

Statement of originality:

This deliverable contains original unpublished work except where clearly indicated otherwise. Acknowledgement of previously published material and of the work of others has been made through appropriate citation, quotation or both.

Table of Contents

List of Tables

List of Figures

List of abbreviations

ADMS	Atmospheric Dispersion Modelling System
AQ	Air Quality
ArF	Agricultural Surface
ARPAE	Agenzia Regionale per la Protezione Ambientale ed Energetica
BC:	Base Case
BLDG_A	Building Area
BLDG_L	Building Length
°C	Degree Celsius
CEH	Centre for Ecology and Hydrology
CERC	Cambridge Environmental Research Consultants
CET	Central Europe Time
Cf	Coniferous Forest
CFD	Computational Fluid Dynamics
D	Deliverable
DEM	Digital Elevation Model
Df	Deciduous Forest
DfT	Department for Transport
EFT	Emission Factors Toolkit
EIA	Environmental Impact Assessment
EMIT	Emission Inventory Toolkit
FA2	Factor of 2
FB	Fractional Bias
GBC	Guildford Borough Council
GI	Green Infrastructure
GIS	Geographic Information System
Gl	Grassland
IPCC	Intergovernmental Panel on Climate Change
KTT	Karush-Kuhn-Tucker
LCZ	Local Climate Zone
LL	Living Lab
LOOV	Leave-one-out-cross-validation

LU	Land Use
LUC_A	Land Use Agricultural Land
LUC_L	Land Use Data Urban
LULC_W	Land Use Waterbody
LUR	Land Use Regression
m	Meter
MAXT	Maximum Temperature
MB	Mean Bias
MINT	Minimum Temperature
MRT	Mean Radiant Temperature
NBV	Normalized Building Volume
NO	Nitrogen monoxide
NO_2	Nitrogen dioxide
NO_x	Nitrogen oxides
O_3	Ozone
OECD	Organisation for Economic Co-operation and Development
OS	Ordnance Survey
PCS	Passive Control System
PET	Physiologically Equivalent Temperature
PM	Particulate Matter
$PM_{2.5}$	Particulate Matter with Aerodynamic Diameter less than 2.5 μm
PM_{10}	Particulate Matter with Aerodynamic Diameter less than 10 μm
PMV	Predicted Mean Vote
POP	Population Density
R	Rural
R^2	Coefficient of Determination
Rs	Rural surface
RBF	Radial Basis Function
RMSE	Root Mean Square Error
SEA	Strategic Environmental Assessment
sec.	Seconds
SO_2	sulphur dioxide
TRAF_HV	Traffic Volume Data of Heavy Vehicles

TRAF_LV	Traffic Volume Data of Light Vehicles
U	Urban
UHI	Urban Heat Island
Us	Urban surface
VOC	Volatile Organic Compounds
WIND	Wind Speed
WHO	World Health Organization
WMO	World Meteorological Organization
WRF	Weather Research and Forecasting
Ws	Water surface
W-SVR	Weighted Support Vector Regression

Executive Summary

This report documents the results of numerical simulations carried out in various iSCAPE cities, namely Bologna, Bottrop, Dublin, Guildford and Vantaa, to assess the effectiveness of various PCSs (Passive Control Systems) in improving air quality and urban thermal comfort. As mentioned in D5.2, these cities are those with a focus on physical interventions (Bologna, Dublin, Guildford, and Vantaa) and infrastructural solutions (Bottrop). The analysis of the results of numerical simulations provide insights into the assessment of the effectiveness of PCSs and infrastructural solutions and contribute to determine the most effective interventions. While D6.2 reports on the results of physical and infrastructural interventions at the neighborhood scale, here the focus is at city scale to highlight what can be expected in terms of solutions more broadly.

This report, therefore, describes the methodologies adopted to carry out numerical simulations in the various iSCAPE cities and provides the results and their analysis about the efficacy of the different PCSs in reducing air pollution and/or reducing the urban heat island (UHI) effect at the urban level. All the numerical simulations carried out in this work were verified by means of data gathered within experimental campaigns presented in D5.2 or from local weather stations.

1 Introduction

This report presents the work and the results obtained within Task 6.3 of the iSCAPE project, which takes outcome from previous Task 6.2 on infrastructure interventions at neighbourhood level further by investigating the effect of the proposed infrastructural solution at city scale on both air quality and UHI. The work is built up on recent research showing that separating areas of densely built-up neighbourhoods with vegetation, barriers from outskirts with low density and low height buildings will improve ventilation and therefore reduce concentration and reduce UHI. In this task, this is done in selected neighbourhoods or on a city-wide scale of the LL-Cities. As each city has a specific different morphology and a different microclimate, each analysis presents unique features on one hand, and on the other hand the investigative approaches here adopted can be transferred to other cities in Europe.

As already reported in D1.4 ('*Report on Climate Change and Air Quality Interactions*[1]') and in D6.1 ('*Assessment of air quality and microclimate in EU selected cities pre-infrastructural solutions*[2]'), the climate in cities usually differs significantly from the average local weather conditions. Cities and metropolitan areas cause local climatic effects due to the different physical properties of their surfaces in comparison to the less built-up and greener surroundings, which are generally summarised under the term 'urban climate'. The consequences of the urban climate are an increased thermal level in comparison to the surrounding countryside ('urban heat island'), often limited ventilation conditions due to partly dense and high buildings (changed wind currents), a strongly modified radiation balance, mostly lower humidity conditions and a deterioration of the urban air quality.

The IPCC (Intergovernmental Panel on Climate Change) has stated that global warming of the climate system is unequivocal (Stocker et al., 2013). Climate change is leading to an increase in average temperatures, especially in urban areas. In addition, it is responsible of an increasing probability of intense and prolonged heat periods (e.g., Meehl et al., 2007, Stocker and Raible, 2005; Tebaldi et al., 2006), which in turn significantly reduces overall climate comfort. Since the urban climate is directly related to the design of the environment, changes in the urban structure can modify the local climate both positively and negatively. In the context of urban microclimates, thermal comfort is the key indicator to describe individuals' subjective experience of temperature in open spaces. It summarises the impact of sun, wind, air temperature and humidity on thermal sensation. However, the interactions between the various climate elements and the city are too complex to be easily assessed. If the effects of an intended change in the urban structure are to be predicted, the use of numerical simulation models is unavoidable.

Furthermore, exposure to air pollution, different particulate and gaseous pollutants, is one of the main health risks in urban environments worldwide (WHO, 2018). The health effects caused by air pollution are serious. The Organisation for Economic Cooperation and Development (OECD), for example, found in a study that in 2010 about 42,500 deaths in Germany were caused by air pollution (OECD, 2014). Even if the emission situation in Germany is not as serious as for example in China or India (Bernard & Kazmin, 2018), the combination of pollutant sources and poorly ventilated areas such as narrow street canyons can quickly lead to the accumulation and local concentration of air pollutants above the air quality standards. In addition, it is known that even prolonged exposures to low concentrations of pollutants can produce adverse effects on human health (Townsend and

---

[1] Report on climate change and air quality
[2] The full report will be made available on the iSCAPE results webpage

Maynard, 2002; WHO, 2018). Besides decreasing the number of emissions, there are different tools to address these issues on an urban planning level. In order to be able to develop adequate urban planning measures and assess their effectiveness, pollutant dispersion models capable to adequately simulate the release, dispersion and (atmospheric) deposition of pollutants are required.

In urban planning, basic studies on climate and air pollution are of great importance for qualified land use planning and development planning in densely populated areas. Against the background of climate change, this importance continues to increase. Since the statements in question refer to a planning area, the use of maps as a basis for information is recommended. In this context, maps are an essential tool for planners, but also an important information carrier for politicians and the interested public. This means that spatial cartographic representations are also necessary for the implementation of climatic and air-hygienic aspects.

This investigation needs to be done by the use of micro- and urban- scale climate modelling. The models are to be regarded as an analysis tool within the framework of the environmental impact assessment which is a legal obligation within the EU for each project or plan which may have significant effects on the environment.

The European Union Environmental Impact Assessment Directive (2011/92/EU amended with the 2014/52/EU Directive) and Strategic Environmental Assessment (SEA) Directive (2001/42/EC) ask for the preparation of an environmental impact assessment report. This report requires,

- a modelled baseline scenario with the current state of the environment without implementation of a project and,

- an assessment of the environmental effects of so called "main alternatives" (defined as "interventions" in ISCAPE). The results are then to be compared in terms of effectiveness in reducing heat stress (as a climatic effect) or improving the air quality as the two protection goods as laid down in Annex I f) of the SEA Directive, which is addressed by the iSCAPE project.

Passive Control Systems (PCSs) or interventions at the urban scale are those PCS or interventions that can be defined or implemented within the framework of urban development projects (see Annex II No. 10 b of EIA Directive). This refers, for example, to designations in legally binding land-use plans. PCSs are generally a method of engineering increased pollutant dispersion in street canyons (King et al., 2009; McNabola, 2010), which include low boundary walls, roadside vegetation, and photocatalytic coating (Gallagher et al, 2015). Even though the most effective method of reducing air pollution is to control the amount of air pollutants created or at least pollutant emissions, it has been recognized that LBWs, avenue trees and deploying GI (Green Infrastructure) (such as trees and hedges) are effective passive controls in air pollution (e.g., Abhijith et al, 2017; Gallagher et al., 2012; Buccolieri et al., 2009; Gromke, 2011). In particular, GI may provide air quality benefit through a combination of the deposition and dispersion effects on air pollutants (Abhijith et al, 2019; Janhäll, 2015).

This document reports the results of numerical simulations carried out in selected iSCAPE cities, namely Bologna, Bottrop, Dublin, Guildford and Vantaa (i.e. those where a physical or infrastructural intervention was carried out) to document and analyse the effectiveness of various PCSs in reducing air pollution and improving urban thermal comfort.

A key output of this investigation is the information on the most effective interventions in reducing air pollution and UHI (see also upcoming D5.3 '*Report on interventions*'). On this basis, a comparative understanding of the benefits provided by the chosen interventions can be

developed. Thus, the outputs of the modelling work carried out in Task 6.3 and presented in this report are the main inputs for D5.3.

Table 1 provides an overview of all the numerical simulations presented in the rest of the report.

City	Scale	Type of PCS/intervention	Research objectives
Bologna	Urban scale: Bologna	Development of enhanced green areas and planning of trees along the most polluted roads	Effects of trees on UHI at the urban scale
Bologna	Urban scale: Bologna	Development of enhanced green areas and planning of trees along the most polluted roads	Effects of trees on air quality at the urban scale
Bottrop	Existing residential area (Heidenheck)	Designations on Road trees	Effects of urban level interventions on small scale city-climate in different urban morphologies; Planning alternatives to be preferred from these points of view
Bottrop	Existing industrial area (Brakerstraße)	Designations on Road trees; Designation on Roof Greening	Effects of urban level interventions on small scale city-climate in different urban morphologies; Planning alternatives to be preferred from these points of view
Bottrop	Planned residential area (Am Lamperfeld)	Designations on Building Structure	Effects of urban level interventions on small scale city-climate in different urban morphologies; Planning alternatives to be preferred from these points of view
Bottrop	Planned inner city area (Saalbau)	Designations on Building Structure	Effects of urban level interventions on small scale city-climate in different urban morphologies; Planning alternatives to be preferred from these points of view
Dublin	Urban scale: Dublin	Designations on Building Structure	Effects of land use on air quality at an urban scale
Guildford	Urban scale: Guildford	Development of GI	Effect of GI on UHI
Guildford	Urban scale: Guildford	Development of trees and grasslands in and around the city	Effects of GI on urban air quality
Vantaa	residential area Malminiitty	Development of enhanced GI	Effect of GI on air pollution caused by traffic in a densely middle high build-up area studied for four main wind directions with and without vegetation
Vantaa	pedestrian area Tikkuraitti	Development of enhanced GI	Effect of GI on air pollution caused by traffic in a pedestrian shopping area studied for four main wind directions with and without vegetation

Table 1. Overview of numerical simulations carried out within Task 6.3 of the iSCAPE project and presented in this report. (Source: this work).

2 Effects of PCSs on the UHI and AQ in the City of Bologna

The complexity of urban climate has been addressed during the early stages of the iSCAPE project. Present climate and air quality conditions in Europe have been presented in D1., with a specific focus on the iSCAPE target cities. In addition, in D6.1, the Urban Heat Island (UHI) effect has been evaluated for the cities of Dublin and Bologna during a period of a strong heat wave, by means of field data and numerical investigations.

This section presents the model simulations carried out at the urban scale on the effects of PCSs on UHI and air quality (AQ) in Bologna. In the first part of the section, a UHI analysis is performed for the city of Bologna to highlight the different distribution of air temperature within the urban environment and its surrounding. Numerical investigations based on a dispersion type model using local energy-balance are performed to evaluate the UHI effect, differently from what was presented in D6.1 where the analyses were based on results of a mesoscale meteorological model. This different approach here adopted will allow us to focus directly on the very local characteristics of the UHI. Specifically, it is highlighted the dependence of air temperature distribution with the urban texture, land use, city morphology and anthropogenic heat. The enhanced spatial resolution gained by this approach will allow us to fulfill the aim of this task in relation to the impacts of GI[3] on the UHI effects at city scale in present scenario and with possible PCS being introduced.

In the second part of the section, an AQ analysis is performed for the city of Bologna to obtain more general and spatially-detailed results of the dispersion of air pollutants. Numerical simulations of both pollutants concentration and temperature are performed at the urban scale, with a higher spatial resolution than that previously utilized with the WRF (Weather Research and Forecasting) mesoscale numerical weather prediction model. In this case, the higher spatial resolution to fulfill the aim of this task in relation to the impacts of GI at urban-scale on AQ effects in present scenario and with PCS being introduced.

The following Table provides an overview of the simulations conducted in Bologna to evaluate the effectiveness of GI in reducing UHI and improving air quality.

---

[3] Similar to D5.2, the wide concept of green infrastructures for Bologna refers to the evaluation of the effect of trees in street canyons. The impact of other green infrastructures elements, such as green roofs and green façades is evaluated by means of numerical simulations carried out in D6.2 using the data gathered within the monitoring campaigns described in D5.2.

City/Scale	Modelled scenarios	Software
Urban scale: City of Bologna	1) BASE: simulation with existing vegetation 2) Scenario Marconi: Simulation with green areas deployed over Marconi St. 3) Scenario Center: Simulation with a land use of the city centre increased in green areas	ADMS-TH module (CERC, 2018)
Urban scale: City of Bologna	1) BASE: simulation with existing vegetation 2) Scenario with trees over the whole Bologna domain	ADMS Urban (CERC, 2011)

Table 2. Overview of numerical simulations carried out in Bologna for the purpose of evaluating the effectiveness of GI in reducing UHI and improving air quality at the urban level (source: this work).

2.1 Impact of GI on UHI in Bologna

2.1.1 Description of the model

As previously described, one of the aims of the task is to highlight the impact of the interventions in mitigating the effect of UHI on the city scale. To fulfill this scope, an advanced short-range dispersion model called ADMS (Atmospheric Dispersion Modelling System; CERC, 2018) is used. The model, generally developed for simulating a wide range of buoyant and passive release to the atmosphere, was developed by the Cambridge Environmental Research Consultants (CERC, http://www.cerc.co.uk/) and includes different modules depending on the scope of the investigation.

In particular, for the current study, the ADMS - Temperature and Humidity (ADMS-TH) Module is used (CERC; 2018). It belongs to the category of models that derives the resulting distributions as a perturbation of an existing field. In particular, ADMS-TH reports the spatial distribution of the temperature and humidity field generated by spatial variations in land use, city morphology and anthropogenic heat emissions with respect to the unperturbed upwind input values (ADMS-Urban, 2018). The performances of the ADMS-Temperature and Humidity (ADMS-TH) model of the perturbation temperature were discussed in Maggiotto et al. (2014a, b) in the application to the city of Lecce (south Italy). In Maggiotto's work, ADMS-TH results have been compared with those obtained with the Computational Fluid Dynamics (CFD) -based ENVI-met model (Bruse and ENVI-Met Team., 2011) also used in this report. Direct comparisons with measured data and statistical indices showed that daily trends were well captured with ADMS-TH, slightly underestimating the diurnal temperature but providing good accordance for nighttime temperatures. Overall, ADMS-TH was found to be simpler in set up and more effective for a fast and accurate (within 0.3°C) assessment of air temperature distribution within the city, while ENVI-met required ad hoc setup of surface boundary conditions to predict nighttime cooling satisfactorily (within 1.6°C).
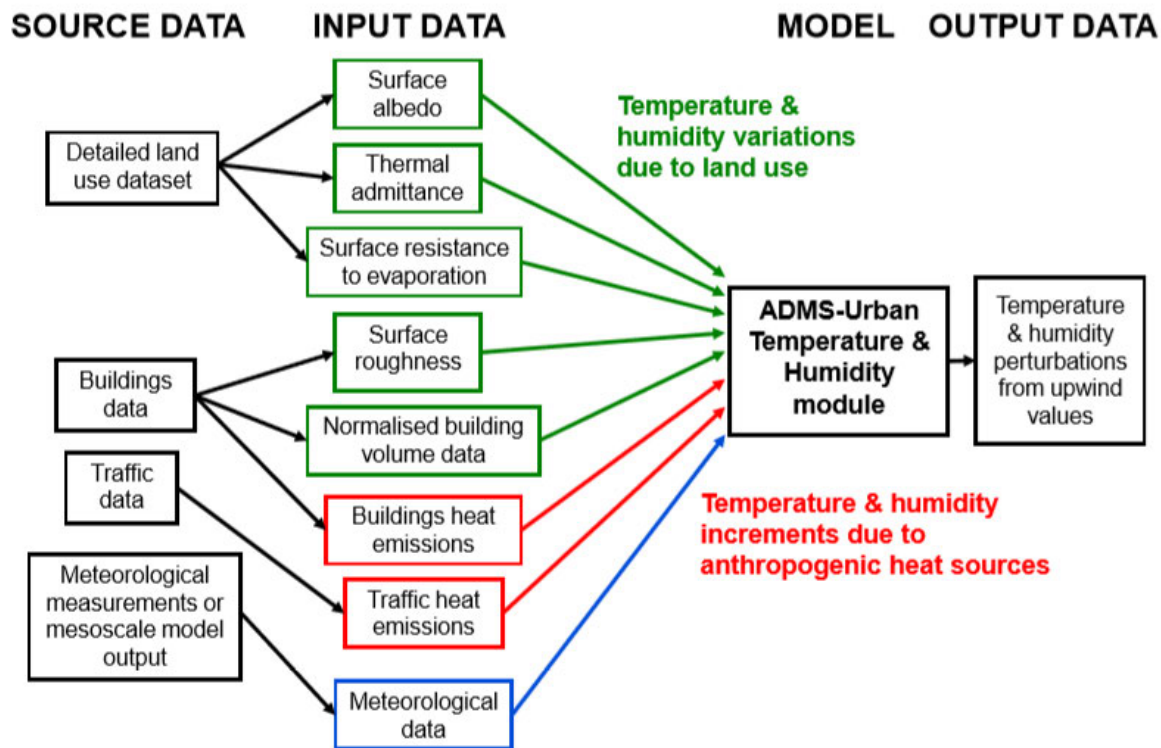
Figure 1: ADMS-Urban Temperature and Humidity flow diagram (source: ADMS-Urban, 2018).

A schematic view of ADMS-TH operational concept is shown in Figure 1. Green boxes highlight the land use dataset, which includes the radiative characteristics of the surface, soil moisture and related exchange processes with the adjoin atmosphere, and the friction force generated by the surface asperities on the air motion. This last input is fundamental when dealing with urban environments since ADMS-TH displays the city texture as a morphologically complex obstacle, treated as a variation of the surface roughness, which perturbates the input meteorological conditions. Moreover, the urban environment is also a source of heat due to the thermal forcing of the materials by which the city structures are built, that as a general inclination to behaves as a black body to solar radiation. Another additional source of heat related to the urban environment is the anthropogenic emission, computed from the thermal release of the domestic heat systems and the road traffic. Last, meteorological data or mesoscale model outputs have to be given in input to assess the atmospheric patterns which will be considered as upwind conditions with respect to the analyzed domain. The model computes a spatial variation of the temperature and humidity fields resulting in the heat fluxes distribution depending on the adopted land use and enhanced by anthropogenic and morphological heat emissions (where necessary), and then a distribution of such temperature and humidity fields according to the meteorological input conditions. The model carries out the computation by solving the linearized forms of the heat transfer equations together with the appropriate boundary conditions.

2.1.1.1 Meteorological input data

The ADMS-TH preprocessor can use the meteorological data in input to derive the heat flux balance equation:

$$Q^* = G + F_{\theta_0} + \lambda_E$$

where Q^* is the net radiation, G is the ground heat storage, F_{θ_0} is the sensible heat flux and λ_E is the latent heat flux. The net radiation term is computed following a 6th grade polynomial formula function of the incoming solar radiation K^+, the temperature expressed in Kelvin T^K, the cloud cover c_L and the surface albedo r (ADMS-Urban, 2018). As a model output the perturbation net radiation field is a bulk difference between the local perturbed-by-domain-characteristics field (marked with a subscript l) and the unperturbed upwind condition computed with the polynomial formula (marked with a u):

$$\Delta Q^* = Q_l^* - Q_u^* = \left(\frac{F(r_l, NBV_l)}{F(r_u, NBV_u)} \, (1 - r_u) \, (1 - r_l) \right) \frac{K^+}{1.12}$$

where NBV is the normalized building volume $NBV = {V_{buildings}}\big/{A_{cell}}$ as the ratio between the buildings volume and the surface area of the grid cell that contains the buildings, and $F\left(r_{l,u}, NBV_{l,u}\right)$ is a modulation of incoming solar radiation by the local environment, tabled depending on albedo and normalized building volume ratios.

The ground heat storage is a first order differential equation defined by Camuffo and Bernardi (1982):

$$G = a_1 \frac{dQ^*}{dt} + a_2 Q^* + a_3$$

Where the a_i coefficients account for the surface radiation differential absorbance during the daytime and the thermal stability conditions especially related to nocturnal boundary layers.

The latent heat flux λ_E depends on the moisture content of the surface and the efficacy of the humidity exchange between the soil and the atmosphere. It is computed directly from the surface resistance to evaporation, an input parameter describing the land use.

Once the perturbation of those three terms is evaluated through the spatial variation of the land use parameters, ΔF_{θ_0} is evaluated.

Those parameters can either be computed by the preprocessor through a derivation from basic meteorological quantities, such as a period of the year, time, wind velocity and direction, temperature, humidity or cloud cover, or be given as an input to the processor (Hourly heat flux data input).

In the end, temperature and humidity perturbed fields are evaluated accounting for the roughness length and the ΔF_{θ_0} distributions.

2.1.1.2 Land use parameters

The essential parameters that define the land use which the model needs to compute the temperature and humidity fields perturbations are the spatial variation of the surface resistance to evaporation and the surface roughness.

In addition, other parameters, such as the surface albedo, the thermal admittance and the normalized building volume, can be specified to enhance the reliability of the simulation. These five parameters are essential to run a simulation with the basic meteorological variables. On the contrary, it is possible to define the land use only by the first two parameters and specify the not radiation and ground heat flux perturbations directly as input. Table 3 presents a recap of these parameters together with a specification of their use in the model.

Parameter	Description	Units	When used
Surface resistance to evaporation	A measure of surface wetness	s/m	All runs
Surface roughness length for momentum transfer	Represents the height of any obstacles present in the model domain	m	All runs
Albedo	A measure of the reflectivity of the surface	-	Basic meteorological input
Thermal admittance	A measure of the ability of the surface to accept or release heating	$J/m^2 s^{1/2} K$	Basic meteorological input
Normalized building volume	A measure of the density of the buildings within the domain	m	Basic meteorological input
The perturbation to the net radiation	Absolute net radiation perturbations	W/m^2	Hourly flux input
The perturbation to the ground heat flux	Absolute ground heat flux perturbations	W/m^2	Hourly flux input

Table 3: Summary of spatially varying parameters that can be entered into the model (source: modified from ADMS-Urban, 2018).

2.1.1.3 Anthropogenic heat emissions

Additionally to the described input parameters, a detailed description of anthropogenic heat emissions can also be provided as input to the model. This term describes the daytime variations of the anthropogenic emissions related to the domestic heat systems (modelled as a building heat release) and the traffic rates. Domestic heat system emissions are generally tabled and vary according to the land use type of the building locations (e.g. residential, hospitals, city centre). The traffic emissions are directly computed by the Emissions Inventory Toolkit (EMIT), a comprehensive tool related to ADMS-Urban for compiling and editing emissions inventories comprehending also greenhouse gases, among which CO_2 emissions. From the emissions, a rate of heat release from a road using fuel i in units of W/km is determined as

$$Q_{FV,i} = \lambda F_i \, EF_{CO_2}$$

where λ is the adimensional heat release factor, F_i is the conversion factor from CO_2 to heat emissions (different from Diesel to Petrol and tabled) in units of J/g, and EF_{CO_2} is the rate of CO_2 in gs/km.

To summarize, the anthropogenic heat emissions in an urban area are modelled as time-dependent volume sources ranges through scales in dependency to the chosen spatial domain. It results in an additional term which perturbs the temperature field inside the urban environment.

2.1.2 Methodological approach

The analysis of the UHI in the city of Bologna was performed testing a suitable period within the two experimental field campaigns carried out in two urban street canyons described in D3.3 ('*Report on footprint of Passive Control Systems*'[4]) and D5.2 ('*Air pollution and meteorology monitoring report*'[5]). In particular, the selected period is the month of August 2017, whose meteorological conditions are described in D5.2.

2.1.2.1 The spatial domain

Figure 2 shows a top view of the spatial domain used for the simulation. Geographical coordinates and dimensions are reported in Table 4. The domain is a 20x40km box centered on the Metropolitan Area of Bologna, southerly limited by the hill chain and surrounded by the countryside plain. As reported in D1.4 and D6.1, the city of Bologna shows a morphology that can be considered typical of most of the European cities (Di Sabatino et al., 2010) characterized by a densely build-up historical city centre surrounded by residential and industrial areas, sharing different morphometry, building or house type, vegetation and road traffic.

Minimum Longitude	Minimum Latitude	Maximum Longitude	Maximum Latitude	Area (m^2)	Perimeter (m)
11°15'18'' E	44°41'78'' N	11°61'53'' E	44°63'31'' N	796591823	118851

Table 4: Geographical coordinates and domain dimension for the test case (source: this work).

The city is located in the southern part of the Po Valley, a well-recognized hot-spot for air pollution (Finardi et al., 2014). A complete description of the city, its location and the Po Valley characteristics in terms of air quality and climate have been addressed in D1.4 and D6.1. The domain includes a portion of the Po Valley plain in a 10-15km radius from the city. This is a rural intensely cultivated area, sparkled by small villages or isolated houses or farms. The southern hill chain delimits the city growth and encloses the Po Valley, modifying the local meteorological dynamics. The hills are densely vegetated, while most of the villages are located in the Reno Valley along the Reno River, south-south-westerly with respect to Bologna.

Detailing the surface characteristics of the domain is fundamental for models operating at local scale inside the boundary layer to have the best possible representation of atmosphere-soil interactions.

---

[4] Report on footprint of passive control systems
[5] The report will be made available on the iSCAPE results webpage.
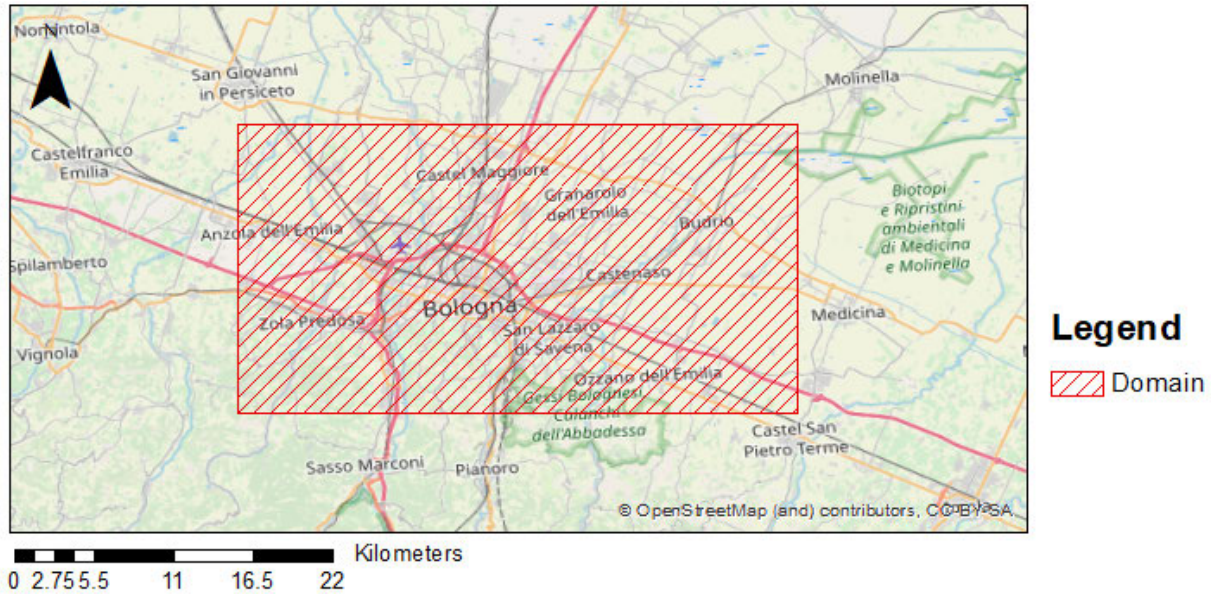
Figure 2: Areal view of the spatial domain (source: OpenStreetMap).

2.1.2.2 Input data: land use

Land use type used for the analysis is derived from the Local Climate Zone (LCZ) classification adopted by Stewart and Oke (2012), which provides a useful framework for the UHI studies. The term LCZ describes regions of uniform surface cover, structure, material and human activity on a defined horizontal spatial scale. Each LCZ has a characteristic temperature regime associated with urban environments, natural biomes and agricultural lands. The classification consists in 17 LCZs, subdivided in *built types* (1-10) related to structural features of the surface, and *land cover types* (A-G) accounting for seasonal and ephemeral properties (Stewart and Oke, 2012).
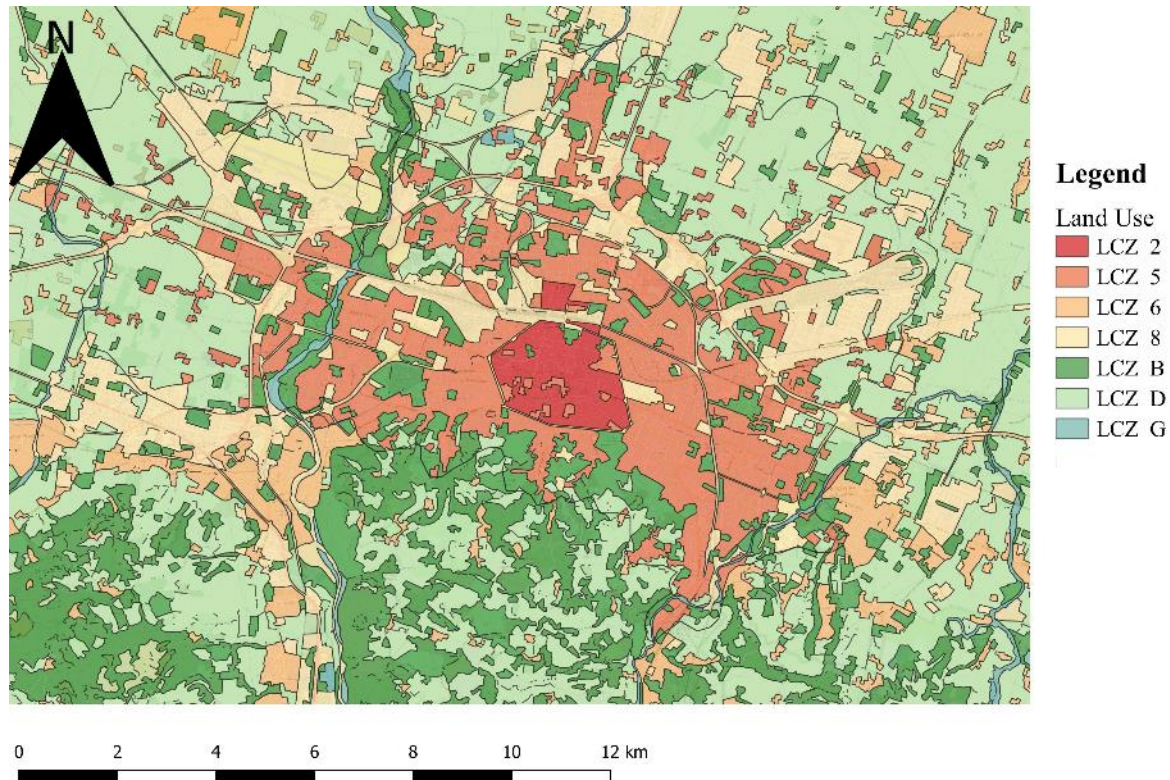
Figure 3: Land use for the simulation domain following LCZ classification (source: Own account).

Following this classification, the domain of the model is subdivided in land use type according to Figure 3. Clearly, not all the classes are used to define the domain. A brief description of the LCZs used in the study is reported in Table 5.
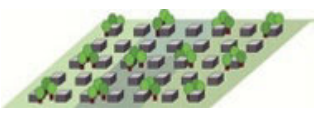
	LCZ 2: Compact Midrise: A dense mix of midrise buildings (3–9 stories). Few or no trees. Land cover mostly paved. Stone, brick, tile, and concrete construction materials.
	LCZ 5: Open Midrise: The open arrangement of midrise buildings (3–9 stories). The abundance of pervious land cover (low plants, scattered trees). Concrete, steel, stone, and glass construction materials.
	LCZ 6: Open Lowrise: The open arrangement of low-rise buildings (1–3 stories). The abundance of pervious land cover (low plants, scattered trees). Wood, brick, stone, tile, and concrete construction materials.
	LCZ 8: Large Lowrise: The open arrangement of large low-rise buildings (1–3 stories). Few or no trees. Land cover mostly paved. Steel, concrete, metal, and stone construction materials.
	LCZ B: Scattered Trees: The lightly wooded landscape of deciduous and/or evergreen trees. Land cover mostly pervious (low plants). Zone function is a natural forest or an urban park.
	LCZ D: Low plants: The featureless landscape of grass or herbaceous plants/crops. Few or no trees. Zone function is natural grassland, agriculture, or an urban park.
	LCZ G: Water: Large, open water bodies such as seas and lakes, or small bodies such as rivers, reservoirs, and lagoons.

Table 5: LCZ classes used to determine the actual domain (source:Stewart and Oke, 2012).

Once the surface types are defined, the land use parameters must be imposed on the model to define the radiative, thermal and friction capacity of the domain. Parameters have been defined in section 2.1.1.2 and in for the current study, the first 5 parameters in Table 3 have been computed and provided as input to the model, following the Basic Meteorological run mode. Parameters are therefore presented in the following maps (Figure 4Figure 8Figure 7). Surface resistance to evaporation assesses the surface capacity to hold its humidity level (Figure 4), so it is crucial for

the evaluation of the humidity perturbation field. The resistance is larger in urban areas, especially in the city centre and for densely packaged arrays of buildings where the bare soil is covered by a complex texture of obstacles covered in concrete and tarmac. Minimum values can be found in the plain, where bare soil, agriculture and low-risen plants offer a weak resistance to evaporation. The hill chain shows an intermediate value between urban and rural environments since the presence of forests inhibits surface evaporation due to the moist entrapment inside the canopy. The surface resistance to evaporation is fundamental for the model to evaluate the latent heat flux of the energy budget equation since it accounts for the percentage thermal loss from the surface depending on the surface type.
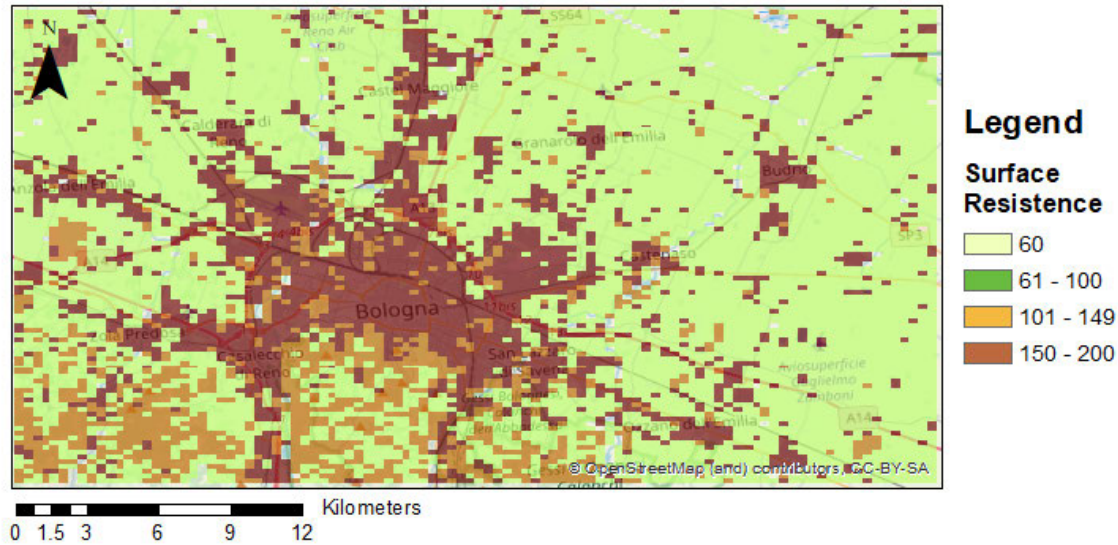
Figure 4: Map of the surface resistance to evaporation over the domain (source: Own account).

Figure 5 shows the surface roughness length, the quantity responsible for the momentum loss due to the interaction of the atmospheric flows with the obstacles on the surface. Together with the surface resistance to evaporation, it is a fundamental parameter for all type of meteorological input because it has a direct impact on the flow. Moreover, it is also the key parameter, together with the spatial variation of the sensible heat flux, which determines the temperature perturbation field. The roughness length is computed following the formulation by McDonald (1998):

$$\frac{z_0}{H} = \left(1 - \frac{d}{H}\right) exp\left(-\left(0.5\beta \frac{C_D}{k^2}\left(1 - \frac{d}{H}\right)\lambda_f\right)^{-0.5}\right),$$

where z_0 is the roughness length (m), H is the mean building height (m), d is the displacement height (m), β is an empirical constant, $\frac{C_D}{k^2}$ is the corrected drag coefficient and λ_f is the frontal area of buildings.
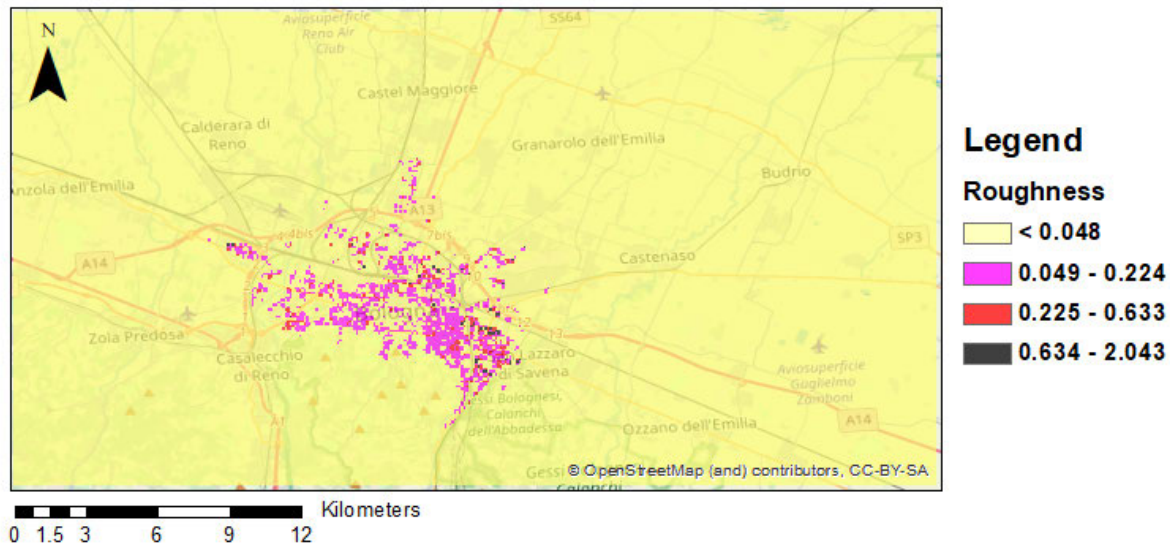
Figure 5: Map of the roughness length over the domain (source: Own account).

Roughness is a characteristic of the obstacles, so the larger values are displayed inside the urban environment, together with the larger and more frequent horizontal gradients. In rural areas roughness is more homogeneous, since despite the different cultivation types, cultivated fields offer small friction to atmospheric flows.

Albedo and NBV are directly related to the net radiation since they influence the absorbance and scattering features of the surface. Surface albedo (Figure 6) is a measure of the reflectivity of materials to the incident solar radiation. Generally, materials like concrete and tarmac have low values for albedo, letting the solar radiation been almost all absorbed and emitted at larger wavelength enhancing the urban temperature. This process is somehow mitigated by the predominance of red rooftops (most of the buildings are covered by red roof tiles) which increases the albedo to levels similar to the countryside.
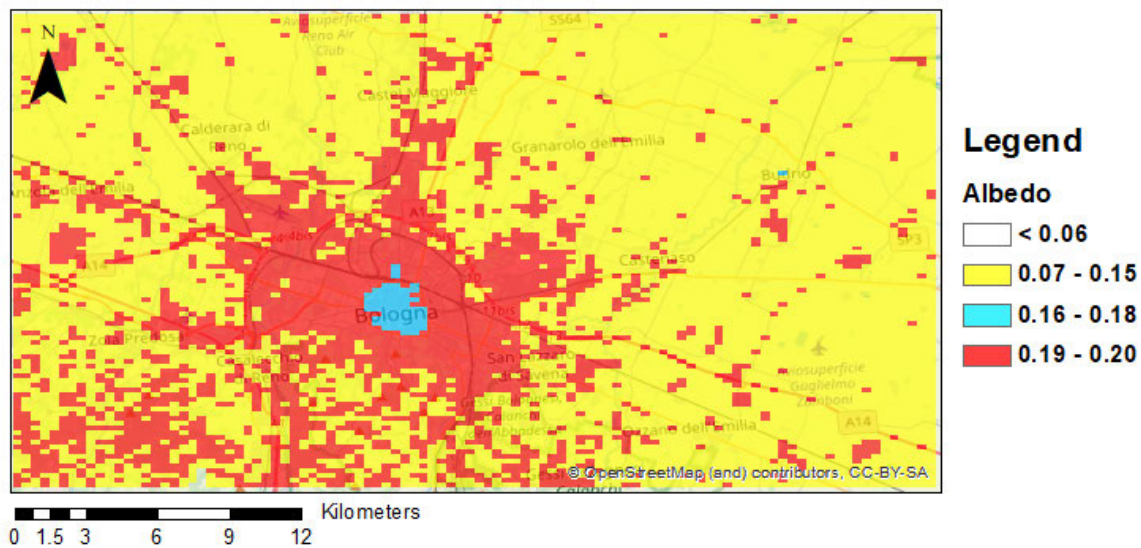
Figure 6: Map of the surface albedo over the domain (source: Own account).

NBV (Figure 7) is an exclusive parameter of the urban environment, describing the volume of built space in every grid cell of the domain. The larger values are located in the city centre, despite some outsiders can be found also in different urban spots related to specific facilities (an industrial area, fair buildings). The more the distance from the city centre is, the less the density of the building packaging will be.
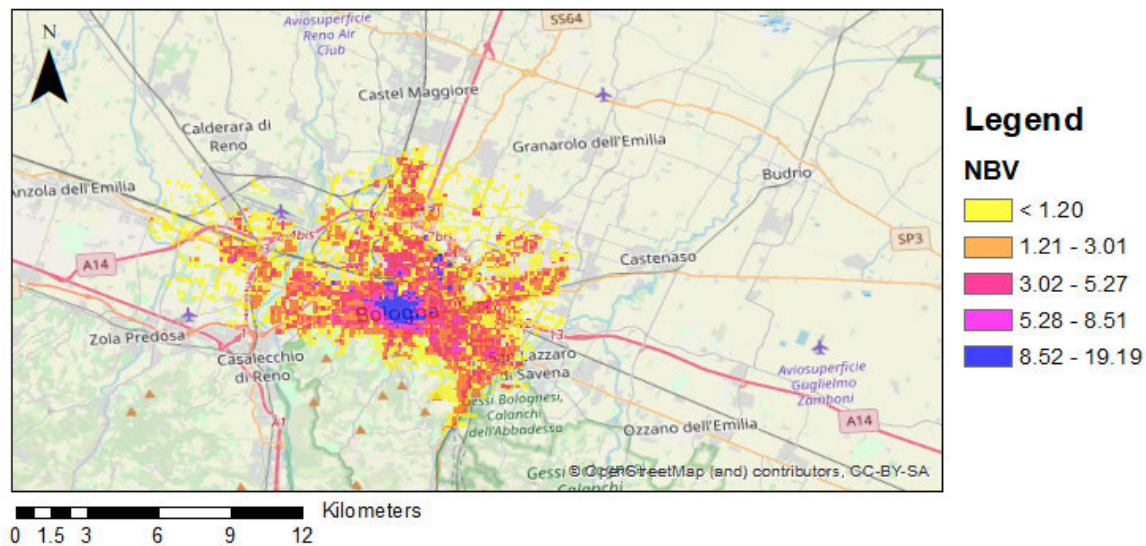
Figure 7: Map of the normalized building volume over the domain (source: Own account).

Finally, the thermal admittance establishes the efficacy of the surface to absorb and emit heat from and to the atmosphere. It is strongly dependent on the material the soil is made of and it is a good indicator of the surface thermal forcing. It reaches maximum values in the city centre and the most urbanized periferical areas, while it rapidly decreases in the countryside.
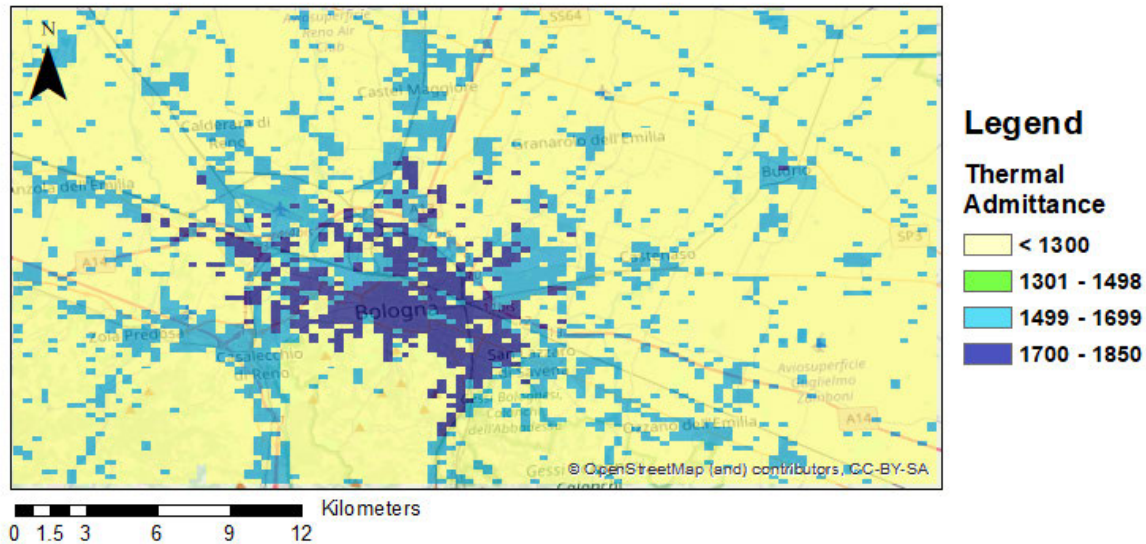
Figure 8: Map of the thermal admittance over the domain (source: Own account).

2.1.2.3 Input data: upwind meteorological conditions

Meteorological input data must be provided as unperturbed upwind conditions with respect to the domain. Therefore, an array of measured meteorological data must be obtained around the simulation domain in order to cover all the possible wind directions.

The chosen setup for the simulation is the basic meteorological mode; the input data in this modeling option consists in date, time, wind velocity and direction, temperature, relative humidity and cloud cover. Data suits the World Meteorological Organization (WMO, 2014) guidelines; therefore, wind velocity and direction are collected at 10 m AGL (above ground level) while temperature and humidity are collected at 2 m AGL. Data are averaged over one-hour mean interval, and have collected from the local environmental protection agency ARPAE (Agenzia Regionale per la Protezione Ambientale ed Energetica) monitoring stations surrounding the domain. First, wind velocity and directions were collected from the station at Bologna Airport, located to the north-east with respect to the city but inside the domain and representative of conditions not affected by the presence of buildings in the city. Since the ADMS model runs with the meteo upwind condition, i.e. undisturbed flow conditions approaching the study area retrieved outside the domain (Maggiotto et al., 2014a,b), the most suitable station to describe upwind conditions with respect to the domain was identified from the analysis of wind directions. All meteorological input data were then collected from different stations surrounding the domain depending on wind directions[6] (φ). Specifically, meteorological input data are collected from meteorological stations located in:

- San Pietro Capofiume (44°39'01'' N, 11°28'53'' E; located 35 km north-east from Bologna) if $20° < \varphi < 90°$;

- Imola (44°21'12'' N, 11°42'51'' E; located 35 km east-south-east from Bologna) if $90° < \varphi < 180°$;

- Sasso Marconi (44°24' N, 11°15' E; located 12 km south-south-west from Bologna) if $180° < \varphi < 300°$;

- Padulle-Sala Bolognese (44°37'49'' N, 11°16'34'' E; located 15 km north-north-west from Bologna) if $300° < \varphi < 20°$.

---

[6] Wind directions are referenced to the meteorological reference frame with 0° to the north and clockwise rotation.
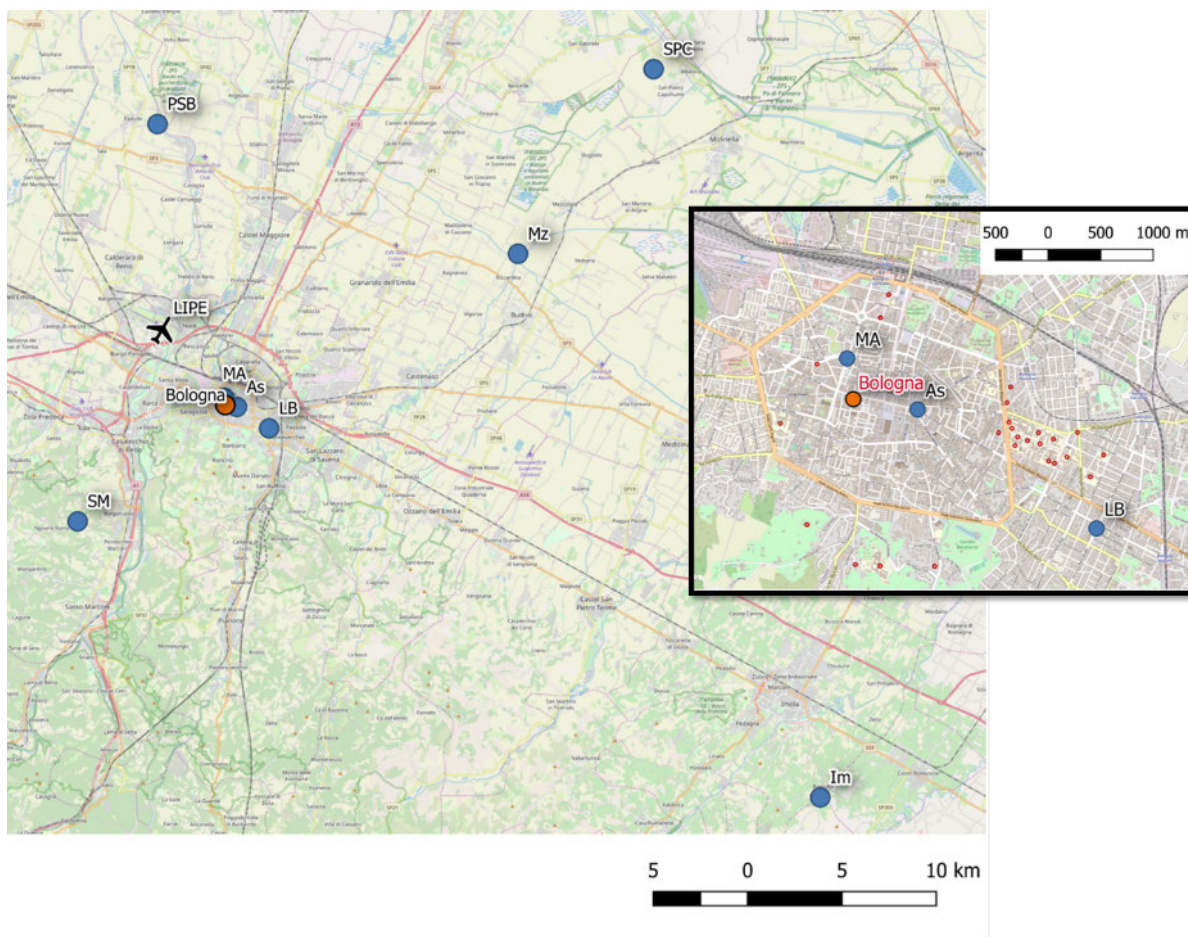
Figure 9. Meteorological stations providing data used for input to the model simulations: San Pietro Capofiume (SPC), Imola (Im), Sasso Marconi (SM), Padulle-Sala Bolognese (PSB), Marconi airport (LIPE); Reference meteorological stations used to evaluate the perfomance of the model simulations: Mezzolara (Mz), Bologna Urbana (BU), Asinelli (As), Marconi mobile station (MA), Laura Bassi mobile station (LB) (source: Own account and OpenStreetMap).

2.1.2.4 Validation

CERC models are validated against available measured data obtained from real world situations, field campaigns and wind tunnel experiments. Validation of the ADMS models has been performed using many experimental datasets that test different aspects of the models. These studies are both short-term as well as annual, and involve tracer gases or specific pollutants of interest. The validation of the ADMS-TH model was performed comparing the model outputs with measured data at several monitored sites around London, showing that the model was able to predict plausible temperature and humidity changes that occur due to changes in land use and anthropogenic emissions (Hamilton et al., 2017). Further validations of the ADMS-TH model were performed in Lecce (Italy) comparing the output of simulations with measured data and with CFD simulations (Maggiotto et al., 2014), which again proved that the model is able to predict correctly temperature and humidity daily trends.

2.1.2.5 Performance evaluation

Model performance was evaluated by comparing hourly temperature modelled values with measured ones. This comparison was carried out for three specific sites corresponding to the reference measurement stations of Bologna Urbana (BU), Asinelli (As) and Mezzolara (Mz) (Figure 9).

The following figures show the time series and scatter plots of simulated values (Mod) and measured data (Obs) for the whole month of August 2017. Figure 10 shows the comparison of observed and simulated temperature values for the entire month of August 2017 at the Bologna Urbana meteorological station. Comparing this figure with the following figures (Figure 12 and Figure 14), respectively showing the meteorological stations of Asinelli and Mezzolara, we might note that the model tends to present a larger overestimation at the Bologna Urbana site. The overestimation could be caused by site-specific parameters that do not emerge in albedo maps, thermal admittance, and surface resistance to evaporation since as previously reported they were created with a resolution which does not take into account changes below 100 meters. The scatterplots (Figure 11Figure 13 and Figure 15) highlight the general good agreement between simulations and observations.
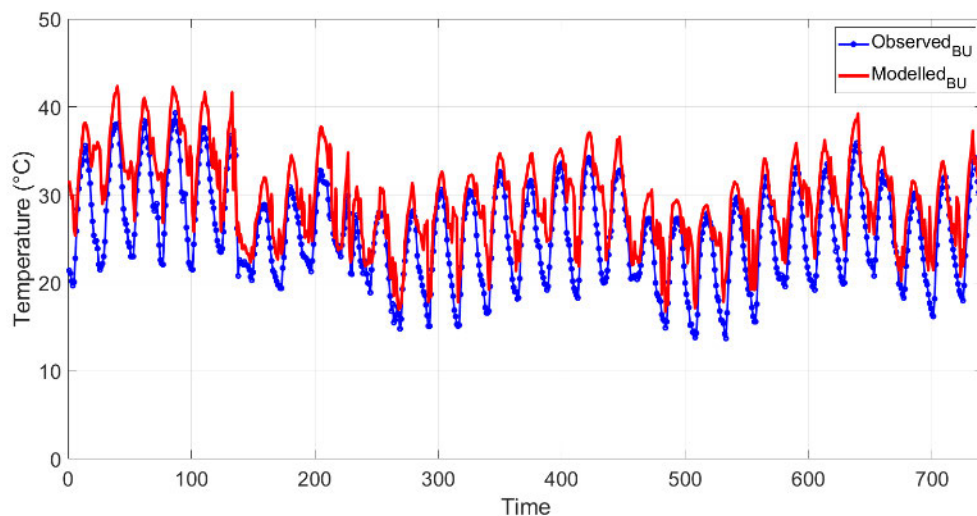
Figure 10. Time series of modelled (red line) and observed (blue dotted line) hourly temperature values for the month of August 2017 (1/08/2017 0:00 – 31/08/2017 23:00) at the Bologna Urbana meteorological station (source: Own account for simulated values, Dext3r website for observations).
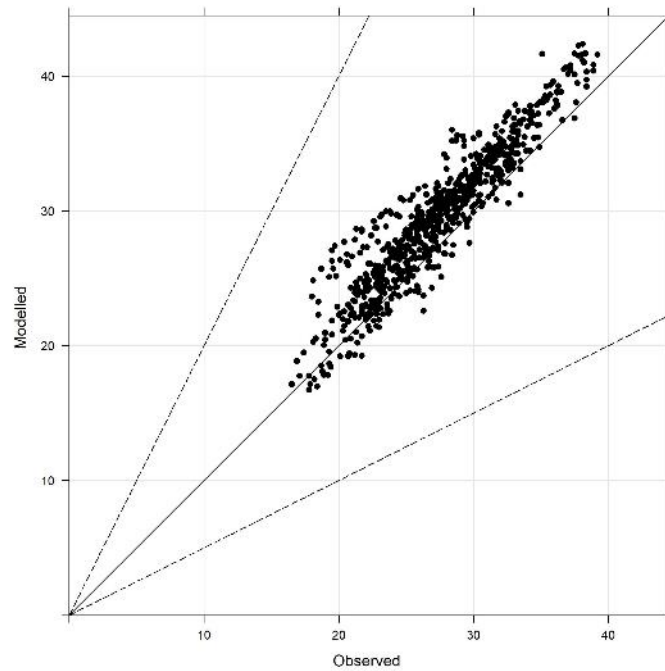
Figure 11: Scatter plot of modelled and observed hourly temperature values for the month of August 2017 (1/08/2017 0:00 – 31/08/2017 23:00) at the Bologna Urbana meteorological station (source: Own account for simulated values, Dext3r website for observations).
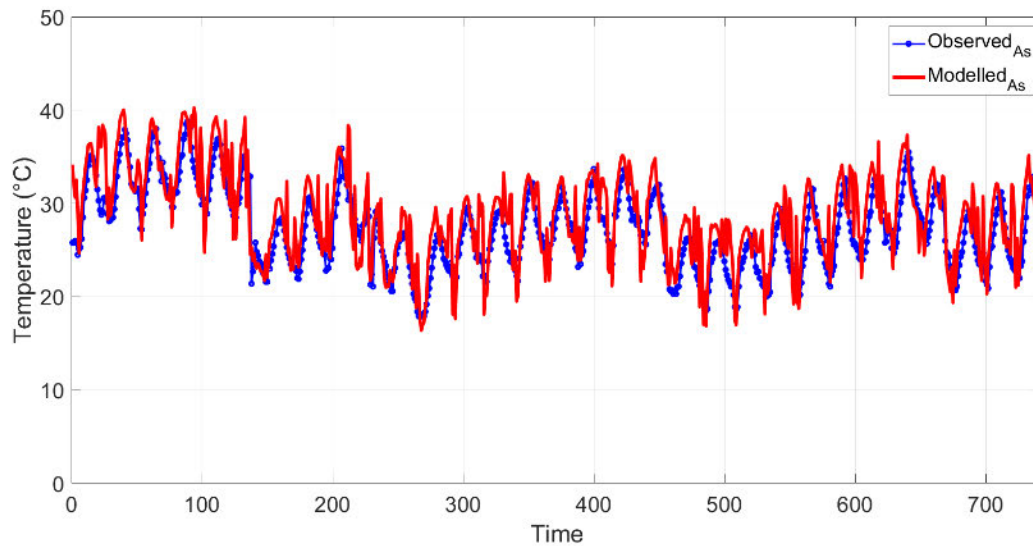
Figure 12. Time series of modelled (red line) and observed (blue dotted line) hourly temperature values for the month of August 2017 (1/08/2017 0:00 – 31/08/2017 23:00) at the Asinelli synoptic meteorological station (source: Own account for simulated values, Dext3r website for observations).
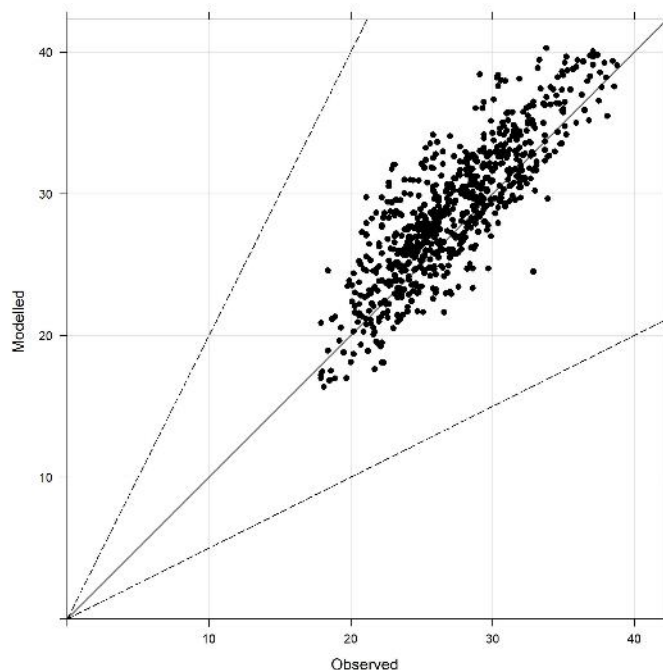
Figure 13: Scatter plot of modelled and observed hourly temperature values for the month of August 2017 (1/08/2017 0:00 – 31/08/2017 23:00) at the Asinelli synoptic meteorological station (source: Own account for simulated values, Dext3r website for observations).
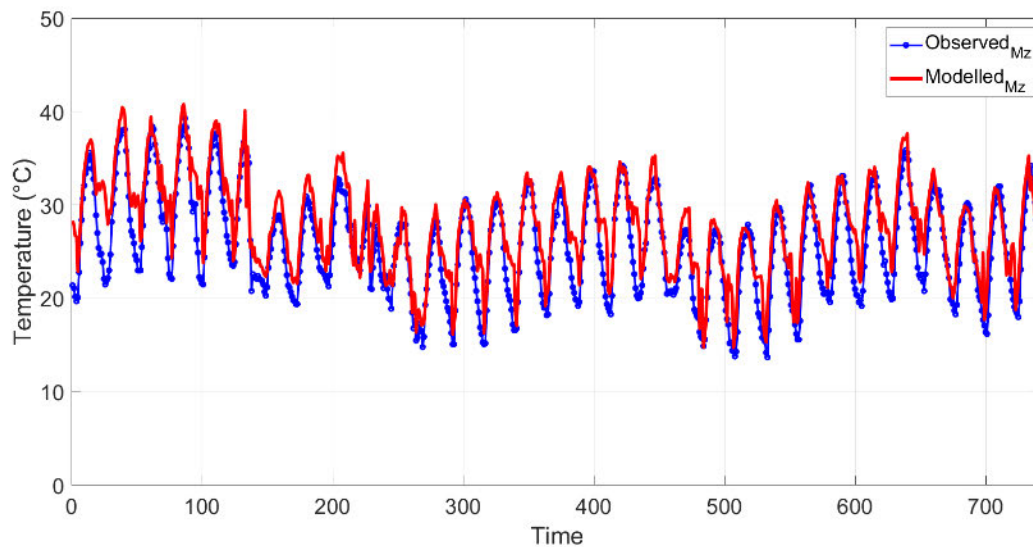
Figure 14. Time series of modelled (red line) and observed (blue dotted line) hourly temperature values for the month of August 2017 (1/08/2017 0:00 – 31/08/2017 23:00) at the Mezzolara rural meteorological station (source: Own account for simulated values, Dext3r website for observations).
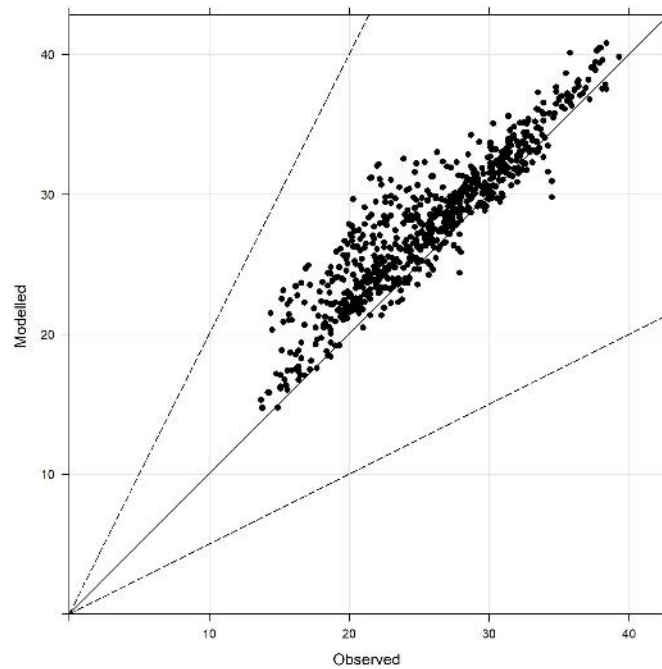
Figure 15: Scatter plot of modelled and observed hourly temperature values for the month of August 2017 (1/08/2017 0:00 – 31/08/2017 23:00) at the Mezzolara rural meteorological station (source: Own account for simulated values, Dext3r website for observations).

In particular, the performance of the ADMS-TH model was evaluated by calculating some statistical parameters, with a methodology developed by Hanna (1993) and summarized by Chang and Hanna (2004). The following indicators were considered for the evaluation of the performance of the ADMS-TH model:

- The mean bias (MB), and the fractional bias (FB), measuring the mean difference between the modelled and observed concentrations
- the normalized mean square error (NMSE), a measure of the mean difference between matched pairs of modelled and observed concentrations
- the factor of two (FA2), i.e. the fraction of modelled concentrations within a factor of 2 of observations
- Pearson's correlation coefficient (r), a measure of the extent of a linear relationship between the modelled and observed concentrations,
- and the coefficient of determination (R^2), the proportion of the variance in the dependent variable that is predictable from the independent variable(s).

Following equations describe the calculations of those statistical parameters:

$$MB = (C_o - C_m)$$

$$FB = \frac{(\overline{C_o} - \overline{C_m})}{0.5(\overline{C_o} + \overline{C_m})}$$

$$NMSE = \frac{\overline{(M - O)^2}}{\overline{MO}}$$

FA2 = the fraction of data for which $0.5 < C_m/C_o < 2$

$$r = \frac{\sum_{i=1}^{n}(C_{o.i} - \overline{C_o})(C_{m.i} - \overline{C_m})}{\sqrt{\sum_{i=1}^{n}(C_{o,i} - \overline{C_o})^2 \sum_{i=1}^{n}(C_{m,i} - \overline{C_m})^2}}$$

$$R^2 = \frac{[\sum_{i=1}^{n}(C_{o.i} - \overline{C_o})(C_{m.i} - \overline{C_m})]^2}{\sum_{i=1}^{n}(C_{o,i} - \overline{C_o})^2 \sum_{i=1}^{n}(C_{m,i} - \overline{C_m})^2}$$

Where C_o denotes observations, C_m denotes model simulations, and the overbar denotes the average over the dataset.

Ideally, FB and NMSE should tend to zero, while FA2, r and R^2 should be equal to 1.

In Table 6 the statistical parameters for all reference stations are presented.

Station	Type	OBS mean + SD	MOD mean + SD	MB	NMSE	R	R²	FA2	Fb
BU	Urban	27.4 ± 3.0	29.5 ± 3.2	2.11	0.01	0.99	0.77	1.00	0.07
AS	Urban	27.3 ± 3.1	28.8 ± 3.1	1.56	0.00	0.97	0.70	1.00	0.06
Mz	Rural	25.7 ± 2.6	27.9 ± 3.1	2.18	0.01	0.99	0.84	1.00	0.08

Table 6. Statistical analyses for evaluating the performance of the ADMS-TH model. Reference station: Bologna Urbana (BU), Asinelli (As), Mezzolara (Mz). Observed data (Obs), modelled data (Mod) (source: Own account for simulated values, Dext3r website for observations).

Overall, temperature values are well predicted, with FA2 results close to 1 showing good agreement between observed and modelled temperature values. Hour by hour comparisons of values show somewhat greater error as shown by normalised mean square error (0.01). The values of the fractional bias are very low (0.07 in BU station and in the range of 0.06 to 0.08), where the low positive values indicate the tendency of the simulations to a slight overestimation of temperature values. Also, R values close to 1, and R^2 values higher than 0.7 and even larger at Bologna Urbana and Mezzolara shows the good performance of the model simulations. The overestimation of the model is also highlighted in the following Figure 16, which shows the weekly time-temperature cycle in Bologna Urbana.
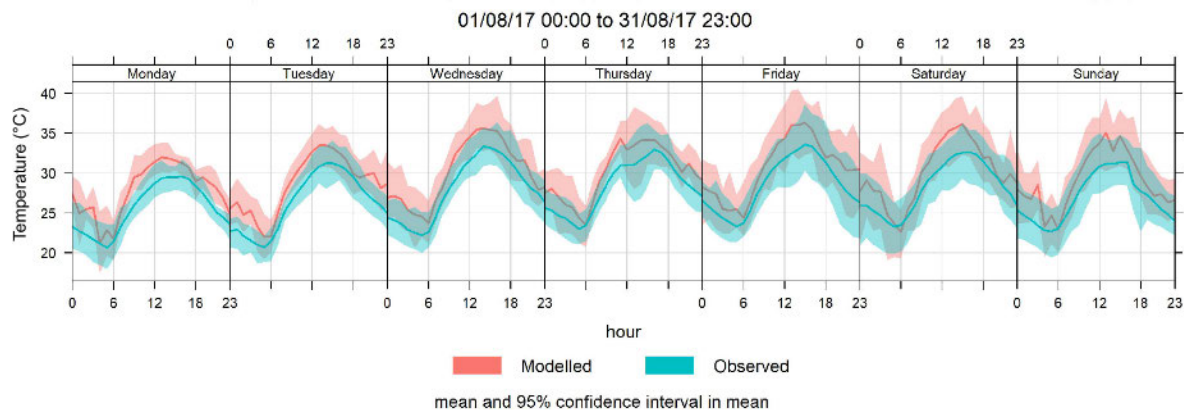
Figure 16. Weekly time temperature cycle in Bologna Urbana, an average of modeled (red line) and measured (blue line) data and 95% confidence interval in the mean in the month of August 2017 (source: Own account for simulated values, Dext3r website for observations).

However, even in the case of Bologna Urbana where the overestimation is larger than in the other cases, it can be observed that the average of the modelled data falls within the confidence interval. Overall the results indicate a very good performance of the ADMS-TH simulations performed for the city of Bologna.

2.1.3 Modelled results and discussion

Since one of the purposes of this deliverable is to highlight the effects of green infrastructure on urban-scale UHI effects, in Bologna the modeling of the current base case scenario was carried out over a period during which an intensive experimental field campaign carried out in two street canyons in Bologna (the summer experimental campaign in August-September 2017, thoroughly described in D3.3 and D5.2). In fact, as described in those Deliverables, within the summer and winter experimental campaigns, instrumentation for the measurement of meteorological and turbulence (and air quality) variables was located along and above two parallel street canyons in the city of Bologna, Marconi St. and Laura Bassi Veratti St. Furthermore, during both campaigns, two days intensive thermographic campaigns involving measurements of the temperature of building facades and asphalt in the two canyons by means of thermographic IR cameras, were also carried out in the two canyons, with the purpose to evaluate the UHI effect at neighbourhood scale. For this reason, the simulations presented below refer to the days 22 and 23 August 2017, when the summer thermographic campaign was carried out in Bologna.

2.1.3.1 Present base case scenario (NO PCSs)

The simulations of the ADMS-TH model in the current scenario, i.e. considering the actual land use and the hourly meteorological variables recorded by ARPAE stations during the 22-23 August 2017, have produced as output hourly maps of temperature at 3m height level. Below, the maps of temperature for four different times of the day are presented:

- At 6 am (early morning);
- At 12 am (noon);
- At 6 pm (i.e., before sunset);
- At 24 (midnight).
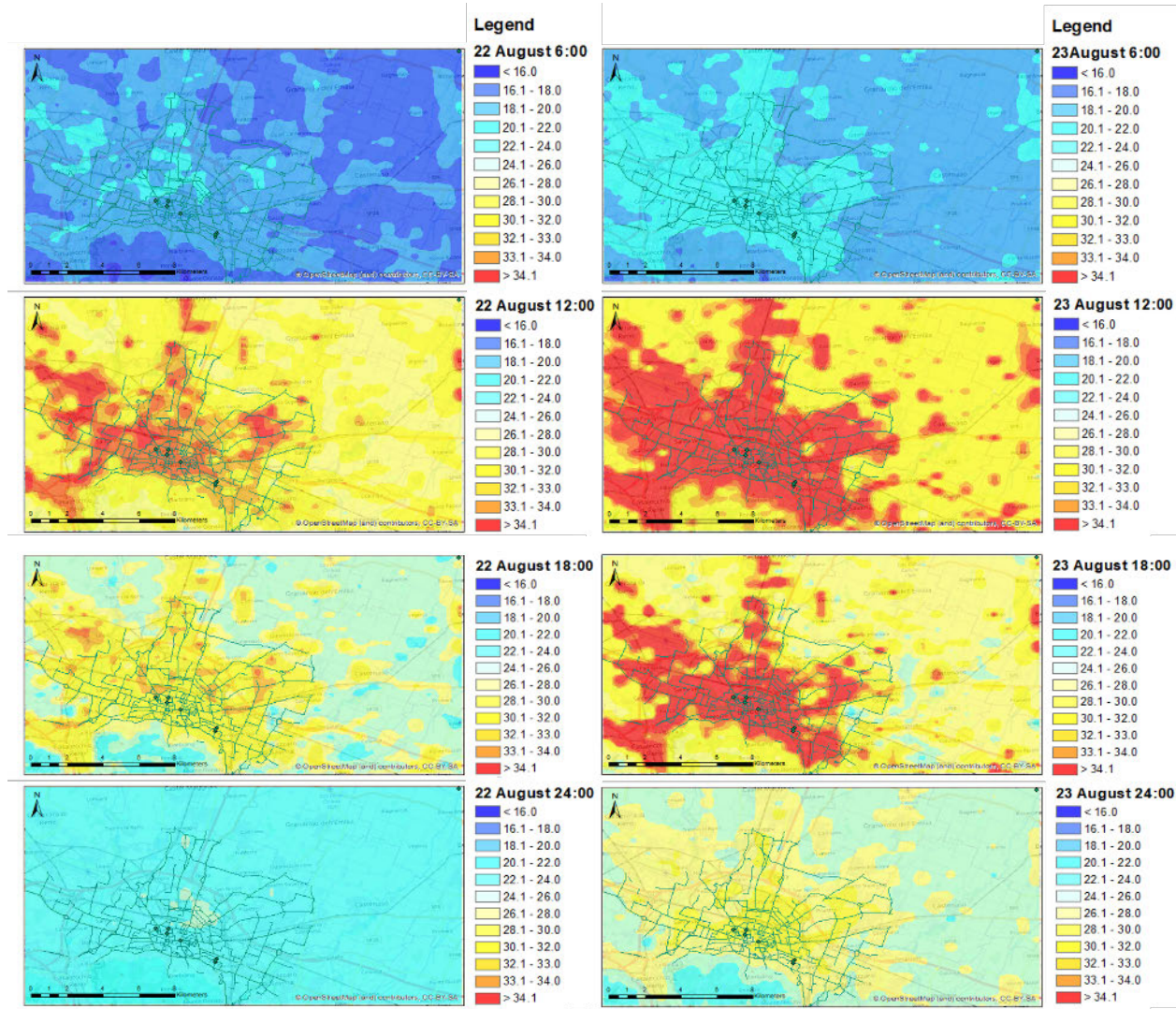
Figure 17: Maps of simulated temperature (°C) at 3m height level, presented for four different hours (from top: 6:00; 12:00; 18:00 and 24:00) of 22 August 2017 (left) and 23 August 2017 (right) for the NO PCSs scenario (base case, current scenario) (source: Own account).

The figures show a higher temperature in the city centre and lower temperatures in rural areas. In urban areas, the high density of buildings traps more heat because of the reduced albedo and the higher absorption of infrared radiation which prevents it from spreading out to space; furthermore, the absence or limited presence of green areas inhibits the dispersion of latent heat from the ground to the detriment of sensible heat, which is also responsible for the increase of temperature.

The temporal evolution of the UHI is characterized by a diurnal cycle: in the early hours of the morning minor differences in temperature between urban and rural areas are noticed, while differences increase during the day until reaching the maximum before sunset. The peak in the hours before sunset is due to the fact that areas characterized by poor urbanization disperse more quickly and more effectively the energy stored during the day compared to the urbanized centre. This is followed by a delay in the dispersion of the absorbed heat by the urbanized areas.

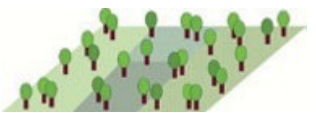Since the centre of Bologna has been classified as "Compact Midrise" (from the previously presented LCZ classification: Dense mix of midrise buildings. Few or no trees. Land cover mostly paved. Stone, brick, tile, and concrete construction materials), the effects that green infrastructures produce on the UHI effect at city scale were evaluated by modifying the LCZ classes. In particular, two scenarios were simulated:

- Marconi St. with trees: considering Marconi St. as a typical representative street canyon in the Bologna city centre (LCZ2), the presence of trees was simulated by modifying the surface parameter of the reference class with that used in the LCZ5 class.
- Centre with trees: the parameter thermal admittance was changed over the whole city centre of Bologna.

One primary reason to perform these two simulation scenarios derives from our observations in D5.2 that the UHI effect is much more pronounced in Marconi St. as compared to Laura Bassi, which was attributed to the presence of vegetation in Laura Bassi and to the location of Laura Bassi a bit further away from the city centre in a residential area characterized by the presence of small houses and apartments.

2.1.3.1.1 Marconi St. with trees (Marconi PCSs)

As described previously, in the first scenario investigated we planted trees in Marconi St. by modifying the surface parameter of the reference class with that used in the LCZ5 class. Figure 18 illustrates graphically this modification in the input surface parameter.
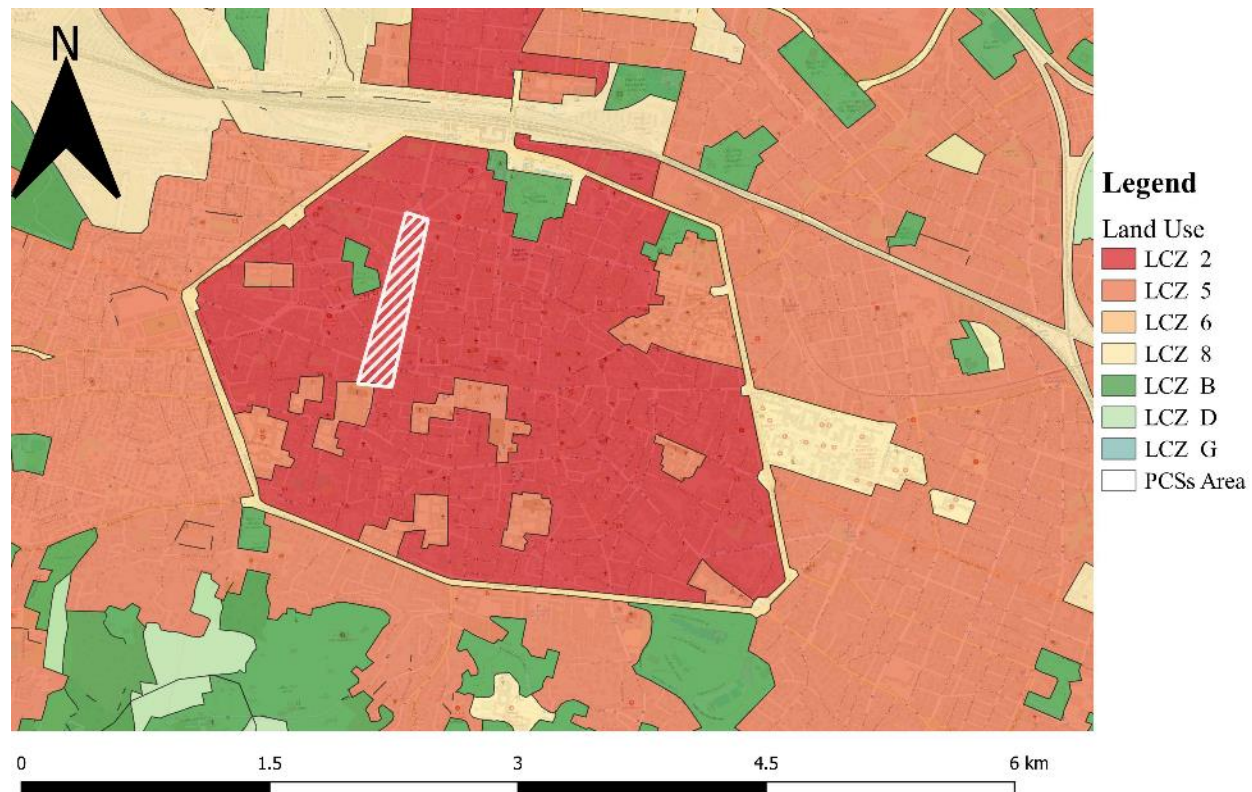
Figure 18. Map showing the modification of the surface parameter from the reference class to the LCZ5 class to introduce trees in Marconi St in the first simulation scenario investigated to evaluate the impact of GI on UHI in Bologna (source: Own account)

A more in-depth analysis of the outputs of this simulation was conducted by comparing the modeled results with data collected during the summer campaign (see D3.3 and D5.2). Figure 19 adds to the hourly values of air temperature observed on 22-23 August 2017 (measured within the experimental campaign and by ARPAE urban and rural stations) and building facades temperatures in the Marconi street canyon (already presented in D5.2) also hourly simulated temperature values in the Marconi street canyon (black line). The model overestimation (already described in section 2.1.2.5) is greater during sunny hours whereas the simulated values are closer to the surface temperature of buildings than to those of air. However, at night, when the model correctly simulates the air temperature, the street canyon is isothermal, with the same observed temperature for the air and for the surface of the building.
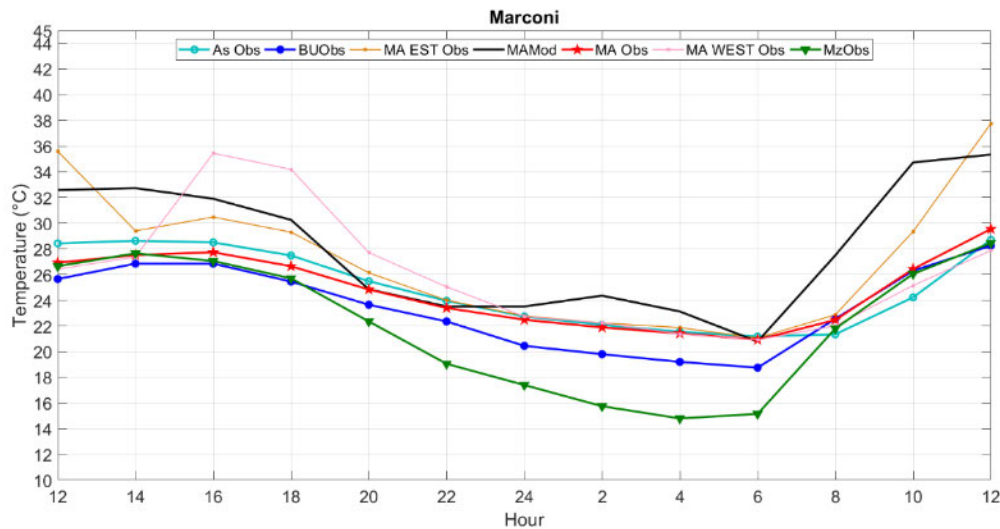
Figure 19: Hourly temperature observed and simulated values in Marconi street canyon and measured at ARPAE urban and rural meteorological stations in the surroundings of Bologna. Specifically, observed temperature values (Obs) in the Asinelli (As), Bologna Urbana (BU) and Mezzolara (Mz) stations and in Marconi St. (MA); temperature values extracted from thermographic analysis of the buildings positioned to the west (MA WEST) and to the east (MA EAST) of Marconi St.; temperature values modeled in Marconi St. 4 meters from the ground (MAMod) (source: Own account, for temperature data measured within the Bologna summer experimental campaign and for simulated values in Marconi St., Dext3r website for data measured at ARPAE meteorological stations).

The temperature simulated by the ADMS-TH model provides us with an indication of the UHI extension at that time. In this way, we may then evaluate the change in the temperature and UHI effect when introducing a variation of land use, which we may consider as an indication of the effect of the introduction of trees in that location (Figure 20). For the period of 22 and 23 August analyzed to date, the UHI in the case trees are added in via Marconi seems to present a similar intensity as that of the base case, but during some hours and especially at night the effect is reduced, with a maximum 0.4°C reduction during the first hours of the day.
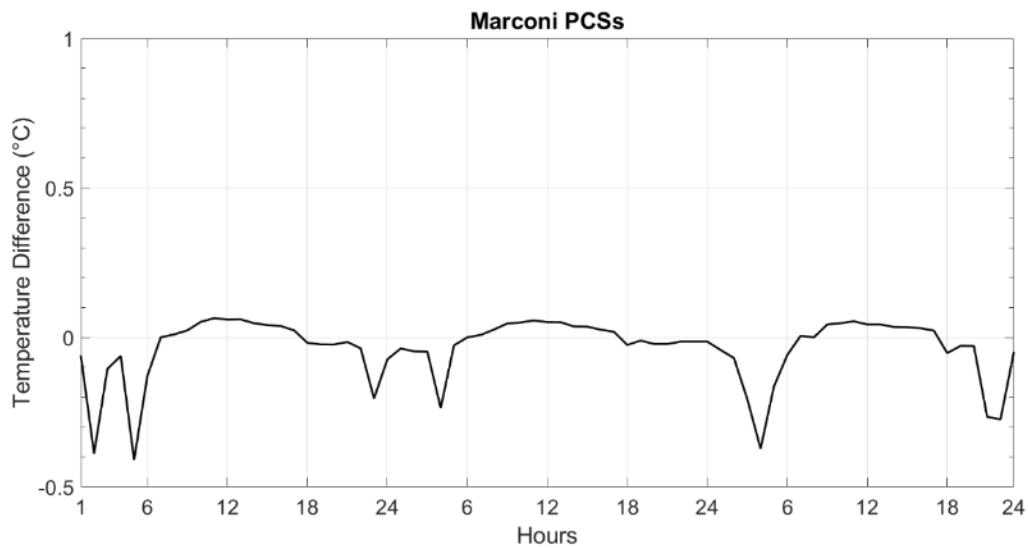
Figure 20. Difference between the temperature before and after the change in land use (source: Own account

Figure 21 shows the map of differences in temperature at 04:00 on 23 August 2017. The values indicate the temperature reduction (in °C) due to the presence of PCSs (here, trees) in Marconi St. The map shows how the introduction of trees over a small area can produce effects over the observed temperature even in the surrounding areas.
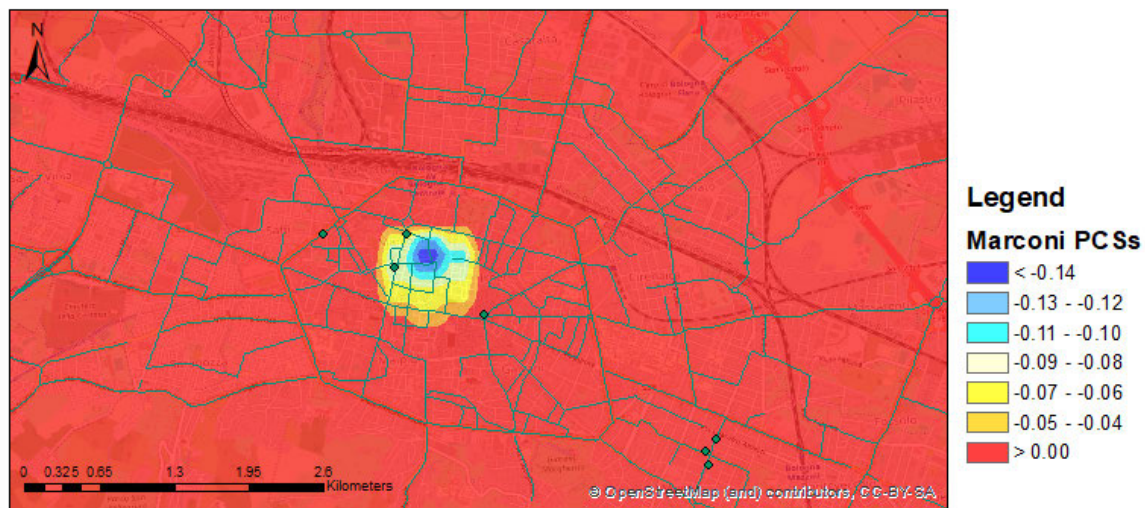
Figure 21. The Difference of temperature (°C) between the NO PCSs (base case) case and Marconi PCSs scenario (trees added in the Marconi street canyon). The difference is expressed in °C (source: Own account).

2.1.3.1.2 Centre of Bologna with trees (Centre PCSs)

In the second scenario simulated we considered a change in land use extended over the whole centre of Bologna. In this case the UHI effect is reduced by the same intensity but affects a larger area. Figure 23 shows the differences in temperature perturbation between the NO PCSs scenario (base case) and the Centre PCSs scenario (whole Centre of Bologna covered with trees). Similar to the previous scenario, it can be observed that the presence of trees induces a temperature reduction (and as such increases the thermal comfort) over a large area covering the city centre and surrounding areas.
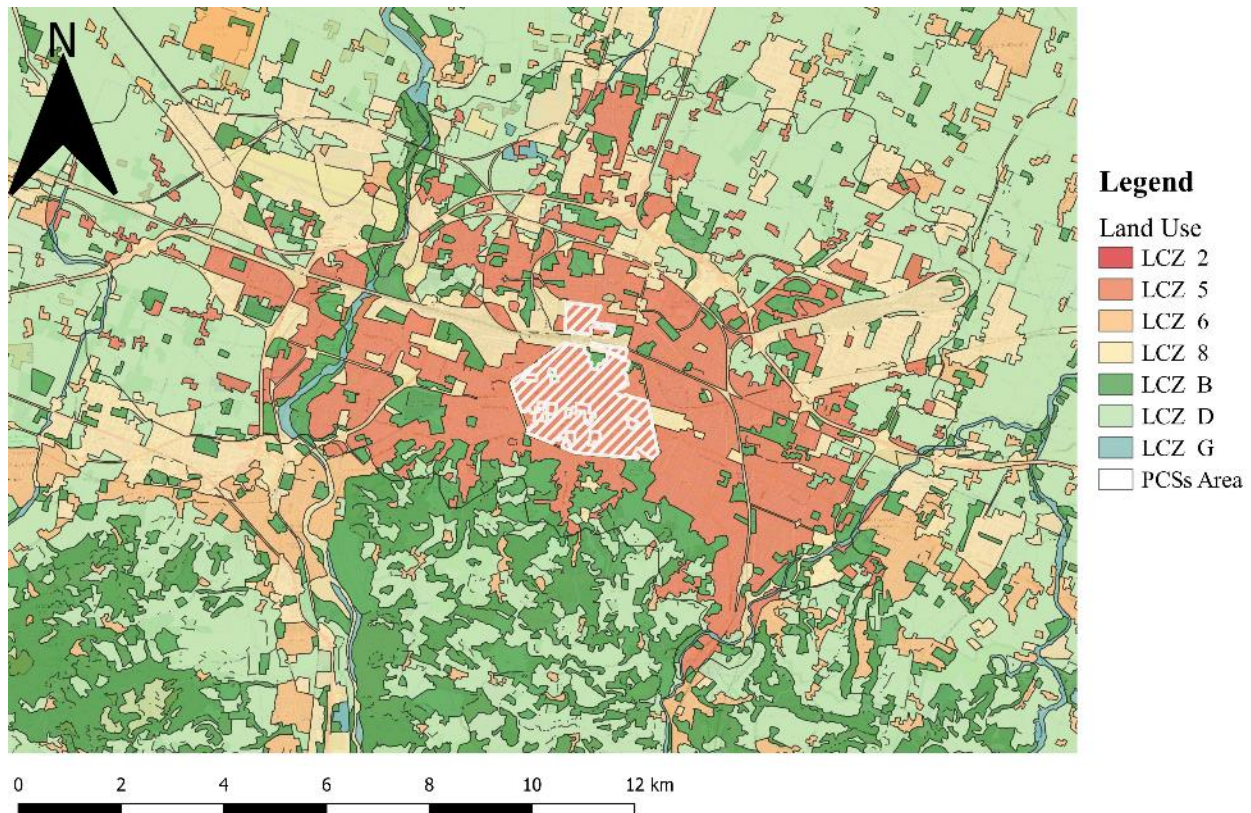
Figure 22. Map showing the modification of the surface parameter from the reference class to the LCZ5 class to introduce trees over the whole Bologna city centre in the second simulation scenario investigated to evaluate the impact of GI on UHI in Bologna (source: Own account).
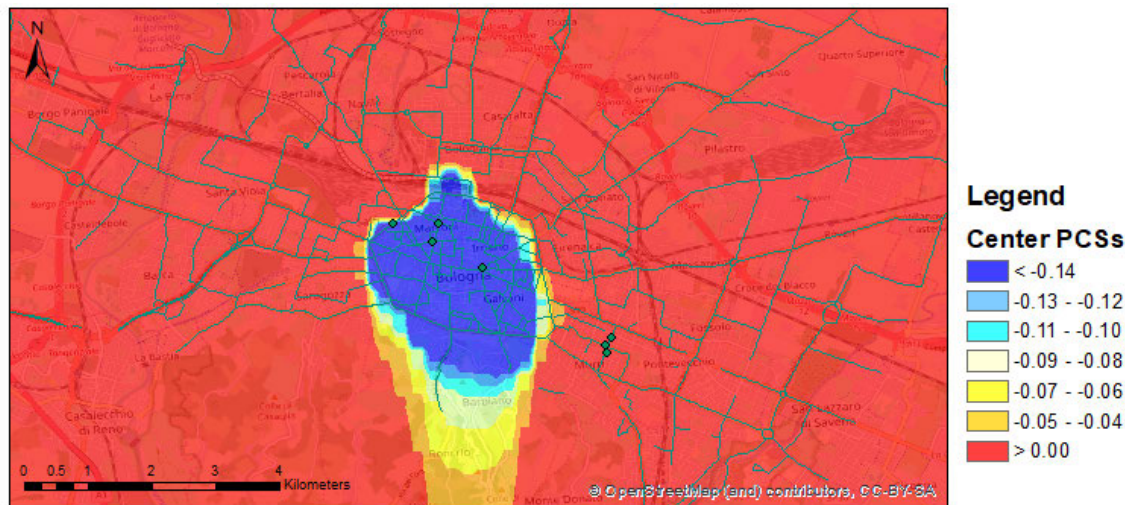
Figure 23. Difference of temperature between the NO PCSs (base case) case and the Centre PCSs scenario (trees added over the whole city centre. The difference is expressed in °C (source: Own account).

2.2 Impact of GI on AQ in Bologna

2.2.1 Description of the model

Similar to D4.5, in this work, the ADMS-Urban model (version 4.1.1.0) developed by Cambridge Environmental Research Consultants (CERC) was used (CERC, 2011) to carry out atmospheric dispersion simulations through which to evaluate the dispersion of air pollutants emitted into the atmosphere from the sources considered in the emission inventory. The ADMS-Urban model is a quasi-Gaussian plume air dispersion model able to simulate a wide range of passive and buoyant releases to the atmosphere. The dispersion of pollutants has been simulated with the Atmospheric Dispersion Modelling System (ADMS; CERC, 2017). This model has been already extensively verified within a large number of studies, and its performance has been compared with other EU and US EPA models, such as CALPUFF and AERMOD for instance (e.g., Carruthers et al., 2000; Di Sabatino et al., 2008; Stocker et al., 2012).

Minimum input data for the modeling setup and for the representation of the modeled domain consists in the emission sources including emission rates and time-varying emission factors, meteorological data (at least: air temperature, wind speed, wind direction, and either cloud cover either sensible heat flux either Monin-Obukhov length for estimating boundary layer height), and background concentrations. Within the model, the dispersion calculations are driven by hourly meteorological profiles of wind speed and direction, characterized through Monin-Obukhov length similarity theory. This is an important difference between the model and traditional analytical stationary dispersion models, which use Pasquill stability classes to describe the stability of the atmospheric boundary layer. ADMS, in fact, uses two measurable physical parameters, i.e. the height of the atmospheric boundary layer and the Monin-Obukhov length, to this scope, which enables a much more realistic description of dispersion phenomena. As such, it is easily understandable that input meteorological data are among the most important input parameters for modeling air pollution dispersion.

The simulations in Bologna were conducted in two different ways:

- Short term – the model calculates one concentration value for each pollutant and for each hour of input meteorological data, with output as hourly means for the first 24 lines of meteorological data only. The output can be a grid or a table containing simulated values for the receptor points and the selected pollutants. This simulation type, in particular, was used for the verification and comparison of model outputs with observations.

- Long term - the concentration output files will contain a single set of concentration data, averaged over all the lines of meteorological data. This means that if the meteorological input file covers one year, the obtained simulated concentrations are yearly means. Also, in this case, it is possible to obtain gridded concentrations over the study area or tables with concentration values at receptor points. This simulation type, in particular, was used for producing concentration maps in the actual scenario (base reference case) and in the scenarios to be compared with it, i.e. when introducing a change in PCSs (here, GI).

Additional options for the simulations include gaseous and particle dry and wet deposition; in case these options are selected, the user needs to include information on dry deposition velocity and washout coefficients for each pollutant for including dry and wet deposition in the dispersion simulations. Further, in case the wet deposition is also considered in the simulations, precipitation needs to be included in the meteorological dataset. The dry deposition velocity contains a diffusive part, the deposition velocity itself, and the terminal velocity of a particle, which is due to gravitational settling in the plume. Both are required in ADMS-Urban for dry deposition modelling. If the values are unknown, they can be estimated by the model. Wet deposition occurs when there is precipitation (rain, sleet, snow, etc.) and it is modelled through a washout coefficient which is dependent on the nature of the pollutant, the rainfall rate and droplet size. This washout coefficient can be taken as a constant value (in which case the wet deposition is independent of the rainfall rate), or it can depend on the rainfall rate. Finally, the model includes the option to include the NO_x photolytic chemistry module, which accounts for fast, near-road oxidation of NO by O_3 to form NO_2 (Smith et al., 2017). In order to consider the NO_2-NO-O_3 chemical reactions in the simulations, meteorological data need to include solar radiation and time and hour of the day. The modelling also uses the ADMS-Urban NO_x photolytic chemistry module, which incorporates both reactions for the photochemical reaction between nitric oxide (NO), nitrogen dioxide (NO_2), volatile organic compounds (VOC) and ozone (O_3), and reactions that govern the oxidation of sulfur dioxide (SO_2) leading to the formation of ammonium sulfate particles, i.e. particulate matter (PM). To use this scheme, solar radiation information and background concentration data for the critical pollutants NO_x, NO_2, O_3 and SO_2 are required.

2.2.2 Methodological approach

The analysis of AQ in the city of Bologna was performed testing a suitable period chosen within the two experimental field campaigns described in D3.3 and D5.2. In particular, the selected period is the month of August 2017, whose specific meteorological conditions are described in D5.2.

An emission inventory is covering the Bologna area and consisting of traffic sources over a domain of 12 x 19 km, was built up with a methodological approach fully described in D4.5 ('*Report on policy options for AQ and CC*'[7]). The year 2017 was selected as a base case, and the validation

---

[7] The report will be made available on the iSCAPE results webpage.

for the base case is thoroughly presented discussed in D4.5. In the following we report only a brief synthesis of the methodology adopted.

The runs use hourly measured meteorological data from Marconi airport for the whole domain, with data available over 95% of hours in 2017. In order to assess the baseline air quality in the modelled area, background pollution concentrations were included in the modelling. Background concentrations of air pollutants were obtained from the ARPAE monitoring network: Via Chiarini (in the western part of Bologna, measuring hourly data for NO_x, NO_2, O_3 and daily data for PM_{10}); Giardini Margherita (in the southern part of Bologna, measuring hourly data for NO_2). No monitoring data are available for CO because the annual average is smaller than the legal limit (0.6 mg/m³). According to the work of Righi et al. (2009) to model well also the CO emissions, it is necessary to insert its background value, in particular considering that it is affected by a "memory effect" that can be corrected taking into account the concentrations of CO present in the hours immediately preceding the specific time considered in the model. For these reasons, here the background CO concentration was inserted as the concentration measured at the ARPAE urban traffic Porta San Felice station during the hour previous to the simulations.

The emissions from air pollution sources are time dependent, so time-varying emission factors for road and grid sources need to be considered. In this study, detailed data of hourly factors for weekdays (24 hours), Saturdays (24 hours) and Sundays (24 hours) (i.e. diurnal profiles) and monthly profiles are defined.

As for the meteorological input, parameters of wind speed, wind direction, surface temperature, precipitation, solar radiation and cloud cover were used. The meteorological dataset contained hourly sequential data measured at the Bologna airport weather station, considered the reference meteorological station for the city of Bologna not influenced by the presence of buildings in the city itself:

- Name: Bologna/Borgo Panigale (Bologna airport);
- WMO number: 16140 and WMO code: LIPE;
- Latitude: 44.5308 and Longitude: 11.2969.

Here it is also worth to mention that the air dispersion simulations carried out in Bologna with the ADMS-Urban dispersion model were verified comparing output air quality concentrations with measured values at ARPAE air quality stations for the whole 2017 year, providing more than satisfactory results for all pollutants. The verification of the dispersion simulations for air quality in Bologna is presented in D4.5.

2.2.2.1 Modeling of trees in ADMS

In order to model the effect of trees on air quality, the dry deposition option was activated in the ADMS-Urban model. As discussed in section 2.2.1, to set up the dry deposition it is necessary to set the deposition velocity (V_{dep}) values for each pollutant. This speed varies according to the type of pollutant (gas, particle), the size, the reactivity, and the type of surface on which it is deposited. Zhang et al. (2003) provided the deposition velocity values for the gaseous substances deposited on a wide range of surfaces, in particular tabulating the values for urban surfaces and different types of trees. In the model, tabulated values for deciduous broad-leaved, the most widespread in Bologna, were used (NO_2=0.0078; SO_2=0.0101 and O_3=0.0078 m s^{-1}). With regard to the deposition velocity values of PM_{10}, the value provided in the report of the National Radiological Protection Board (NRPB, 2001) was used (0.099 m s^{-1}).

2.2.3 Modelled results and discussion

In order to evaluate the effect of PCSs on the AQ, two scenarios are investigated: base case scenario (Bologna without trees) and PCSs scenario (Bologna with trees) where the deposition velocity values were set to take into account that the trees extend over 30% of the Bologna area. Similar to what presented in the previous section for UHI effects in Bologna, the modeling of the scenarios was carried out for August. The results are illustrated below with deposition maps of NO_x and PM_{10} for the base case, while in order to evaluate the effect of PCSs, the scenario with PCSs is compared with the base case scenario through differences maps.

2.2.3.1 Base case scenario (NO PCSs)

The following figures show the spatial distribution of the concentration of NO_x and PM_{10} in the base case for August 2017 (Base Case scenario), averaged over the period considered.
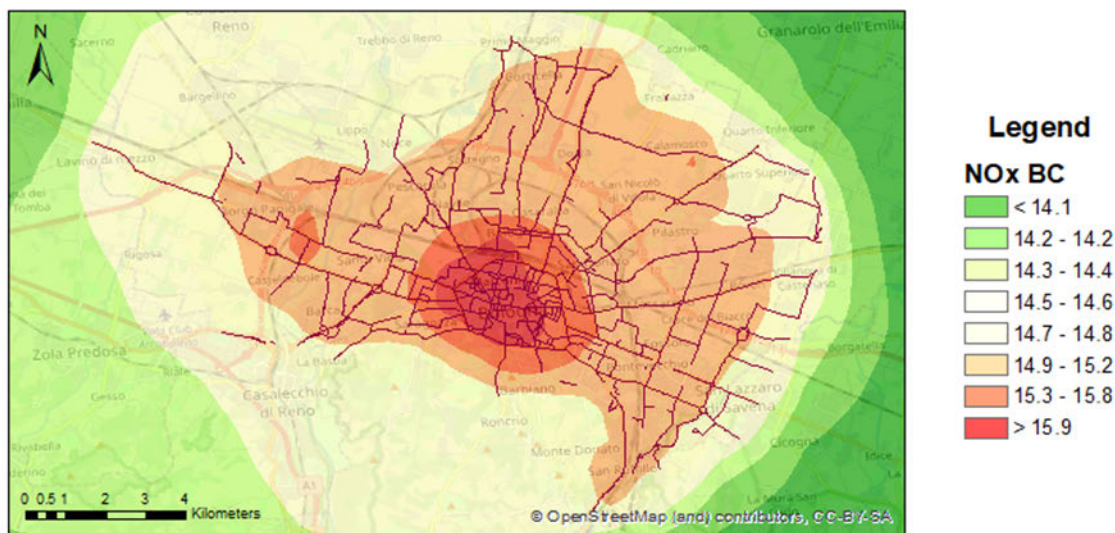
Figure 24. Map of NO_x concentrations (µg m³) in the base case for Bologna. The maps represent concentrations averaged over the period considered (August 2017) (source: Own account).
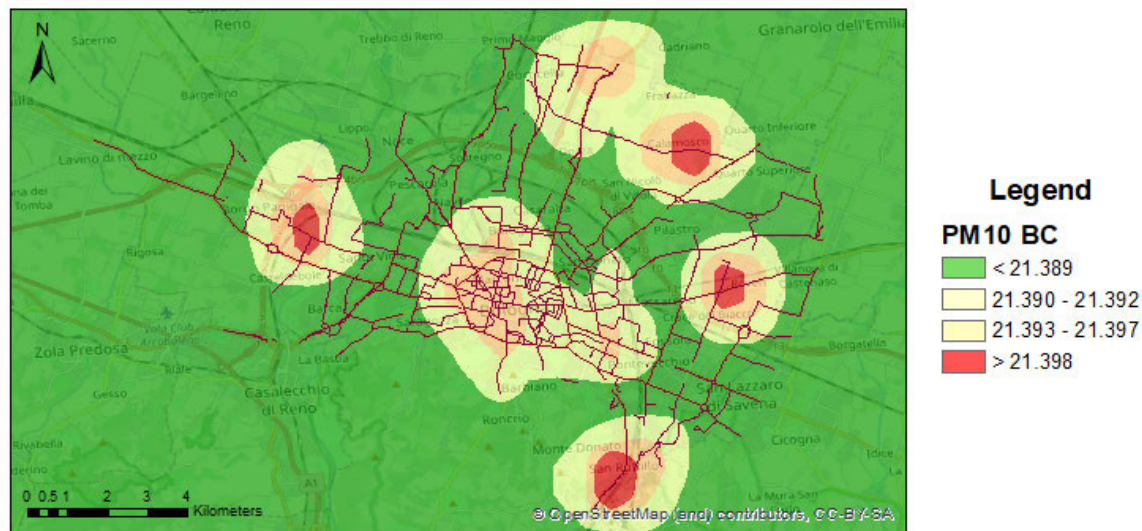
Figure 25. Map of PM$_{10}$ concentrations (µg m^3) in the base case for Bologna. The maps represent concentrations averaged over the period considered (August 2017) (source: Own account).

The following figures show the spatial distribution of the deposition of NO$_x$ and PM$_{10}$ in the base case for August 2017 (Base Case scenario).
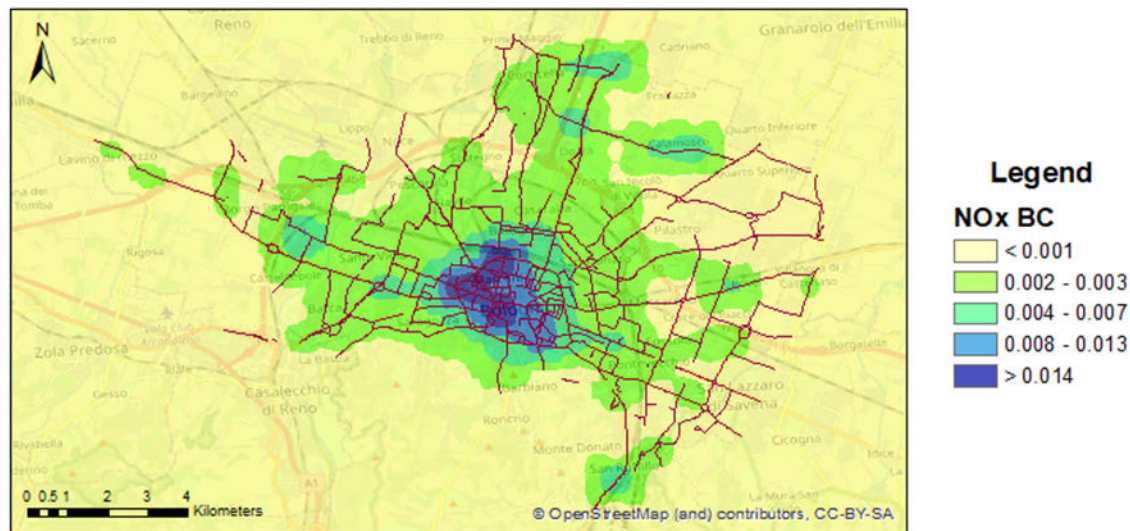
Figure 26. Deposition map (µg / m^2 / s) for NO$_x$ in the base case for Bologna. The map represents deposition values averaged over the period considered (August 2017) (source: Own account).
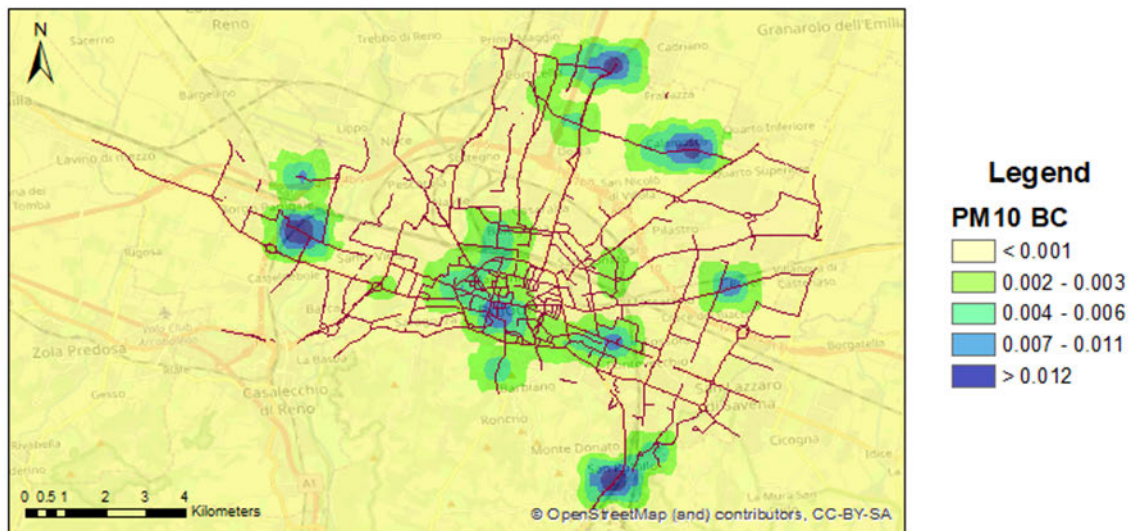
Figure 27. Deposition map (µg / m² / s) for PM₁₀ in the base case for Bologna. The map represents deposition values averaged over the period considered (August 2017) (source: Own account).

The NO$_x$ and PM$_{10}$ deposition maps (Figure 26 and Figure 27) show that the spatial deposition pattern follows the spatial concentration pattern so that the deposition is larger in the most trafficked areas.

2.2.3.2 Bologna with trees scenario (PCSs)

The following figures show the spatial distribution of the deposition of pollutants in the PCSs scenario for August 2017.
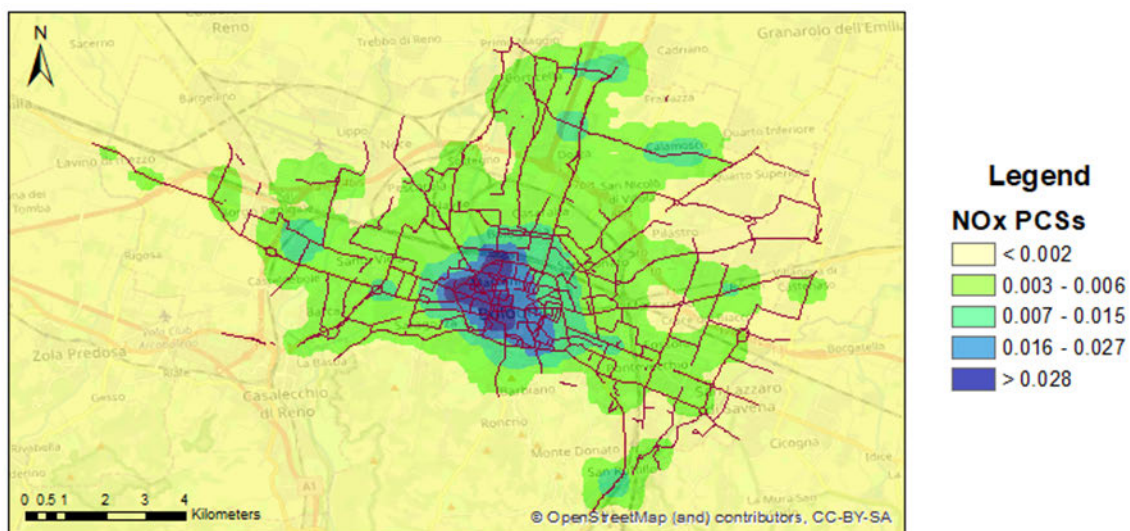
Figure 28. Deposition map (µg / m² / s) for NO$_x$ in the PCSs scenario for Bologna. The map represents deposition values averaged over the period considered (August 2017) (source: Own account).
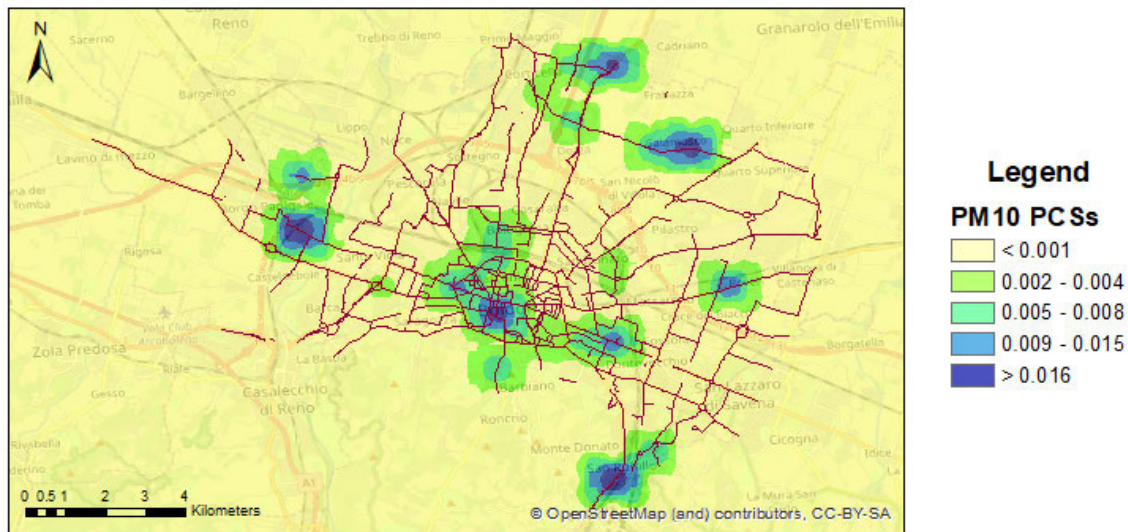
Figure 29. Deposition map (µg / m² / s) for PM₁₀ in the PCSs scenario for Bologna. The map represents deposition values averaged over the period considered (August 2017) (source: Own account).

The concentration maps show the same spatial deposition pattern of the base case scenario. To compare the base case with the PCSs scenario, maps of difference in a deposition in the two scenarios are presented in the following.
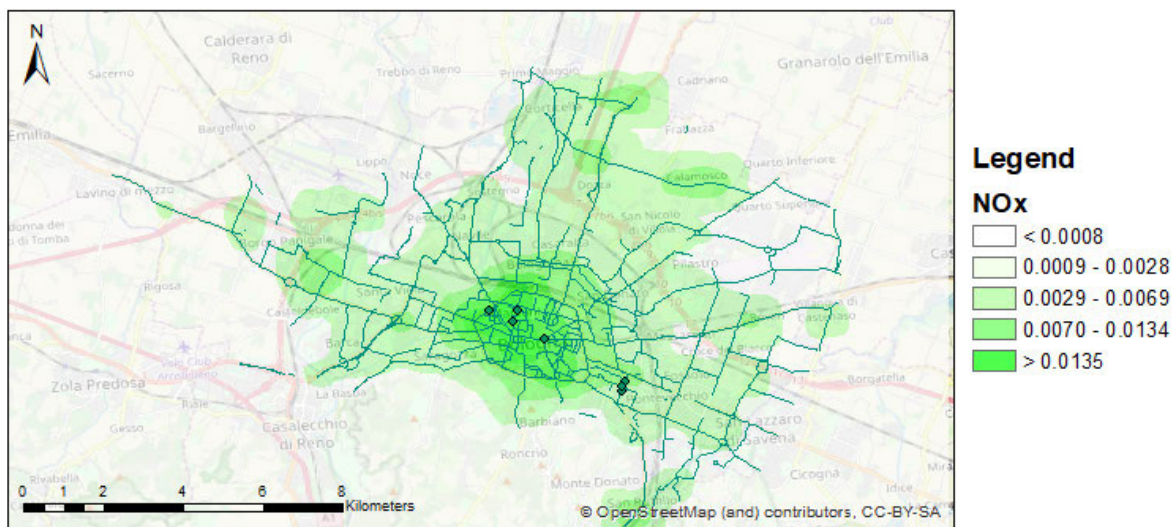
Figure 30. Maps of differences in deposition (µg / m² / s) between the two scenarios for NOₓ. The differences are calculated between the PCSs scenario and the Base Case Scenario (source: Own account).
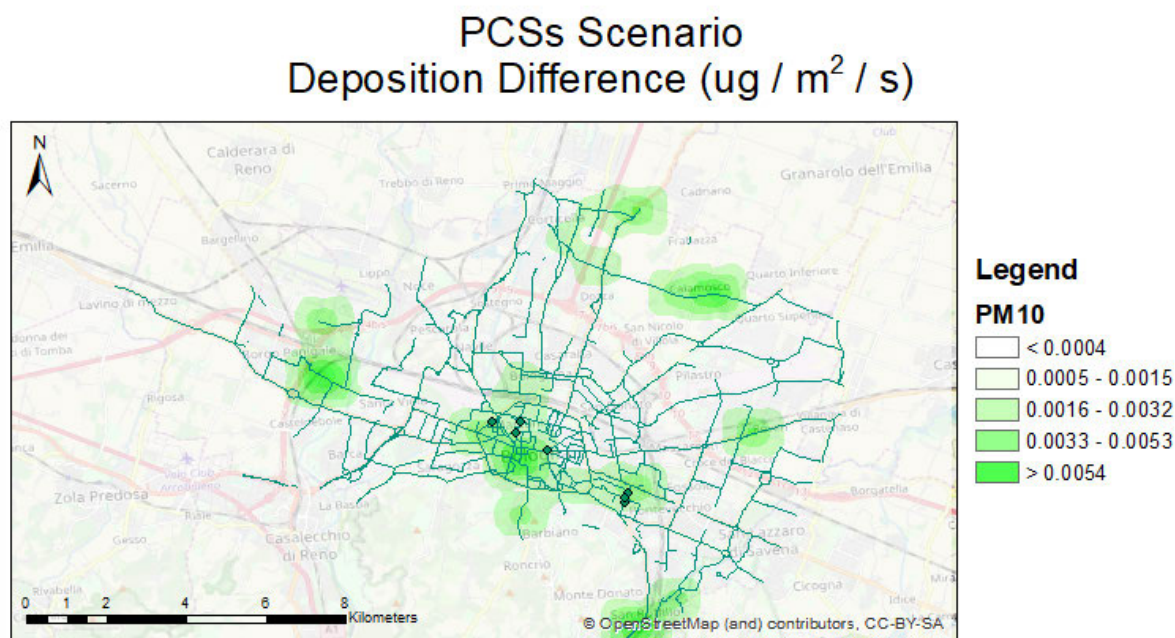
Figure 31. Maps of differences in deposition (µg / m² / s) between the two scenarios for PM₁₀. The differences are calculated between the PCSs scenario and the Base Case Scenario (source: Own account).

The maps of difference in deposition show an increase in a deposition in the same areas where the deposition is more active. In order to quantify the increase in deposition due to PCSs, a proxy of the reductions in concentrations, the percentage of increase maps (Table 7) was calculated both at the Porta San Felice receptor (SF) located at the urban traffic ARPAE air quality station in Bologna and considering the maximum value of the maps (max Grid).

	BC ($\mu g\ m^{-2}\ s$)	PCSs ($\mu g\ m^{-2}\ s$)	Difference ($\mu g\ m^{-2}\ s$)	Deposition increase (%)
NO_x (max Grid)	0.014	0.028	0.014	100%
PM_{10} (max Grid)	0.012	0.016	0.004	33%
NO_x (SF)	0.071	0.140	0.966	97%
PM_{10} (SF)	0.111	0.165	0.485	49%

Table 7. Summary of deposition data calculated from the map (max Grid) and at Porta San Felice receptor (SF). NO_x and PM_{10} deposition values for the base case (BC) and PCSs scenario (PCSs); deposition differences between PCSs scenario and the base case, percentage of increase in deposition due to PCSs (source: Own account).

3 Microscale modelling for investigation areas in the City of Bottrop

As described in the introduction to this report, studies on air quality and urban climate (heat stress) are also becoming increasingly important for spatial planning. In urban planning, basic studies on climate and air are of great importance for qualified land use planning and development planning in densely populated areas. Against the background of climate change, this importance continues to increase. Since the statements in question refer to a planning area, the use of maps as a basis for information is recommended. In this context, maps are an essential tool for planners, but also an important information carrier for politicians and the interested public. This means that spatial cartographic representations are also necessary for the implementation of climatic and air-hygienic aspects.

The aim of the following investigations was to simulate both the thermal situation (comfort) and air pollution in selected areas of the city of Bottrop. The various neighbourhoods in accordance with the DoW of Task 6.3 represent 'different morphology and microclimate' within the City of Bottrop. They have been selected in the living lab in collaboration with the City of Bottrop. Thus, the results of this investigation will be used on the ground for further land-use planning by the City of Bottrop. Consequently, the chosen approach must follow the legal requirements laid down in the aforementioned European framework directives. This guarantees for a visible impact of the iSCAPE project.

According to the German building code (§ 1 Abs. 6 Nr. 7 a) BauGB), impacts on the climate as an object of protection are described as relevant for consideration and include local impacts of climate change. According to Annex IV No. 5 lit. f) BauGB, the EIA report must contain a description of the effects of the project on the climate (e.g. type and extent of greenhouse gas emissions) and the vulnerability of the project to climate change. In addition, a description of the aspects of the current environmental status (the so-called baseline scenario) and an overview of its likely development if not implemented are required (Battis et al., 2015: 59-61). The baseline scenario will change as a result of climate change. It is therefore possible that, under the signs of climate change, additional significant environmental changes, which may not be compensable, are to be expected (e.g. due to the intensification of the heat island effect in cities), which ultimately raises the question of the eligibility of a project or plan for approval in the weighing process.

As a result of the new environmental assessment regulations, a distinction must, therefore, be made between four areas of impact:

1. effects of projected climate change (changed reference state) on existing spatial structures and land uses, taking into account planned climate adaptation measures.

2. effects of the climate (climatic situation and projected climate change) on planned land use

3. effects of planning on the climate:
   - Effects on the global climate,
   - Effects on today's local climate and climatic changes in the future.

4. the impact of planning on major accidents and disasters.

Microscale modelling, for example, enables urban planners to simulate and compare the effects of targeted climate change adaptation measures or measures for air pollution control within

different planning scenarios without the area or planning measures under investigation having to exist in reality.

The case studies in the city of Bottrop focus on the possibilities of heat reduction and general improvement of the quality of stay in highly sealed urban spaces. From a climatic and air-hygienic point of view, the low presence of green spaces in heavily anthropogenically overshadowed areas can generally be regarded as disadvantageous. This applies in particular to large sealed and overheated areas. In addition to greening measures, improving ventilation can also produce positive climatic effects and improve air quality.

As presented in the Introduction section, the case study in the city of Bottrop is based on following overall research questions:

- What effects do selected urban-level interventions have on the small-scale city climate and air quality in different urban morphologies?

- Which planning alternatives are to be preferred in these aspects?

The following Table presents an overview of the model simulations carried out in Bottrop to address the above research questions.

City/Scale	Modelled scenarios	Software
Existing residential area (Heidenheck)	1) Baseline scenario (status quo) 2) Scenario A (Designation on Road Trees): Simulation with additional road trees	ENVI-met V4.3.2 Summer18 (inklusive BIO-met)
Existing industrial area (Brakerstraße)	1) Baseline scenario (status quo) 2) Scenario A (Designation on Road Trees): Simulation with additional road trees 3) Scenario B (Designation on Roof Greening): Simulation with roof greening on flat roofs	ENVI-met V4.3.2 Summer18 (inklusive BIO-met)
Planned residential area - Legally binding plan (Am Lamperfeld)	1) Baseline scenario (status quo) 2) Scenario A (Designations on Building Structure): Simulation with a block development 3) Scenario B (Designations on Building Structure): Simulation with a loose development / single building	ENVI-met V4.3.2 Summer18 (inklusive BIO-met)
Planned inner city area - Legally binding plan (Saalbau)	1) Baseline scenario (status quo) 2) Scenario A (Designations on Building Structure): City preferred development design	ENVI-met V4.3.2 Summer18 (inklusive BIO-met)

Table 8. Details on numerical simulations carried out in Bottrop presented in the following (source: own account).

3.1 Model Bottrop 1 – Road Trees – Existing Residential Area (Heideneck)

3.1.1 Description of the model

In the focus of the first microclimatic investigation in the area of the Bottrop city centre are the larger surroundings of the street Heideneck. The modelled area has a size of 426 x 296 m. The existing area is characterised by living close to the city centre in open construction with greenery. At the same time, the residential area is crossed by numerous streets, some of which are heavily trafficked and air-hygienically polluted. Parts of the south of the study area were part of the 2018 Wanderbaumparade.

The study area is characterised by mostly open construction and green housing estates, which usually cause rather weak heat islands, sufficient air exchange and mostly good bioclimates. They can also be described as climatic favourites in the city centre. In spite of the loose building structures, the building density causes heat islands with limited exchange conditions, partly unfavourable bioclimates and increased air pollution (especially with high traffic volumes). Wind discomfort in the area of street canyons and open spaces.

Figure 32: Model Bottrop 1 (Heideneck) – Location of the investigated area (source: own account, data: City of Bottrop).

In the baseline scenario, the building stock was modeled as a status quo (simplified modelling). In scenario A, additional road trees were modelled in addition to the existing trees (trees marked in red on the map). In order to reduce the heating of urban surfaces, it makes sense to plant street trees with climate-adapted tree species. It should be noted here that in street canyons with increased traffic, the ventilation situation can be restricted by a closed canopy so that air pollutants can no longer be easily removed. In such situations, trees with smaller canopies or with sufficient spacing or other vegetation measures should be avoided.

3.1.2 Methodological approach

The use of a microscale climate model is necessary to enable a comparison between the actual state and the plan variant/s. The model ENVI-met 4.3.0.0 is used for this purpose (Bruse, 2004; ENVI-met website: www.envi-met.com, ENVI-met GmbH 2017/18).

3.1.2.1 Description of the Software

ENVI-met is a three-dimensional prognostic numerical flow-energy balance model. The physical basics are based on the laws of fluid mechanics, thermodynamics and atmospheric physics. The model is used to simulate wind, temperature and humidity distribution in urban structures. It captures urban structures as an overall system and describes dynamic climatological processes.

This microscale model simulates the interactions between surfaces, plants and the atmosphere in an urban environment. Parameters such as building surfaces, soil sealing, soil properties, vegetation and solar radiation are included. Due to the interaction of sun and shade as well as the different physical properties of the materials (specific heat, reflection properties, ...) different surface temperatures develop in the course of a simulated day, which in turn release their heat more or less strongly into the air depending on the wind field. In order to simulate interactions between vegetation and the atmosphere, the physiological behaviour of plants is simulated. This includes opening and closing the stomata to control the exchange of water vapour with the environment, the absorption of water via the roots or the change in leaf temperature during the day (Website envi-met 1).

The possible spatial resolution of the model lies between 0.5 and 10 m depending on the size of the total area and is temporally accurate up to 1-5 sec. The model includes the simulation of the following parameters:

- Flow field (also around the building)

- Exchange processes for heat and moisture

- Air temperature and humidity distribution

- Turbulence

- Exchange processes with vegetation

- Bioclimatology

- Pollutant dispersion

In the context of the urban microclimate, thermal comfort is an essential indicator to describe the subjective experiences of people with outdoor temperature. Thermal comfort summarises the influence of sun, wind, air temperature and humidity on the perception of heat. Assessing the microclimate conditions of an urban space means finding out how pedestrians feel under certain climatic conditions - especially their thermal and wind comfort - and how this affects behaviour within the urban structure. In addition, appropriate thermal conditions can play a key role in the economic success of outdoor facilities such as cafes, shopping streets or recreation areas. Different thermodynamic models in ENVI-met allow a holistic evaluation of stationary and transient thermal comfort conditions (Website envi-met 1).

In order to characterise or determine the intensity of the urban climate and the urban heat island, climate elements such as air temperature, humidity or radiation properties of surfaces are usually used. However, it makes sense to limit the urban climate not only to atmospheric or surface properties but also to the resulting effects. Simple indices or combined variables that only take air temperature or humidity into account are rather unsuitable for this purpose. Methods that describe and quantify the effects of the human thermal environment in thermo-physiological terms are particularly suitable here. They are based on the energy balance of the human body and can be expressed using thermal indices (e.g. physiologically equivalent temperature, PET) (Matzarakis, 2013).

A bioclimate index makes sense since the heat load felt by humans or the weather-related load on the organism does not depend solely on the air temperature, but also on other influencing variables within the thermal effect complex. The most important influencing variables which influence the sensation in the thermal effect complex and which are used for the calculation of the

PET are, e.g. air temperature, humidity, wind speed and the mean radiation temperature. In addition, there is the physical activity of humans and the thermal resistance of clothing. The PET value used here is described according to the ENVI-met tool BioMet as: *"Physiological equivalent temperature. Based on the Gagge-2-node model, it relates skin and core temperature generated by the outdoor environment to the indoor air temperature resulting in the same temperatures"* (Biomet description of PET). BioMet input data (ENVI-met output data):

- Buildings

- Vegetation / trees

- Air temperature

- Mean radiant temperature

- Horizontal wind speed

- Specific humidity

The PET value is calculated in ENVI-met with the specially developed program Biomet for the output data sets of the simulations. The default setting in Biomet remains unchanged for this purpose and is designed for a slim 35-year-old man.

Age of person	35 y
Gender	Male
Weight	75 kg
Height	1.75 m
Surface area	1.91 m²
Static clothing insulation	0.90
Total metabolic rate	164.49 W

Table 9. Setup of personal human parameters for PET (source: own account).

Besides the climatic conditions, the air is one of the most important factors of the habitat for humans, animals and plants. Due to the interrelationships, it is obvious to consider the topics of urban climate and air hygiene together: *"The pollutant dispersion model of ENVI_MET allows the synchronous release, dispersion and deposition of up to six different pollutants including particles and passive and reactive gases. Sedimentation and deposition on surfaces and vegetation is taken into account as well as the photochemical reaction between NO, NO_2 and Ozone (O_3) [NO-NO_2 ozone chemistry] and the release of (B)VOC through plants."* (Website envi-met 1). The results can be used to better understand the dynamics of local pollutant dispersion and help to develop urban streetscapes and green infrastructure for improving air quality and human well-being.

Nitrogen oxides (NO_X) is the generic term for nitrogen monoxide (NO) and nitrogen dioxide (NO_2). Nitrogen oxides are formed almost exclusively during combustion processes in engines and large combustion plants. These combustion processes primarily produce nitrogen monoxide, which is quickly converted into harmful nitrogen dioxide in the atmosphere. In large cities, the concentration of NO as a primary, short-lived exhaust emission product is a 'traffic indicator'. The concentration of NO_2 as a secondary, comparatively stable and more harmful conversion product is rather a measure of the effects of traffic in the interaction of the underlying influencing variables. NO_2 is more harmful to health than NO and acts as an irritant gas on the mucous membranes of the respiratory tract. Acute health effects such as disorders of the lung functions can be observed in certain persons (bronchiatrists and asthmatics) above a certain stress level. In addition to volatile organic compounds, nitrogen oxides also play an important role as precursors for summer ozone formation.

The main cause is transport, followed by power stations, industry, households and small consumers. While nitrogen oxide emissions from power plants have been significantly reduced in recent years by the installation of denitrification systems, the share of road traffic - despite the catalytic converter - has fallen only slightly due to the unchanged increase in driving and transport volumes.

3.1.2.2 Input data and setup

The methodology for the mapping of all four model areas in the City of Bottrop was carried out in three steps:

1. the mapping of the building structures (shape and height),

2. the mapping of the streets and footpaths (flooring),

3. and the mapping of the green areas - mainly trees (shape and height).

The mapping was carried out on the basis of existing maps, aerial photographs and on-site inspections. In the next step, the recorded data of the three mappings were transferred to the ENVI-met program where they were used for virtual modelling of the actual state of the study area and as a basis for various greening and planning/building measures (scenarios).

One summer radiation day over 24 hours was simulated to achieve maximum warming in the model area. In addition to the building, vegetation and surface structure of the model area, meteorological parameters were determined for a micro-scale modelling of the actual state as well as the variants. These values correspond to the typical initial conditions of a summer radiation weather situation with the heat load. The initial values of the meteorological parameters are chosen the same for all variants. Summer radiation days are usually weak wind weather conditions. The exit wind speed at the height of 10 metres should, therefore, be less than 1.5 m/s. The wind speed at the end of the day should, therefore, be less than 1.5 m/s.

All results determined with ENVI-met are representative for the daily situation with the values for 4 p.m. CET and a height of 1.5 meters.

Start date	21/06/2018
Start time	20:00
Total simulation time	24 h
Output interval for files	60 min

Table 10 Start and duration of the model run in Bottrop (source: own account)

Wind speed at 10 m height	2 m/s
Wind direction	60° (from NE)
Roughness length	0.01
Specific humidity at the model top (2500 m)	5 g/kg
Simple Forcing of temperature and humidity is activated	
MIN – Temperature	14°C at 6:00

MAX – Temperature	28°C at 16:00
MIN – Relative humidity	50% at 16:00
MAX – Relative humidity	70% at 6:00
Solar radiation	No modification of calculated radiation
Clouds	No clouds in the model run
Turbulence model	Standard TKE Model (Mellor & Yamada 1982)

Table 11 Meteorology settings for the Bottrop models (source: own account)

Initial conditions for soil – soil wetness (%) / initial temperature (K)	
Upper layer (0-20 cm)	40% / 300 K
Middle layer (20-50 cm)	45% / 298 K
Deep layer (50-200 cm)	50% / 297 K

Table 12: Soil data conditions for the Bottrop models.
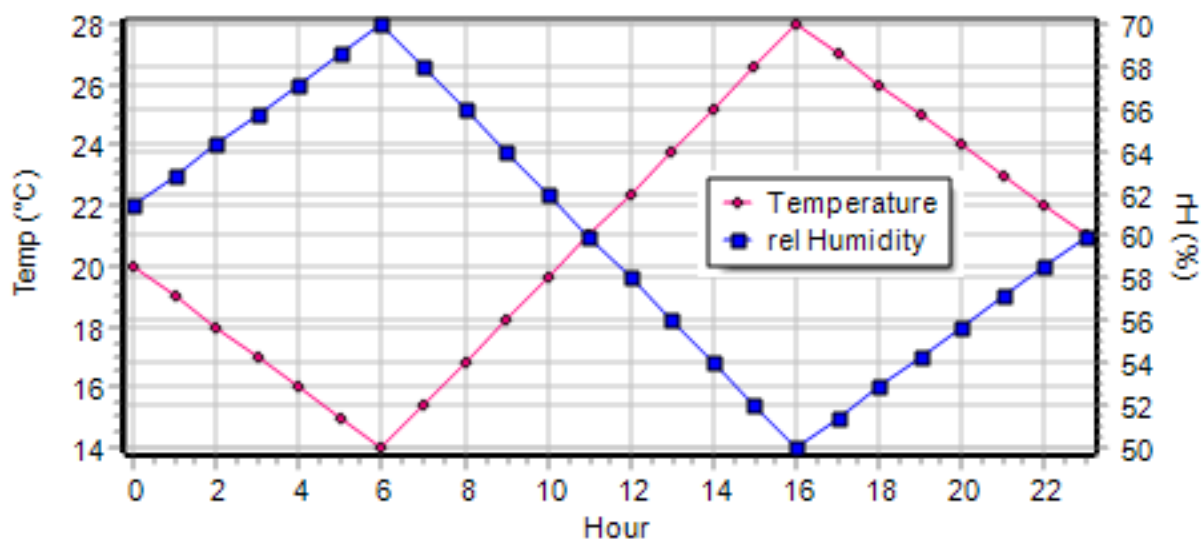
Figure 33: Specification of the hourly course of temperature and relative humidity (simple forcing) (source: own account according to the ENVI-met software setup)
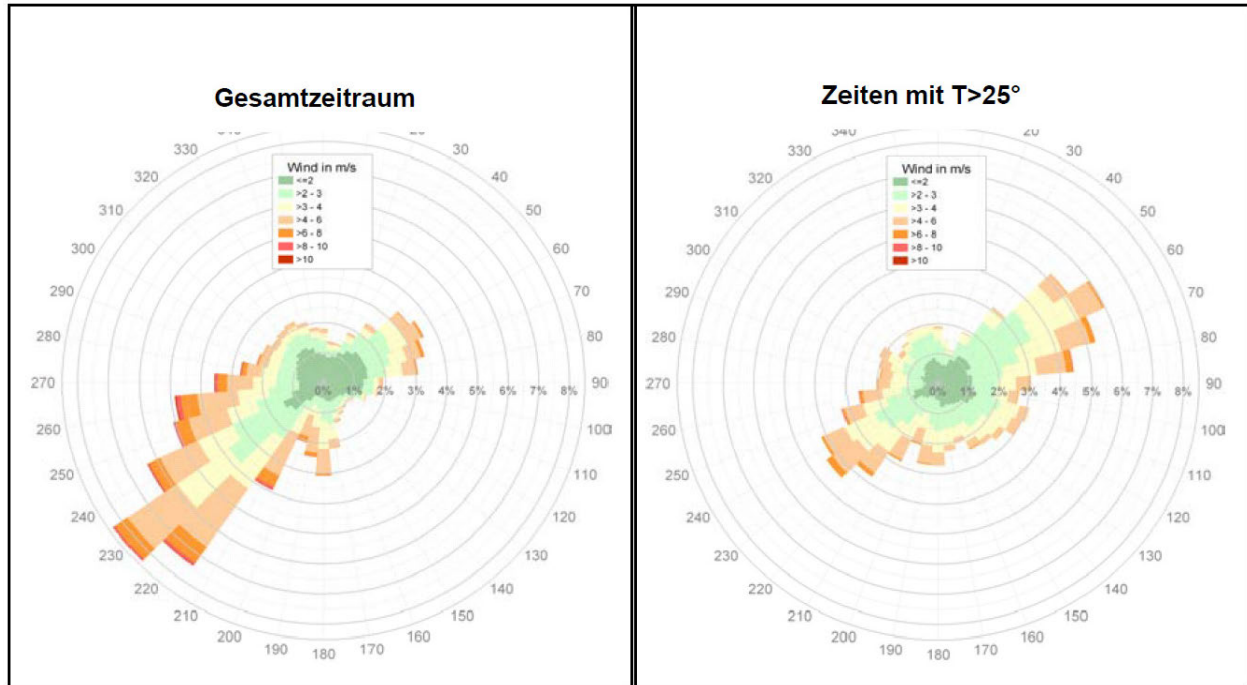
Figure 34: Wind direction distribution at the Bottrop-Welheim station from 1986 to 2005 (source: Stadt Bottrop, 2014)

Figure 34 compares graphical analyses of the wind direction distribution for two scenarios. For the left wind rose, all data of the investigation period were evaluated, while the right wind rose only contains the cases where the air temperature is above 25°C.

3.1.2.3 Model validation and verification

The areas of the models were selected in coordination with the Environmental Office of the City of Bottrop. The aim was to select a broad range of different types of land-use (residential area, industrial area and a dense inner city area). The selection of the modeled scenarios and the methodological approach were also developed and coordinated in cooperation with the Environmental Office of the City of Bottrop. For input data, official data of the City of Bottrop were used; meteorological input data are based on local weather data.

The selection of the areas, the development of the scenarios and the methodological approach (e.g. the ENVI-met setup) were discussed and agreed with representatives of the City of Bottrop and other stakeholders at a stakeholder workshop in October 2018.

For model validation, the modelled results for heat stress were compared with the corresponding values of existing ENVI-met simulations within the framework of the Climate Adaptation Concept Bottrop and measured values of local weather stations (Stadt Bottrop, 2014).

3.1.3 Modelled results and discussion

The evaluation and analysis of the results of all four model calculations were carried out with the Leonardo program, which is available for visualizing the results of ENVI-met model runs. So it was possible to create maps in various vertical and horizontal sections as results and difference maps, each of which displays the desired parameters (here air temperatures and PET values). In the following, the microclimatic situation of the actual state is presented by describing air temperature. For the analysis of the bioclimatic situation the PET values are discussed here. The shown day situation is described as representative with the values for 4 p.m. CET at the height of 1.5 meters.
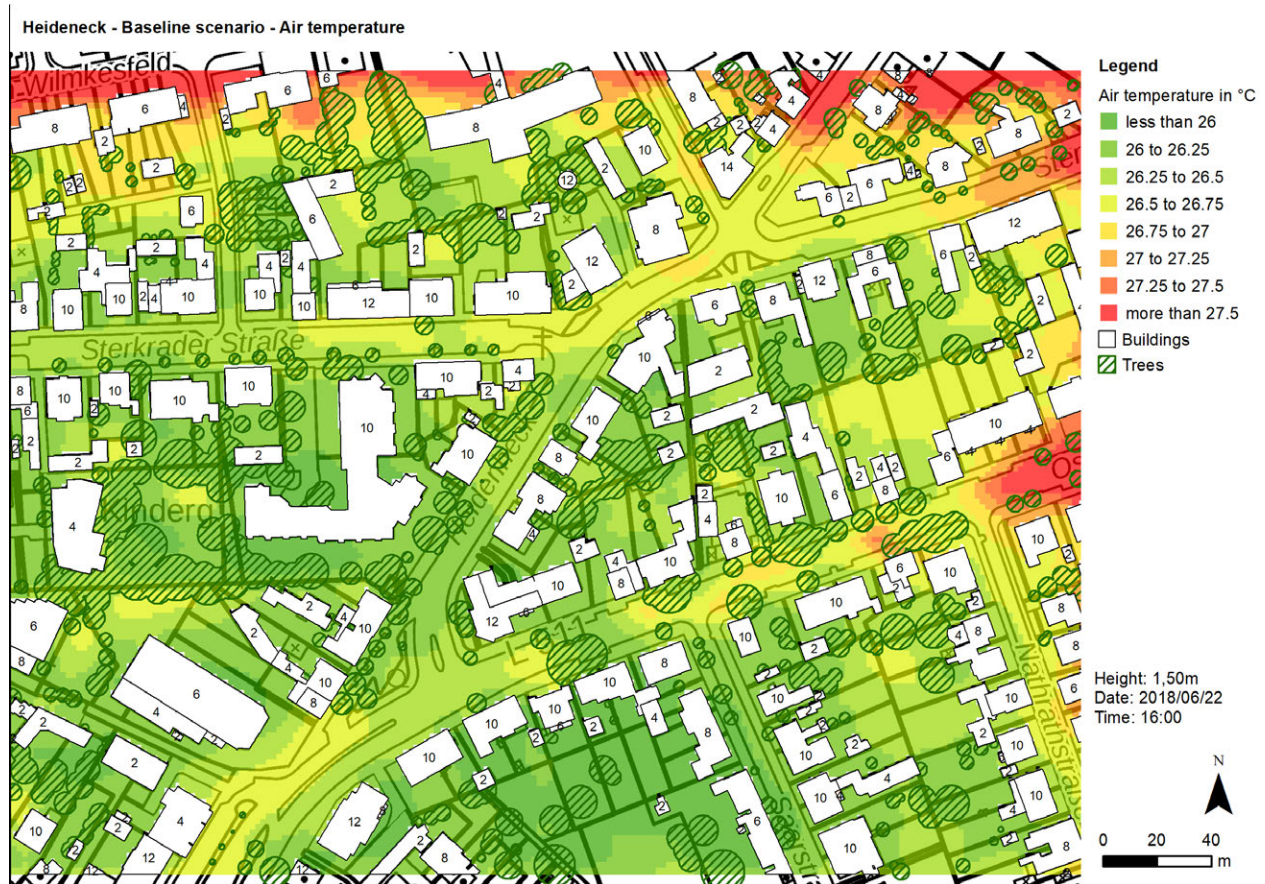
Figure 35: Model Bottrop 1 (Heideneck): Baseline scenario - ENVI-met calculated air temperature (source: own account, data: City of Bottrop).

The high temperatures at the northern and eastern edge of the model area are not to be considered since the ENVI-met program only provides valid results in the core model. The highest air temperatures in the baseline scenario with over 27.5°C (Figure 35, red) occur over the asphalt surface of the Osterfelder Straße. The areas sealed here and the inadequate shading lead to a warming of the air. In the areas with open residential buildings and green inner courtyards, the lowest air temperatures occur with values between less than 26.0 and up to 26.5 °C. The lowest air temperatures are found in the areas with open residential buildings and green inner courtyards. In the area between Sterkrader Straße and Heideneck, building shading can also reduce to a small extent the heating of the sealed surface in the street space and thus the increase in air temperature.

Figure 36: Model Bottrop 1 (Heideneck): Baseline scenario - ENVI-met calculated PET values (source: own account, data: City of Bottrop).

With an additional focus on the residential areas, the quality of stay is examined on the basis of the bioclimatic conditions for the daytime situation at 4 p.m. CET. The PET values for the actual situation in the study area (Figure 36) show that in particular the sealed traffic areas and the buildings lead to a very high bioclimatic load with PET values of more than 48 °C. According to the PET scale, these areas shown in red in Figure 36 represent a considerable heat load. In particular, the green inner courtyards of residential buildings show reduced PET values and the effect of trees. In the area of the shadows cast by the buildings, the PET values are in some cases much lower than for the unshaded areas. In these shaded areas, a somewhat lower thermal load is felt.

The bioclimatic situation is significantly lower in spots with vegetation than in areas without vegetation. The reduction of the PET values remains locally limited but can improve the quality of the stay in the areas without other shading by buildings. The greened inner courtyards and the already existing roadside greenery thus represent an important contribution to the small-scale improvement of the micro-climatic situation.

Figure 37: Model Bottrop 1 (Heideneck): Scenario A – Difference of air temperature, scenario A minus baseline scenario (source: own account, data: City of Bottrop).

The change of the air temperatures in scenario A (with additional road trees) in direct comparison to the actual situation shows a clear cooling in the area of the Sterkrader Straße by up to 0.3°C (Figure 37). The range of the cooling by 0.1 to 0.2°C in the vicinity covers both the streets Heideneck and Osterfelder Straße as well as the garden/inner courtyard areas of the buildings. In these areas, the additional vegetation locally improves the microclimate. In some areas, however, the air temperature may rise by up to 0.2°C. This can be attributed to the deteriorated ventilation of individual street sections by additional trees. This affects the Sterkrader Straße/Am Lamperfeld intersection in the north, the forecourt of the supermarket on Osterfelder Straße/Heideneck in the south and Saarstraße on the eastern edge, where additional trees have a negative effect on ventilation and thus increase the air temperature.

Figure 38: Model Bottrop 1 (Heideneck): Scenario A – Difference of PET values, scenario A minus baseline scenario (source: own account, data: City of Bottrop).

The described changes in air temperature from the baseline scenario to scenario A of the model are also reflected in the bioclimatic situation (Figure 38). The PET values are up to 12°C lower in the area of additional shading by road trees than in the actual situation. However, these considerable improvements are only achieved in the immediate vicinity of the additional vegetation by shading. In some areas, additional roadside greenery leads to a reduction in wind speeds and thus to a deterioration of PET values. Due to the new trees, the positive effects of their shadowing and the negative effects act as a flow obstacle and locally limited areas with no relevant effect are created. The red areas with a slight increase in the PET values by a maximum of 3 °C indicate a trend towards a reduction of the quality of stay. However, this is far too low to have a strong effect on humans. In addition, the improvement in the quality of stay prevails in the areas of the sidewalks.
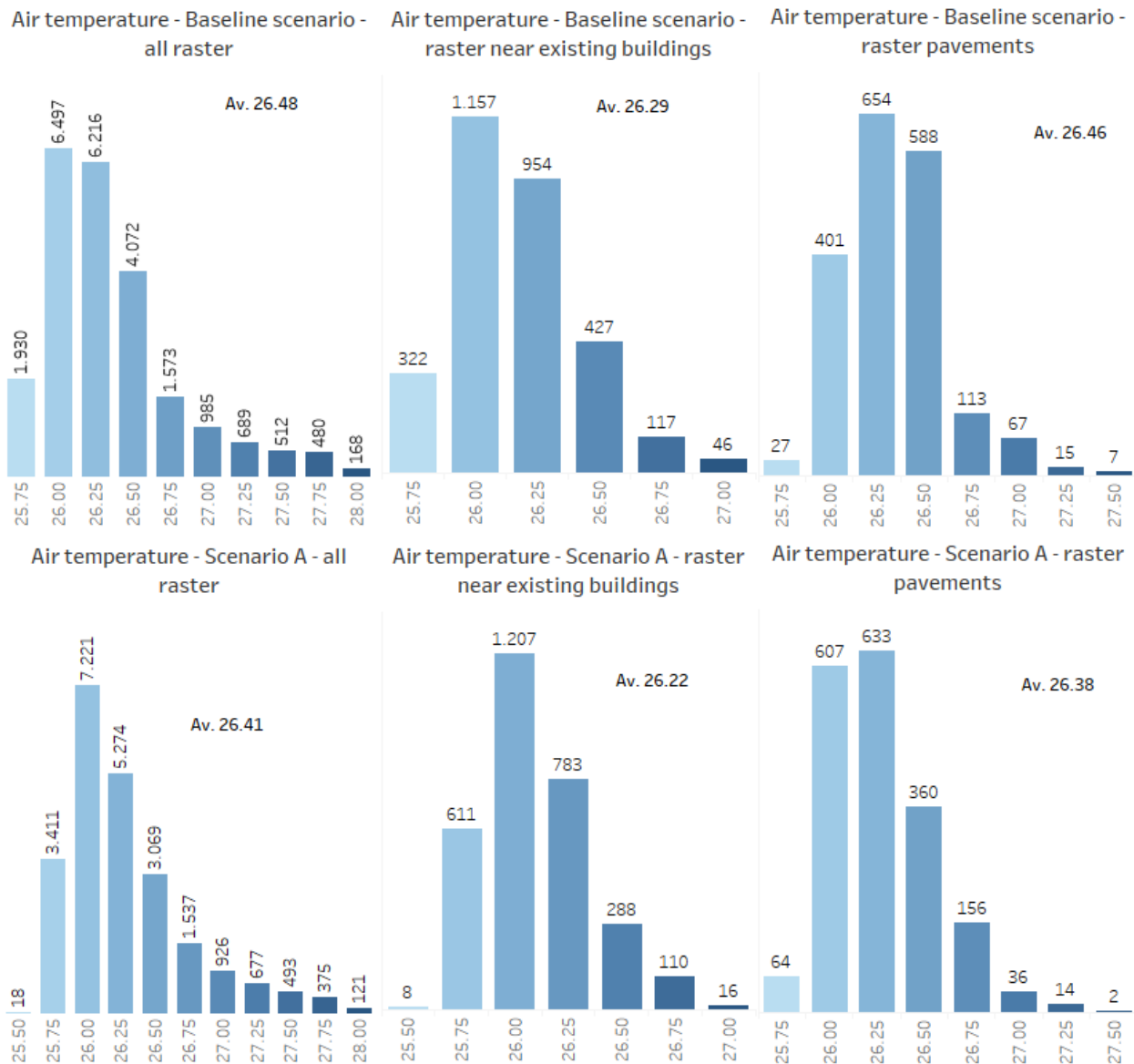
Figure 39: Analysis of changes in air temperature in single grid cells (Heideneck) (source: own account)

The microclimatic overall situation in the study area is characterised by the open building structures with gardens and inner courtyards as well as the sealed traffic areas. In areas with strong greening, shading and ventilation are somewhat better, which means that the heat load is slightly less pronounced. Small-scale shading by buildings or large trees shows a very locally limited somewhat higher quality of stay. In the areas of traffic areas exposed to radiation, comparatively stronger warming of the sealed surfaces is achieved.

For scenario A with additional street trees, the microclimatic changes remain locally limited. In the scenario, ventilation in areas of unshaded road junctions is reduced if these are surrounded by additional trees. From the point of view of urban climate, scenario A with additional vegetation

makes sense. The overall impact of the changed climate function of the planned area can be classified as very low. For the extensive gardens, inner courtyards and parking areas, further partial desertification or additional vegetation is recommended. When redesigning surfaces (including buildings), the lightest possible materials should be used, as these heat up much less.

The most extensive microclimatic changes can be seen in sidewalk areas. The additional shading by road trees outweighs any changes in ventilation due to flow obstacles. Nevertheless, when using and selecting street trees to improve the urban climate, the benefits of additional shading should be weighed against any changes in the ventilation situation. The greening and design of private courtyard and house areas can contribute to a significant and sustainable improvement and upgrading of the housing situation. In addition, synergies can be exploited, as the supported measures also contribute to climate adaptation. In particular, the planting of inner courtyards, spacing areas and front gardens, roof and façade greening, as well as light or white building paints and façade insulation in the course of restoration, also contribute to improving the urban climate and indoor climate.

3.2 Model Bottrop 2 – Road Trees and Roof Greening – Existing Industrial Area (Brakerstraße)

3.2.1 Description of the model

The second research area for the city of Bottrop is located around Brakerstraße in an industrial and commercial area close to the city centre (Figure 40). The modelled area has a size of 256 x 296 m. The area has a high degree of sealing, which is influenced in particular by asphalted areas/company premises, roof areas and traffic areas. The area has a low proportion of greening.
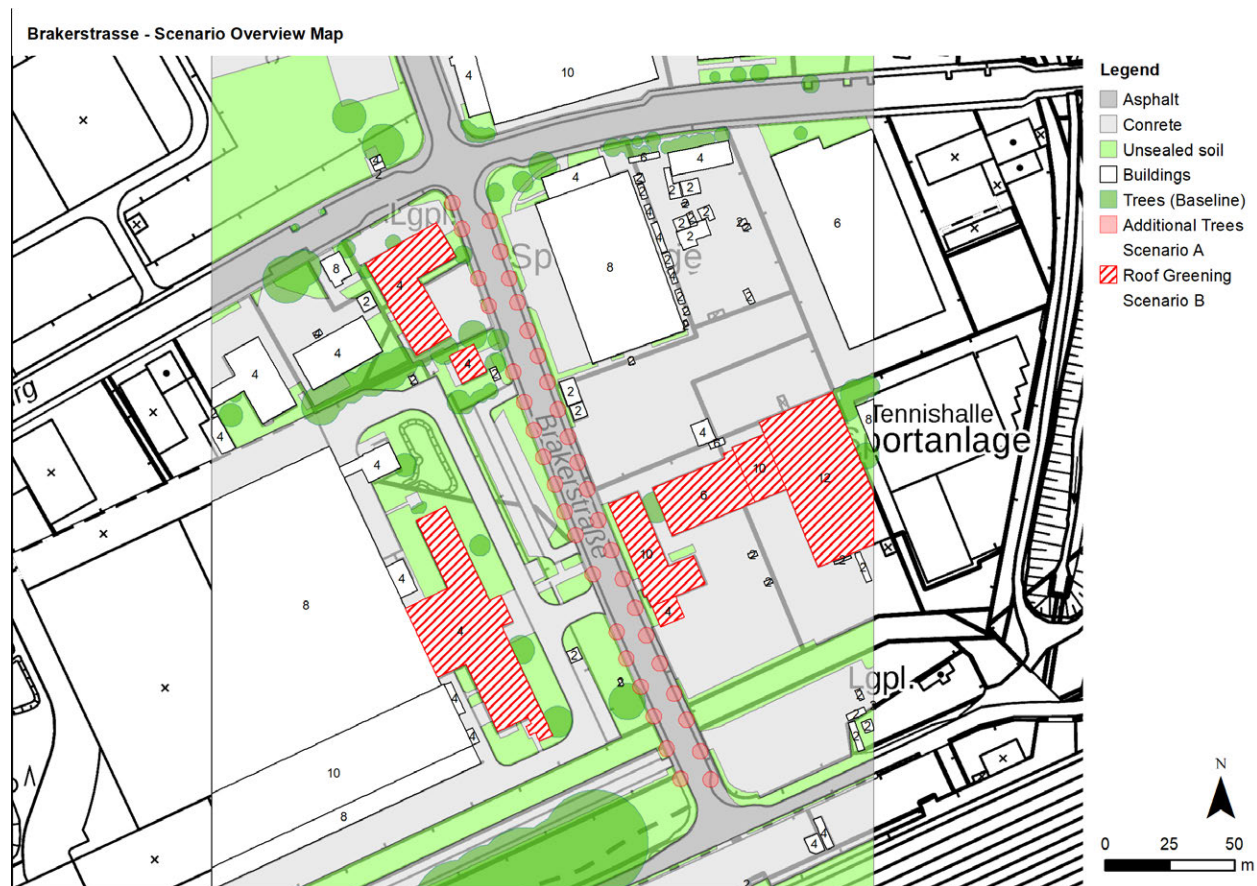
Figure 40: Model Bottrop 2 (Brakerstraße) – Location of the investigated area (source: own account, data: City of Bottrop).

The vulnerability of industrial and commercial enterprises to extreme weather conditions such as heat is comparatively high. Due to their spatial location, structural and operational characteristics and the density of asset values, they may be more vulnerable than other urban areas. The climate in commercial and industrial areas is characterised by a high degree of sealing and thus strong summer heating (heat stress). In addition, there are emissions of noise and pollutants as well as waste heat pollution. Many industrial and commercial enterprises are located in endangered

areas, also for historical reasons, and are located in watercourses or in densely populated inner-city areas. In addition, the heat load of the industrial and commercial areas in Bottrop is sometimes very high. Rising temperatures, especially in the summer months, can lead to a reduction in the efficiency of the working population, which triggers additional cooling requirements. Summer heat in the workplace, both indoors and outdoors, can cause workers to suffer from fatigue, poor concentration and cardiovascular stress. This can lead to a decrease in motivation and performance.

The existing status quo was modelled in the baseline scenario. In scenario A, additional road trees were modelled in addition to the existing trees (trees marked in red on the map). The modelling of scenario B also takes into account roof greening. Roof, facade and courtyard greening can be enhanced by cooling effects and increased air humidity. Urban greenery thus assumes numerous climate-relevant functions and improves the urban climate. Thus it counteracts health burdens, produces oxygen, binds dust and filters air pollutants. In addition, open and unsealed areas protect buildings from climatic effects by retaining rainwater, seep it away and release it again through evaporation.

3.2.2 Methodological approach

The methodological approach, the software used, the data and the setup have already been described in section 3.1.2 and are identical for all models for the city of Bottrop.

3.2.3 Modelled results and discussion

In the following, the microclimatic situation of the actual state is presented by describing air temperature. For the analysis of the bioclimatic situation the PET values are discussed here. The shown day situation is described as representative with the values for 4 p.m. CET at the height of 1.5 meters.
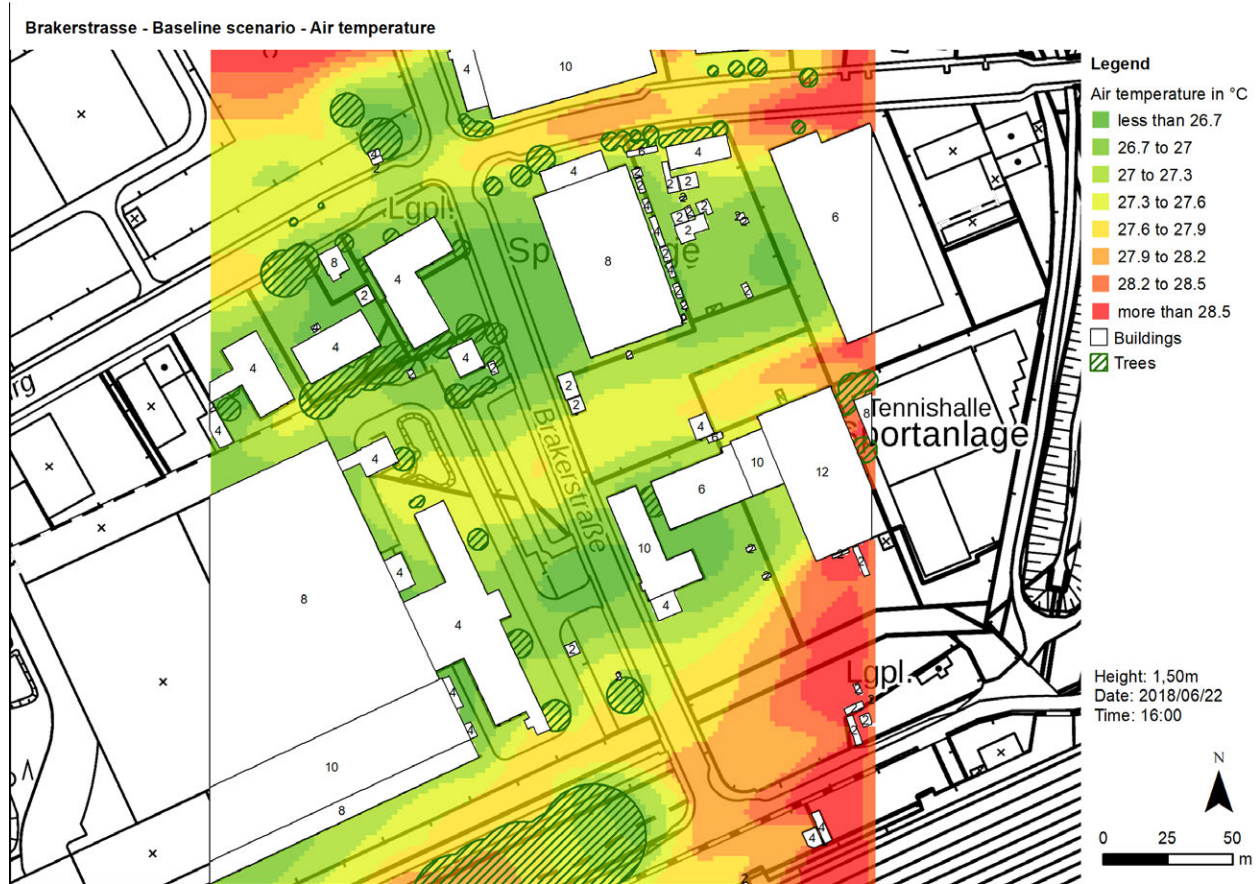
Figure 41: Model Bottrop 2 (Brakerstraße): Baseline scenario - ENVI-met calculated air temperature (source: own account, data: City of Bottrop).

The highest air temperatures in the baseline scenario with over 28.5°C (Figure 41, red) occur over the asphalt surface of the street An der Knippenburg and in particular over sealed areas, such as the storage area at the bottom right and the junkyard in the middle right. In the areas with open residential buildings and green inner courtyards, the lowest air temperatures occur with values up to less than 26.7°C. The lowest air temperatures are found in the areas with small buildings and vegetation.

Figure 42: Model Bottrop 2 (Brakerstraße): Baseline scenario - ENVI-met calculated PET values (source: own account, data: City of Bottrop).

The PET values for the baseline scenario in the study area (Figure 42) show that in particular the sealed traffic areas and the buildings lead to a very high bioclimatic load with PET values of more than 48°C. According to the PET scale, these areas shown in red in Figure 42 represent a considerable heat load. The effects of sealed plots and large buildings, which heat up during the day, are clearly visible. Cooling effects from existing trees are very local and mainly due to shading. The effects of sealed plots and large buildings, which heat up during the day, are clearly visible. It also shows that the effects of the heat emitted by the building outweigh any effects of the shadows cast by the buildings. Cooling effects from existing trees are also very local and mainly due to shading.

Figure 43: Model Bottrop 2 (Brakerstraße): Scenario A – Difference of air temperature, scenario A minus baseline scenario (source: own account, data: City of Bottrop).

The change of the air temperatures in scenario A (with additional road trees) in direct comparison to the actual situation shows different effects in the area of the Brakerstraße by up to 0.2°C (Figure 43). The change of the air temperatures in scenario A (with additional road trees) in direct comparison to the actual situation shows a clear heating in the area of Brakerstraße. These effects can be explained by the additional road trees and thus flow obstacles that restrict the exchange of air and thus promote heating of the air. In contrast, there are only minor positive cooling effects due to the additional vegetation.

Figure 44: Model Bottrop 2 (Brakerstraße): Scenario A – Difference of PET values, scenario A minus baseline scenario (source: own account, data: City of Bottrop).

The described changes in air temperature from the baseline scenario to scenario A of the model are also reflected in the bioclimatic situation (Figure 44). On the one hand, the PET values are up to 3°C higher in the area of additional road trees, which hinder the exchange of air. On the other hand, the additional street trees have local effects that lead to cooling by up to 12°C compared to the baseline scenario by casting shadows. Due to the new trees, the positive effects of their shadowing, but also the negative effects, act as a flow obstacle and locally limited areas with no relevant effect are created. This can have a positive effect on the quality of stay along the sidewalks and make outdoor activities more pleasant.
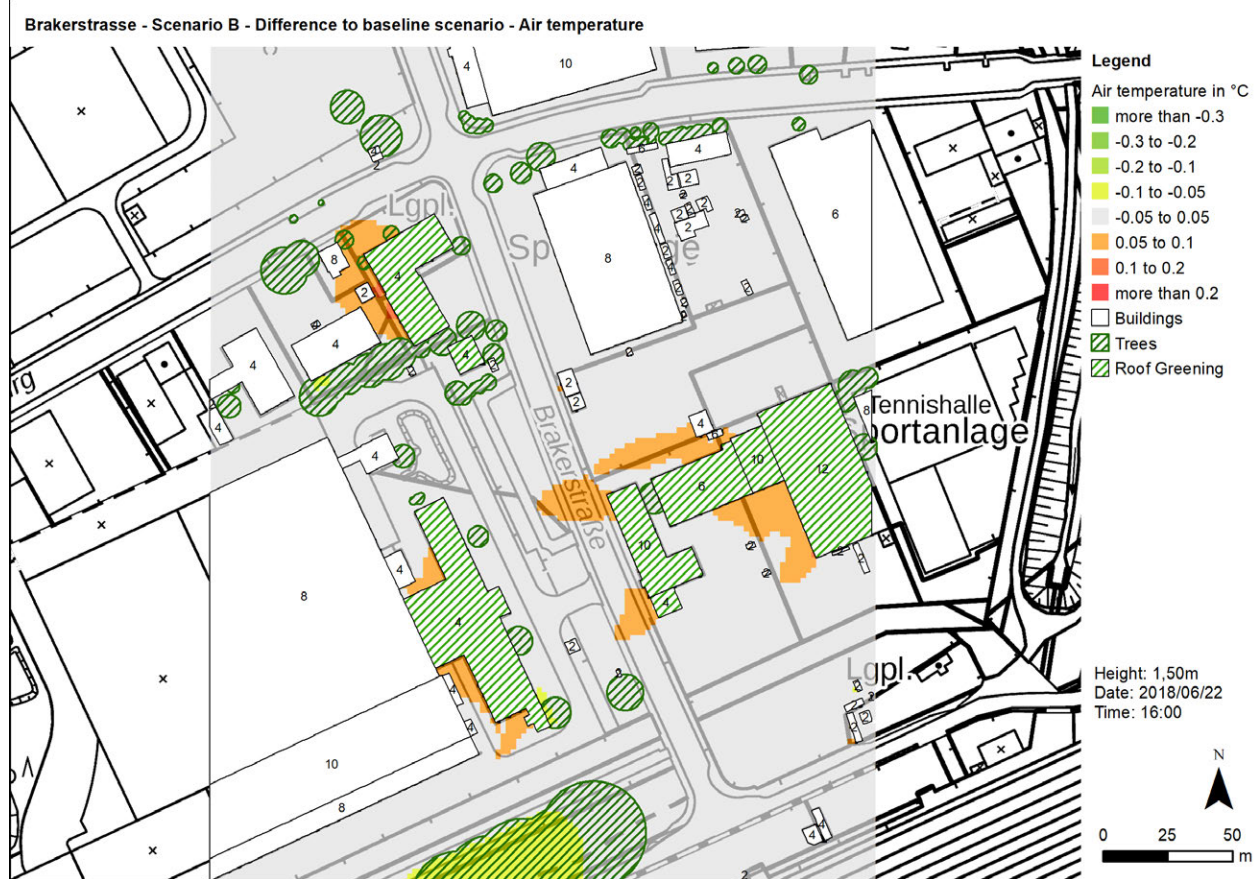
Figure 45: Model Bottrop 2 (Brakerstraße): Scenario B – Difference of air temperature, scenario B minus baseline scenario (source: own account, data: City of Bottrop).

For scenario B with additional roof greening of the buildings, an intensive greening with up to 50 cm high grass was modelled. It should be noted that the measurement height was limited to 1.5 m due to the direct effective height for humans (at a maximum height of 2 m). Therefore, the compensating effects achieved for the surroundings are relatively low, whereas green roofs can have considerable positive effects on the indoor climate of buildings. The increase in air temperature by up to 0.05°C (Figure 45, orange) can, therefore, be neglected when interpreting the results. These changes can also be explained by a change in the roughness of the roof surfaces and thus changes in the flow conditions.
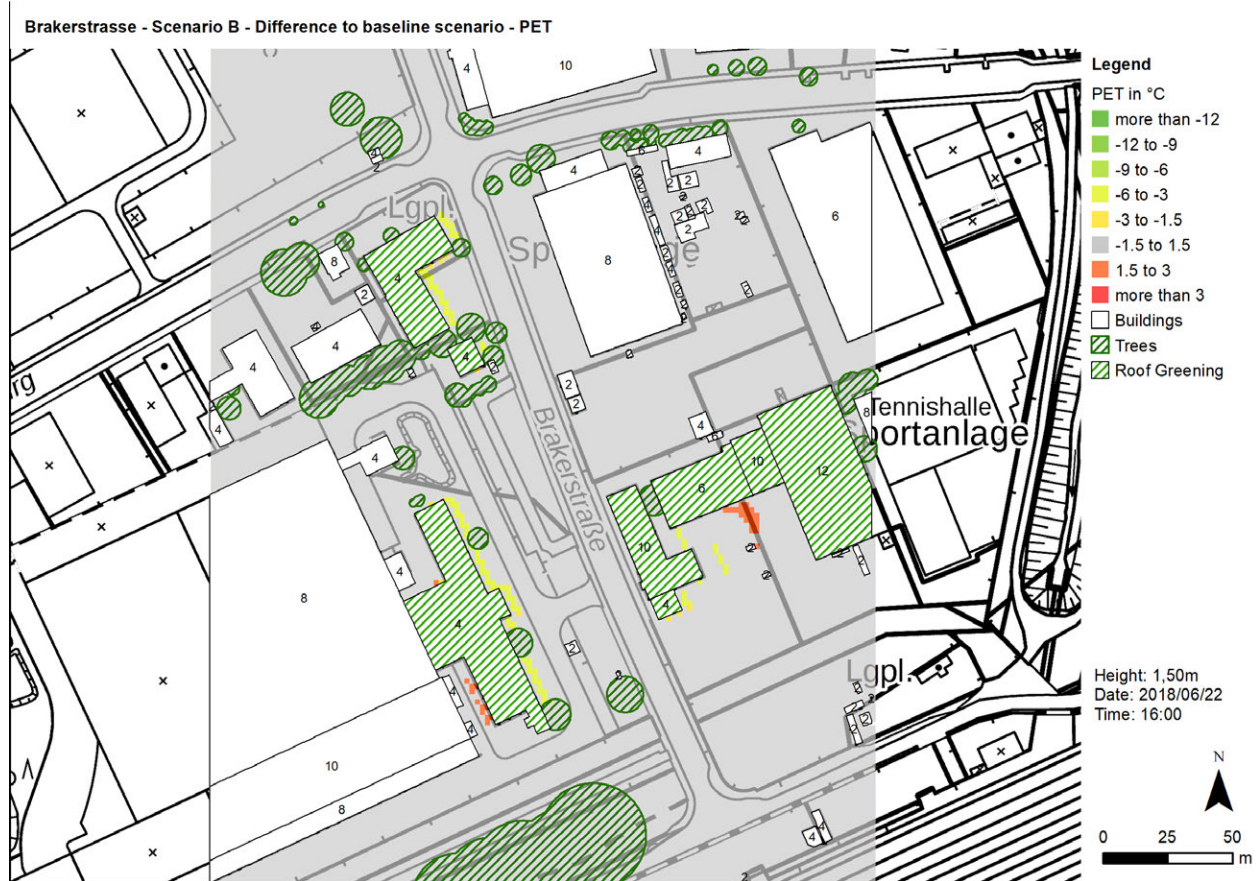
Figure 46: Model Bottrop 2 (Brakerstraße): Scenario B – Difference of PET values, scenario B minus baseline scenario (source: own account, data: City of Bottrop).

When considering the difference in PET values, the bioclimatic situation in the model area was slightly improved in scenario B. The PET values in the immediate surroundings of the greened buildings decreased by 1.5 to 3°C (Figure 46, yellow). Here, however, the importance of building shading in combination with relatively high wind speeds, which lead to a better bioclimatic situation, must also be taken into account. In scenario A, on the other hand, the PET value was reduced in some areas due to the reduction of wind speed.
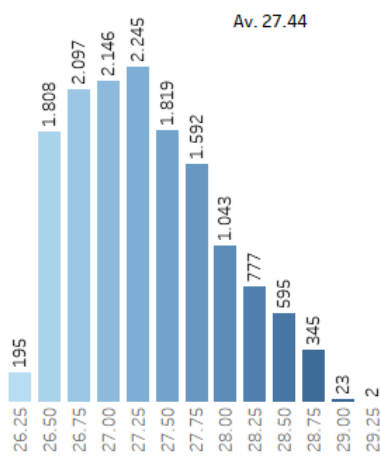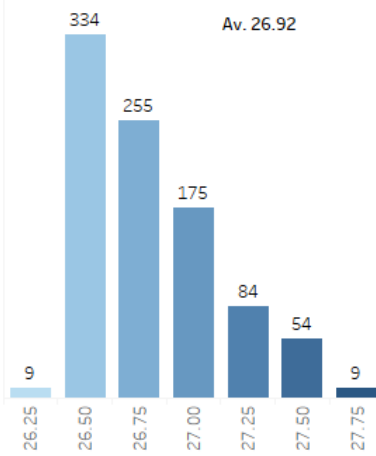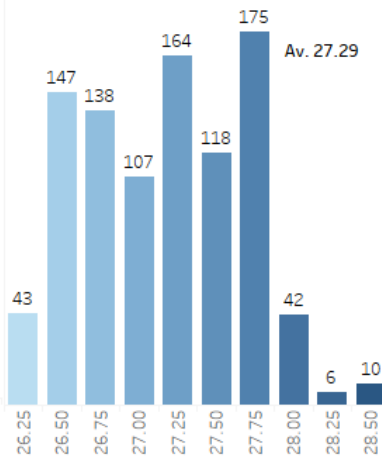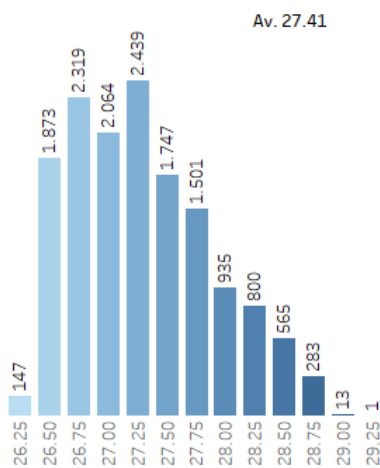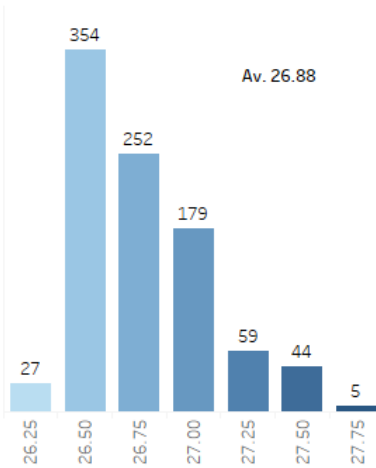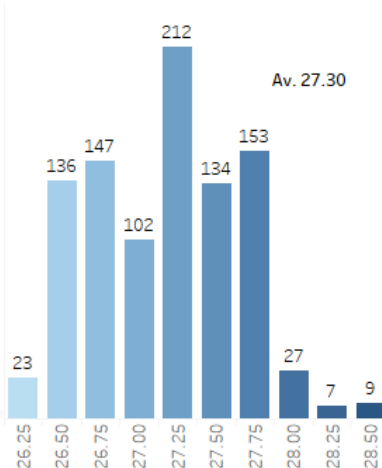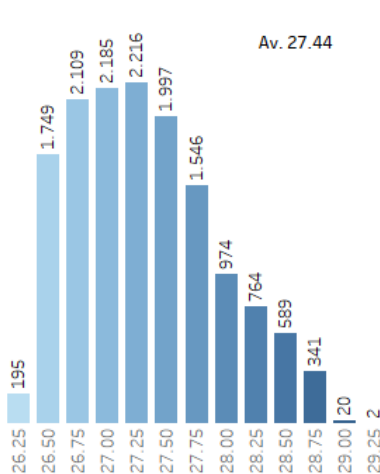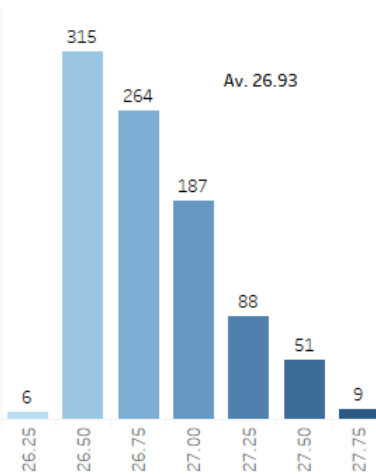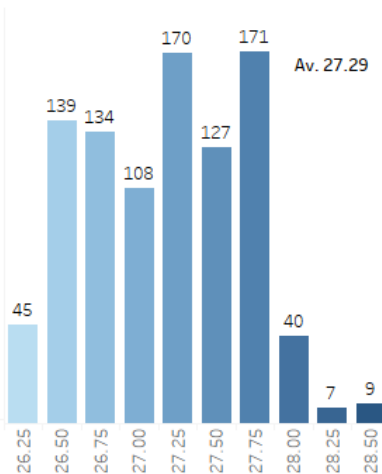
Figure 47: Analysis of changes in air temperature in single grid cells (Brakerstraße) (source: own account)

The study area Brakerstraße is in a microclimatic unfavourable initial situation due to the high degree of sealing in the actual situation. The bioclimatic situation of many areas with PET values of up to 48°C can be classified as a burden and is perceived as very hot by humans. From the findings of the investigation, the use of street trees in areas which are still unshaded in the actual situation and where trees have only minor effects as a flow obstacle results in the use of street trees. As road trees, species with a deciduous trunk should be used in order to keep the flow resistance as low as possible.

The extensive roof greening for buildings up to 4 m height has a minor effect on the air temperatures at 1.5 m height. In combination with roof greening, the air temperatures for the entire investigation area can be reduced slightly. By combining adaptation measures, a slight improvement for parts of the model area could be achieved in the scenarios. Despite the use of the adaptation measures described here, the microclimatic situation for the model area Brakerstraße remains almost unchanged. For future adaptation and construction measures, further microclimatic investigations such as measuring and modelling should be recommended.

3.3 Model Bottrop 3 – Building Structure – Planned residential area (Am Lamperfeld)

3.3.1 Description of the model

The third model area for the city of Bottrop is an area in an existing mixed area close to the city centre (residential, commercial, sports). The modelled partial area is the area between the stadium and the street Am Lamperfeld, which is currently being redeveloped (residential use). The modelled area has a size of 380 x 352 m. The model area is currently still undeveloped and characterized by quite dense vegetation and the immediate proximity to the Jahnstadion (stadium), with sports grounds and northern and southern parking lots.
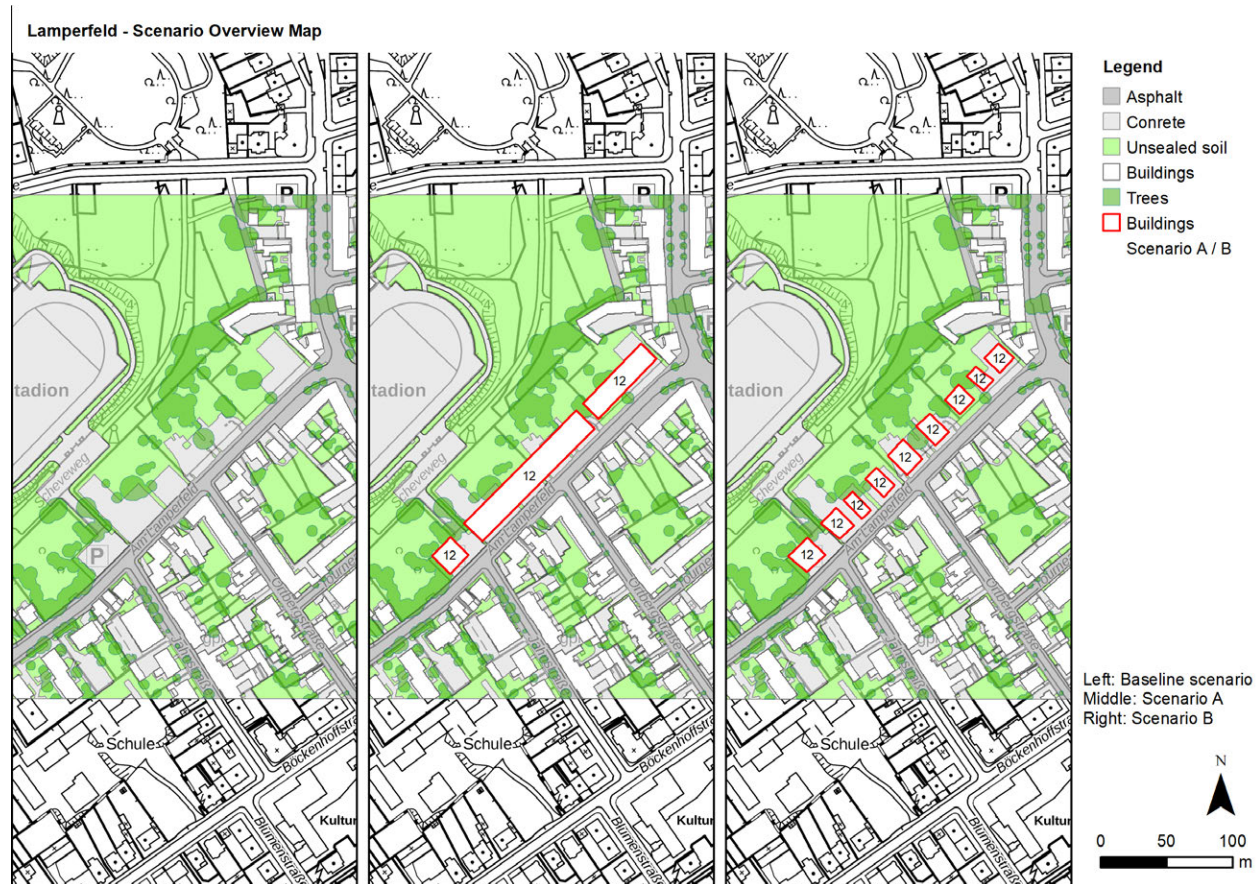
Figure 48: Model Bottrop 3 (Am Lamperfeld) – Location of the investigated area (source: own account, data: City of Bottrop).

The basic scenario shows the status quo. In scenario A, the implementation of a row development with a height of 12 m is modelled. In scenario B, loose buildings with 9 town houses are modelled with the building height remaining unchanged. The model results should, in particular, provide information about the shading and ventilation situation as well as any local climatic changes caused by the planning. With the aim of improving the quality of stay for the residents and

minimising changes to the local climate, recommendations for action can be derived for construction measures and measures to improve the microclimatic situation.

3.3.2 Methodological approach

The methodological approach, the software used, the data and the setup have already been described in section 3.1.2 and are identical for all models for the city of Bottrop.

3.3.3 Modelled results and discussion
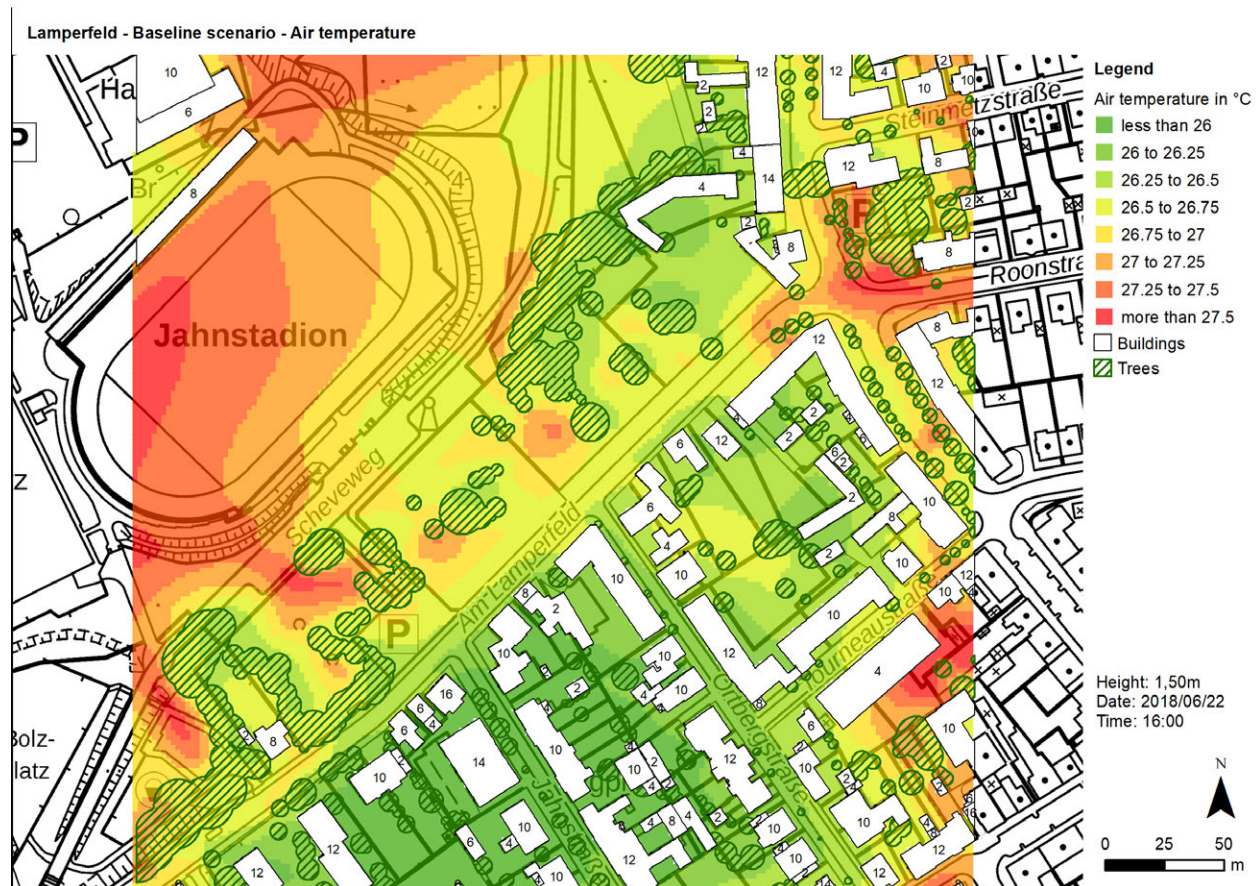
Figure 49: Model Bottrop 3 (Am Lamperfeld): Baseline scenario - ENVI-met calculated air temperature (source: own account, data: City of Bottrop).

The highest air temperatures in the baseline scenario with over 27.5°C (Figure 49, red) occur over the open area of the Stadium and the unshaded street intersection Am Lamperfeld and Kirchhellener Straße in the north-east. In the areas with open residential buildings and green inner courtyards, the lowest air temperatures occur with values between less than 26.0°C.
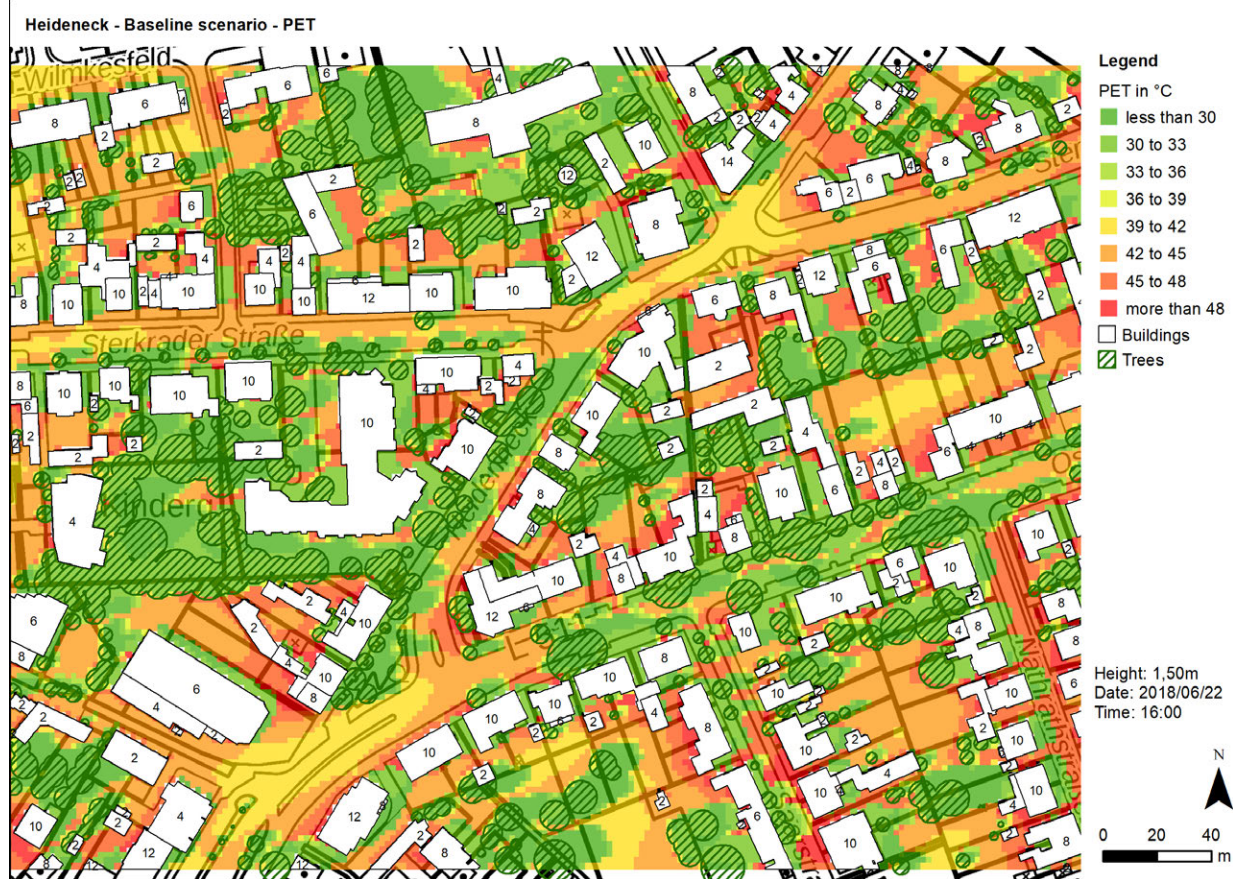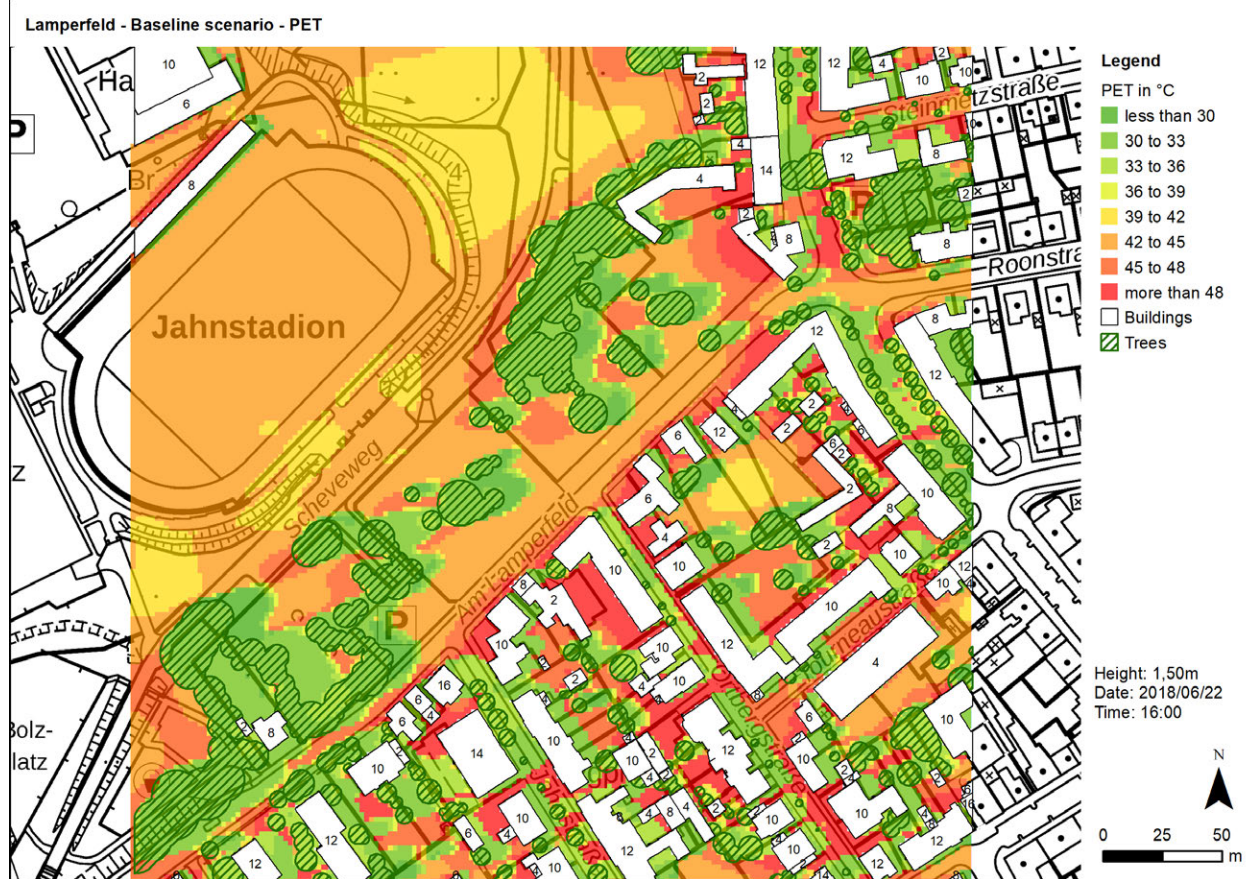
Figure 50: Model Bottrop 3 (Am Lamperfeld): Baseline scenario - ENVI-met calculated PET values (source: own account, data: City of Bottrop).

The PET values for the actual situation in the investigation area are shown in Figure 50. The high proportion of open, sealed or unplanted areas and the dense development in the southeast lead to a high bioclimatic load on parts of these areas. This also applies to a large extent to areas of the inner courtyards where PET values of up to 48°C can be achieved despite greening (Figure 50, red).

The moderate bioclimatic situation within the buildings is also due to the building density and thus moderate ventilation of the residential area. Areas of the shadow cast by buildings and greened inner courtyards of the buildings show slightly reduced PET values between 39 and 33°C in some parts. In areas where buildings cast shadows, the PET values are much lower than in unshaded areas. In these shaded areas, a somewhat lower thermal load is felt.

PET values tend to be somewhat lower in street areas and partly also on the stadium surface, but remain at a very high load level. The bioclimatic situation is significantly lower in areas with vegetation than in areas without vegetation. The reduction of the PET values remains locally limited, but can improve the quality of stay in areas without other shading by buildings. The greened inner courtyards, as well as the already existing roadside greenery, thus represent an important contribution to the small-scale improvement of the microclimatic situation.
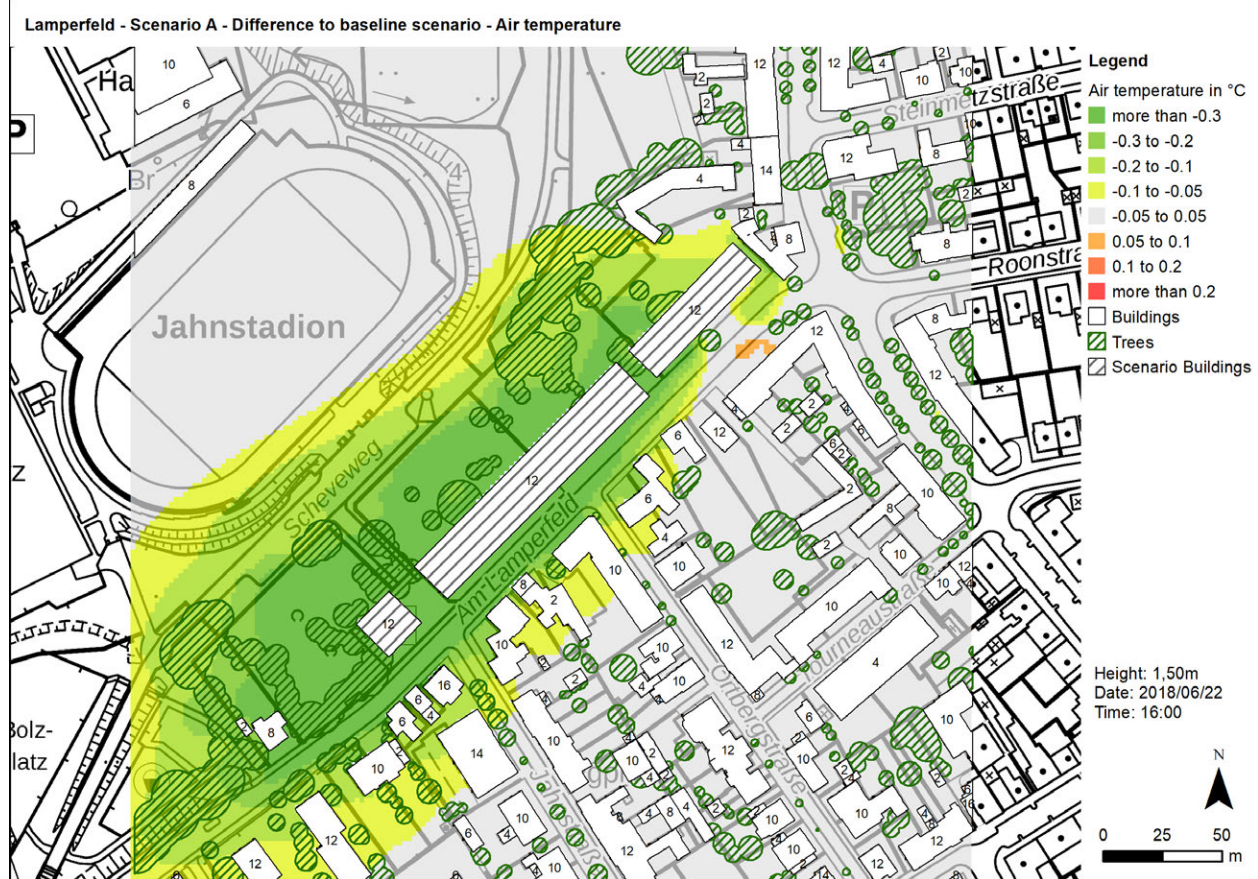
Figure 51: Model Bottrop 3 (Am Lamperfeld): Scenario A – Difference of air temperature, scenario A minus baseline scenario (source: own account, data: City of Bottrop).

The changes in the air temperature in scenario A show the cooling effects of up to 0.3°C (Figure 51, green). In the model, this circumstance is due to changes caused by shading and changes in the wind field as a result of the new row development. The shading reduces the heating of the soil surface. In addition, a street canyon is formed at the street Am Lamperfeld, which increases wind speeds and can positively influence the ventilation of the study area.
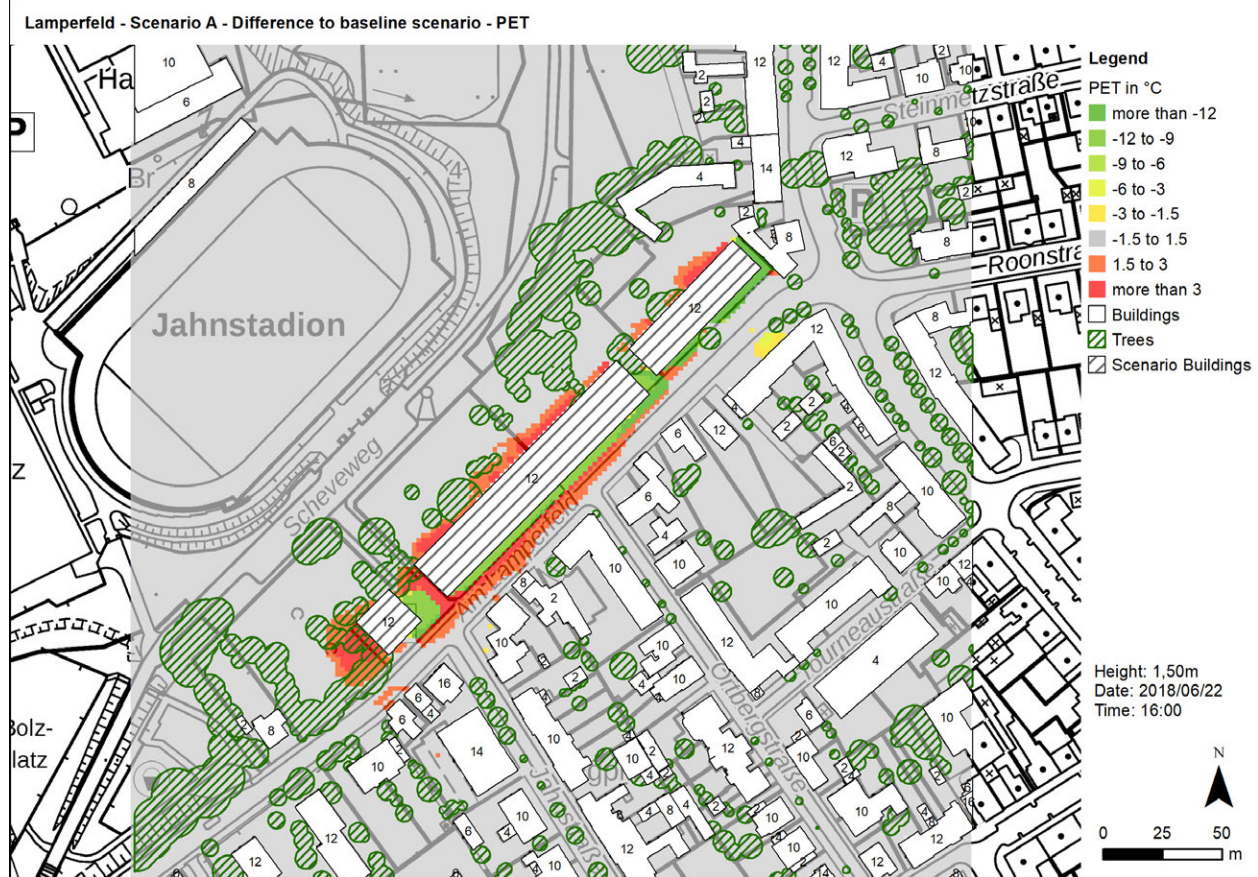
Figure 52: Model Bottrop 3 (Am Lamperfeld): Scenario A – Difference of PET values, scenario A minus baseline scenario (source: own account, data: City of Bottrop).

For the representation of the biometeorological situation the differences with respect to the actual situation were calculated. The changes in PET values due to the new buildings are shown in Figure 52. The PET values are up to 12°C lower in the area of building shading than in the actual situation. These improvements are located at a maximum of 10 m directly at the new buildings. The red areas with a very slight increase in PET values of up to 3°C indicate a trend towards a reduction in the quality of stay. However, this is far too low to have a noticeable effect on humans. The visible changes are very locally limited to the immediate surroundings of the new buildings.
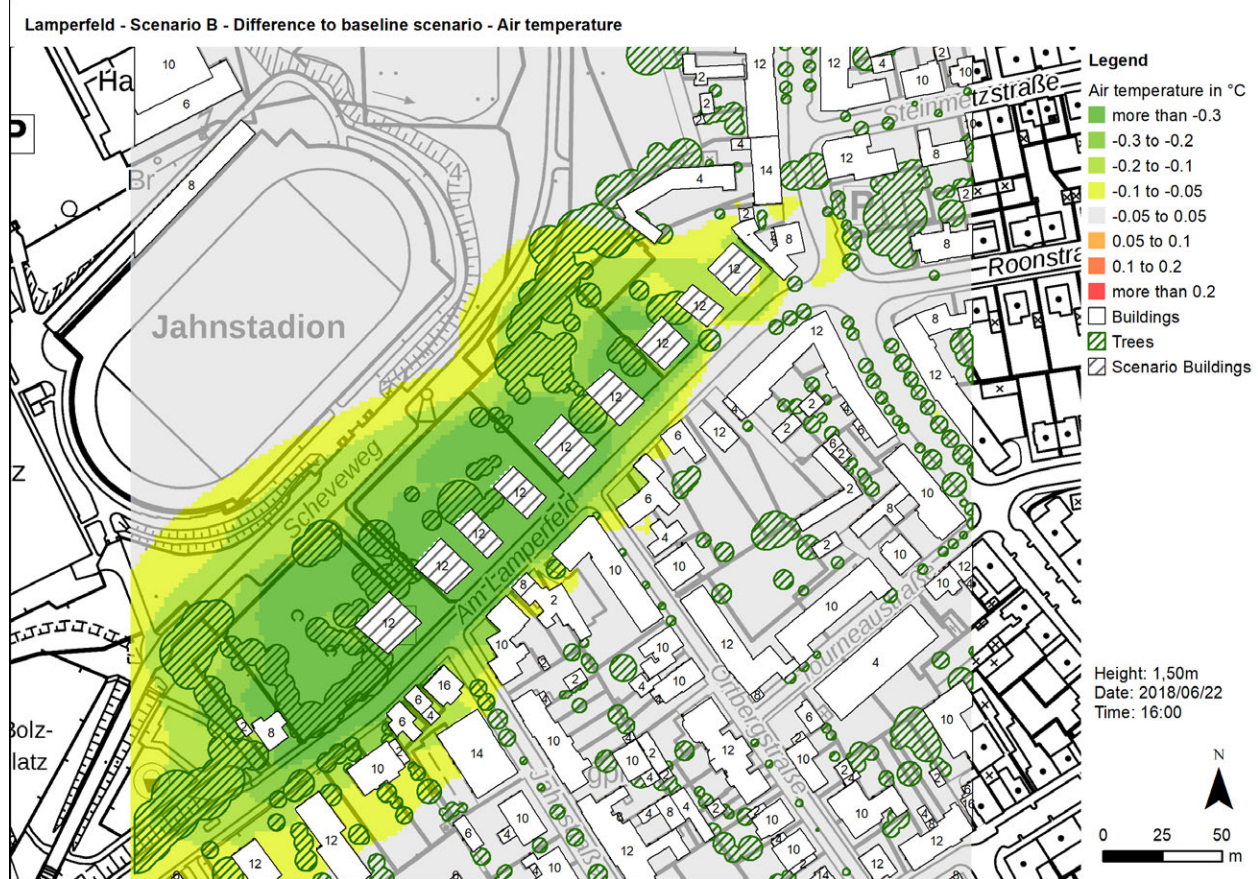
Figure 53: Model Bottrop 3 (Am Lamperfeld): Scenario B – Difference of air temperature, scenario B minus baseline scenario (source: own account, data: City of Bottrop).

The changes in air temperature in scenario B show cooling effects of up to 0.3°C (Figure 53), as in scenario A. The changes in the building structure are too small to lead to significant changes in the microclimatic situation. As in scenario A, the improvement of the air temperature in the model is due to the new shading and changes in the wind field as a result of the new buildings. The shading reduces the warming of the soil surface. In addition, the wind speeds at the Am Lamperfeld road increase, which can have a positive effect on the ventilation of the study area.
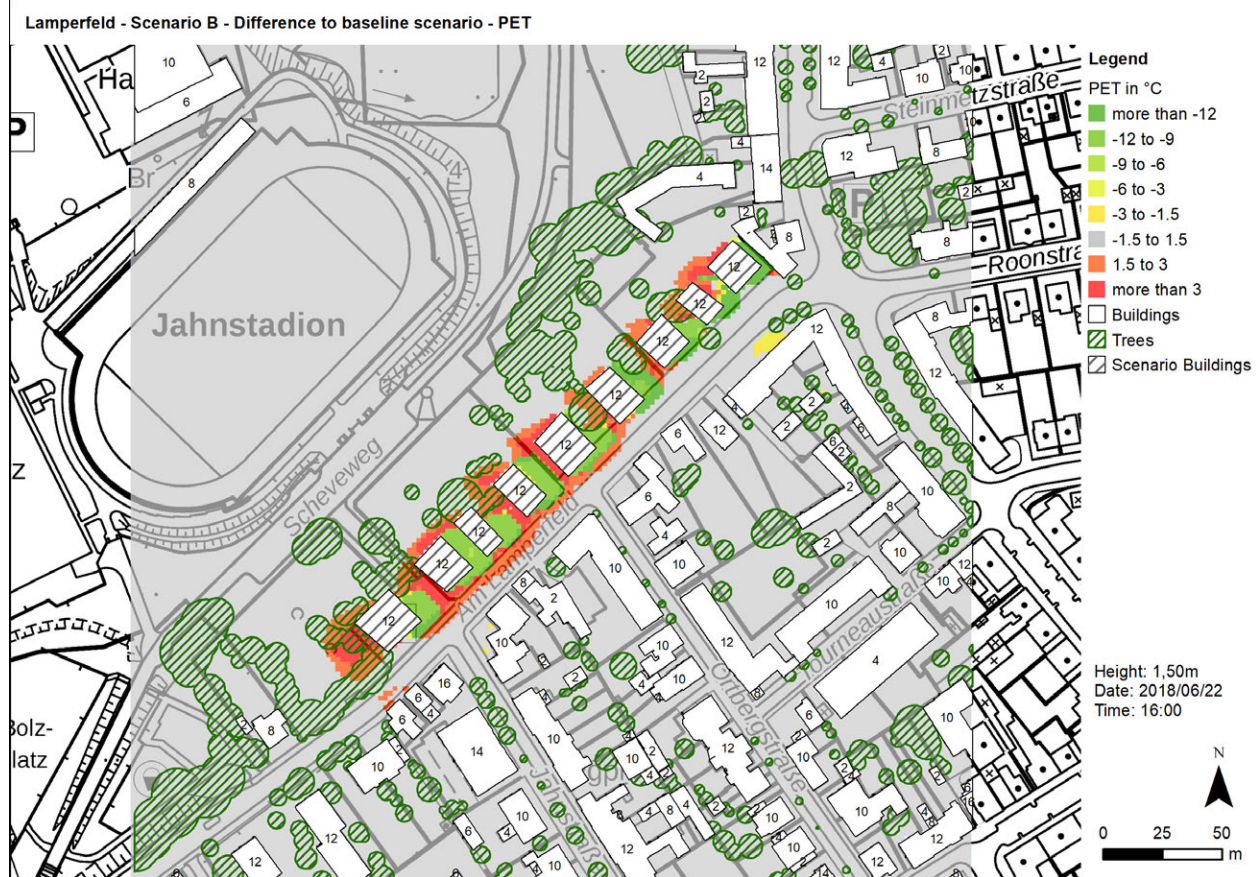
Figure 54: Model Bottrop 3 (Am Lamperfeld): Scenario B – Difference of PET values, scenario B minus baseline scenario (source: own account, data: City of Bottrop).

The changes in PET values due to the new buildings in scenario B are shown in Figure 54. The PET values in the area of building shading are up to 12°C lower than in the current situation. These improvements are located at a maximum height of 10 m directly at the new buildings. The red areas with a very small increase in PET values of up to 3°C indicate a trend towards a reduction in the quality of stay. However, this is far too low to have a noticeable effect on people. The visible changes are very locally limited to the immediate surroundings of the new buildings. Compared to scenario A, there are additional shaded areas between buildings where the quality of stay improves.

Air temperature - Baseline scenario - all raster

Av. 26.75

Value	Temp
2.183	25.75
2.073	26.00
3.824	26.25
5.399	26.50
4.652	26.75
3.796	27.00
3.293	27.25
1.297	27.50
213	27.75
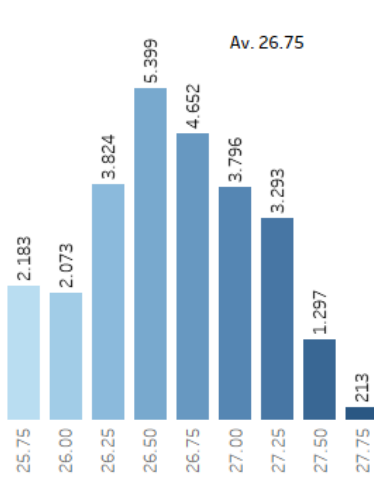
Air temperature - Baseline scenario - raster near existing buildings

Av. 26.24

Value	Temp
357	25.75
464	26.00
487	26.25
189	26.50
45	26.75
10	27.00
5	27.25
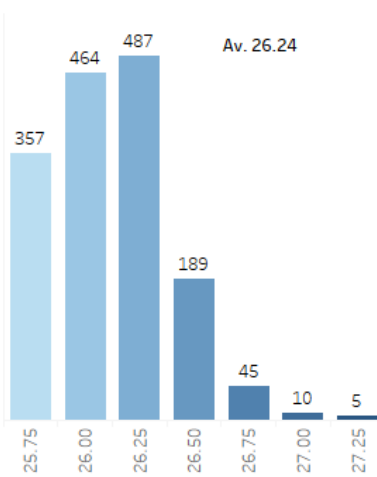
Air temperature - Baseline scenario - raster pavements

Av. 26.45

Value	Temp
103	25.75
237	26.00
339	26.25
378	26.50
115	26.75
44	27.00
21	27.25
4	27.50
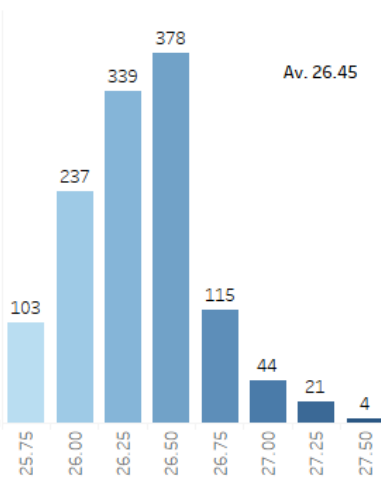
Air temperature - Scenario A - all raster

Av. 26.66

Value	Temp
49	25.50
3.037	25.75
3.713	26.00
4.197	26.25
4.016	26.50
3.954	26.75
3.501	27.00
2.910	27.25
1.141	27.50
212	27.75
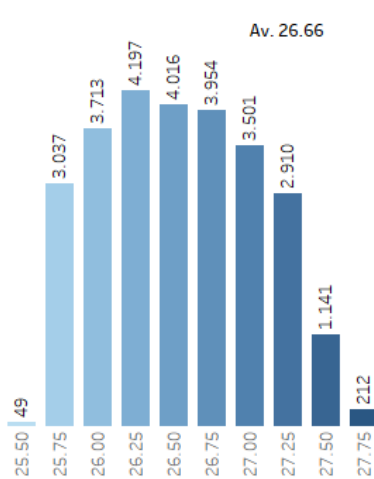
Air temperature - Scenario A - raster near existing buildings

Av. 26.18

Value	Temp
12	25.50
451	25.75
475	26.00
437	26.25
144	26.50
24	26.75
9	27.00
5	27.25
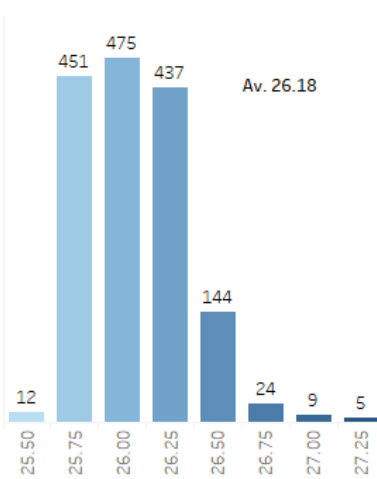
Air temperature - Scenario A - raster pavements

Av. 26.28

Value	Temp
2	25.50
309	25.75
363	26.00
225	26.25
201	26.50
86	26.75
39	27.00
12	27.25
4	27.50
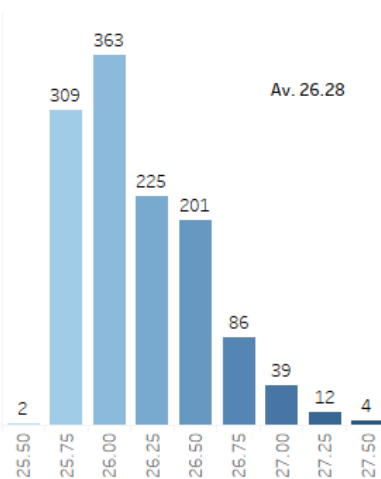
Air temperature - Scenario B - all raster

Av. 26.67

Value	Temp
2.824	25.75
3.569	26.00
4.442	26.25
4.131	26.50
3.962	26.75
3.537	27.00
2.934	27.25
1.131	27.50
200	27.75
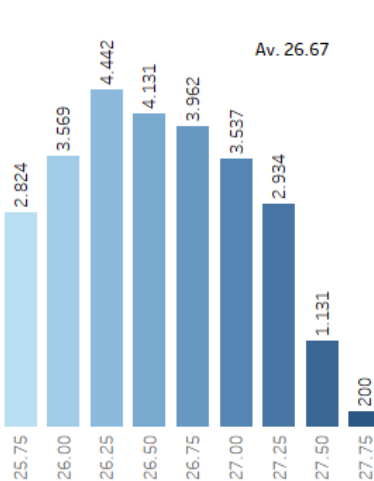
Air temperature - Scenario B - raster near existing buildings

Av. 26.18

Value	Temp
439	25.75
486	26.00
452	26.25
142	26.50
24	26.75
9	27.00
5	27.25
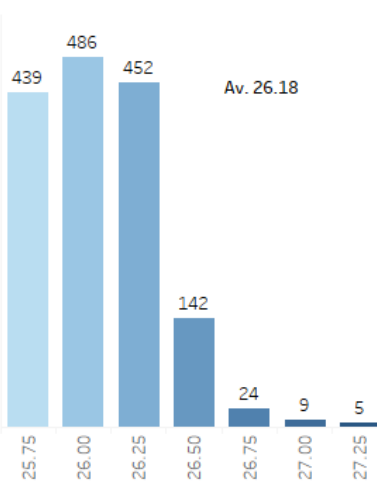
Air temperature - Scenario B - raster pavements

Av. 26.31

Value	Temp
242	25.75
364	26.00
298	26.25
202	26.50
78	26.75
43	27.00
10	27.25
4	27.50
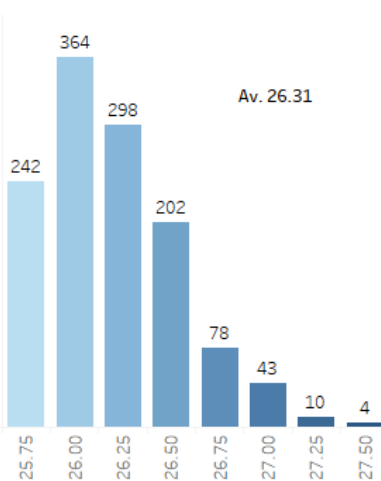
Figure 55: Analysis of changes in air temperature in single grid cells (Lamperfeld) (source: own account)

The overall microclimatic situation in the study area is characterised by dense development in the southeast and a high proportion of open, unvegetated space in the area of the stadium. In locations with a stronger greening, the shading and ventilation are somewhat better, which means that the heat stress is slightly less pronounced. Small-scale shading by buildings or large trees shows a very locally limited somewhat higher quality of stay. In the areas of the traffic areas exposed to radiation and the stadium, very strong heating of the sealed surfaces is sometimes achieved.

For both scenarios with different building types, the microclimatic changes remain locally limited. In both scenarios the shading and ventilation changes. From the climatic point of view, scenario B with open buildings is preferable to scenario A. For both scenarios, additional extended adaptation measures to improve the quality of stay should be considered. For this purpose, shading of the parking areas by large trees and/or technical solutions can be used as design elements. For the extensive parking areas, a partial desedimentation is also possible. When redesigning surfaces (including buildings), the lightest possible materials should be used, as these heat up much less. Depending on the building structure, an increase in the thermal level caused by the buildings remains locally limited. The overall effect of the changed climate function of the planned area can be classified as rather low.

3.4 Model Bottrop 4 – Building Structure – Planned inner city area (Saalbau)

3.4.1 Description of model

The fourth research area of modelling for the city of Bottrop is located at Droste-Hülshoff-Platz in the city centre of Bottrop in the immediate vicinity of the Rathhaus (Figure 56). The entire area is crossed by numerous streets, some of which are highly frequented. The modelled area has a size of 328 x 256 m. The area is currently covered with a so-called Saalbau (event hall), which is to give way to a new inner-city quarter in the near future. The city is planning an administrative extension to the historic town hall for the site. The area of the current Saalbau is to be part of these plans for the design and development of neighbouring areas at Droste-Hülshoff-Platz. Great importance will be attached to environmentally friendly construction, which will take into account both energy-related environmental standards and the use of rainwater and green roofs. This is part of the claim as a climate model city Innovation City.

Figure 56: Model Bottrop 4 (Saalbau) – Location of the investigated area (source: own account, data: City of Bottrop).

In the baseline scenario, the current situation is modeled. Scenario A contains the preferred variant of the future development that the city of Bottrop is planning.

3.4.2 Methodological approach

The methodological approach, the software used, the data and the setup have already been described in section 3.1.2 and are identical for all models for the city of Bottrop.

3.4.3 Modelled results and discussion
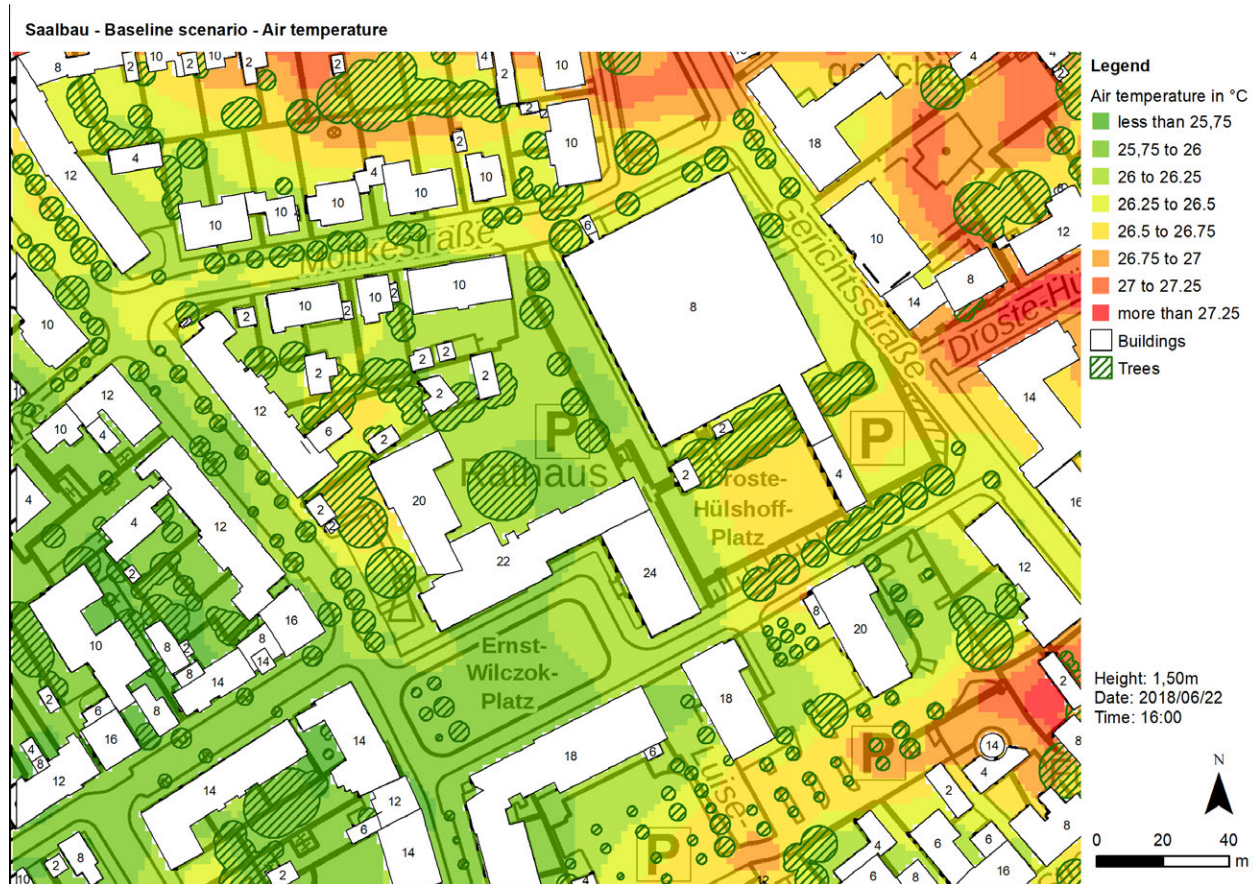
Figure 57: Model Bottrop 4 (Saalbau): Baseline scenario - ENVI-met calculated air temperature (source: own account, data: City of Bottrop).

The highest air temperatures in the baseline scenario with over 27.25°C (Figure 57, red) occur over the asphalt surface of the Droste-Hülshoff-Straße in the north-east and the parking lot in the south-east. The areas sealed here and the inadequate shading lead to a warming of the air. In the areas with open residential buildings and green inner courtyards, the lowest air temperatures occur with values between less than 25.75°C. The lowest air temperatures are found in the areas with large trees and green inner courtyards.
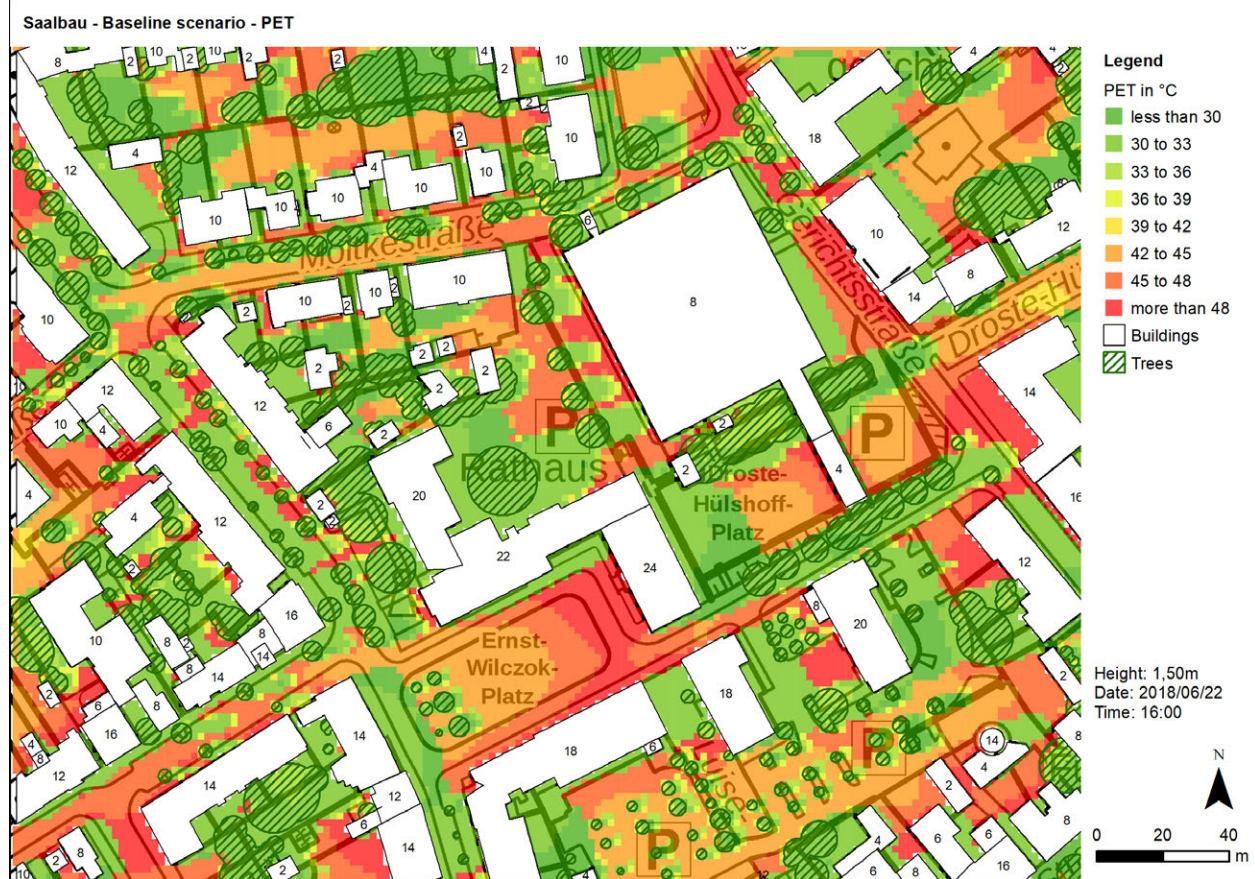
Figure 58: Model Bottrop 4 (Saalbau): Baseline scenario - ENVI-met calculated PET values (source: own account, data: City of Bottrop).

The PET values for the actual situation in the study area (Figure 58) show that in particular the sealed traffic areas and street trains lead to a very high bioclimatic load with PET values of more than 48°C. The PET values for the test area are also very high. According to the PET scale, these areas shown in red in Figure 58 represent a considerable heat load. In particular, the green inner courtyards of residential buildings and greened street sections show reduced PET values. In the area of the shadows cast by the buildings, the PET values are sometimes significantly lower than in the unshaded areas. In these shaded areas, a somewhat lower thermal load can be felt. The bioclimatic situation in areas with vegetation is significantly lower than in areas without vegetation. The reduction of the PET values remains locally limited, but can improve the quality of stay in areas without another shading by buildings. The greened inner courtyards and the already existing street greenery thus represent an important contribution to the small-scale improvement of the microclimatic situation.
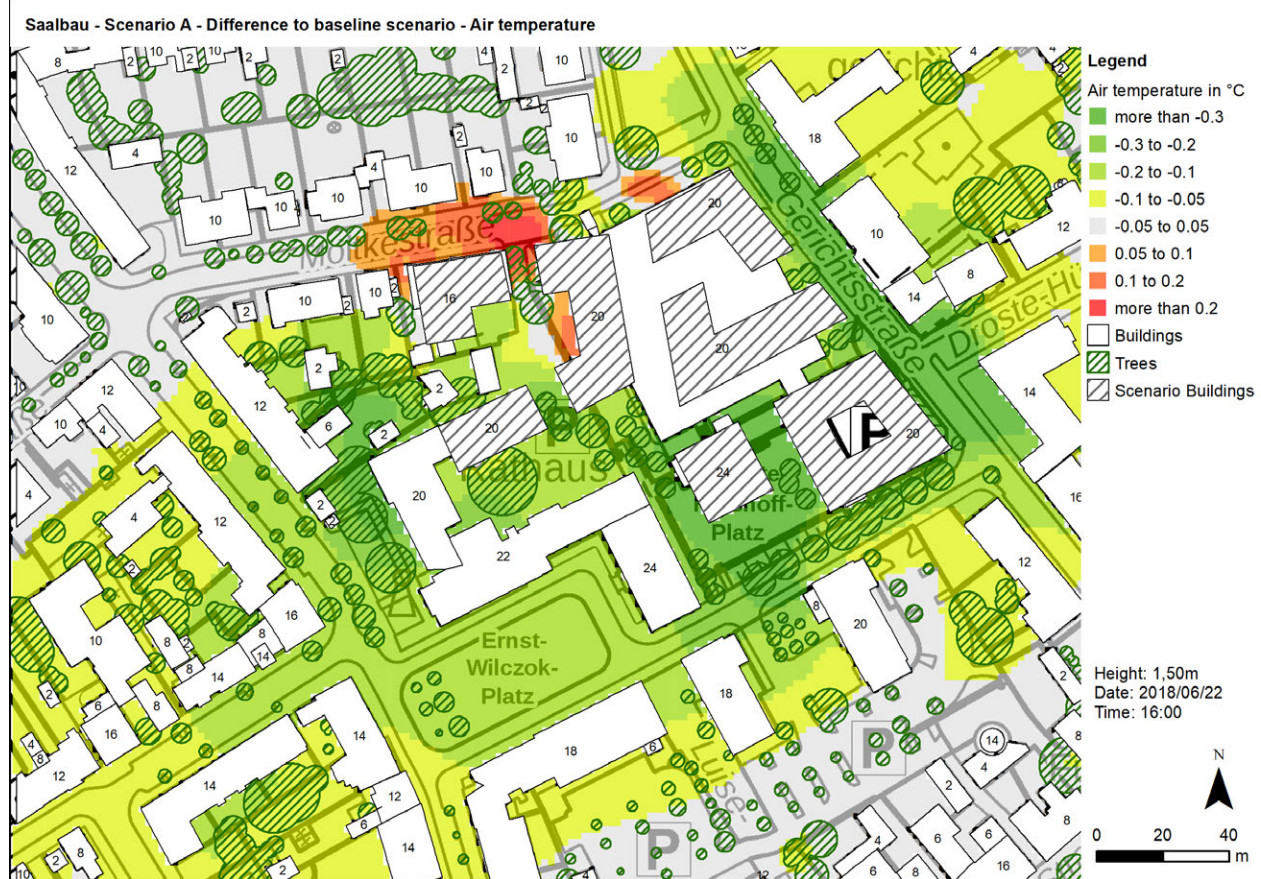
Figure 59: Model Bottrop 4 (Saalbau): Scenario A – Difference of air temperature, scenario A minus baseline scenario (source: own account, data: City of Bottrop).

The change of the air temperatures in scenario A (with new buildings) in direct comparison to the actual situation shows a slight cooling in the investigated area of up to 0.3°C (Figure 59). In the area of Moltkestraße, changes in the wind field lead to a slight increase in air temperature of up to 0.2°C. In areas with vegetation, the local microclimate is generally slightly better. The changes in the microclimatic situation in the study area can be regarded as minor, even if the planned construction project is implemented.
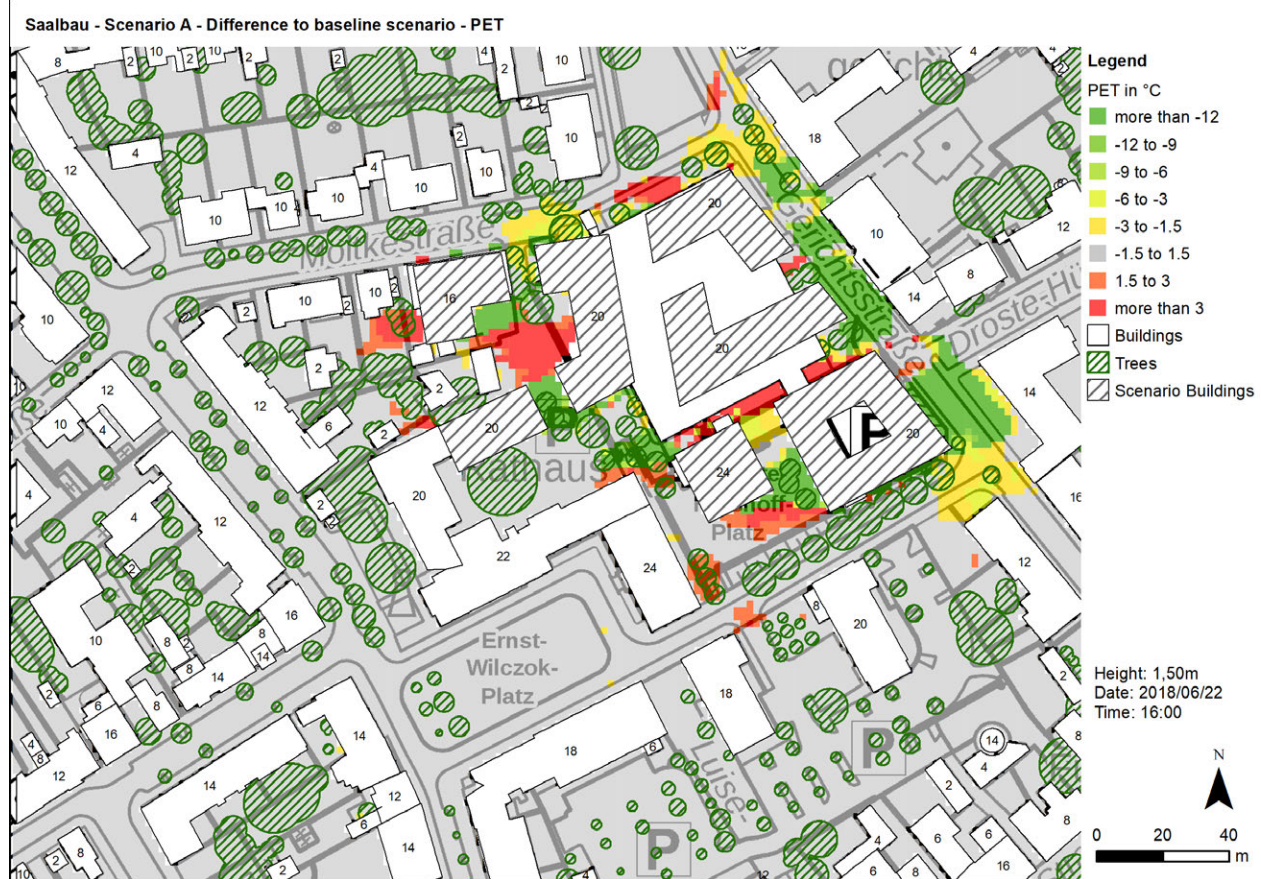
Figure 60: Model Bottrop 4 (Saalbau): Scenario A – Difference of PET values, scenario A minus baseline scenario (source: own account, data: City of Bottrop).

The described changes in air temperature from the baseline scenario to scenario A of the model are also reflected in the bioclimatic situation (Figure 60). The PET values change exclusively in the immediate vicinity of the new buildings. Here, both improvement and deterioration of the quality of stay can be seen. An increase of the PET values takes place exclusively in areas of newly emerging passages as well as open areas without vegetation (red). However, this is too low to have a strong effect on humans. In addition, the improvement of the quality of stay predominates in the areas of the sidewalks. Here there are improvements in the bioclimate due to shading and improvements in ventilation due to the new buildings.
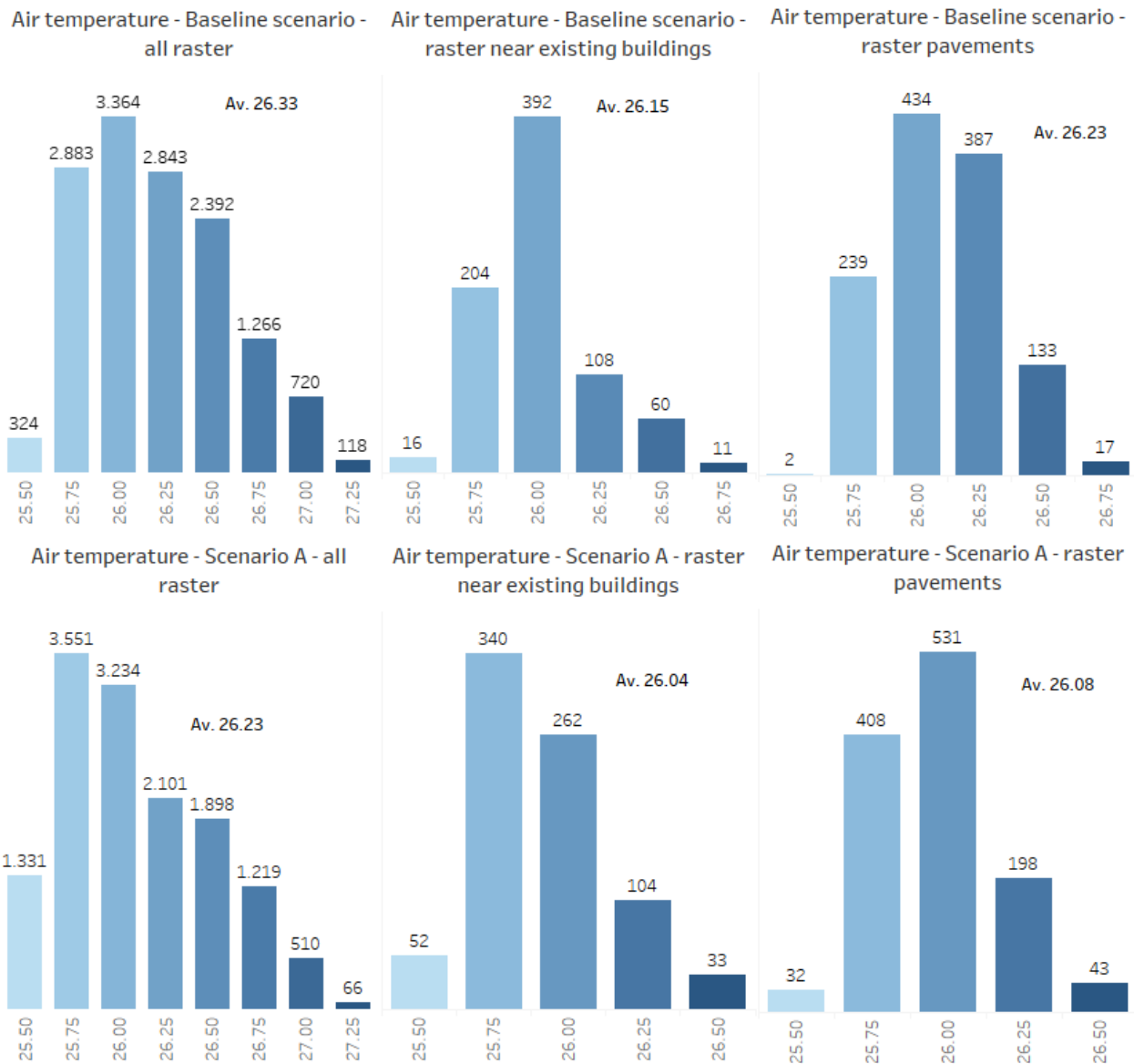
Figure 61: Analysis of changes in air temperature in single grid cells (Saalbau) (source: own account)

The overall microclimatic situation in the study area is characterised by a typical urban climate in densely built-up areas. In locations with stronger vegetation, the shading is slightly better, which means that heat stress is lower. Small areas shaded by buildings or large trees show a very locally limited, higher quality of stay. In the radiation-exposed areas of traffic areas and squares, a very strong warming of the sealed areas is sometimes achieved.

In scenario A with new buildings, the microclimatic changes remain locally limited. From a climatic point of view, scenario A has no significant negative effects compared to the baseline scenario. Depending on the building structure, an increase in the heat balance caused by the buildings is locally limited and is even partly compensated by new shading. The overall effect of the changed climate function of the planned area can be classified as rather small.

4 Land Use Regression Model for the City of Dublin

Several epidemiological studies have indicated that present-day outdoor pollution can have significant adverse effects on public health (Brunekreef and Holgate, 2002; Pope and Dockery, 2006). In 2015 it has been shown that approximately 6.4 million deaths worldwide were caused by air pollution (Landrigan, 2017). The pollutants with severe health concerns include particulate matter (PM), nitrogen dioxide (NO_2) and ozone (Brunekreef and Holgate 2002). The major challenge in epidemiological analyses of the long-term impact of air pollution exposure on human health is to quantify the exposure of the population in a city. Cohort studies often fail to account for the small-scale variation in pollution levels between individuals living within the same geographic region. Studies have shown that the variation in particulate matter air pollution within a city can be higher than the variation between cities (Miller et al., 2007), moreover other studies (Briggs et al., 2000; Zhu et al., 2002; Gilbert et al., 2003) noted that the variation in air pollution could be significant at a scale of meters within a geographic location. Most epidemiological studies of air pollution effects on health depend on measurements obtained from a small number of fixed monitoring sites covering a large geographical area (Pope et al. 1995). This fails to capture the small scale spatial variability in the pollutants' distributions (McCreddin et al., 2015; Dimakopoulou et al., 2017).

The development of models to assess air pollution exposure within cities has become important in health studies (Brunekreef and Holgate, 2002; Brauer et al., 2003; Moore et al., 2007). These exposure assessment methods include exposure indicator variables (e.g. traffic intensity at the residential address or distance to a major road), geostatistical interpolation models (e.g. kriging, inverse distance weighing), dispersion models, and Land Use Regression (LUR) models. LUR modelling commonly uses multiple linear regression to analyse associations between measured pollutant concentrations at a number of monitoring sites and Geographic Information System (GIS) covariates (predictor variables) such as traffic, land use, topography and population characteristics. The main strength of LUR is the empirical structure of the regression mapping (e.g. selection of optimized buffer size), its relatively simple inputs, and low cost as compared with dispersion modeling (Jerrett et al., 2005).

LUR models have been developed to perform epidemiological studies on air pollutants in either the spatial or temporal domain. Traditionally LUR models used only spatial covariates to predict long-term pollutant concentrations over a geographical area. In situations where the modelling was performed over a spatial domain, annual average concentrations of the pollutant obtained by using concentration data observed over the period of one year were used to develop the regression equations. To obtain exposures to air pollutant during specific time periods of interest, the developed regression model was extrapolated forward (Morgenstern et al., 2008; Ryan et al., 2008) or backwards in time by assuming that temporal changes are constant across the study area (Brauer et al., 2008; Cesaroni et al., 2008; Clark et al., 2010; Karr et al., 2009a, b; Morgenstern et al., 2006, 2008; Slama et al., 2007).

The development of spatial LUR models requires observed pollutant data from a large number of monitoring stations to determine concentrations as accurately as possible and to minimize exposure misclassification (Alam and McNabola, 2015). Fixed urban background air quality measurement stations in routine monitoring networks are widely used to represent the exposure of subjects residing within large geographic areas surrounding these monitoring stations. In

situations where a sufficiently high number of fixed monitoring station data are available, GIS-based spatial interpolation approaches (such as kriging) and statistical techniques can be used to interpolate from ambient monitoring data. However, as the number of ambient monitoring sites is often limited, these methods do not adequately capture the smaller-scale spatial variations in pollutant concentrations such as those occurring near roadways, which leads to the popularity of LUR models in scientific communities.

A limitation of existing LUR models is the selection of proper predictors for each monitoring station. Selection of spatial covariates (predictors) at appropriate distances of influence (e.g., distance to road, industrial land use, etc.) is important for determining final model performance. The appropriate distance (circular buffer) of influence for exposure analysis is, in general, estimated by considering different buffer distances (Basu et al., 2019). Typically less than 10 circular buffer distances are considered to assess correlations with the dependent variable (Henderson et al., 2007; Aguilera et al., 2007). Because of the differences in topography, meteorology, land use, traffic and population composition of one urban area to another, the buffer distances suitable for one urban area might not be the best choice for another. Furthermore, most of the LUR models are based on ordinary least square regression, which can only account for linear dependence between the predictors and the air pollution concentration. The relationship between air pollution concentrations and the predictors in question is often non-linear (Alam and McNabola, 2015; Basu et al., 2019).

This analysis addresses the aforementioned challenges by considering a nonlinear regression based LUR model while modelling the spatial variation of PM_{10} air pollutant in greater Dublin, Ireland. The nonlinear regression considered in the analysis is termed as weighted support vector regression that can quantify the non-linear relationship present between the set of predictors and the air pollution concentration. The study introduces a weight function to account for uncertainty in different types of data due to the variation of record lengths between long term and short term station data. Finally, the study also considers a systematic approach to the selection of buffer distance optimization, based on the approach described in Basu et al. (2019).

The following Table provides an overview of the two models developed for simulating air quality in Dublin at the urban scale.

City/Scale	Model	Model category	Purpose
Dublin: urban scale	Weighted Support Vector Regression approach for cold season	Land Use Regression	Obtain map of PM_{10} concentrations at the urban scale in the cold season
Dublin: urban scale	Weighted Support Vector Regression approach for warm season	Land Use Regression	Obtain map of PM_{10} concentrations at the urban scale in the warm season

Table 13. Details on models developed in Dublin presented in the following (source: own account).

4.1 Methodology and input data

4.1.1 Study Area and Experiment design

The study area considered in the analysis is the greater Dublin area, which is the capital and most populated city in Ireland (see Figure 62). The model was developed to understand the spatial variation of ambient particulate matter (PM_{10}) concentrations across the city. PM_{10} concentrations measured at a daily time scale from 13 fixed monitoring stations were obtained from the Environmental Protection Agency (EPA), Ireland for the chosen study area. Data from those EPA monitoring stations were collected continuously using an automated system. The stations are part of the Cleaner Air for Europe Directive network and follow the 4th Daughter Directive and national implementation regulations. Details of those stations are provided in Table 14.

To understand the variation of PM_{10} concentration across different time periods of a year, the monthly mean concentration of PM_{10} for each station were estimated and plotted in Figure 63. The figure indicates that the PM_{10} is slightly higher during the colder months (November to April) and lower in the warmer months (May to October). Furthermore, it can be noted from the figure that the monthly mean concentration for all stations ranges between 8 $\mu g/m^3$ to 32 $\mu g/m^3$, which is less than the European Union legislation requirement of 40 $\mu g/m^3$ (European Environmental Agency, 2017). From Table 14 it can be noted that the number of days the daily concentration of PM_{10} averaged over a day exceeds 50 $\mu g/m^3$ (as per EU legislation requirement) is less than 3% for each station, except for Coleraine Street, where 5% of the days the PM_{10} pollution exceeds the specified threshold concentration.
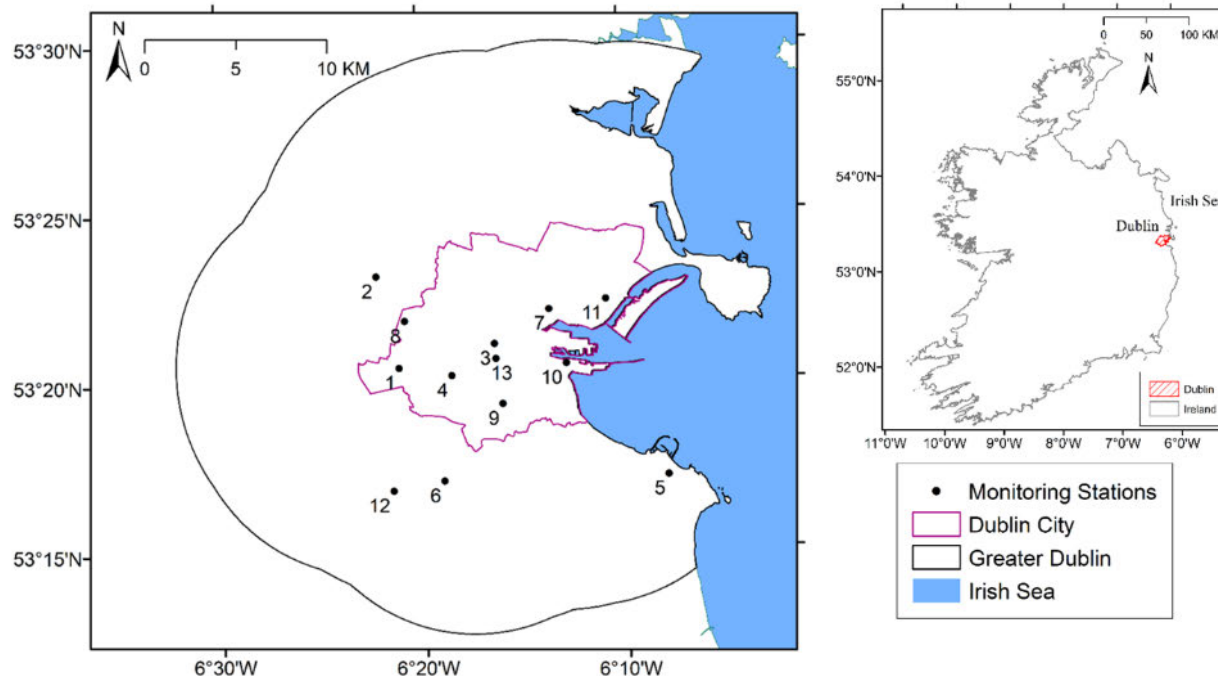
Figure 62: Study area (Dublin city and Greater Dublin Area), and locations of monitoring stations (source: own account)

St. No.	Station Name	Location details		Data duration	PM$_{10}$ concentration ($\mu g/m^3$)			Percentage of days PM$_{10}$ concentration exceeds 50 $\mu g/m^3$
		Latitude	Longitude		Annual	Colder months	Warmer months	
1	Ballyfermot	53.340	-6.352	16/09/2003 to 31/12/2016	13.23	15.35	11.36	1.05
2	Blanchardstown	53.386	-6.370	01/01/2008 to 31/12/2016	17.68	20.15	14.88	2.58
3	Coleraine Street	53.352	-6.273	01/01/2001 to 22/12/2008	21.66	25.15	18.29	5.04
4	Davitt Road	53.336	-6.309	01/01/2013 to 31/12/2016	13.16	15.16	11.49	0.53
5	Dun Laoghaire	53.286	-6.132	01/01/2008 to 31/12/2016	14.40	17.49	11.58	1.41
6	Knocklyon	53.285	-6.317	01/01/2008 to 31/12/2008	17.18	20.83	15.96	0.48
7	Marino	53.368	-6.228	06/12/2000 to 22/12/2008	16.14	18.89	13.19	2.21
8	Phoenix Park	53.364	-6.347	03/02/1996 to 31/12/2016	12.80	14.66	10.95	1.04
9	Rathmines	53.322	-6.267	17/01/1996 to 31/12/2016	17.36	20.77	14.10	2.52
10	Ringsend	53.341	-6.214	05/04/2009 to 11/03/2012	19.47	23.78	15.04	2.94
11	St Annes	53.373	-6.181	01/01/2013 to 31/12/2015	17.28	17.97	16.60	0.46
12	Tallaght	53.280	-6.359	03/01/2008 to 31/12/2016	13.84	16.05	11.57	0.94
13	Winetavern Street	53.344	-6.272	10/01/2001 to 31/12/2016	18.01	20.87	15.22	2.56

Table 14: Details on data of 13 EPA monitoring stations (source: own account)

Based on Table 14, it can be noted that some of those monitoring stations have longer records, while others have relatively short records. Differences in the record lengths for each monitoring station affects the associated uncertainty in the estimation of average PM_{10} concentration and needs to be accounted for while developing the LUR model.
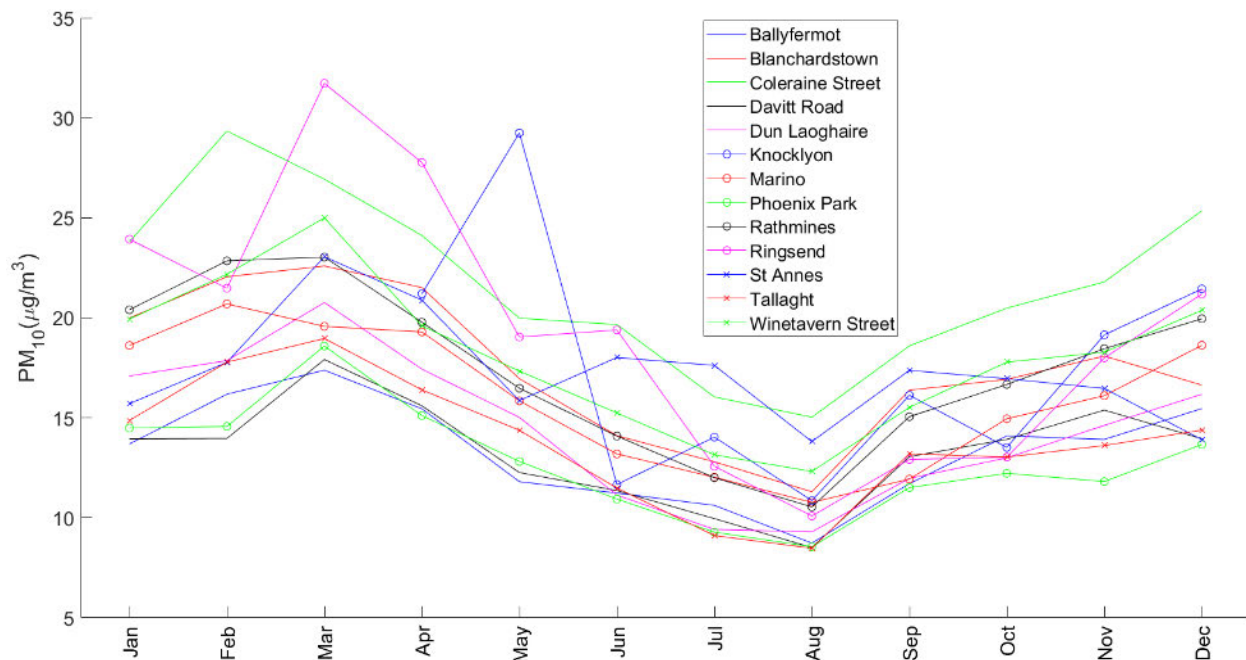
Figure 63: Monthly mean concentration of PM_{10} for 13 monitoring stations in Dublin (source: own account).

Before developing the LUR model, a set of predictor variables needs to be identified that could influence the predicted seasonal average PM_{10} concentration for colder and warmer seasons. Based on previous literature (Alam and McNabola, 2015; Basu et al. 2019), the following variables have been selected as potential predictors that can influence the particulate matter air pollution in Greater Dublin area:

1. Digital Elevation Model (DEM): obtained from Shuttle Radar Topography Mission (SRTM) website (http://srtm.csi.cgiar.org) at 90 m resolution.

2. Population density (POP): obtained from Ireland census board (http://www.cso.ie/en/census/census2011boundaryfiles).

3. Building length (BLDG_L) and building area (BLDG_A): obtained from OpenStreetMap (http://download.geofabrik.de/europe/ireland-and-northern-ireland.html).

4. Land use data (urban: LUC_U; agricultural land: LULC_A; waterbody: LULC_W): obtained from CORINE landcover report 2012.

5. Traffic volume data of light (TRAF_LV) and heavy (TRAF_HV) vehicles at annual average: obtain from Dublin City Council.

6. Hydro-meteorological variables: Rainfall, Maximum and Minimum Temperature and Wind speed obtained from Met Eireann (the Irish Meteorological service) (www.met.ie).

The spatial extent of influence for each of the aforementioned potential predictor variables (except the meteorological variables) was not known a priori. Corresponding to each monitoring station, 20 different buffer lengths were therefore selected for the analysis. The buffer lengths considered were: 100, 200, 300, 400, 500, 600, 700, 800, 900, 1000, 1200, 1400, 1600, 1800, 2000, 2200, 2400, 2600, 2800 and 3000 m. Subsequently, the values of each of the potential predictors (covariates) corresponding to each buffer distance were extracted, and the correlation between those covariates and PM_{10} concentration were estimated. The correlation values corresponding to each potential predictor are plotted in Figure 64. The figure indicates that increasing the buffer length, the correlation between the predictor and predictand changes considerably, and the correlation value tends to become constant as the buffer length is considerably higher. Based on the correlation analysis, the covariates having the highest correlation with the predictand (seasonal average PM_{10} concentration) were identified for both seasons (see Table 15) which constitute the set of selected predictors.
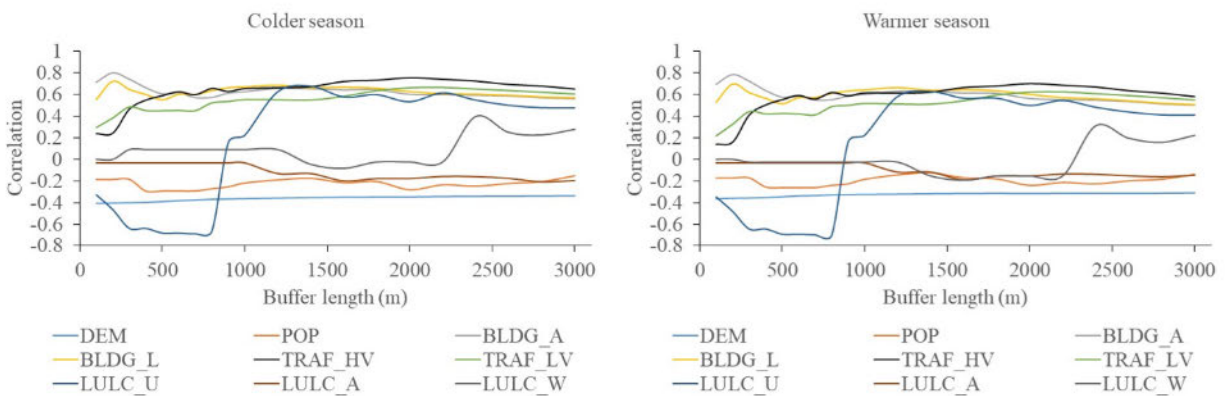
Figure 64: Correlation plot between predictors and predictand (PM_{10} concentration) corresponding to different buffer lengths (source: own account).

It can be noted from Table 15 that waterbody was not selected as a covariate since the area of waterbodies is low in Dublin. It is to be noted that in situations where the correlation between the covariates and predictand takes both positive and negative values corresponding to different buffer lengths, only realistic correlations were considered (for example, increase in urban area is expected to increase the pollution concentration; for low buffer length the correlation between predictand and urban area was found to be negative and was not considered).

Sl. No.	Selected Variables	Abbreviation	Colder season	Warmer season
1	Digital Elevation Model	DEM	100m	100m
2	Building Area	BLDG_A	200m	200m
3	Building length	BLDG_L	200m	200m
4	Heavy vehicles	TRAF_HV	2000m	2000m
5	Light vehicles	TRAF_LV	2000m	2000m
6	Urban land use	LULC_U	1400m	1400m
7	Agricultural land use	LULC_A	2800m	2800m
8	Rainfall	RAIN	NA	NA
9	Maximum Temperature	MAXT	NA	NA
10	Minimum Temperature	MINT	NA	NA
11	Wind speed	WIND	NA	NA

Table 15: List of selected predictors (covariates) and the corresponding buffer lengths for colder and warmer seasons (source: own account).

It is to be noted that the meteorological variables (rainfall, maximum and minimum temperature and wind speed) are available from at-site location data, whose locations are different from the stations where PM_{10} data were collected. Weighted averages of those meteorological variables (Y_s) for a station s can be estimated based on Equations 1 and 2 (Basu et al., 2019).

$$Y_s = \sum_{i=1}^{N_m} \gamma_i X_i \qquad\qquad (1)$$

where

$$\gamma_i = \frac{1/d_{si}}{\sum_{j=1}^{N_m} 1/d_{sj}} \qquad\qquad (2)$$

where *s* is an air quality monitoring station (either fixed or mobile), Y_s is the average value of the meteorological variable (either rainfall, maximum or minimum temperature or wind speed) for the

site s, N_m is the total number of meteorological stations for which data were available, X_i is the seasonal average (colder or warmer) value of the meteorological variable, γ_i is the weighing factor and d_{si} is the distance between the monitoring station s and the meteorological station i. Details on the location and average values of those meteorological stations are provided in Table 16-Table 18. Values of the selected set of predictors for each monitoring stations are provided in Table 19.

Sl. No.	Location	Latitude	Longitude	Average Rainfall in	
				Colder season	Warmer season
1	Phoenix Park	53.358	-6.342	2.15	2.19
2	Dublin Airport	53.423	-6.238	2.01	2.12
3	Malahide Castle	53.44	-6.157	1.89	1.96
4	Glasnevin	53.369	-6.269	1.98	2.02
5	Glenasmole DCWW	53.237	-6.367	3.43	2.95
6	Ringsend	53.338	-6.208	1.87	1.88
7	Ballyedmonduff House	53.233	-6.222	3.40	2.76
8	Casement	53.303	-6.437	2.02	2.04
9	Merrion Square	53.338	-6.252	1.97	1.91
10	Supt's Lodge	53.237	-6.358	3.45	2.87
11	Ballyboden	53.272	-6.303	2.57	2.11
12	Simmons Court	53.322	-6.222	2.04	2.06
13	Glenaraneen	53.251	-6.451	2.88	2.83
14	Dun Laoghaire	53.285	-6.126	2.17	2.20

Table 16: Average values of meteorological variables along with their location details obtained from Irish Meteorological department – a) Rainfall (source: own account).

Sl. No.	Location	Latitude	Longitude	Average Maximum Temperature in		Average Minimum Temperature in	
				Colder season	Warmer season	Colder season	Warmer season
1	Phoenix Park	53.358	-6.342	9.89	17.85	2.96	9.23
2	Dublin Airport	53.423	-6.238	9.29	16.68	3.19	9.07
3	Casement	53.303	-6.437	10.15	17.60	3.79	10.23
4	Wellington Lane	53.328	-6.244	9.39	17.10	2.77	8.65
5	Wilton Place	53.334	-6.249	9.99	17.29	4.84	11.13
6	Richmond Row	53.33	-6.265	10.08	17.32	4.59	10.96

Table 17: Average values of meteorological variables along with their location details obtained from Irish Meteorological department – b) Maximum Temperature (source: own account)

Sl. No.	Location	Latitude	Longitude	Average Wind Speed in	
				Colder season	Warmer season
1	Dublin Airport	53.423	-6.238	11.397	9.169
2	Casement	53.303	-6.437	11.821	9.175

Table 18: Average values of meteorological variables along with their location details obtained from Irish Meteorological department – c) Wind Speed (source: own account)

St. No.	DEM	BLDG_A	BLDG_L	TRAF_HV	TRAF_LV	LULC_U	LULC_A	RAIN	MAXT	MINT	WIND
1	41.0	10164.3	1070.7	51900	2368768	217.1	0.0	2.36	9.84	3.33	11.653
2	54.5	8677.3	2376.4	64317	2756568	91.8	18.0	2.35	9.81	3.41	11.635
3	15.6	31984.2	4636.1	290811	12424374	139.7	0.0	2.19	9.96	3.94	11.532
4	24.5	16160.9	4170.3	106560	5108545	128.7	0.0	2.33	9.87	3.65	11.591
5	28.9	8420.3	3164.9	31218	1915236	106.4	0.0	2.23	10.04	4.46	11.551
6	70.0	12381.2	1020.8	69285	3413335	109.0	46.5	2.53	9.84	3.68	11.637
7	13.0	8053.8	2831.3	117874	5825014	104.1	0.0	2.18	9.86	3.91	11.483
8	51.8	7532.1	1566.3	33214	1620067	107.4	13.5	2.26	9.87	3.16	11.623
9	26.1	24817.9	3639.5	167387	8079773	150.2	0.0	2.26	9.92	4.10	11.559
10	5.0	6086.9	2076.1	141086	3621075	215.3	0.0	2.07	9.88	4.01	11.513
11	20.3	1221.5	203.5	19542	2036557	91.0	9.0	2.20	9.82	3.86	11.492
12	99.4	10087.5	5510.1	25273	2418525	116.4	48.8	2.65	9.78	3.51	11.692
13	15.3	49495.4	9770.9	323622	13092705	74.3	0.0	2.21	9.94	4.03	11.539

*Table 19: Set of selected predictors based on correlation analysis for each monitoring stations – a) Colder season[8]
(source: own account)*

---

[8] DEM: Digital Elevation Model; BLDG_A: Building Area; BLDG_L: Building length; TRAF_HV: Heavy vehicles; TRAF_LV: Light vehicles; LULC_U: Urban land use; LULC_A: Agricultural land use; RAIN: Rainfall; MAXT: Maximum Temperature; MINT: Minimum Temperature; WIND: Wind speed.

St. No.	DEM	BLDG_A	BLDG_L	TRAF_HV	TRAF_LV	LULC_U	LULC_A	RAIN	MAXT	MINT	WIND
1	41.0	10164.3	1070.7	51900	2368768	217.1	0.0	2.26	17.56	9.56	9.173
2	54.5	8677.3	2376.4	64317	2756568	91.8	18.0	2.25	17.46	9.62	9.172
3	15.6	31984.2	4636.1	290811	12424374	139.7	0.0	2.12	17.41	10.24	9.171
4	24.5	16160.9	4170.3	106560	5108545	128.7	0.0	2.21	17.45	9.90	9.172
5	28.9	8420.3	3164.9	31218	1915236	106.4	0.0	2.21	17.32	10.81	9.171
6	70.0	12381.2	1020.8	69285	3413335	109.0	46.5	2.28	17.38	9.89	9.172
7	13.0	8053.8	2831.3	117874	5825014	104.1	0.0	2.12	17.30	10.14	9.170
8	51.8	7532.1	1566.3	33214	1620067	107.4	13.5	2.22	17.70	9.41	9.172
9	26.1	24817.9	3639.5	167387	8079773	150.2	0.0	2.15	17.35	10.36	9.171
10	5.0	6086.9	2076.1	141086	3621075	215.3	0.0	2.03	17.31	10.26	9.171
11	20.3	1221.5	203.5	19542	2036557	91.0	9.0	2.14	17.26	10.07	9.170
12	99.4	10087.5	5510.1	25273	2418525	116.4	48.8	2.41	17.37	9.69	9.173
13	15.3	49495.4	9770.9	323622	13092705	74.3	0.0	2.13	17.39	10.31	9.171

Table 20: Set of selected predictors based on correlation analysis for each monitoring stations – b) Warmer Season[9] (source: own account)

---

[9] DEM: Digital Elevation Model; BLDG_A: Building Area; BLDG_L: Building length; TRAF_HV: Heavy vehicles; TRAF_LV: Light vehicles; LULC_U: Urban land use; LULC_A: Agricultural land use; RAIN: Rainfall; MAXT: Maximum Temperature; MINT: Minimum Temperature; WIND: Wind speed.

4.1.2 Spatial Land Use Regression Model

The commonly used LUR model develops a multiple linear regression between the selected predictors (spatial covariates) and the predictand (PM_{10} concentration at a given location in the study area) by providing equal weight to each monitoring station data. However, in situations where the record length of each of those monitoring stations are considerably different, different weight needs to be provided in each monitoring station while developing the regression relationship between the selected predictors and the predictand. Values of weights corresponding to each monitoring station were estimated based on the approach defined in Basu et al. (2019), as explained below.

The weight-uncertainty covariance matrix was estimated based on the approach considered by Tasker (1980), summarized in Equations 3-5.

$$\Lambda_{ij} = \begin{cases} \sigma_\delta^2 + c_1 \left(\frac{1}{m_i} \right) & (i = j) \\ 0 & (i \neq j) \end{cases} \tag{3}$$

where

$$c_1 = max \left[0, \bar{\sigma}^2 \left(1 + \frac{\bar{K}^2}{2} (1 + 0.75\bar{G}^2) + \bar{K}\bar{G} \right) \right]; \sigma_\delta^2 = max \left[0, \sigma_{OLS}^2 - c_1 \left(\frac{1}{N} \sum_{p=1}^N \frac{1}{m_p} \right) \right] \tag{4}$$

where σ_δ^2 is the model-error variance estimated using Equation (6.3.4), m_i is the record length of ith station (in days), σ_{OLS}^2 is the observed mean square error of the estimate of seasonal average PM_{10} concentration using OLS regression obtained between the predictors and predictands in situations where equal weight was assumed for each station. $\bar{K}$ is the arithmetic average of the log Pearson type III deviates of all station PM_{10} concentration data, $\bar{G}$ is the arithmetic average of the skewness of all stations, and $\bar{\sigma}$ is the arithmetic average of the standard deviation of all N stations. The weight value for each station can be estimated based on the uncertainty matrix as:

$$\delta_i = \frac{1/\Lambda_{ii}}{1 / \min_{\forall j}(\Lambda_{jj})} ; 0 < \delta_i \leq 1 \tag{5}$$

Based on the equation, the station having least weight-uncertainty will have a weight equal to unity and the remaining stations will have a weight between 0 and 1.

It can be noted from Equation 3 that with an increasing record length of station data, the associated weight-uncertainty value decreases. Also, when the model-error variance is less, the weight-uncertainty for the station reduces. This indicates that the reliability of the air pollution-related information extracted from the station is high and more importance (weight) should be provided for the station while developing LUR model. It can be observed from Equation 5 that the associated

weight is corresponding to a station increases when the weight-uncertainty for that station decreases.

Furthermore, in most real-world scenarios, the assumption of a linear relationship between the selected predictors and the predictand does not hold true, indicating that a multiple linear regression based LUR model developed between the selected predictors and the predictand may not yield accurate results. To investigate the relationship between each of the selected predictors and the predictand (seasonal average PM_{10} concentration), scatter plots between those variables were prepared (see
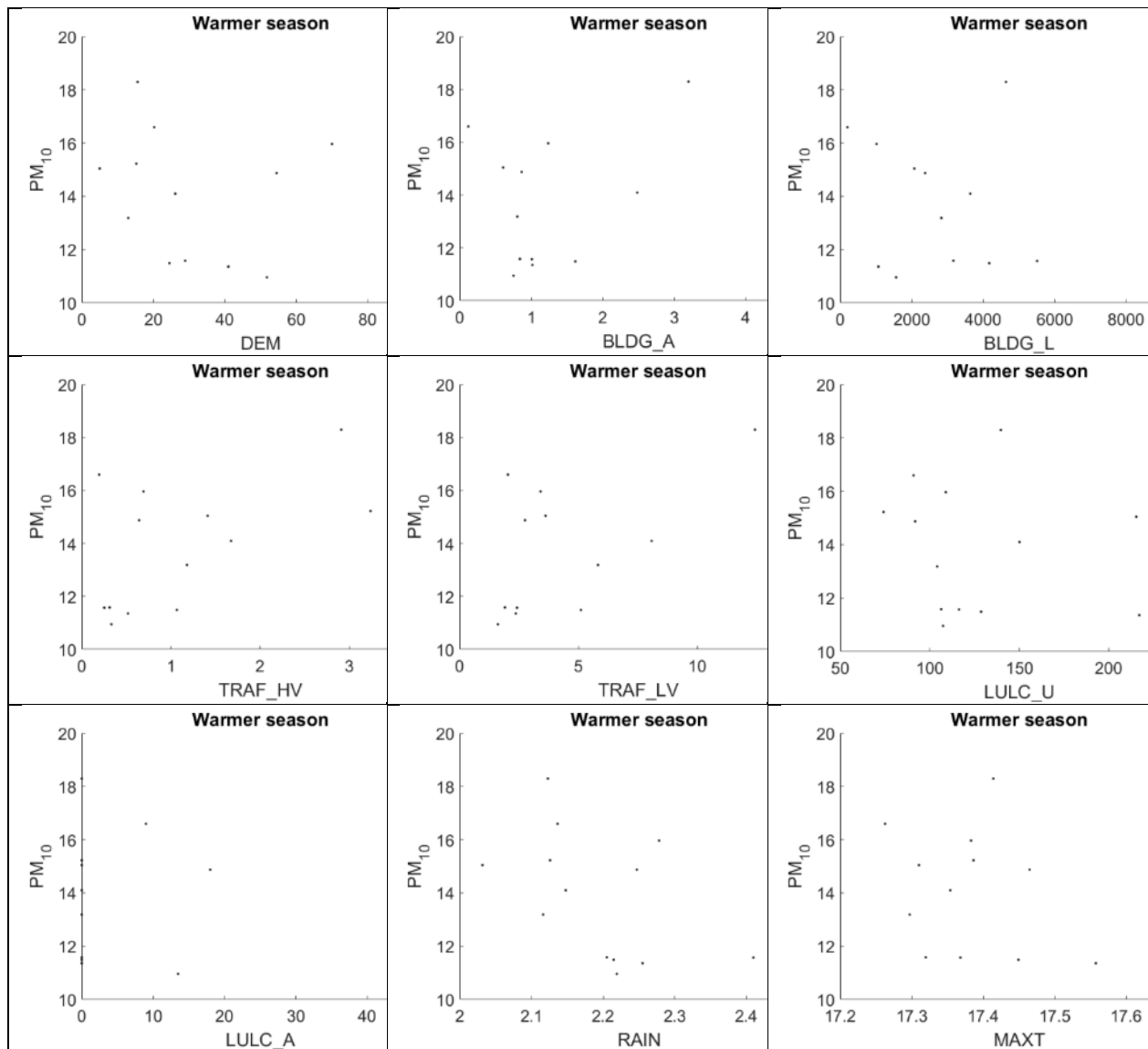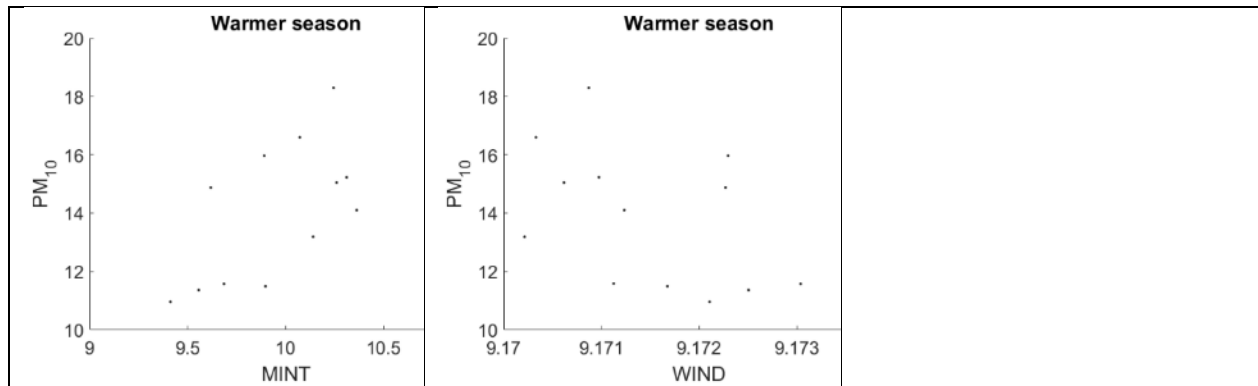
Figure 66). The figure indicated that the relationships between the selected predictors and predictand deviate from linear relationships and are found to be nonlinear. As the conventional multiple linear regression-based approaches fails to capture the associated nonlinearity in the data, an alternative weighted support vector regression (W-SVR) based LUR model has been developed in the study to model the seasonal average PM_{10} concentration in the Greater Dublin area. The W-SVR model can account for both nonlinearity in the data and can consider different weight on monitoring stations due to unequal record lengths while developing the regression relationship (Basu et al., 2019). Details of the W-SVR model are provided in Section 4.1.3.
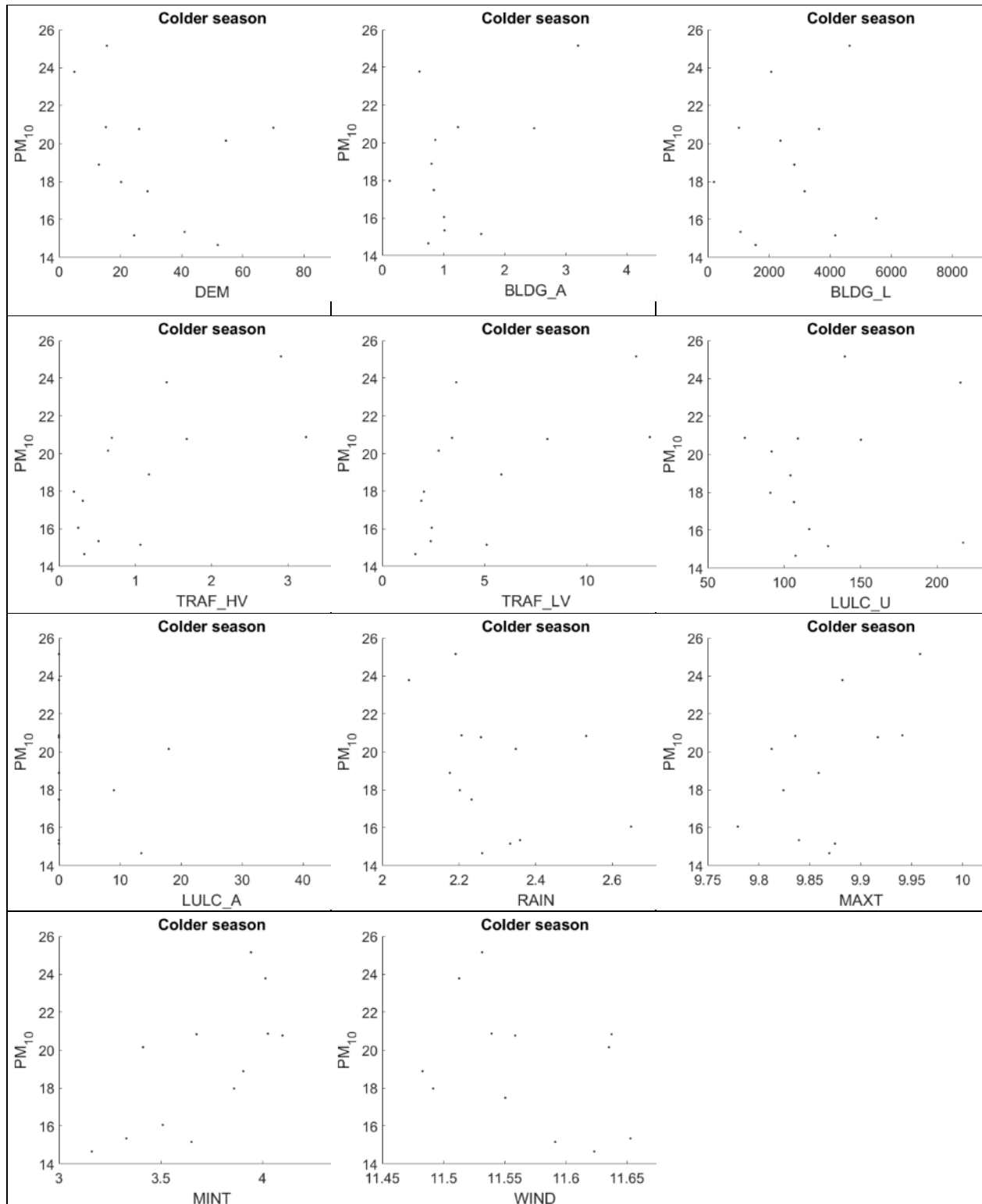
Figure 65: Scatterplot between selected predictors and predictand (PM$_{10}$) for colder seasons (source: own account).
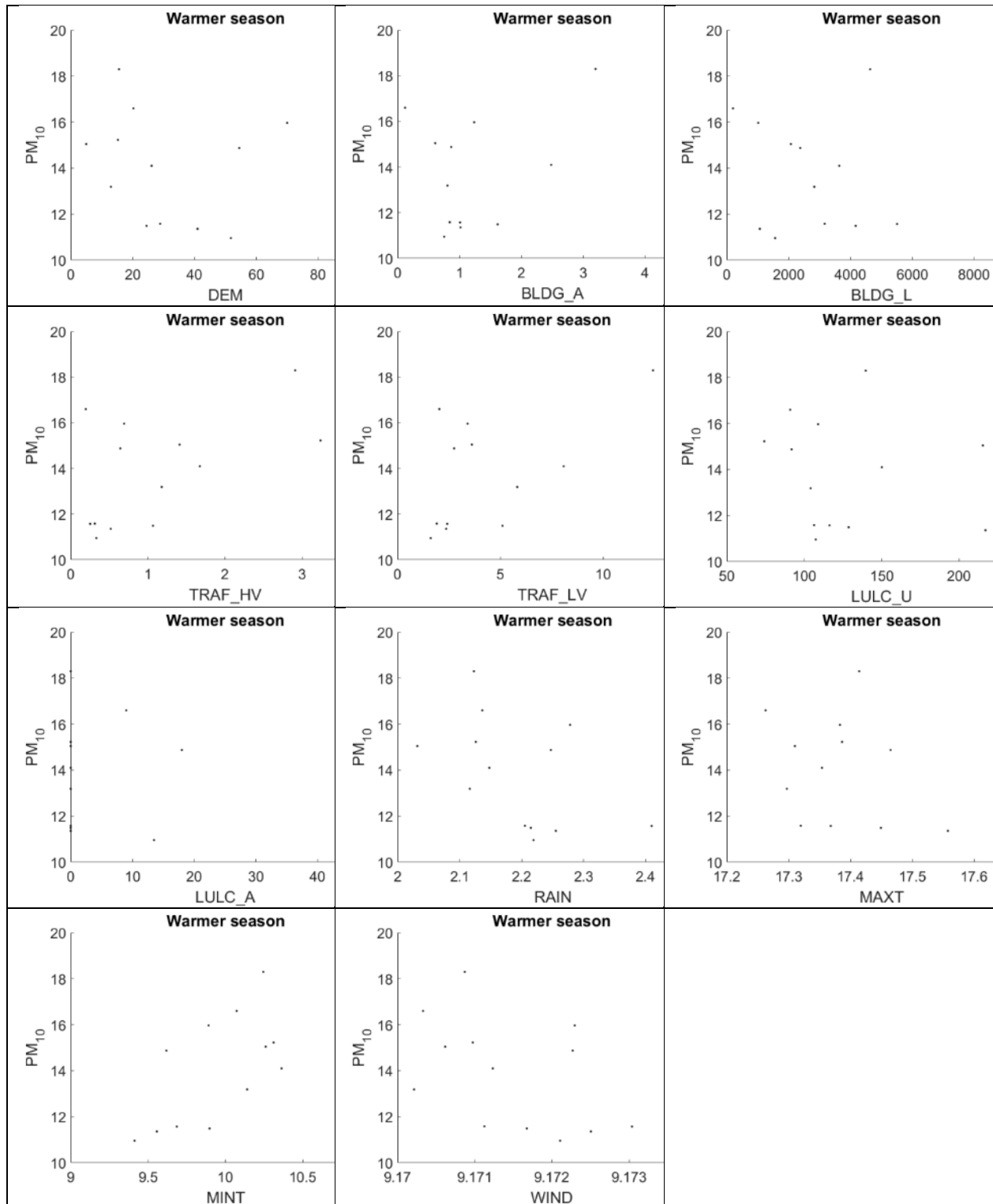
Figure 66: Scatterplot between selected predictors and predictand (PM$_{10}$) for warmer seasons (source: own account).

4.1.3 Weighted Support Vector Regression approach (W-SVR)

Details of the W-SVR approach have been adopted from Basu et al. (2019). The W-SVR based LUR model considers a nonlinear relationship between the selected predictors (covariates) and the predictand for site $\{i, i = 1, \cdots, N\}$ as:

$$y_i = f(\overrightarrow{x_i}) \tag{6}$$

where $\{f(\cdot); \Re^K \to \Re\}$ is a nonlinear transformation function and $\overrightarrow{x_i} = (x_{i1}, x_{i2}, \cdots, x_{iK}) \in \Re^K$. The principle of the W-SVR approach is to map the data $\vec{x}$ at a higher *p*-dimensional space using a mapping function $\phi(\cdot)$, where a linear relationship exists between $\phi(\vec{x})$ and observed output y. Projecting the data in higher dimension introduces new variables in the data that considers the nonlinear terms as new variable(s), which in turn can linearize the original dataset through this transformation (Basu and Srinivas, 2014).

The linear relationship can be defined as:

$$\hat{y} = \phi(\overrightarrow{x_i}) \times w + b \tag{7}$$

where $w = [w_1 \quad \cdots \quad w_p]^T$, b are the unknown model parameters, and $\hat{y}$ is the model prediction. The objective of the model is to reduce the empirical risk, given as:

$$R_{emp} = \frac{1}{N} \sum_{i=1}^{N} |y_i - \hat{y}_i|_\varepsilon \tag{8}$$

where $|y_i - \hat{y}_i|_\varepsilon$ is the Vapnik's ε-insensitive loss function (Vapnik, 1995) defined as:

$$|y_i - \hat{y}_i|_\varepsilon = \begin{cases} 0; & if \ |y_i - \hat{y}_i| \le \varepsilon \\ |y_i - \hat{y}_i| - \varepsilon; & otherwise \end{cases} \tag{9}$$

The parameter $\varepsilon \ge 0$ is a non-negative number to be specified by the modeler. In situations where the difference between observed and model predicted value of the predictand (model prediction error) is less than ε, the W-SVR algorithm considers that the prediction error is zero (please see Equation 9). The most stringent condition arises when $\varepsilon = 0$, as selected in the present study.

To reduce the structural risk for ensuring that the developed model is not over-fitted, the following cost function is minimized (Huang and Shen, 2008):

$$\min_{w,\xi,\xi^*} \frac{1}{2} \|w\|^2 + C \sum_{i=1}^{N} \delta_i(\xi_i + \xi_i^*) \tag{10}$$

subject to the constraints,

$$
\begin{aligned}
y_i - \left((\phi(\overrightarrow{x_i}) \cdot w) + b\right) &\leq \varepsilon + \xi_i \quad for\ i = 1, \cdots, N \\
(\phi(\overrightarrow{x_i}) \cdot w) + b - y_i &\leq \varepsilon + \xi_i^* \quad for\ i = 1, \cdots, N \\
\xi_i &\geq 0 \quad for\ i = 1, \cdots, N \\
\xi_i^* &\geq 0 \quad for\ i = 1, \cdots, N
\end{aligned}
\tag{11}
$$

where ξ_i and ξ_i^* are positive slack variables and C is a positive real-valued constant that determines the amounts up to which the deviation from ε are tolerated. The weight value for each station was denoted as δ_i, and can be estimated by using Equation (5). A considerably lower value of C gives more importance to the structural risk, and hence might under-fit the model, whereas a considerably higher value of C gives more importance to the empirical risk and tends to over-fit the model. The optimal value of the parameter C needs to be selected by the modeler to ensure equal importance is provided to reduce both structural and empirical risk. The optimization problem can be solved by introducing the Lagrange function given as:

$$
\min_{w,b,\xi_i,\xi_i^*} \mathcal{L} = \frac{1}{2}\|w\|^2 + C\sum_{i=1}^{N}\delta_i(\xi_i + \xi_i^*) - \sum_{i=1}^{N}(\eta_i\xi_i + \eta_i^*\xi_i^*) - \sum_{i=1}^{N}\alpha_i(\varepsilon + \xi_i - y_i + (\phi(\overrightarrow{x_i}) \cdot
$$
$$
w) + b) - \sum_{i=1}^{N}\alpha_i^*(\varepsilon + \xi_i^* + y_i - (\phi(\overrightarrow{x_i}) \cdot w) - b)
\tag{12}
$$

subject to

$$
\alpha_i, \alpha_i^*, \eta_i, \eta_i^* \geq 0
\tag{13}
$$

where $\alpha_i, \alpha_i^*, \eta_i, \eta_i^*$ are termed as Lagrange multipliers. The objective of this optimization problem is to minimize the value of $\mathcal{L}$ by identifying optimal values of w and b. Partially differentiating $\mathcal{L}$ with respect to w gives,

$$
w - \sum_{i=1}^{N}\alpha_i\phi(\overrightarrow{x_i}) + \sum_{i=1}^{N}\alpha_i^*\phi(\overrightarrow{x_i}) = 0 \Rightarrow w = \sum_{i=1}^{N}(\alpha_i - \alpha_i^*)\phi(\overrightarrow{x_i})
\tag{14}
$$

Based on Equation 7, the W-SVR based estimate for a site s can be expressed as:

$$
\hat{y}_s = \phi(\overrightarrow{x_s}) \times w + b = \phi(\overrightarrow{x_s}) \times \sum_{i=1}^{N}(\alpha_i - \alpha_i^*)\phi(\overrightarrow{x_i}) + b = \sum_{i=1}^{N}(\alpha_i - \alpha_i^*)\phi(\overrightarrow{x_s}) \cdot \phi(\overrightarrow{x_i}) + b =
$$
$$
\sum_{i=1}^{N}(\alpha_i - \alpha_i^*)K(\overrightarrow{x_s}, \overrightarrow{x_i}) + b
\tag{15}
$$

where $K(\overrightarrow{x_s}, \overrightarrow{x_i}) = \phi(\overrightarrow{x_s}) \cdot \phi(\overrightarrow{x_i})$ is a kernel function satisfying Mercer condition (Haykin, 2003). The choice of the kernel function includes linear, polynomial, splines, sigmoid and radial basis

function (RBF). In this study, a RBF function was considered for mapping the data from its original space to higher p-dimensional space. The RBF function considered is given as:

$$K(\overrightarrow{x_i}, \overrightarrow{x_j}) = exp\left(-\frac{\|\overrightarrow{x_i} - \overrightarrow{x_j}\|^2}{2\sigma^2}\right) = exp\left(-\nu\|\overrightarrow{x_i} - \overrightarrow{x_j}\|^2\right) \qquad (16)$$

where σ is called the width of the RBF kernel, and $\nu = \frac{1}{2\sigma^2}$. In situations where the data is highly nonlinear, the data needs to be projected in higher dimensions and the width σ will be high. The value of σ (or ν) needs to be specified by the modeler.

For estimating the bias parameter b, the Lagrange multiplier can be partially differentiated with respect to b, ξ_i and ξ_i^* and equated to zero, which yields the following equations:

$$\sum_{i=1}^{N} \alpha_i - \sum_{i=1}^{N} \alpha_i^* = 0 \qquad (17)$$

$$C\delta_i - \eta_i - \alpha_i = 0 \Rightarrow \eta_i + \alpha_i = C\delta_i \qquad (18)$$

$$C\delta_i - \eta_i^* - \alpha_i^* = 0 \Rightarrow \eta_i^* + \alpha_i^* = C\delta_i \qquad (19)$$

Replacing values of $w, \eta_i, \eta_i^*, \xi_i$ and ξ_i^* in the Lagrange function yields a Wolfe dual function, expressed as:

$$\max_{\alpha_i, \alpha_i^*} \mathcal{L}^* = -\frac{1}{2}\sum_{i=1}^{N}\sum_{j=1}^{N}(\alpha_i - \alpha_i^*)(\alpha_j - \alpha_j^*)\phi(\overrightarrow{x_i}) \cdot \phi(\overrightarrow{x_j}) - \varepsilon\sum_{i=1}^{N}(\alpha_i + \alpha_i^*) + \sum_{i=1}^{N} y_i(\alpha_i - \alpha_i^*) \qquad (20)$$

subject to $\sum_{i=1}^{N} \alpha_i - \sum_{i=1}^{N} \alpha_i^* = 0, \ 0 \leq \alpha_i \leq C\delta_i$ and $0 \leq \alpha_i^* \leq C\delta_i$. This optimization function can be used to solve for values of the Lagrange multipliers α_i and α_i^*.

Based on Karush-Kuhn-Tucker (KKT) conditions, the product between Lagrange multipliers and constraints must be equal to zero (Karush, 1939; Kuhn and Tucker, 1951). The KKT conditions yield:

$$\alpha_i(\varepsilon + \xi_i - y_i + \phi(\overrightarrow{x_i}) \cdot w + b) = 0 \qquad (21)$$

$$\alpha_i^*(\varepsilon + \xi_i^* + y_i - \phi(\overrightarrow{x_i}) \cdot w - b) = 0 \qquad (22)$$

$$(C\delta_i - \alpha_i)\xi_i = 0 \qquad (23)$$

$$(C\delta_i - \alpha_i^*)\xi_i^* = 0 \qquad (24)$$

Based on the KKT conditions, it can be noted that for situations:

$$when\ 0 < \alpha_i < C\delta_i, b = y_i - \phi(\overrightarrow{x_\iota}) \cdot w - \varepsilon = y_i - \sum_{j=1}^{N} K(\overrightarrow{x_\iota}, \overrightarrow{x_J}) - \varepsilon \qquad (25)$$

$$when\ 0 < \alpha_i^* < C\delta_i, b = y_i - \phi(\overrightarrow{x_\iota}) \cdot w + \varepsilon = y_i - \sum_{j=1}^{N} K(\overrightarrow{x_\iota}, \overrightarrow{x_J}) + \varepsilon \qquad (26)$$

While developing the W-SVR model, the constant C and the RBF function width σ are not known a priori and need to be estimated. For this purpose, the stations data have been subdivided in two sets, the calibration set and the validation set. Data corresponding to the calibration set were used to develop the model for different combinations of those W-SVR parameter values. Subsequently, the developed model is used to predict the seasonal average PM_{10} concentration for stations in the validation set and the error in average PM_{10} concentration between the predicted and observed values were noted. The optimal parameter pair of W-SVR model for which the error in model performance was minimized has been selected. As the developed model does not consider the data corresponding to the validation set, the developed model can be reliably used to predict the seasonal average PM_{10} concentration in any location in the study area. In this study, the validation set consists of 90% of the data and the validation set consists of the remaining dataset. The analysis is repeated several times by randomly selecting the calibration and validation set to remove any bias in the identification of the optimal parameters.

4.1.4 Model Performance measures

Performance of the W-SVR model for both colder and warmer season was evaluated by using a leave-one-out-cross-validation (LOOCV) experiment, where air pollution concentrations for one station were considered to be unavailable, and the W-SVR based LUR model was developed by using the data from the remaining stations. Once the LUR model was developed, the pollution concentration for the ungauged/omitted site was predicted using the model. This procedure was repeated for *N* times, each time omitting one of the *N* stations. The error in the model's predicted and observed concentrations was quantified by using the following four performance measures:

$$Bias = \frac{1}{N}\sum_{i=1}^{N}(\hat{y}_i - y_i) \tag{27}$$

$$ABias = \frac{1}{N}\sum_{i=1}^{N}|\hat{y}_i - y_i| \tag{28}$$

$$RMSE = \sqrt{\frac{1}{N}\sum_{i=1}^{N}(\hat{y}_i - y_i)^2} \tag{29}$$

$$R^2 = 1 - \frac{\sum_{i=1}^{N}(\hat{y}_i - y_i)^2}{\sum_{i=1}^{N}(y_i - \bar{y})^2} \tag{30}$$

where y_i is the observed concentration for site *i*, $\hat{y}_i$ is the model predicted concentration for the site, and $\bar{y}$ is the mean observed concentration for all the sites, estimated as $\bar{y} = \sum_{i=1}^{N} y_i/N$.

Performance of a model can be considered to be adequate if the values of Bias, ABias and RMSE are closer to zero and the Coefficient of Determination (R^2) was closer to 1.

4.2 Modelled Results and discussion

Performance of the two developed models (one for colder season and the other one for warmer season) were evaluated using a LOOCV experiment, as described in section 4.1.4 As the optimal parameters v and C of W-SVR based LUR models for colder and warmer season are not known *a priori*, both the parameters were varied from 100 to 5000 with an increment of 100. The two optimal parameters for W-SVR based LUR models are found to be $v = 7300, C = 3800$ for colder season and $v = 6100, C = 5200$ for warmer the season, based on the approach described in section 6.3.2.3. The weight values corresponding to each station that were used to develop the W-SVR based LUR model are provided in Table 21. It can be noted from the table that the weighted uncertainty of each station in colder season are considerably higher than that for the warmer season, indicating that the variability in daily PM_{10} concentration for the colder season are more when compared to the warmer season. Further, the weights are higher for Phoenix Park, Rathmines and Winetavern Street (Stations no. 8, 9 and 13 respectively) where the available records of PM_{10} concentration are longer.

St. No.	Colder months		Warmer months	
	Weights	Weighted uncertainty	Weights	Weighted uncertainty
1	0.5399	0.6073	0.6006	0.2648
2	0.3972	0.8255	0.3452	0.4607
3	0.4252	0.7711	0.4361	0.3648
4	0.1978	1.6578	0.2329	0.6831
5	0.4510	0.7271	0.4899	0.3247
6	0.0169	19.3522	0.0502	3.1659
7	0.3822	0.8579	0.3510	0.4531
8	1.0000	0.3279	1.0000	0.1591
9	0.8899	0.3685	0.9198	0.1729
10	0.1571	2.0878	0.1514	1.0508
11	0.1743	1.8810	0.1771	0.8980
12	0.4197	0.7813	0.4042	0.3935
13	0.8791	0.3730	0.8931	0.1781

Table 21: Weights (estimated based on Equation 5) and the weighted uncertainty (estimated based on Equation 3) of each station for colder and warmer months (source: own account)

The developed models were then used to predict the PM_{10} concentration in LOOCV experiment, as described in Section 4.1.4. The model performance/error measures in terms of Bias, Abias, RMSE and R^2 for the colder and warmer season are provided in Table 22.

Season	Bias	Abias	RMSE	R^2
Colder	-0.073	0.707	0.979	0.905
Warmer	-0.063	0.685	0.930	0.832

Table 22: Performance measure of developed W-SVR based LUR models in LOOCV framework for colder and warmer seasons (source: own account).

The model performance measures provided in Table 22 indicated that the bias for the colder season is -0.073 µg/m³ while that for the warmer season is -0.063 µg/m³. Negative values of bias suggest that the model slightly underestimates the actual PM_{10} concentration in the study area, however, the amount by which the model under-predicts is close to zero. The Abias and RMSE indicated that the error in prediction, on average, is within the range of ±1 µg/m³ for both colder and warmer months. The bias, Abias and RMSE for the colder season are found to be slightly higher than that for the warmer season, though the R^2 value for the colder season is better than that of the warmer season, indicating that the model performance is better for colder season. The reason for having slightly higher values of Bias, Abias and RMSE for the colder season is the higher concentration of PM_{10} in that season. In general, the lower values of Bias, Abias and RMSE and high values of R^2 indicate that the developed W-SVR based LUR model can be used to predict seasonal average PM_{10} concentration in greater Dublin area.

The spatial variation of PM_{10} concentration obtained based on the developed W-SVR based LUR model for the study area is shown in Figure 67. The figure indicates that the PM_{10} concentration is higher in the city centre and southern part of the city and low in the western part of the city for both colder and warmer season. The concentration is found to be highest at the city centre during colder months.

It is worth to note that differently from the PCSs objective of the interventions in the other iSCAPE cities, installation of low boundary walls (LBWs) for urban scale is not feasible in real world scenario. Furthermore, unlike other passive control structures, LBW cannot remove any pollution, and it only diverts pollution from one location to another location. For this purpose, installation of LBWs at some small portion of the city would not affect the overall pollution in the city/large scale. Furthermore, it can be noted that the air pollution in Dublin is considerably low as per EU guidelines. Hence, since installation of LBWs for entire city is unrealistic and the pollution in Dublin is considerably lower, installation of LBWs are not considered.

It can be noted from Figure 67 that the PM_{10} concentration during colder season is slightly higher than that in the warmer season. However, the highest daily average concentration of PM_{10} are noted to be 24.5 µg/m³ and 17.39 µg/m³ respectively, for colder and warmer months. The noted concentration is considerably lower than 40 µg/m³, which is the requirement as per European Union legislation. Due to the low concentration in Dublin, installation of low boundary walls (LBWs) as passive control structure at city scale is not deemed necessary for the study area. Furthermore, it needs to be noted that unlike other passive control structures, LBW cannot remove any pollution, as it only transit pollution from one location to another location. Hence, installation of LBWs at a small portion of the city would not affect the overall pollution at the city scale. It can also be noted that it is impractical and infeasible to install LBWs for the entire city in real world scenario, particularly in cities where the pollution is considerably lower than the permissible limit. Due to the aforementioned reasons, installation of LBWs as passive control structure are not considered for the city of Dublin.
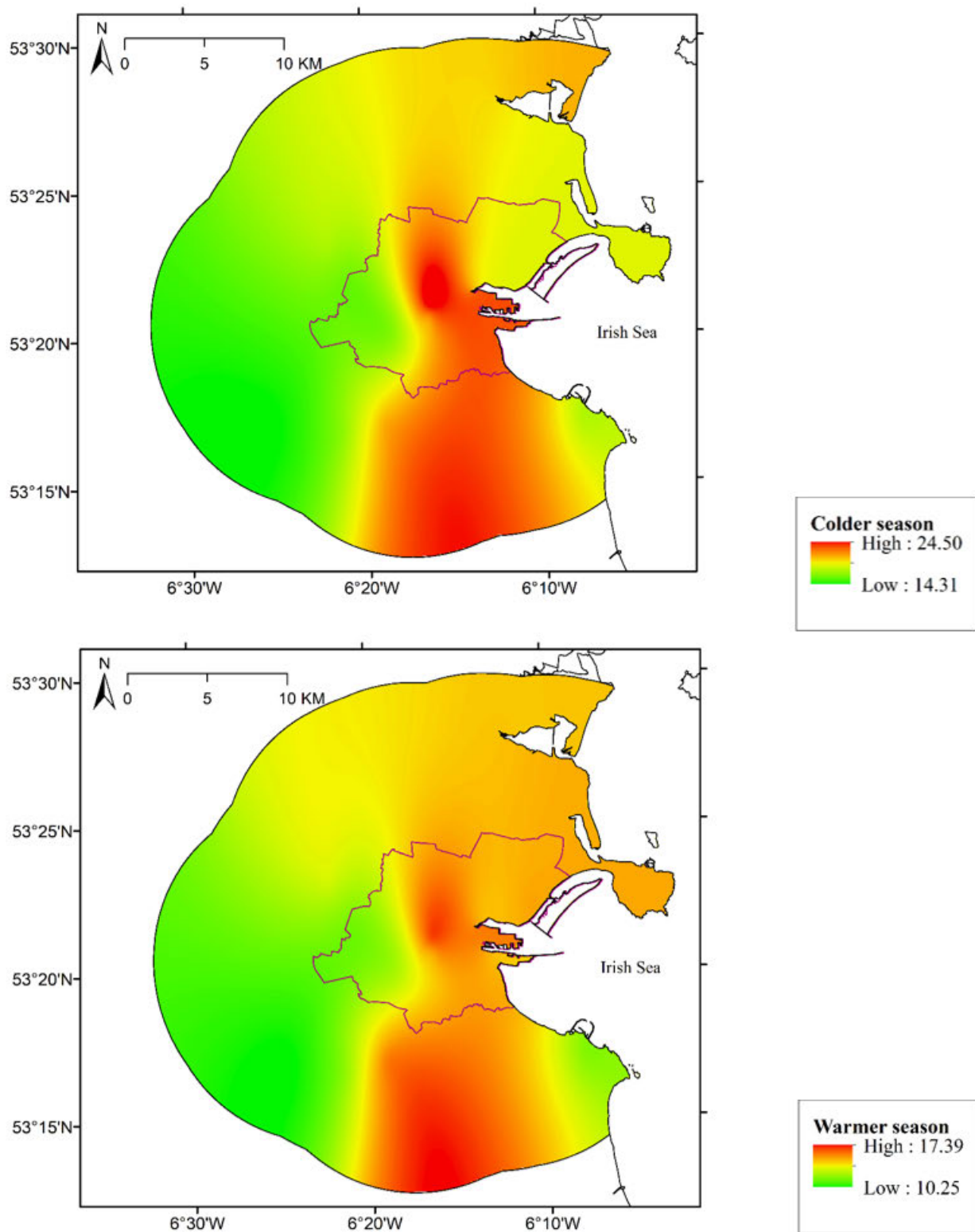
Figure 67: Spatial variation of PM$_{10}$ concentration obtained for the colder and warmer season using WSVR based LUR model prediction (source: own account).

5 Assessments of AQ and UHI for the City of Guildford

This part of the report includes two types of assessments, i.e. to provide indications on the impacts of GI on (i) air quality (AQ), and (ii) Urban Heat Island (UHI) in iSCAPE city Guildford.

Following Table provides an overview of the model simulations presented in the following sections to tackle the two assessments.

City/Scale	Modelled scenarios	Software
Guildford: Urban scale	1. 2015-BASE- Baseline scenario for the year 2015 with existing vegetation 2. 2015-BASE-NoGI- the year 2015 without any GI.	ADMS-Urban
Guildford: Urban scale	1. Existing baseline scenario with existing vegetation. 2. The scenario with No Green Infrastructures (GI).	ADMS-Urban Temperature and Humidity Module (ADMS-TH)

Table 23. Overview of model simulations carried out in Guildford and presented in the following sections (source: own account).

5.1 Air quality assessment for Guildford

The present study is primarily targeted at accessing the potential of urban vegetation or green infrastructure (GI) in helping cities and boroughs in the UK to comply with the UK air quality standard for NO_2 concentration around roads - the only standard that UK is currently failing to meet (DEFRA, 2017) and also assess the reduction in PM_{10} as well as $PM_{2.5}$ concentration. For example, in the borough of Guildford, an estimated 52 roads exceeded the annual mean limit (40 $\mu g/m^3$) for NO_2 in 2017. In order to comply with the current and future air quality standards, the UK government is undertaking several nationwide programs, which include fleet modernisation and promoting public transportation. Despite those efforts, it is estimated that 45 roads in Guildford will exceed the annual mean limit for NO_2 in 2020 falling to 27 roads in 2030 (DEFRA, 2017). Since high NO_2 concentrations occur in certain places due to highly localised reasons, the onus has been put on local authorities to tackle this issue through a host of innovative approaches such as planting new GI. Increasing vegetation can be an effective way of improving air quality and can assist the local city planners in meeting their air quality targets. The approach presented here (Section 5.1.1) may help in filling the existing knowledge gap on the efficiency of GI, which prevents the practical implementation. Therefore, through this investigation, we have evaluated the potential of existing urban vegetation in controlling the NO_x, PM_{10} and $PM_{2.5}$ concentrations for Guildford in 2015, which can serve as a case study for replication amongst other cities and boroughs across the UK and Europe. The year 2015 has been chosen to represent the current situation in Guildford since data for the model inputs are freely available for this year.

The current section focuses on the evaluation of the potential of existing urban GI in air quality. The aim of this study to estimate the reduction in pollutant such as NO_x, PM_{10} and $PM_{2.5}$ concentration levels in Guildford due to existing GI in and around in the year 2015. It also aims to estimate the amount of pollutant deposited over the surface offered by urban GI. To achieve the above-mentioned aims, air pollutant dispersion models had been set-up under two scenarios

(Section 5.1.5). Many previous studies used ADMS-Urban for air pollution dispersion modelling at the city scale (Barnes et al., 2014; Righi et al., 2009; Tiwary et al., 2009).

5.1.1 Description of the model

The area of interest in this study is the urban area of Guildford, which is a large town in Surrey county, located southwest of central London. The Guildford is one of iSCAPE city and town similar to other UK town with respect to land cover and meteorological condition. The integrated modelling approach described below will be used to study the air quality benefits of the existing vegetation cover for a 19 km × 26 km area that encompasses the complete Guildford borough in the UK (borough area = 270.9 km^2) as shown in Figure 68. The land use in Guildford is predominantly residential, and about half of the city's population (population estimated at around 130,000) lives within the urban area of Guildford town, located in the centre of Guildford borough (GBC, 2016).
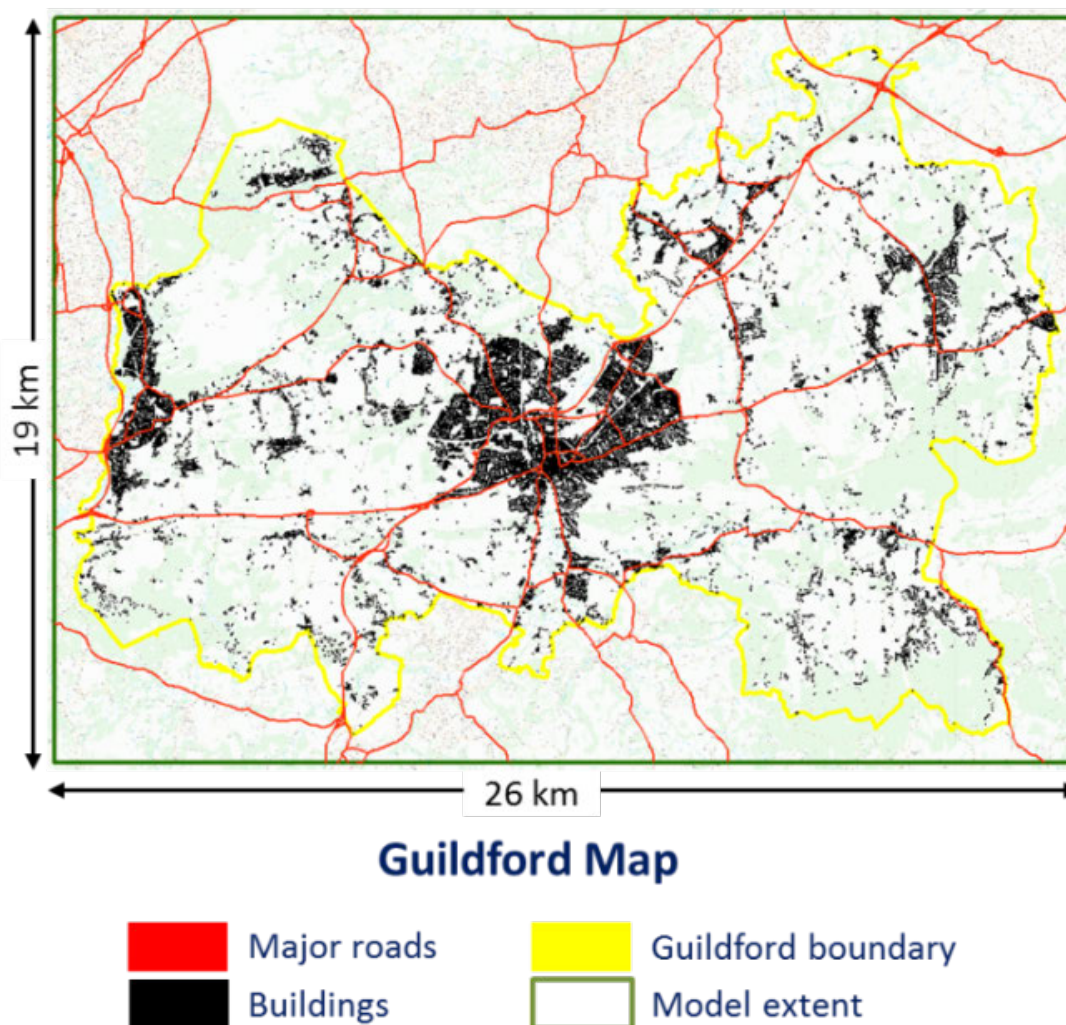
Figure 68: Modelled domain of Guildford borough along with the major roads and buildings (source: Website ordnancesurvey 2019).

To ensure the air quality in urban areas, it is required to assess the effect of development on air quality and enforce the counter measurement well in advance. In this study, we have assessed the potential of existing urban vegetation on air quality on the city-scale model with the help of integrated modelling approach that combines air quality maps generated through dispersion modelling by using Gaussian plume model (ADMS-Urban) and air pollutant concentration maps based on pollutant deposition over vegetation as source in dispersion modelling (Eq. 31). Mathematically,

$$C_{ij} = \sum_{m=0}^{n} D_j \ (1 - v_{dj})$$

(31)

Where C_i is the resultant concentration of air pollutant species i at point j, Dj is the total concentration of air pollutant species i at point j from n number of air pollution sources, v_{dj} is the deposition velocity of air pollutant i at point j.

The Gaussian plume model has been chosen to reduce the simulation time and resource instead of other modelling approaches such as CFD. For instance, Jeanjean et al. (2017) reported CFD simulation time of 3 days for domain size of 3.2 x 2.6 km^2 for air pollutant dispersion modelling in London. On other hand, the United States Forest Service developed i-Tree tool has been used to estimate the annually-averaged air pollutant removed by deposition over GI canopies (Nowak, 1994). However, i-Tree is unavailable to capture the reduction in air pollutant concentrations due to enhanced atmospheric dilution through increased surface roughness. Furthermore, the below approach has been used because many Gaussian plume models such as RLINE, ADMS-Road, CALPUFF including AMDS-Urban either neglect the dry deposition or assume constant throughout the domain which leads to uncertainty in the estimation of air pollutant concentration levels.

5.1.2 Model set-up

This detailed approach for assessing the effect of GI on air quality consists of a series of steps:

Step 1: Development of the spatio-temporal air quality maps for Guildford by using traffic emission as a prime source and other sources as background for air pollutant dispersion in ADMS-Urban. The other influential parameters (meteorology, topography and land cover) are provided as meteorological data, terrain data and surface roughness respectively as inputs in the ADMS-Urban.

Step 2: Estimation of air pollutants deposition over the vegetation surface according to land cover, pollutant concentration (from step-1) and meteorological condition.

Step-3: Development of the spatio-temporal air quality maps by using air pollutant deposited amounts (as grid sources) in ADMS-Urban. The other influential parameters are kept the same as in step (1) as inputs in the ADMS-Urban.

Step-4: Assessment of the air quality due to the presence of urban GI by combining the air quality map from Step 1 and Step 3.

Step 5: Development of air quality for Guildford same as step-1 with altered surface roughness to take account the absence of GI.

Step 6: Comparison of the pollutant concentrations in Guildford with and without vegetation under the different scenarios (Section 5.1.5) to assess the effects of a proposed vegetation planting strategy on air quality.

5.1.3 Model input

Traffic: Road traffic is the major source of air pollution in Guildford (GBC, 2016), and the major roads (M roads, A roads, and B roads) in Guildford are shown in Figure 68. In the modelled domain, there are 16.6 km of M roads (motorways) and 232.9 km of A roads, henceforth referred to as "major roads", 99.6 km of B roads and C roads (classified unnumbered), henceforth referred to as "minor roads", and 1379.0 km of U roads (unclassified unnumbered); henceforth referred to as "Local roads". A majority of the traffic volume passes through the major and minor roads; whereas local roads have relatively much lower traffic volumes. In order to estimate the pollutant emissions from the roads, the EFT (Emissions Factors Toolkit) v8.0.1 developed by DEFRA (2016) is used, which requires vehicle counts, fleet composition, and traffic speed as inputs (Mumovic et al., 2006). We obtained the data for the traffic counts and fleet composition in Guildford from the Department for Transport (DfT; https://data.gov.uk/dataset/gb-road-traffic-counts), the UK which operates ~130 traffic counters for "major roads", and ~30 traffic counters for "minor roads". The traffic speed was taken to be the average traffic speed in the UK as from Table 24 (https://www.gov.uk/government/collections/speeds-statistics), and assumed to be constant on the roads. The road category is based on type on road (A, B, C, U and M roads) and locality (U-urban and R-rural).

Speed (Km/h)

Road Category	Vehicle Type				
	Car	Bus	Motorcycle	LGV	HGV
AU	48	41	48	48	41
AR	97	82	97	97	82
BR	24	21	24	24	21
BU	48	41	48	48	41
CR	24	21	24	24	21
CU	48	41	48	48	41
UR	32	27	32	32	27
UU	16	14	16	16	14
MM	97	82	97	97	82

Table 24: The speed of different vehicles based on the road category (source: own account).

Meteorology and topography: Meteorological variables such as wind velocity and direction, temperature, relative humidity, and cloud cover are required to solve the transport equations in the ADMS-Urban model. The hourly data for those variables were obtained for the year 2015 from

a weather station located in South Farnborough (latitude = 51:28N longitude = 00:77W, and altitude = 65 metres above mean sea level), which is at distance of 14.5 km from the centre of the modelled domain. The dominating wind direction was South-West as per wind rose diagram in Figure 69.

The land-cover data for the modelled domain was obtained for the year 2015 land cover map as shown in Figure 70, which is produced by the centre for ecology and hydrology (CEH), UK based on satellite imagery and digital cartography at a resolution of 25 m (Rowland et al., 2017). The domain was divided into seven types of land cover which are deciduous forest (Df), coniferous forest (Cf), grassland (Gl), rural surface (Rs), water surface (Wf), agriculture surface (Arf) and urban surface (Us). The percent land cover for the year 2015 in Guildford model domain mention in Table 25. The variable surface roughness value was used based on the type of land cover. The effect of variation in topography on dispersion was incorporated in the modelled domain by use terrain data for 2017, which is generated by the Ordnance Survey (OS) and available under Open Government Licence (https://www.ordnancesurvey.co.uk). It is assumed that the topography has negligible change over the year from 2015 to 2017. The geometry of roads has obtained the Department for Transport (DfT; https://data.gov.uk/dataset/gb-road-traffic-counts/resource/fe120864-7618-4da5-bcd7-c6fa06a3140d).

Land Cover	Percentage area	Land Cover	Percentage area
Grassland	37.8	Coniferous forest	8.2
Rural Surface	21.4	Urban Surface	2.2
Deciduous forest	20.3	Water surface	0.8
Agricultural Surface	9.2		

Table 25: Type of land cover and contribution to the total area (source: own account)
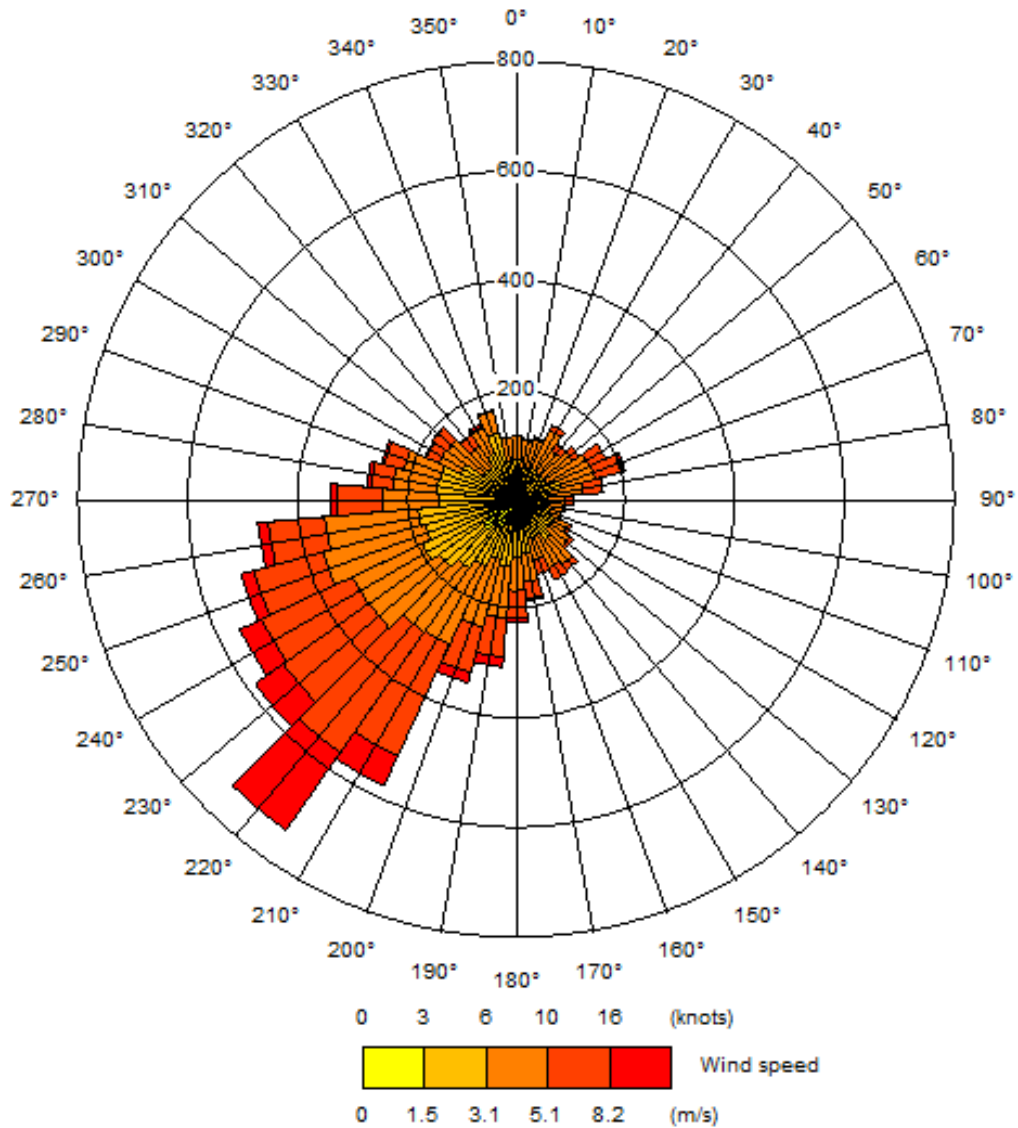
Figure 69: Windrose diagram at a 65m above mean sea level at South Farnborough meteorological station (source: Metrological department, UK).

| | Improved grassland | | Heather | | Heather grassland | | Sub-urban | | Broadleaved woodland | | Arable and horticulture | | Coniferous woodland | | Urban | | Freshwater |
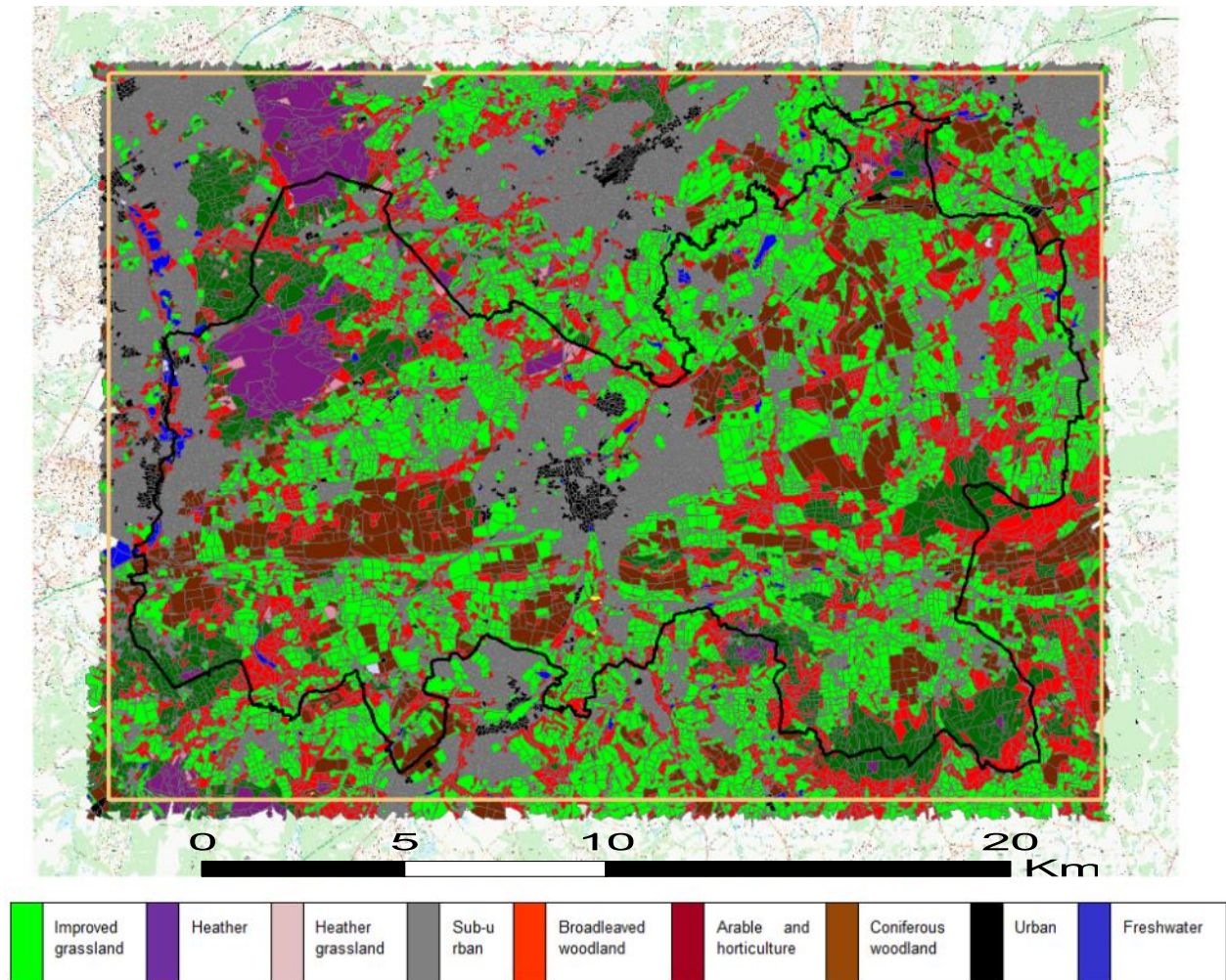
Figure 70: Map showing spatial distribution of different land covers at 25 m resolution in modelled domain over Guildford city (source: Digimap, UK).
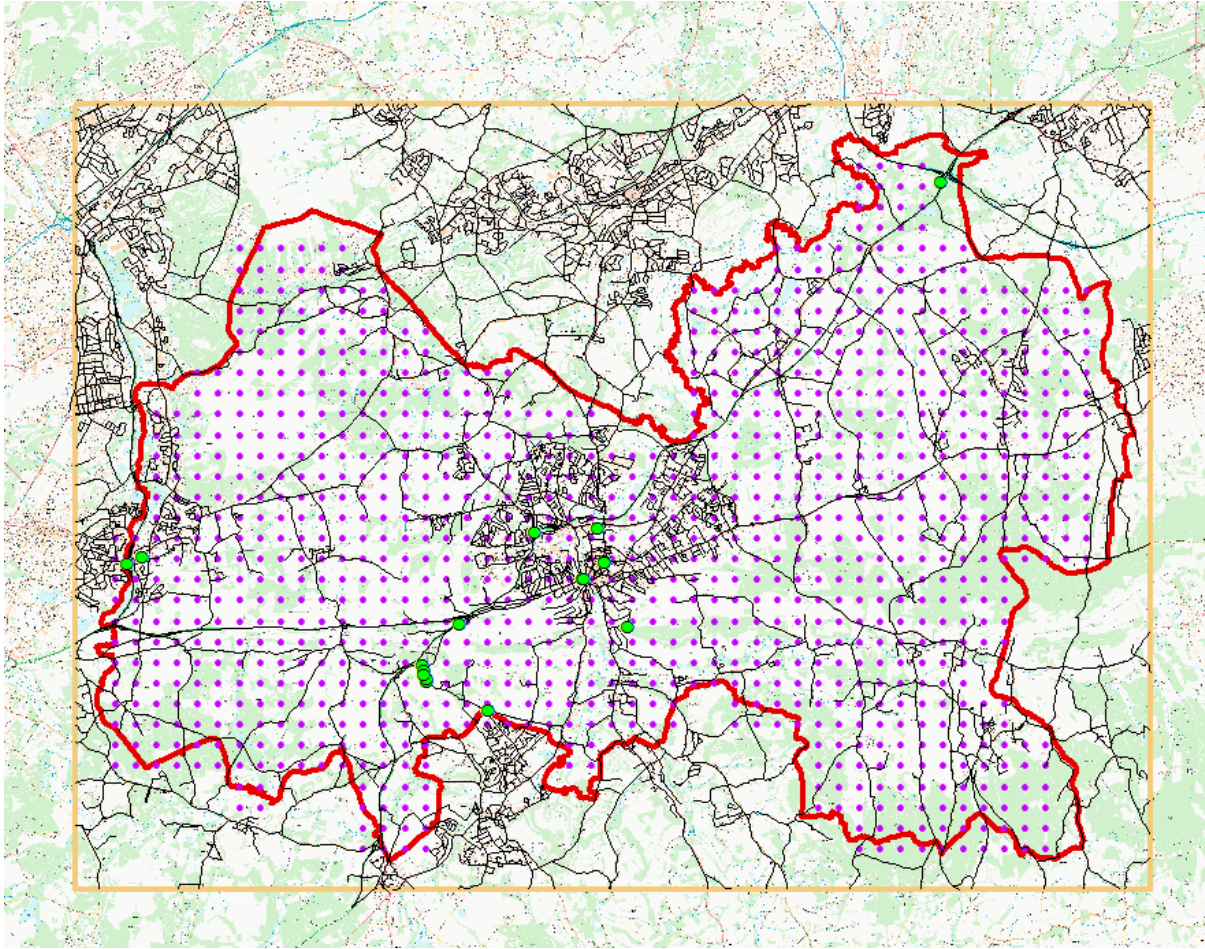
Figure 71: GBC monitored points (green) and output grid points (purple) along with the road network (source: own account).

Deposition Modelling: Urban vegetation such as urban forests, parks, gardens and hedges act as a sink for atmospheric pollutants. When harmful gaseous pollutants and airborne particles pass over the surface of vegetation, can be deposited over it. The deposited amount (F; g m^{-2}) to GI is proportional to the deposition velocity (V_d; m s^{-1}), time of exposure (t; sec) and pollutant concentration (C; g m^{-3}) (Bottalico et al., 2016; Jeanjean et al., 2016; Tiwary et al., 2009).

$$F = V_d \times C \times t$$

(32)

V_d for different gaseous pollutants (Eq. 3) can be calculated as the inverse sum of aerodynamic resistance (R_a; s m^{-1}), quasi-laminar boundary layer resistance (R_b; s m^{-1}) and canopy resistance (R_c; s m^{-1}) (Janhäll, 2015; Jayasooriya et al., 2017; Tallis et al., 2011; Tiwary et al., 2009; Wesely, 1989) and for particles (Eq. 4), the deposition velocity is estimated using virtual resistance ($R_a.R_b.V_s$), aerodynamic resistance and quasi-laminar layer resistance should be considered in a series and the whole term in inverse will be calculated in parallel to settling velocity (V_s) without canopy resistance (Seinfeld and Pandis, 2006; Wesely, 2000).

For gases:
$$V_d = \frac{1}{R_a + R_b + R_c}$$
(33)

For particles:
$$V_d = V_s + \frac{1}{R_a + R_b + R_a R_b V_s}$$
(34)

The year 2015 hourly meteorological data were used to estimate R_a and R_b (Tiwary et al., 2009) and R_c (for gases) was calculated depending upon land cover and seasonal category as per Wesely (1989). LCM2015 maps have 21 classes based on the UK terrestrial Broad Habitats (Jackson, 2000) and out of them, only nine classes are available in the modelled domain that has been divided into seven type of land cover. V_s (only for particles) was evaluated for particles diameter up to 50 mm according to the Stokes law (Eq. 5)

$$V_s = \frac{d_p^2 g (\rho_p - \rho_a) C_c}{18 \mu_a}$$
(35)

ρ_p is the density of the particles, ρ_a is the density of the ambient air, d_p is particle diameter, and g is the gravitational acceleration.

The total deposition of air pollutant over GI and other surfaces have been estimated by a combination of pollutant concentration level estimated by dispersion modelling and vegetation characteristics (deposition velocity). The sources are defined as area sources as land cover size, and exit velocity was taken as deposition velocity over the surface.

5.1.4 Methods of validation

The air quality modelling is the combination of dispersion and deposition modelling. The spatio-temporal deposition modelling was done by reverse dispersion modelling by ADMS- Urban. Model validation is performed (for 2015-BASE only) by comparing the model results for the annual mean hourly NO_x concentration in Guildford in 2015 (2015-BASE scenario described) with the corresponding concentrations measured at 17 different sites in Guildford as shown in Figure 71, as measured (diffusion tube) by the Guildford borough council (GBC, 2016) and modelled annual mean hourly background concentration for air pollutants NO_x, PM_{10} and $PM_{2.5}$ provided by Defra (https://uk-air.defra.gov.uk/data/laqm-background-maps?year=2015) for year 2015, as shown in Figure 72. Those measurements include roadside, urban background, and rural background concentrations of NO_2. The coefficient of determination (R^2) for modelled annual mean hourly concentration with GBC measured NO_x concentration was 0.74 (at red dots, air quality could be simulated through micro-scale model because these are near to traffic lanes) and with DEFRA modelled annual mean hourly concentration for NO_x, PM_{10} and $PM_{2.5}$ were 0.82, 0.81, and 0.75 respectively. In addition, the air quality model was further developed to evaluate the contribution of GI in improving the air quality in Guildford.
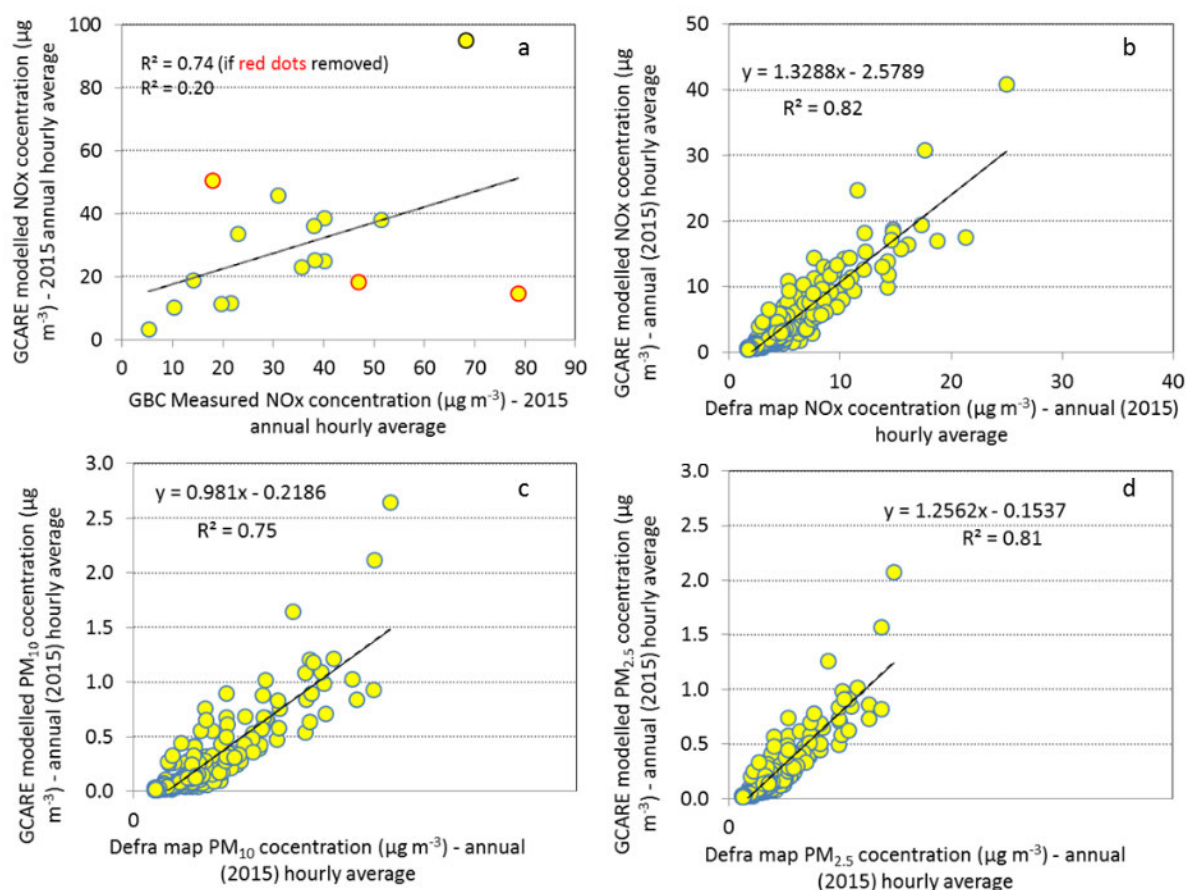
Figure 72: Comparison of modelled hourly average pollutants concentration for the year 2015 with a) GBC measured NO_x; b) Defra modelled NO_x; c) Defra modelled PM_{10} d) Defra modelled $PM_{2.5}$ (source: own account).

5.1.5 Scenarios

In order to evaluate the benefits of planting vegetation in Guildford vis-à-vis reducing the traffic-related air pollutants NO_x, PM_{10} and $PM_{2.5}$ concentration and complying with the relevant standards. We have investigated two scenarios with and without urban vegetation for the year 2015 as described below.

2015-BASE$_{AQ}$: This is the baseline case for the year 2015 with the currently estimated vegetation cover around Guildford city. The air quality is estimated by a combination of dispersion and deposition of air pollutant by ADMS-Urban.

2015-BASE-NoGI$_{AQ}$: This is a hypothetical scenario for the year 2015, which assumes that there does not exist any urban vegetation and land is covered by only urban area. This case has been estimated by changing the surface roughness to zero for existing vegetation throughout the domain. By comparing this scenario with the 2015-BASE, we will be able to estimate the air quality benefits provided by the existing GI in Guildford.

5.1.6 Modelled results and discussion

5.1.6.1 Spatial distribution of pollutant deposition

The spatial distribution of NO_x, PM_{10} and $PM_{2.5}$ depositions are shown in Figure 73. The preliminary results show that the vegetation has removed 1.16 t yr^{-1} km^2 NO_x, 0.18 t yr^{-1} km^2 PM_{10} and 0.06 t yr^{-1} km^2 $PM_{2.5}$ from the atmosphere. The deposition amount offered by vegetation is dependent on the percentage cover of GI and pollutant concentration level. The modelling approach used here for estimation of dry deposition, of NO_x, PM_{10} and $PM_{2.5}$, is as the inverse sum of all resistances (R_a, R_b, R_c) (Janhäll, 2015; Jayasooriya et al., 2017; Tallis et al., 2011; Tiwary et al., 2009; Wesely, 1989). The results indicate that maximum air pollutants concentration reduction is near the traffic source because the deposition amount is proportional to pollutant concentration. The PM_{10} removal rate for scenario-1 (2015-Base$_{AQ}$) is 0.002 t ha^{-1} yr^{-1} which is lesser than 0.004 t ha^{-1} yr^{-1} for Chicago (Nowak, 1994) and 0.009 t ha^{-1} yr^{-1} for Beijing (Laumbach et al., 2015) because of high wind velocity, in Guildford, reduces the deposition velocity. Furthermore, the removal rate of $PM_{2.5}$ is lesser than PM_{10} due to lower settling velocity for small particles. However, the net removal amount (0.06 t yr^{-1} km^2) of $PM_{2.5}$ is higher with compare to Nowak et al. (2013) studies for Los Angeles (0.013 t yr^{-1} km^2) and Atlanta (0.036 t yr^{-1} km^2) because this study also included the deposition over grassland which was neglected in other studies. Most of the studies used the UFORE model that has a number of assumptions to address the more complex deposition process. The UFORE model only estimates the dry deposition over GI and does not consider the effect of surface roughness that reduces the air pollutant concentration over GI due to the increase in atmospheric turbulence.
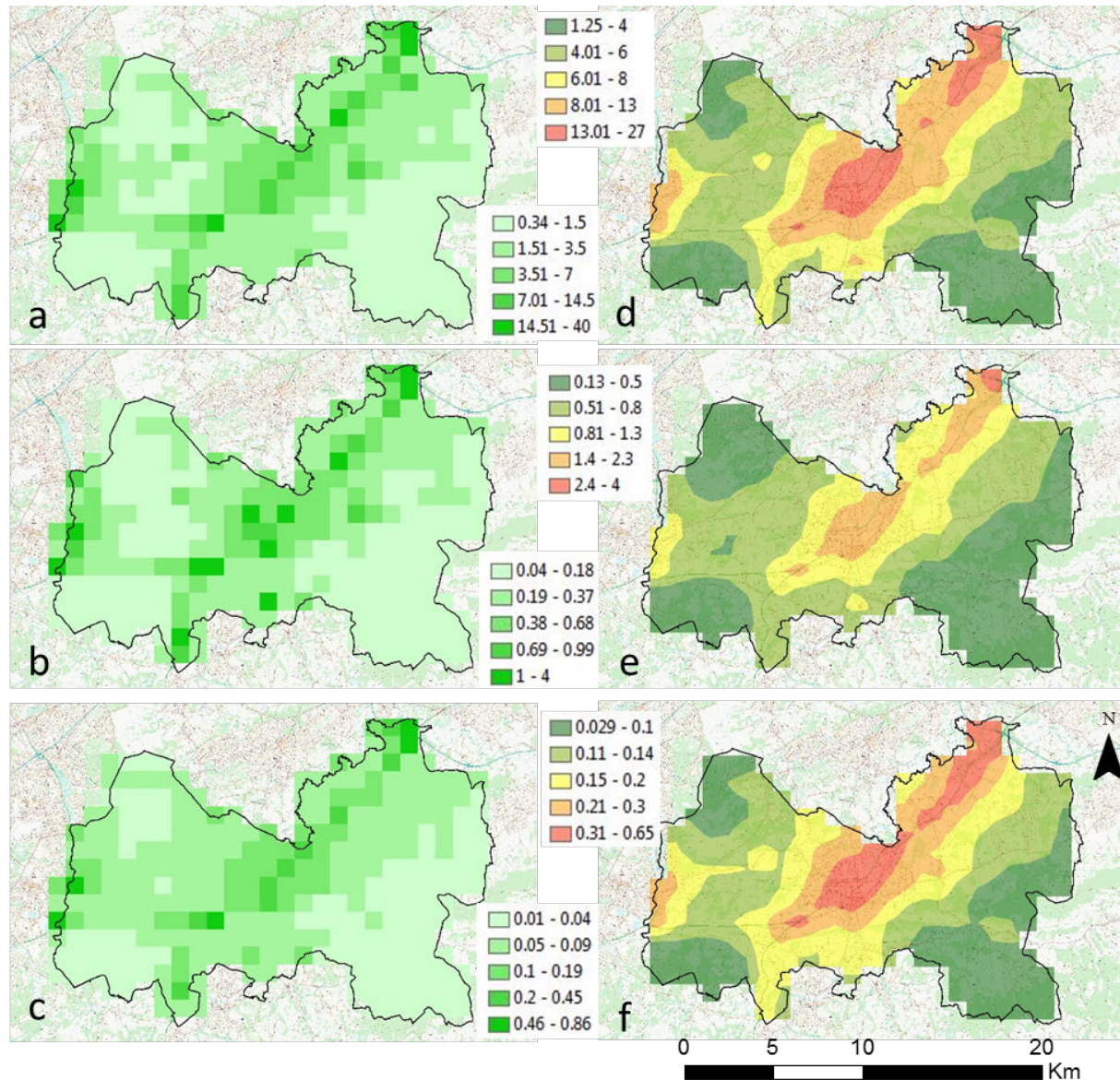
Figure 73: Spatial distribution of deposition (t yr^{-1} km^{-2}) in modelled domain over GI (a) NO$_x$ (b) PM$_{10}$ (c) PM$_{2.5}$ and hourly averaged concentration reduction (µg m^{-3}) in modelled domain for 2015 (d) NO$_x$; (e) PM$_{10}$ and (f) PM$_{2.5}$ (source: own account, data: City of Guildford).

5.1.6.2 Spatial distribution of pollutant concentrations reduction under different scenarios

The spatial distribution of NO$_x$, PM$_{10}$ and PM$_{2.5}$ concentration both with GI and without GI within study domain are shown in Figure 74. This study suggests that the level of pollutant reductions is dependent on the both percentage surface available for deposition and pollutant concentration (Table 26). The preliminary results show that the average hourly pollutants concentration reduction varies between 1.37-34.14 µg m^{-3}; 0.14-4.61 µg m^{-3} and 0.03-1.05 µg m^{-3} for NO$_x$, PM$_{10}$ and PM$_{2.5}$

respectively at height 1.5 m. The vegetation, due to higher deposition velocity, has relatively higher capacity to reduce NO_x concentration than PM_{10} and $PM_{2.5}$ concentration.
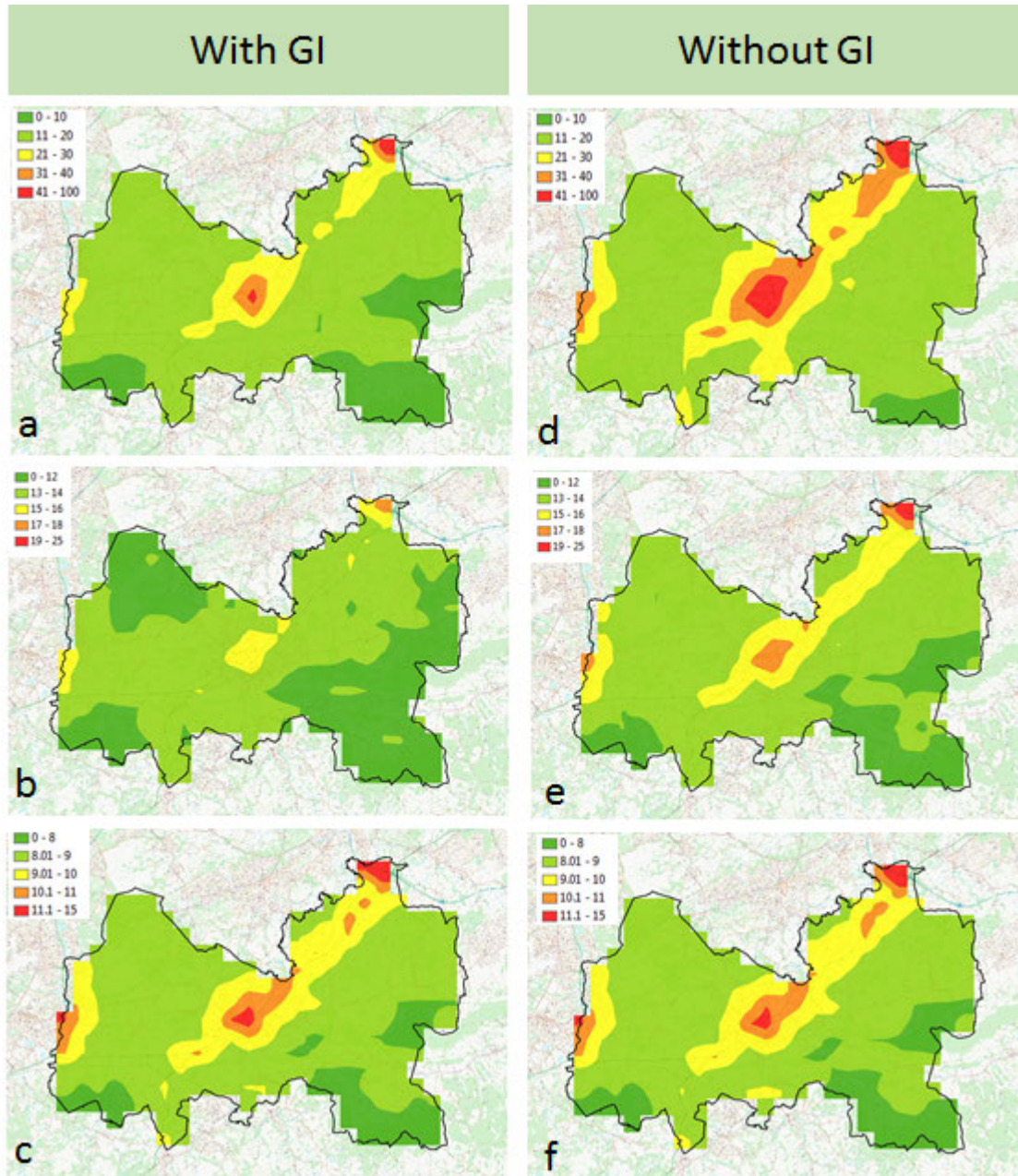
Figure 74: Hourly averaged modelled concentration (µg m⁻³) in modelled domain for 2015-BASE$_{AQ}$ (a) NO$_x$ (b) PM$_{10}$ (c) PM$_{2.5}$ and 2015-Base-NoGI$_{AQ}$; (d) NO$_x$; (e) PM$_{10}$ and (f) PM$_{2.5}$ (source: own account, data: City of Guildford).

Pollutant	NO_x	PM_{10}	$PM_{2.5}$
Max. Concentration without GI ($\mu g\ m^{-3}$)	73.66	19.97	12.76
Max. Concentration with GI ($\mu g\ m^{-3}$)	39.51	15.42	11.71
Max. Concentration reduction ($\mu g\ m^{-3}$)	34.15	4.61	1.05
Min. Concentration without GI ($\mu g\ m^{-3}$)	9.38	11.17	7.54
Min. Concentration with GI ($\mu g\ m^{-3}$)	6.81	11.00	7.49
Min. Concentration reduction ($\mu g\ m^{-3}$)	1.37	0.14	0.03

Table 26: The maximum and minimum pollutant concentration levels and reductions (source: own account).

Two scenarios 2015-BASE$_{AQ}$ and 2015-Base-NoGI$_{AQ}$ have been simulated to assess the impact of GI on urban air quality and preliminary results have been discussed. These scenarios are developed to assess the effect of GI on Guildford is air quality through integrated dispersion-deposition modelling. The input parameters such as traffic emission, metrological, topographical, surface cover data have been collected from different sources, and air quality have been simulated for Guildford city in 2015. The sources of NO_x, PM_{10} and $PM_{2.5}$, were modelled using ADMS-urban (4.1, Cambridge Environmental Research Consultants, UK) to calculate the pollutant deposited amounts and annual hourly pollutants concentration for the year 2015 at height 1.5 m (human breathing zone) for 494 km^2 study area. The computational model has been validated against measured NO_x concentration by GBC and background concentration modelled by DEFRA for NO_x, PM_{10} and $PM_{2.5}$. The coefficient of determination (R^2) for modelled concentration with GBC measured NO_x concentration was 0.74 (at red dots, air quality could be simulated through micro-scale model because these are near to traffic lanes) and with DEFRA modelled concentration for NO_x, PM_{10} and $PM_{2.5}$ were 0.82, 0.81, and 0.75 respectively.

5.2 UHI assessment for Guildford

The urban population growth had led to a prerequisite for infrastructure development causing drastic changes in urban climate (Guildford Society, 2014) by rising the temperature in urban areas than the rural areas. The temperature difference between urban and rural areas occur majorly due to the properties of urban fabric, surface materials capacity to absorb, store and release the incoming solar radiation, which implies that more thermal energy is stored in urban areas. Buildings and other urban fabrics generally have a lower albedo than vegetation and thus cooling is slower in urban areas (Oke, 1982, 1995). Consecutively, local morphology of the urban areas and its characteristics such as building density, height to width ratio (Svensson, 2004), in addition to the emissions from various anthropogenic activities (vehicles, industries and air conditioners) plays a vital role in increasing the urban heat and causing a significant rise in air temperatures (Hinkel & Nelson, 2007). Additionally, the lack of vegetation and moisture in the urban surfaces reduces the evapo-transpiration process (Akbari, Pomerantz & Taha, 2001), which leads to a decline in the heat transfer process leaving more thermal energy to the city, which in turn creates urban heat islands (UHI). The project iSCAPE and its objectives addresses the various factors accountable for deteriorating the quality of air and effects of UHI formation in micro environments. The need for effective ways to estimate and reduce the urban temperature had been formed up with solutions involving implementation of GIs. In this regard, this deliverable examines and discusses the effect of these GI's on urban heat island (UHI). Numerous studies on UHI shows a robust relation between urban area and its characteristics to the rise in temperatures at an urban scale (Roth & Chow 2012; Maggiotto et al., 2014; Jin et al., 2018), since these urban areas were found to contribute around 70% greenhouse gas emissions from the anthropogenic activities in urban areas (Hien & Ignatius, 2016).

The current deliverable emphasizes the need for implementing GI's on a city scale and estimate the perturbations in local temperature in the view of improving the air quality and to reduce the effects of UHI. Furthermore, suitable scenarios will be constructed to estimate the effect of GI's on an urban scale. Simuilar to what done in Bologna, the modelling in Guidlford has been carried out using a dispersion model ADMS (Atmospheric Dispersion Modelling System) developed by Cambridge Environmental Research Consultants (CERC, http://www.cerc.co.uk/). The present investigation utilizes ADMS-TH (ADMS-Temperature and Humidity Module) a deterministic model, which calculates land-use related temperature perturbations relative to upwind meteorological conditions. The model utilizes morphological and meteorological inputs with spatially varying data relating to surface properties (albedo, thermal admittance, surface resistance to evaporation, normalized building volume and surface roughness) to define the capacity of various urban building materials to absorb, store and reradiate heat. Hence, the proposed study approach will enable us to achieve the objective to estimate and highlight the impact of GI's and its necessity on reducing UHI effects by relating with existing scenario

5.2.1 Description of the model

The area of interest in this study is the urban area of Guildford, which is a large town in Surrey County, located southwest of central London. Guildford is one of the target city in iSCAPE project and a town similar to other towns in UK with respect to land cover and meteorological condition. The land use in Guildford is predominantly residential, and about half of the city's population (population estimated at around 130,000) lives within the urban area of Guildford town, located in the centre of Guildford borough (GBC, 2016). Guildford's climate is classified as warm and

temperate and categorized as Cfb (Marine west coast climate) by the Köppen-Geiger classification system. The temperatures are highest during June-July with an average temperature of around 17.4 °C.
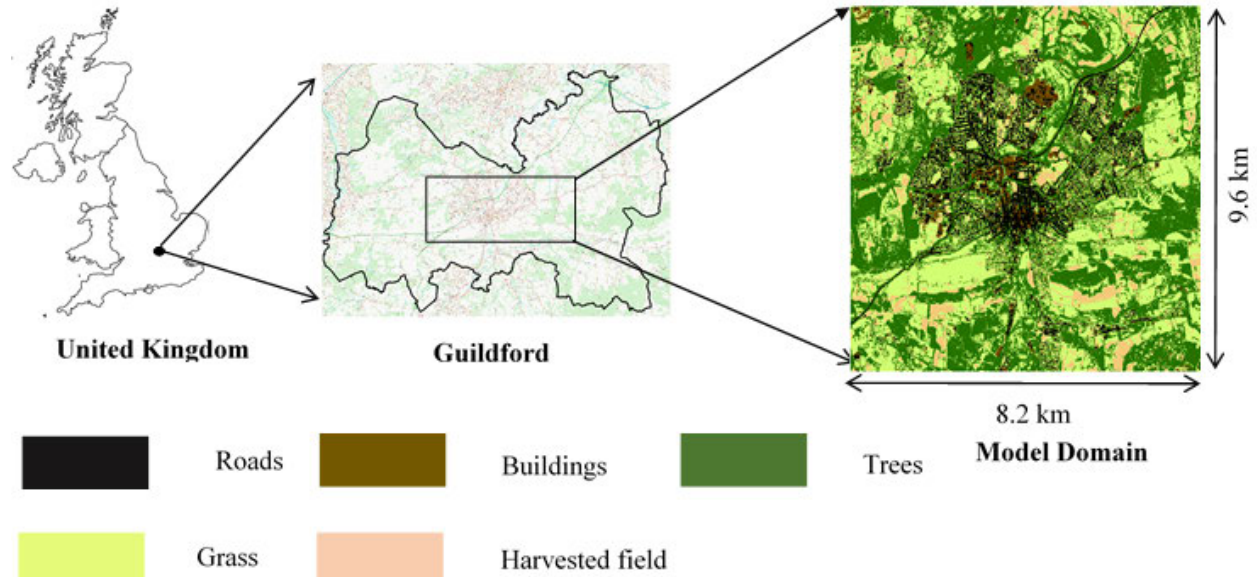
Figure 75: Land use data for Guildford with a resolution of 10m×10m (source: own account, data: City of Guildford)

The modelling has been carried out using a dispersion model ADMS (Atmospheric Dispersion Modelling System) developed by Cambridge Environmental Research Consultants (CERC, http://www.cerc.co.uk/).
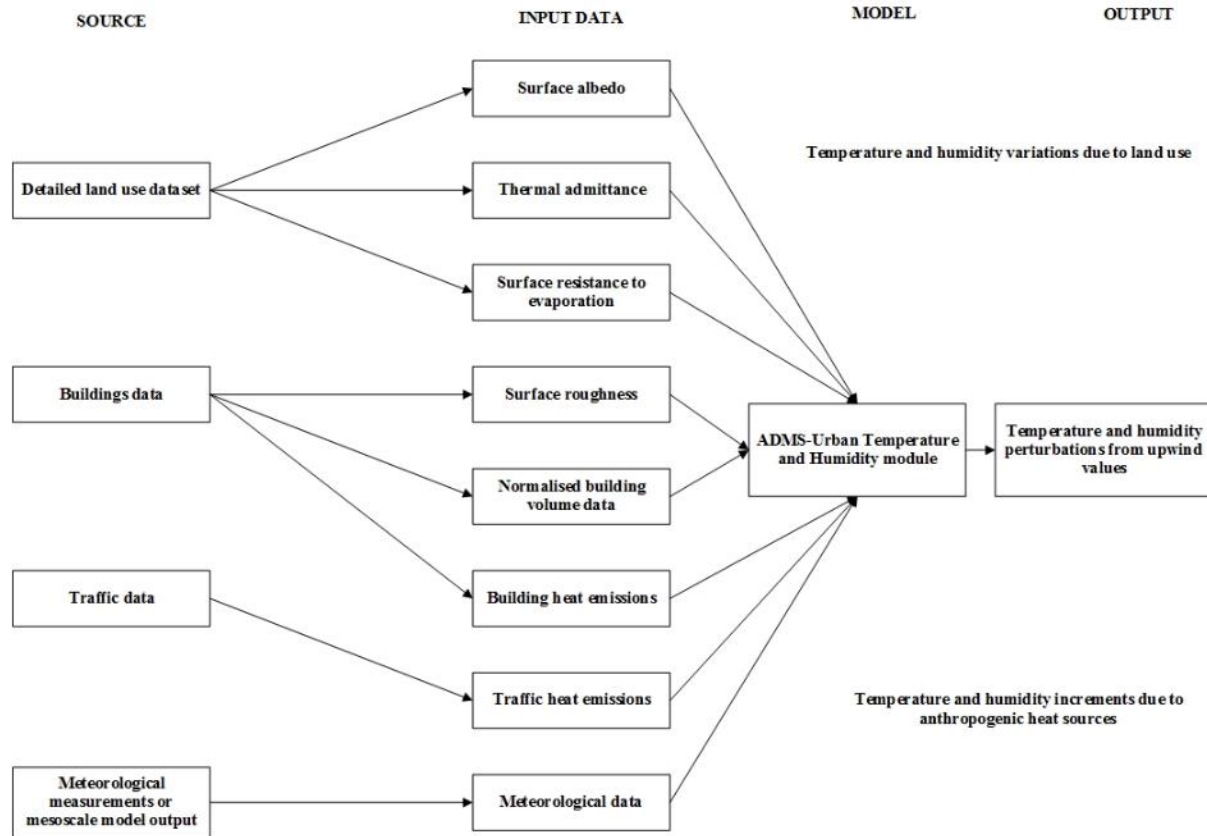
Figure 76: Schematic representation of ADMS-TH model process (source: own account, adapted from CERC)

ADMS meteorological pre-processing module (Thomson, 2010) has been adapted with outputs from LondUM model and ADMS module for flow over complex terrain. These have been modified to calculate perturbations of temperature (ϑi) and humidity ($q i$) (Carruthers, D J Weng 1992). ϑi and $q i$ are calculated from the governing conservation equations using the uncoupled variables a and b in Fourier space, which are related to ϑi and $q i$ over the complex surface by

$$\vartheta_i = \frac{a+b}{pC_p\,(S+1)}$$

(36)

and

$$q_i = \frac{Sa-b}{p\lambda\,(S+1)}$$

(37)

$$S = (\lambda/C_p)dq_3/dT$$

(38)

where S is evaluated at T = T_0, q_s is the saturated specific humidity at temperature T, Cp is the specific heat capacity of air, ρ is the density of air and λ is the latent heat for the vaporization of water. The model takes the inverse Fourier transforms and calculate the perturbations in potential temperature (ϑ_i) and specific humidity (q_i).

5.2.2 Model setup

Simulation runs using ADMS-TH were done with a domain size of 9.6×8.2 km, meshed by a resolution of 10m × 10m covering the major part of urban areas in Guildford (Figure 75: Land use data for Guildford with a resolution of 10m×10m (source: own account, data: City of Guildford)). According to the obtained land use data, (buildings, roads, trees, grass and harvested field), each cell in the computational grid is allocated with a weighted average value of each parameter (albedo, surface resistance to evaporation, thermal admittance, normalised building volume and surface roughness) (CERC, 2018; Hamilton et al., 2014). The hourly meteorological data for the year 2015 acquired from Farnborough meteorological station (www.metoffice.gov.uk/public/weather/forecast/map/gcp7wrjcg#?map=SignificantWeather&zoom=8&lon=-0.77&lat=51.28&fcTime=1550437200) has been used, which includes wind velocity and direction, temperature, cloud cover and relative humidity.
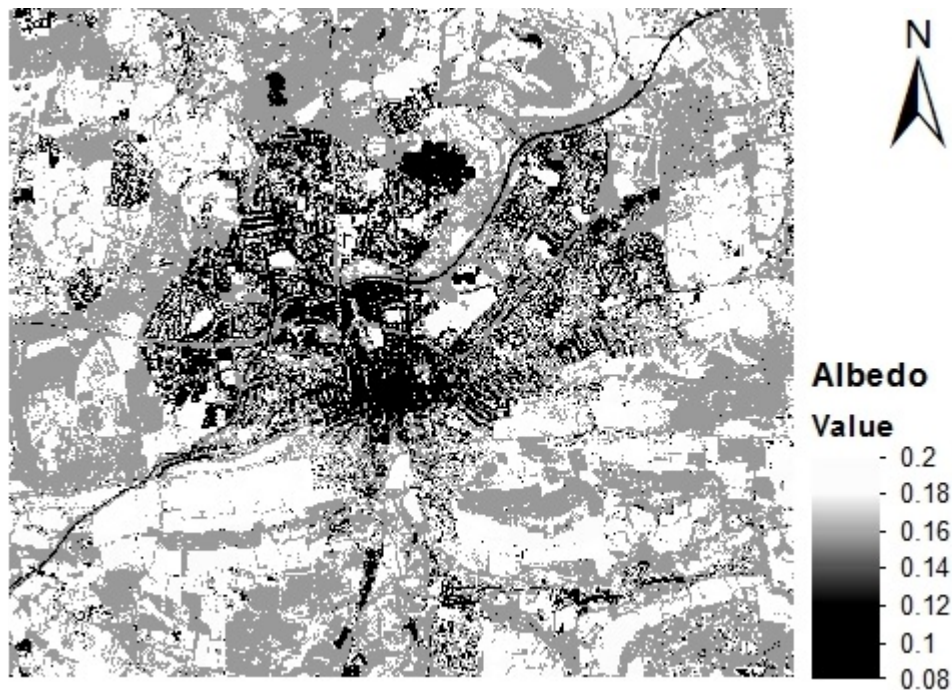
Figure 77: Map of Albedo (source: own account, data: City of Guildford).
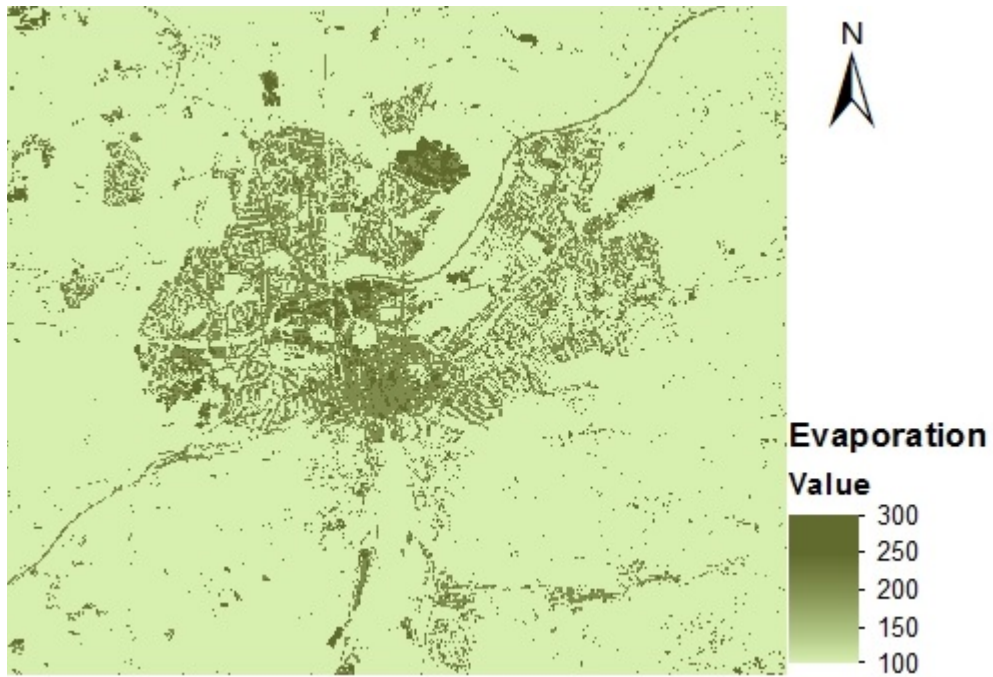
Figure 78: Map of surface resistance to evaporation (source: own account, data: City of Guildford)
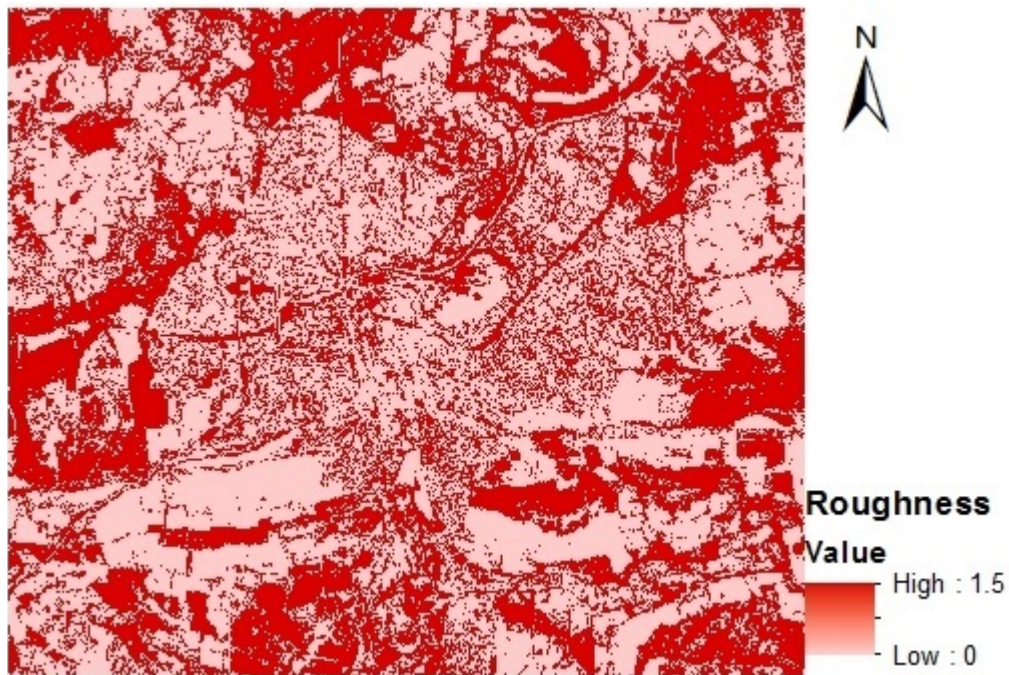
Figure 79: Map of surface roughness (source: own account, data: City of Guildford)
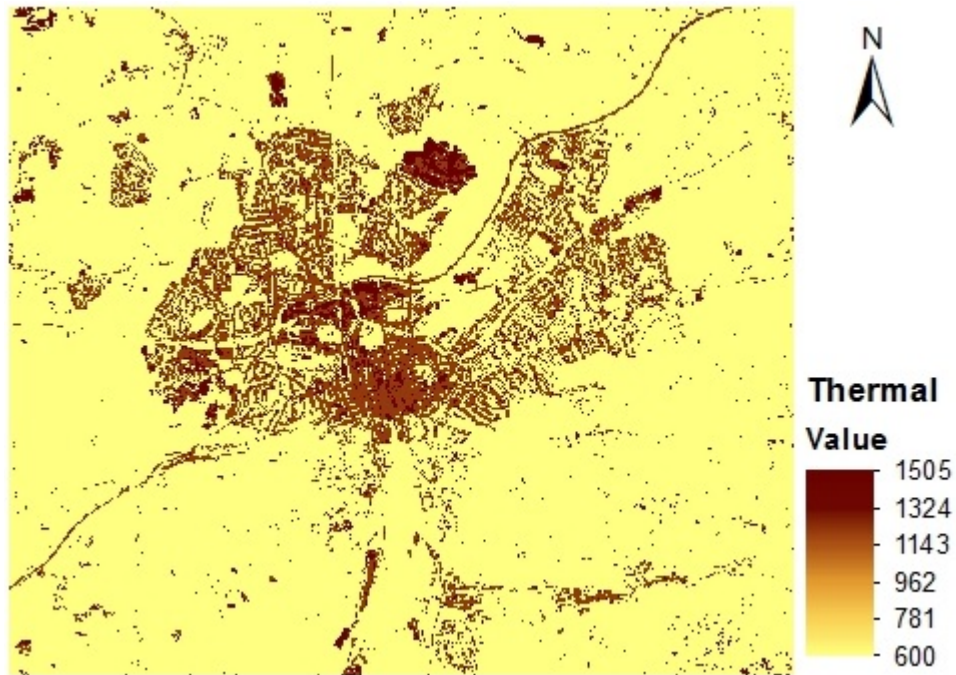
Figure 80: Map of thermal admittance (source: own account, data: City of Guildford)
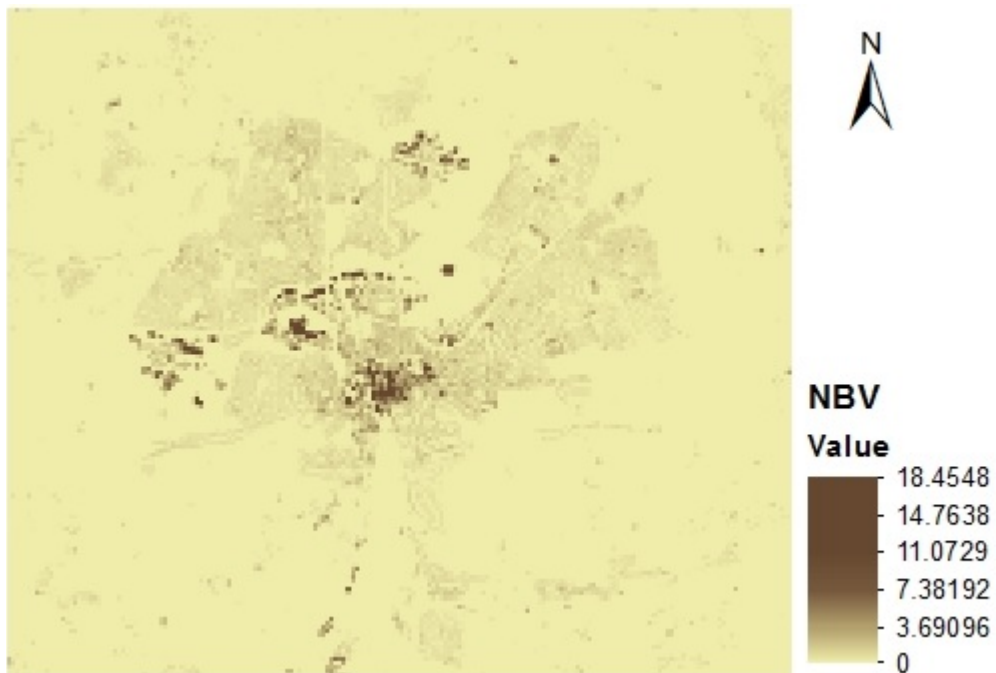
Figure 81: Map of normalized building volume (source: own account, data: City of Guildford)

5.2.3 Model input

5.2.3.1 Meteorological and spatial variation

The model requires spatial variation of surface properties within the model domain, especially input parameters such as surface resistance to evaporation, thermal admittance, albedo and surface roughness (Figure 77-Figure 81). The other meteorological data such as wind speed, wind direction and temperature are obtained from the meteorological station (outside the modelling domain) as discussed in section 5.1.3.

The above-mentioned parameters will be calculated using the land use pattern and morphology of the domain of interest. In this context, the present study utilizes the land use pattern to analyse and estimate the surface properties within the model domain.

5.2.3.2 Anthropogenic heat inputs

The local temperature perturbations for any urban area does not depend only on land use and meteorological changes, but also with heat generated from anthropogenic emissions. Vehicular emissions from the roads and building heat emissions were found to be major in any urban area. Hence, the ADMS-TH model defines a heat concentration parameter which is compared with pollutants emissions such as CO_2. Furthermore, the model assumes the heat dispersion in way similar to dispersion of air pollutants by using Gaussian plume dispersion model to forecast the anthropogenic heat distribution from buildings and roads.

A count of vehicles with respect to the roads covering the urban area had been carried out and normalised building volume for Guildford urban area had also been calculated to estimate the emissions input for modeling the UHI.

5.2.4 Scenarios

The UHI and its intensity to raise the temperature of any built environment should be predicted approximately for the study area, Guildford. An inclusive set of future control scenarios have been made and simulated to find the effects of various morphological changes for the town.

The study for the existing scenario had been carried out and a suitable future scenario have been made and modelled and simulated to estimate and predict the changes in UHI for Guildford.

2015-BASE-GI$_{UHI}$: The baseline scenario simulations were run using the existing land use pattern and vegetation cover for the year 2015. UHI formation and its effect of temperature perturbations were simulated and analysed using ADMS-TH.

2015-BASE-NoGI$_{UHI}$: No-GI scenario is constructed from 2015-BASE-NoGI$_{UHI}$ except for the change in GI's (replacing the existing GI into urban structures).

The proposed scenarios and their impacts are analysed to understand the temperature perturbations created by the existing urban areas on UHI and local meteorology.

5.2.5 Model validation and verification

Conventionally UHI validation has been carried out by comparing the temperatures observed at independent sites with the modelled temperatures (Farhadi et al., 2019; Hamilton et al., 2014; Maggiotto et al., 2014). Unfortunately, there are no meteorological stations within the modelled domain. Therefore, a regional scale atmospheric reanalysis dataset (the COSMO-REA6) was used as validation data. Various aspects of the Consortium for Small-Scale Modelling (COSMO) model, which is used for filling the space and time between the observations, has been validated in a range of previous studies (Baldauf, 2019; Duniec and Mazur, 2018; Klasa and Walser, 2018; Kunz et al., 2017; Shrestha et al., 2018) and this model is therefore used for the present validation exercise.

5.2.5.1 COSMO-REA6

The COSMO-REA6 is an atmospheric reanalysis dataset with a spatial resolution of 6 km and a temporal resolution of 15 mins for 2D fields such as temperature. The high spatial and temporal resolution allows the comparison between the ADMS calculations and the reanalysis dataset. In this dataset, the COSMO Limited Area Model has been used to fill the space and time between observations in an physically consistent fashion. The measurement data are assimilated into the model through a nudging approach described in (David R.Stauffer and Nelson L.Seaman, 1989; Davies, 1977). The observations used as input for the data assimilation come from the German Weather Service's operational database. The initial and boundary conditions are interpolated from the ERA-Interim dataset (Dee et al., 2011). The first year of the reanalysis is 2011, so there should not be any effects of spin-up in the data for the present study from 2015.

5.2.5.2 Validation using Reanalysis data (Temporal variability and Correlation analysis)

The simulation runs using ADMS-TH had been carried out for specific grid points for a 4 day period (01/06/2015 to 04/06/2015) corresponding to the coordinate system used in COSMO REA6. The data obtained from COSMO REA is for a 6km grid size at a height of 2m from the ground and the ADMS modelling domain has a grid size of 10m × 10m. Though the grid size is not identical, the data had been extracted from identical points in the grids from both the domains for comparison. The data from COSMO-REA6 is obtained in GRIB 1, a rotated spherical format which has been converted to netcdf format and the extracted data is compared with the modelled measurements. The time series plot (Figure 82) shows a uniform pattern between the observed data and the modelled data and the trends are found to be similar. However, the diurnal cycle shows strong similarities among the datasets.
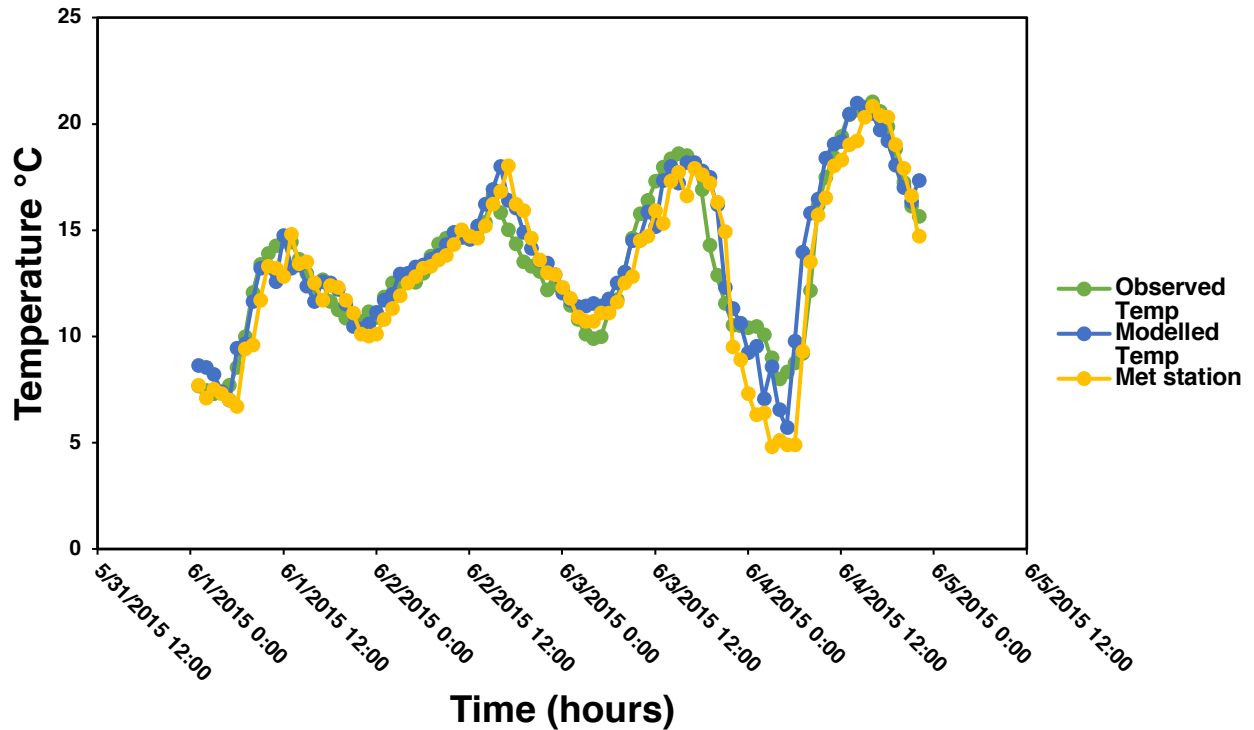
Figure 82: Temporal variation of observed temperatures from COSMO REA6 (green line) and modelled temperatures from ADMS-TH (blue lines) and met station data from Farnborough station (yellow line)

Apart from the time series plot, a residual plot (Figure 83) with residuals of modelled (ADMS-TH) temperatures and residuals of observed (COSMO REA 6) temperatures and Met station data (Farnborough station) has been plotted to study the variation among COSMO REA6 and Met. Station datasets. The linear lines in the residual plot depicts the variation among COSMO REA6 and Farnborough station data. It is clearly evident that the bias between observed (COSMO REA6) and modelled (ADMS-TH) is lower compared to the residual plot between observed (COSMO REA6) and met station data (Farnborough station). This plot shows that, the residuals from observed and modelled temperatures is not showing substantial temporal trend which confirms the performance of the ADMS modelling.
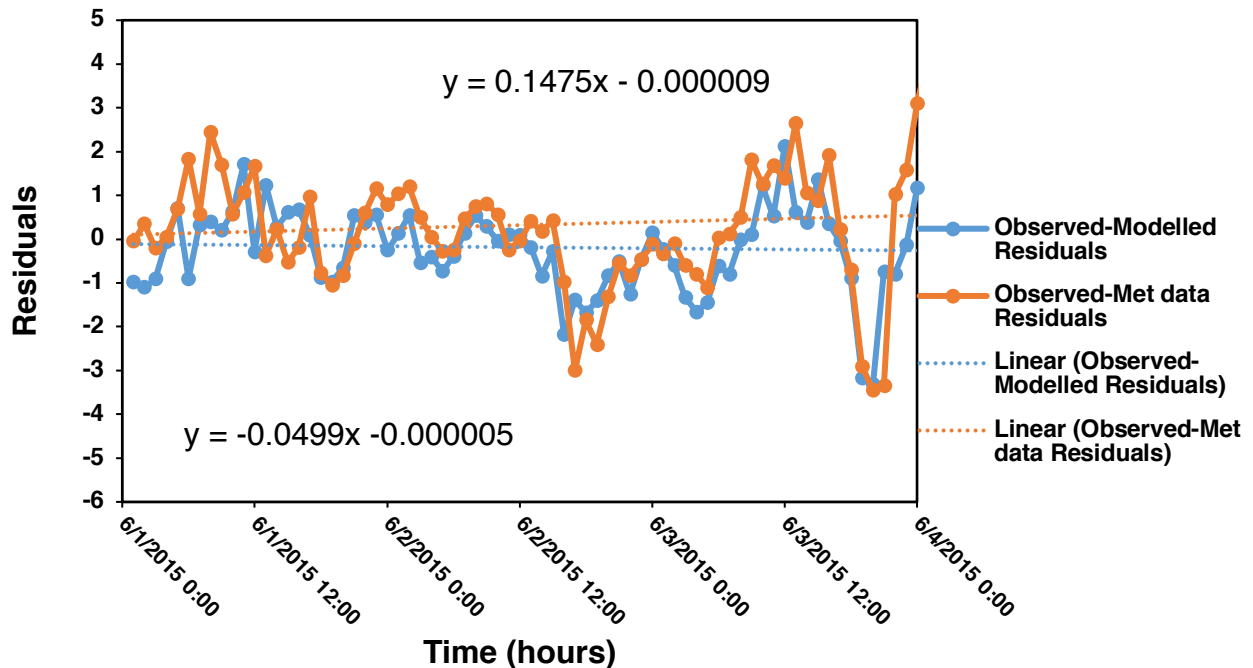
Figure 83: Residual plots between observed temperatures (COSMO REA6) and modelled temperatures (ADMS-TH) (blue line) compared with residuals from Observed temperatures (COSMO REA6) and met station data from Farnborough station (Orange line).

The observed and modelled datasets are further subjected to statistical analysis to determine the correlation among them. The coefficient of determination (R^2) is calculated to estimate the correspondence between the measurements. This analysis will further pose tangible reasons to show the model validity. The scatter plot (Figure 84) between the observed and modelled temperatures resulted in an R^2 value of 0.89. In addition to that, certain other statistical investigations have also been carried out to further support the data validation(Hanna et al., 1991; Kumar et al., 1993).

Statistical Parameters	Obs (COSMO REA 6) – Model (ADMS-TH)	Obs (COSMO REA 6) - Met data (Farnborough)
Mean Absolute Deviation (MAD)	0.844	1.096
Mean Squared Error (MSE)	1.425	2.281
Root Mean Square Error (RMSE)	1.194	1.510
Mean Absolute Percentage Error (MAPE)	7.090	9.073

Fractional Bias (FB)	-0.015	0.030
Geometric Mean Bias (MG)	0.985	1.030
Geometric Mean Variance (VG)	0.970	1.061

Table 27: Comparison of statistical parameters between Observed (COSMO REA 6) and Modelled (ADMS-TH) and met station data (Farnborough station).

The statistical analysis (Table 27) substantiates the agreement between the two datasets. The statistical parameters clearly show that the data obtained from COSMO REA6 can be used for validating the modelled data (ADMS-TH) of the present study.
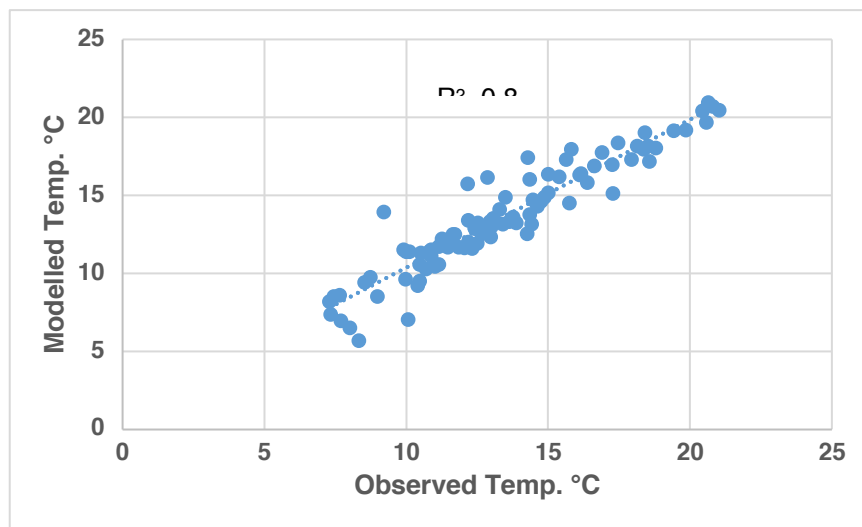
Figure 84: Scatter plot comparing observed temperatures (COSMO REA6) and modelled temperatures (ADMS-TH)

5.2.6 Modelled results and discussion

The ADMS-TH has been used to calculate the temperature perturbations due to land use and anthropogenic heat emissions (Building and Vehicle emissions) for Guildford. The temperature predictions have been carried out for hourly basis on a regular output grid. The modelling was carried out for June 2015 which falls as the first month of summer in Guildford. The modelled results would portray the temperature perturbations (24 hours) for the different proposed scenarios. The simulated results will be estimated and suitable conclusions would be made upon the same.

Temperature perturbation comparison for 2015-BASE-GI$_{UHI}$ and 2015-BASE-No GI$_{UHI}$

The modelled temperature perturbations for the four different hours (01, 07, 13 and 19 hours) for both scenarios are shown in Figure 85 and Figure 86. The modelled results show the temperature to be highest in the mid-day compared to early morning or evening.

The temperature perturbations for both the scenarios had been shown (Figure 85). The 2015-BASE-NoGI$_{UHI}$ scenario at midday around 13:00 hrs has the highest perturbation in temperature with a difference of 0.8°C compared with 2015-BASE-GI$_{UHI}$. The second highest with 0.72°C in the early morning at 7:00 hrs. Similarly, the perturbation in temperature for 1:00 and 19:00 hours were found to be 0.5°C and 0.16°C respectively. The perturbation during the early morning hours (generally said to be busy working hours with higher density of vehicular fleet) would have resulted from the vehicular emissions since, Guildford town is packed with urban infrastructure possessing numerous narrow street canyons which traps the heat from these vehicular emissions.
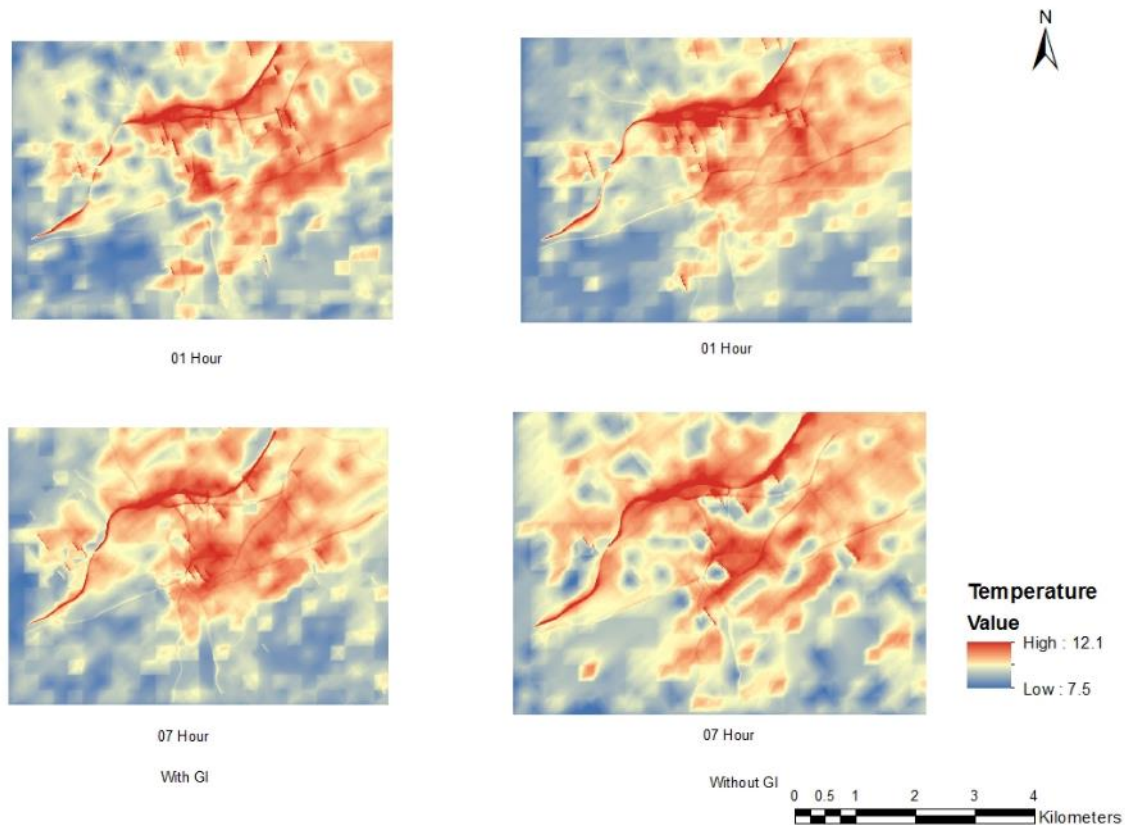
Figure 85: Hourly modelled temperature perturbation (°C) for 01 and 07 hours 2015-BASE-GI$_{UHI}$ (a-b) 2015-BASE-NoGI$_{UHI}$ (c-d) (source: own account, data: City of Guildford).

The mid-day difference in temperature would have been due to the emissions from buildings, since the time of the day is found to be busy with various anthropogenic activities resulting in emissions from various sources than anytime of the day. These emissions will be at the peak during this hour of the day with the meteorological conditions playing a constructive role in trapping the heat and increasing the temperature (Kolokotroni & Giridharan, 2008; Hamilton et al., 2014). Thus the

modelling approach depicts that the scenario without GI's (2015-BASE-NoGIUHI) will cause a rise in temperature during the hours of early and mid-day (7:00 and 13:00 hrs).

The obtained results illustrate the importance of implementing GI's, which pose to exhibit a possible solution in reducing the temperature in any urban infrastructure (Chen, 2013). Even though, in the presence of anthropogenic emissions, the GI's were found to reduce the temperature up to 0.7° to 0.8°C effectively (Figure 86), since the reduction of temperature on a scale of 0.5° - 1°C for any urban infrastructure can be named as a significant reduction (Kolokotroni & Giridharan, 2008; Chen, 2013). The implementation of GIs could further increase the reduction in temperature and have a positive impact on climate change in micro environments.
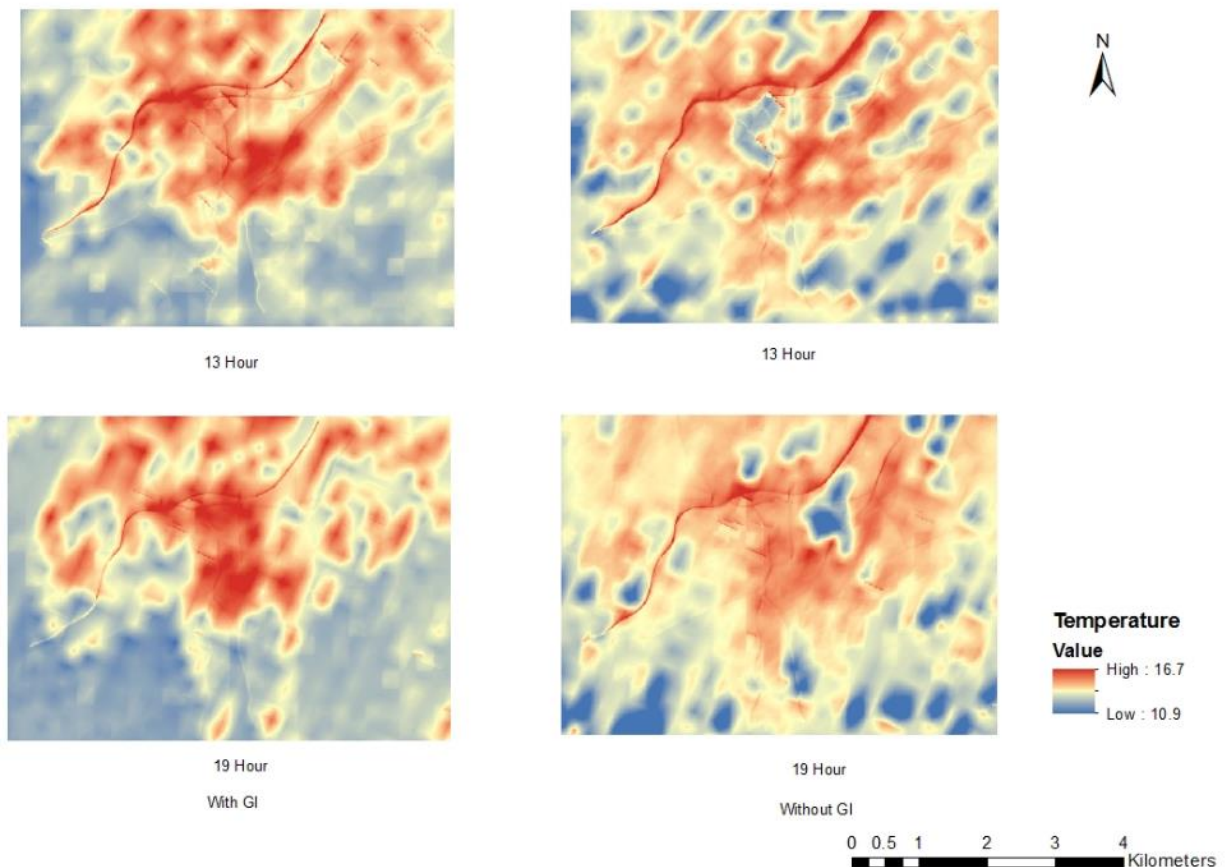
Figure 86: Hourly modelled temperature perturbation (°C) for 13 and 19 hours for 2015-BASE-GIUHI (e-f) 2015-BASE-NoGIUHI (g-h) (source: own account, data: City of Guildford).
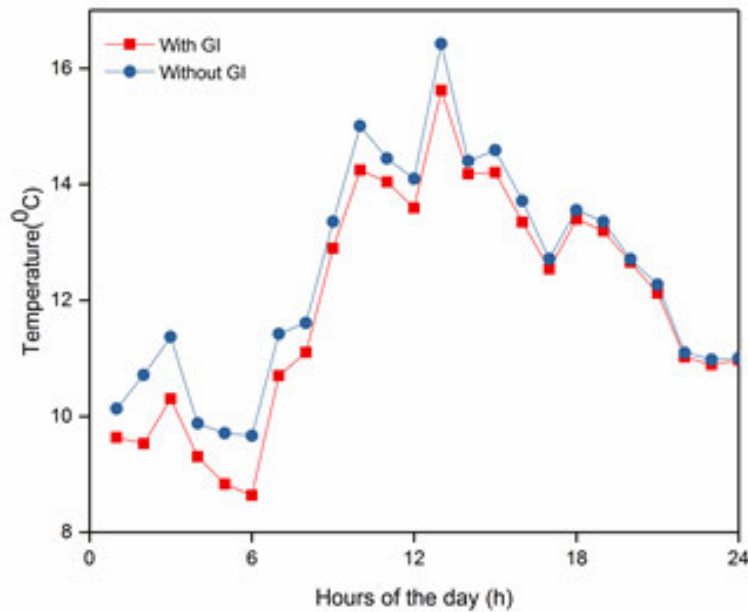
Figure 87: Modelled temperature variations during different hours of the day for Guildford urban area (source: own account, data: City of Guildford)

The study on urban heat islands for Guildford involves two scenarios (2015-BASE-GI$_{UHI}$ and 2015-BASE-NoGI$_{UHI}$). These scenarios were constructed in a view to estimate the impact of GI's in temperature reduction. The study uses ADMS Temperature and Humidity model to estimate the perturbations to near-surface air temperature. The model inputs such as albedo, surface evaporation to resistance, thermal admittance and surface roughness have been obtained from various sources and heat emissions from roads and building had also been considered to model the temperature perturbations for Guildford. The study revealed that the GI's play an important role in reducing the UHI effects to a scale of up to 1$_{o}$C on a midday in the presence of anthropogenic sources, since these sources coupled with urban fabric of any urban area were found to sway in rising the temperature and leading to UHI formation. The role of GIs and their ability to reduce temperatures, as the evapotranspiration from vegetation (Green roofs, Hedges, Trees in large street canyons etc...) was clearly highlighted by this study.

6 Local-scale surface interaction for the City of Vantaa

Vantaa is with about 225 000 inhabitants the fifth largest city in Finland. In the greater area of Tikkurila, the administrative centre of Vantaa, about 40 000 people live. Here the Tikkuraitti pedestrian zone in the middle of build-up area is one of the research areas. In the 1980s Tikkuraitti was one of the main streets of Tikkurila (Asematie). In the municipal development it was foreseen to convert the street to a pedestrian area for recreation with shops and restaurants. Most of the buildings were detached houses. In the course of time the houses were replaced with 4- to 8-storyed buildings on the south site and the 3- to 5-storyed buildings on the north site. But there still few houses only with ground floor level height. The pedestrian zone is placed in almost direct west-east direction. The length is about 250 metre.

Tikkurila is mostly build on soft loam underground. Renewing the building or even construct higher buildings need piled foundation. Still Tikkurila and Tikkuraitti are very popular as the city centre. One primary reason for their attractiveness is that most of the public administration and health service are accessible by foot.

The other research area Malminiitty residential area lies in the northern part of the greater part of Tikkurila, about 2.2 kilometres to the north. In the 1960s and 1970s it was in Finland very common to plan new storey-housing areas apart from single detached-housing area. Nowadays the city growing reached these areas and integrate them into the city over-all development.

The original Malminiitty residential area consists of 12 buildings with 7 storeys surrounded in the west, south and east with 2- to 3-storeyed buildings and lower row houses. That means that Malminiitty residential area was one of the largest housing areas in Finland at that time. In Finland it is very common to protect at least trees during the constructing period and therefore GI is almost immediate available after construction.

Nowadays the Malminiitty residential area is surrounded with all kind of low houses. These buildings are gradually built from the 1980ies until today. During the last five years the city of Vantaa aims for a denser urban structure. A achieve the aims several new buildings were built or are under construction.

The Tikkuraitti pedestrian zone is under reconstruction considerations to give the area a more city-like expression. During the summer time Tikkuraitti is a very popular place for people to meet. During other seasons the area is used as a fairground.

Figure 88 shows the location of the two areas of Tikkuraitti and Malminiitty in Vantaa, located in the north of Helsinki, the capital of Finland, with about 15 kilometres distance to the Bay of Finland, the most easterly part of the Baltic Sea.

GI plays an important role in both areas. In residential areas the door thermal conditions influence above all the comfort of elderly people and children. For public places like the Tikkuraitti pedestrian area all age groups benefit from good arrangement of GI. The interventions show the thermal differences for both areas with their GI as status quo and the areas without any GI.

The relevant influence of GI in Finland is restricted to the growing season. Generally the growing season is defined as the period of the year when the mean air temperature is above 5°C. In southern Finland the growing season covers about 170 days, starting normally at the end of April

and lasting until the beginning of October. From year to year there are notable difference in the length of the growing season.
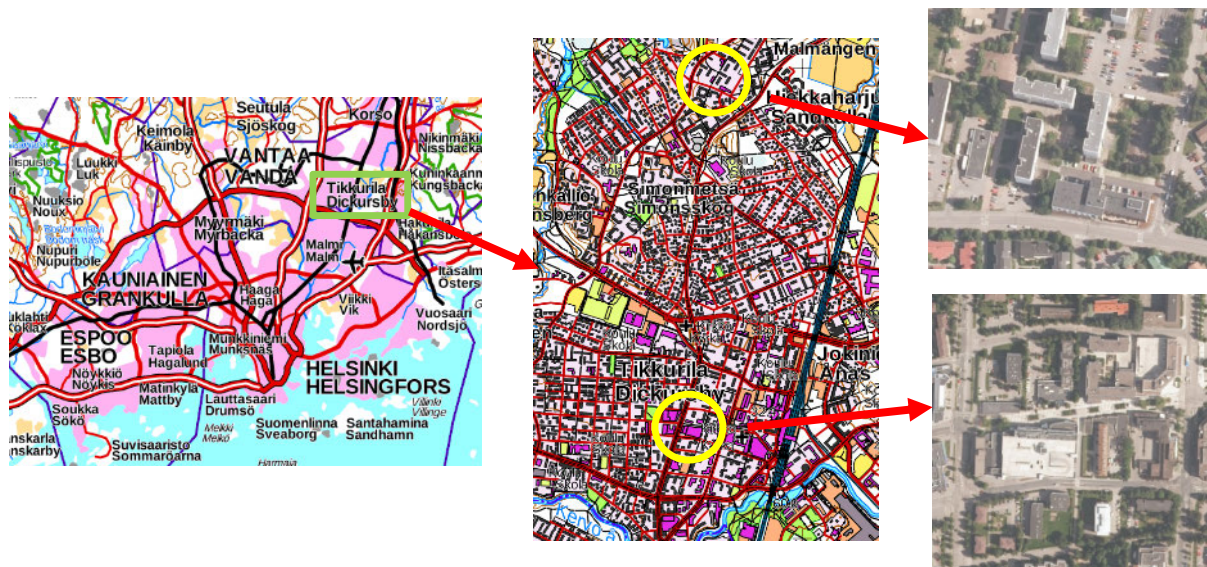
Figure 88: left, the location of the Vantaa administrative centre Tikkurila in the metropolitan area of Vantaai; middle, the location of the two research areas, at the bottom the Tikkuraitti pedestrian area and at the top the Malminiitty residential area; right, aerial photos of the research areas (source: maps and pictures: kansalaisen.karttapaikka.fi).

Table 28 below provides an overview of the model simulations carried out in Vantaa to fulfil the objective of detailing and providing results on the effectiveness of GI in reducing UHI.

City/Scale	Modelled scenarios	Software
- City of Vantaa - residential area Malminiitty	1) Baseline scenario with vegetation with the prevailing wind direction south-west 2) Baseline scenario without vegetation with the prevailing wind direction south-west	ENVI-met V4.3.2 Summer18 (inklusive BIO-met)
- City of Vantaa - pedestrian area Tikkuraitti	1) Baseline scenario with vegetation with the prevailing wind direction south-west 2) Baseline scenario without vegetation with the prevailing wind direction south-west	ENVI-met V4.3.2 Summer18 (inklusive BIO-met)

Table 28: Overview of numerical simulations carried out in Vantaa within this task and presented in the following Sections (source: own account).

6.1 Model Vantaa 1 – Residential Area Malminiitty

6.1.1 Description of the model

The Malminiitty residential area lies in a slightly hilly area with approximately 30% forest and other green space. Malminiitty core area exits of nowadays fifteen up to 8-storey buildings surrounded with detached houses and up to 3-storey row houses. Around the detached house little front and back yard increase noticeable the amount of green space. The main building materials are concrete and wood. Most of the higher houses have a white metal wall covering. The modeled area includes the westerly part of high build-up area. The size covers 240 square meters with about 20 different houses. The modeled area is presented in 3D in Figure 89.
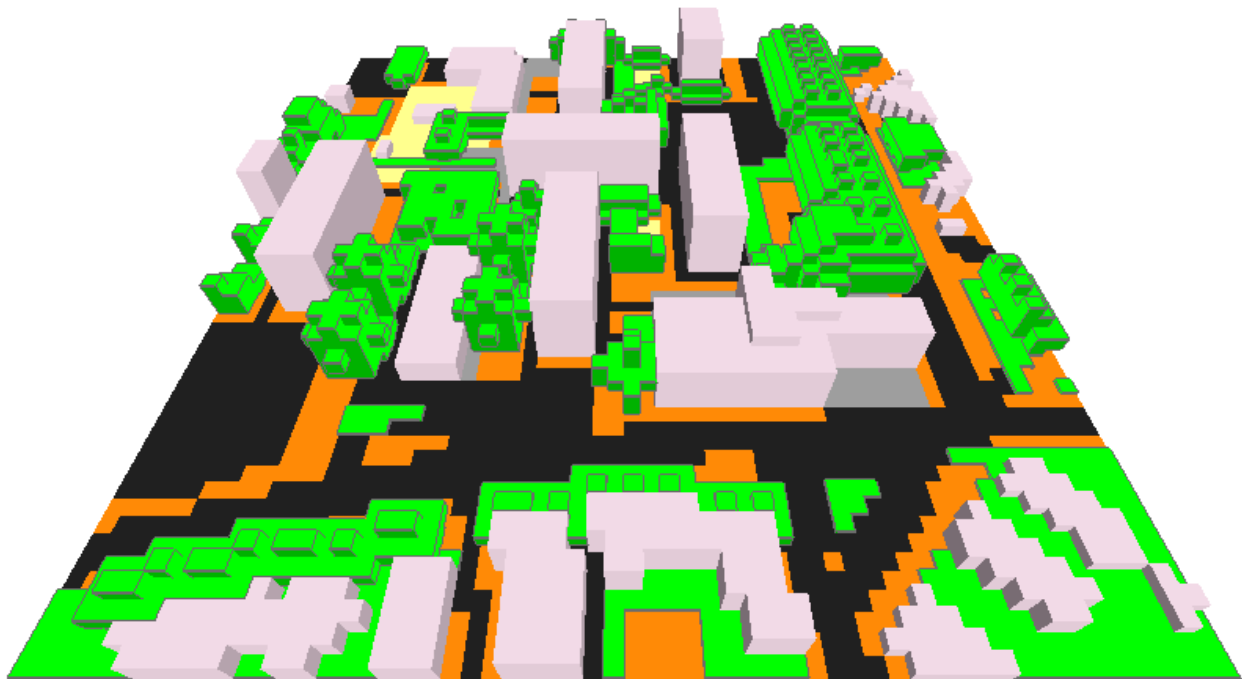
Figure 89: three-dimensional model of the Malminiitty residential area, black: asphalt roads, orange: loamy unsealed areas, yellow: sandy unsealed area, green: vegetation; ENVI-met setup-tool SPACE (Figure: www.envi-met.com).

6.1.2 Methodological approach

To simulate the thermal comfort and thermal differences between areas with GI and without GI the ENVI-met simuliation software is used. The current version for the ENVI-met software is 4.4, but for this research the version 4.3.2 was used (Huttner and Bruse, 2009). ENVI-met V4 is a holistic three-dimensional non-hydrostatic model for the simulation of surface-plant-air interaction. The model is capable to simulate in grid cell sizes from 50 centimeters to 10 meters using normally a time frame from 24 to 48 hours with a time step interval from between 1 and 5 seconds. The used grid size for the Malminiitty residential area was 4x4x4 meters. The simulation was run in a 60x60x30 grid space. Therefore, the modeled area covers a 240x240 meters terrain. The simulation time was set to 12 hours to cover the highest sun elevation for maximum influence of the solar irradiation. The inflowing wind condition was set to south-westerly wind with an average wind speed of 2 meter per second for elevation of 10 meters above undisturbed ground. For the

analyzes a height of 1.2 to 1.5 meters was chosen. ENVI-met calculates out of this the common wind speed for urban areas. For the thermal conditions under observed clear-sky situations long air temperature and humidity observations from the near-by synoptical weather station Helsinki-Vantaa airport was used (Figure 90). The ENVI-met model architecture consists of 4 modules: an atmospheric model, soil model, vegetation model, and build environment and building system model. For further information see http://envi-met.info/doku.php?id=intro:modelconcept. For more detailed information about the ENVI-met basic settings including the bio-climatological settings as well the definition of physiologically equivalent temperature, (PET, Table 29), see the section about the micro-scaled simulation in the area of the city of Bottrop.
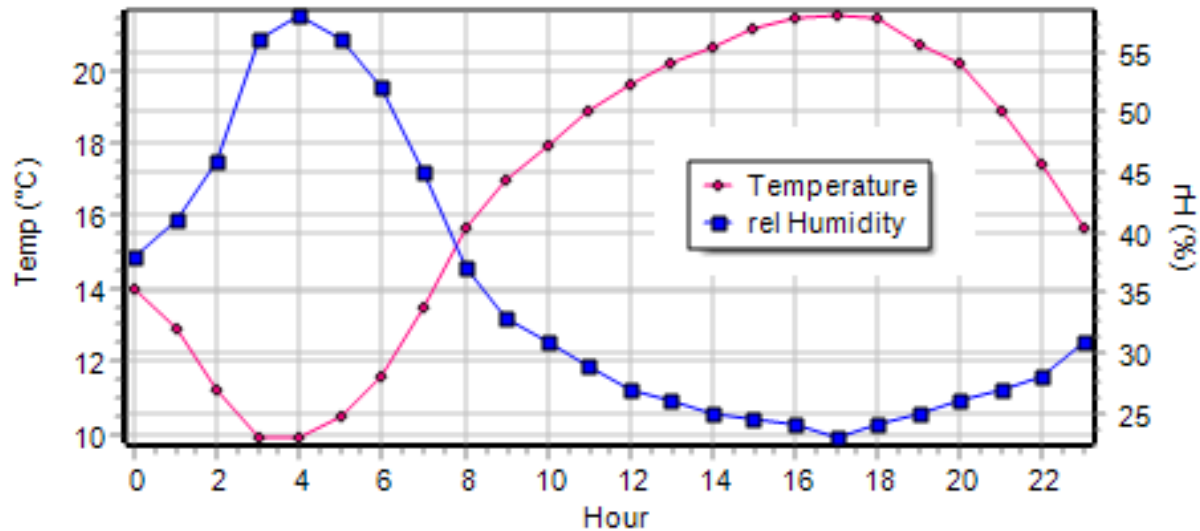
Figure 90: an idealized temperature and humidity curve for a clear-sky midsummer day in Malminiitty based on long-term observation from Helsinki-Vantaa airport, ENVI-met setup-tool ConfigWizard)(source: own account, ENVI-met).

PET (°C)	Thermal Perception	Physiological stress level
<4	Very Cold	Extreme Cold Stress
4-8	Cold	Strong Cold Stress
8-13	Cool	Moderate Cold Stress
13-18	Slightly Cool	Slight Cold Stress
18-23	Comfortable	No Thermal Stress
23-29	Slightly Warm	Slight Heat Stress
29-35	Warm	Moderate Heat Stress
35-41	Hot	Strong Heat Stres

Table 29: Threshold values of PET for different grades of thermal sensation and physiological stress on human beings, during standard condition (source: own account after Matzarakis, 1999)

The micro-scale simulation runs were limited to midsummer season around the 21st of June. The micro-scale simulations backgrounds contain the environmental status quo where the environmental conditions like housing, roads, surfaces, and vegetation were implemented into the model as precise as possible. One restriction concerning the vegetation was taken into account, the type of deciduous trees as main source of evaporation and shading were chosen by height and width and not by the type of species.

6.1.3 Model validation and verification

A meteorological observation station was arranged to monitor the weather condition inside the Malminiitty residential area. The station consisted of an acoustical anemometer, sensors for air temperature and humidity and a 4-component net radiometer. The instruments were installed out-site of a balcony at the sixth floor in 20 meters height faced to south-south-east. The data was collected in a one-second interval. Meteorological conditions in 20 meters height differ from those collected near ground. Nevertheless, the results of the meteorological station and of the micro-scaled simulation point into the same direction.

6.1.4 Modelled results and discussion

The modeled results of two runs were shown, a fully vegetated run and a run where the vegetation was completely removed. To demonstrate the influence of the solar irradiation on human thermal comfort the simulations were conducted for 12 hours from 7.00 o'clock AM until 7:00 o'clock PM. The results for midday air temperature simulation is shown in Figure 91. Results for the human thermal comfort calculation for the same time and day are shown in Figure 92.
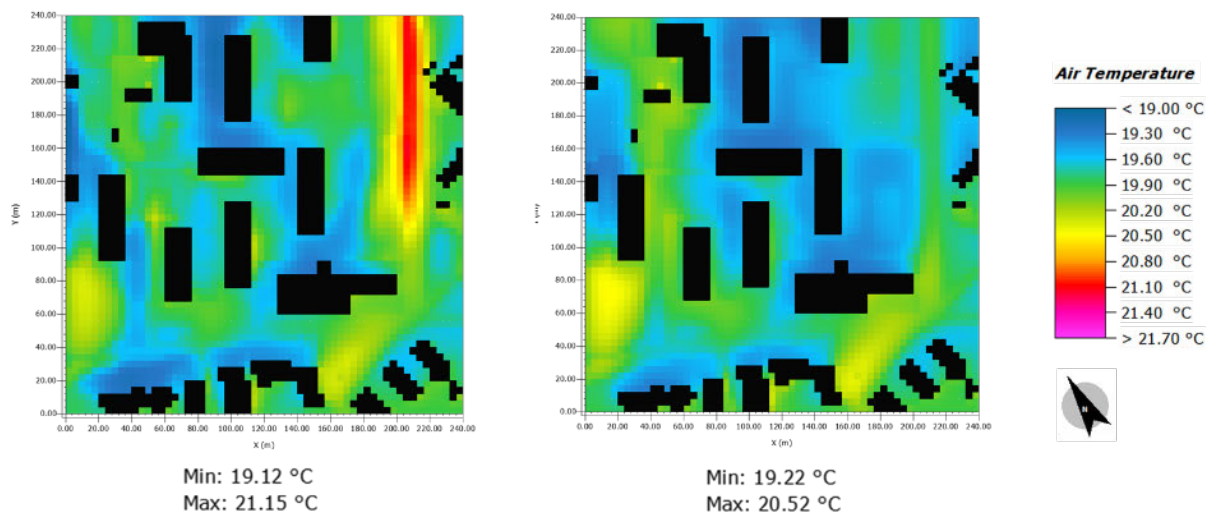
Figure 91: Malminiitty residential area temperature simulation, 21.06., 12:00 o'clock, inflowing wind temperature 19.6°C: left, with vegetation; right, without vegetation (source: own account)

Min: 19.60 °C
Max: 45.79 °C

Min: 20.60 °C
Max: 49.80 °C
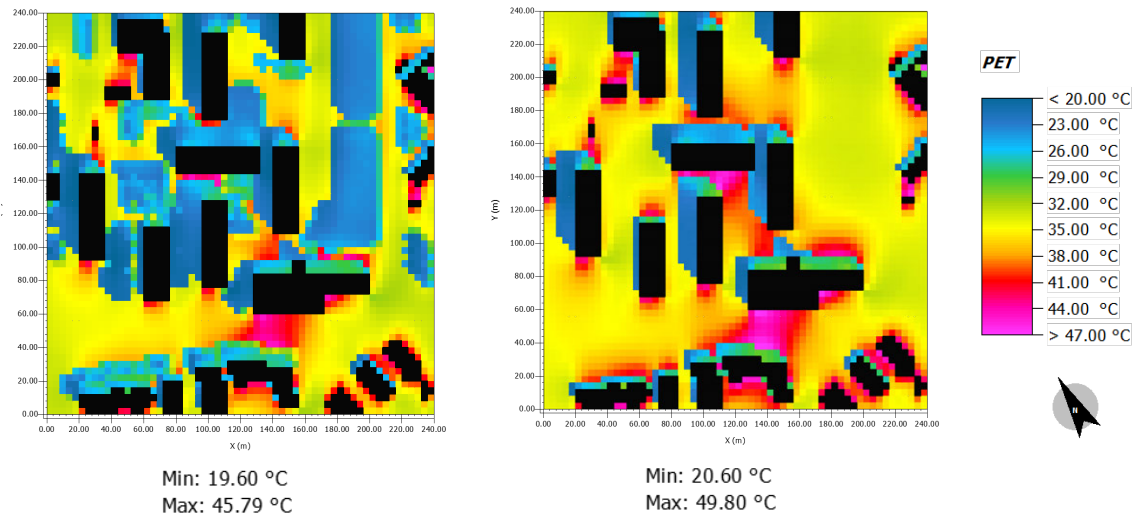
Figure 92: Malminiitty residential area PET calculation based on simulation presented in Figure X7, 21.06., 12:00 o'clock, inflowing wind temperature 19.6°C: left, with vegetation; right, without vegetation (source: own account).

Figure 93: Malminiitty residential area temperature simulation for 21.06., 12:00 o'clock, inflowing air temperature 19.6°C: absolute air temperature difference ((with vegetation) minus (without vegetation)) (source: own account).
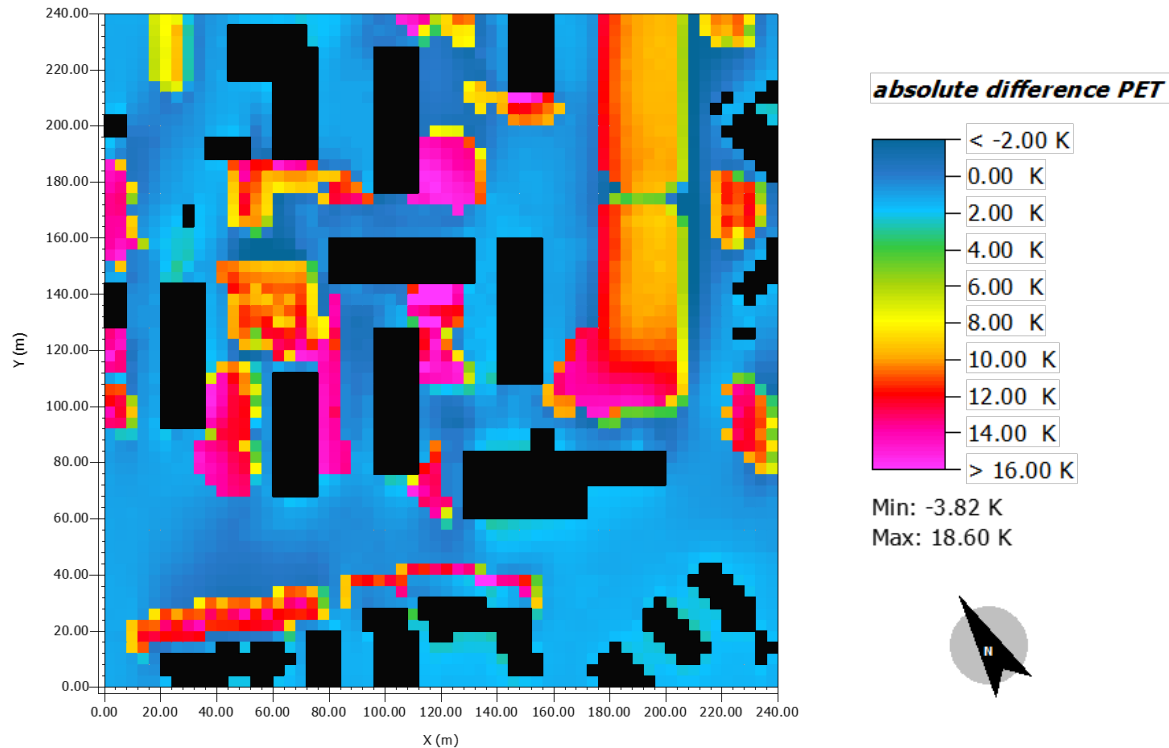
Figure 94: Malminiitty residential area PET differences based on calculation for 21.06., 12:00 o'clock, inflowing air temperature 19.6°C: PET difference ((with vegetation) minus (without vegetation)) (source: own account).

Figure 93 shows the comparison of the air temperature simulation for a clear-sky midsummer day, vegetation minus without vegetation. For the calculation of PET the comparison is shown in Figure 94, here again vegetation minus without vegetation.

The ENVI-met simulation software provides a tool to simulate and analyze microclimatological conditions in comprehensive way. Areas up to 500 meters are as normally objective of the interventions. Only the computing capacities restrict larger model. In the Vantaa the westerly part of the Malminiitty residential area of about 240x240 meters were simulated and analyzed for the prevalent air temperature and the human comfort indices PET. In Finland the Sun even during midsummer never rises higher than 53° above the horizon. Therefore higher buildings cause generally a larger area of shading. Shaded areas are consistently colder than locations in the sun. Also the insulation during the midday hours is normally weaker than in countries at lower latitudes. Vice versa the cleanliness of the atmosphere in Finland produced during the summertime adequate thermal conditions like in more southerly countries.

The simulated area of Malminiitty residential area consists of 3601 grid cell. In the analyzed height of 1.5 meters 723 grid cells contain some kind of housing elements. Two grid cells contain vegetation with a leaf area density (LAD) below 0.5. In 38 grid cells the LAD is between 0.5 and 1. The average temperature simulated for the two grid cells with LAD <0.5 is 19.99°C, while the average temperature in grid cells with LAD between 0.5 and 1 decrease to 19.56°C. It must be state once again, that the analyzed height is between 1.2 and 1.5 meter, therefore clearly under the canopy layer of the trees. Furthermore, solar irradiation causes an average increase of temperature of house up to 22.95°C and is therefore 3.35°C warmer than the inflowing air

temperature. The overheating of the street area in the easterly part of the simulated area is due to the clear-sky condition, prevalent wind direction from south-west and the position of the street, where the wind blows a long way over an overheated street surface.

A clear conclusion that can be drawn from this result is the increase in PET in the simulation runs without vegetation. Here the maximum PET temperature increased from 45.8 to 49.8°C. Notable is that the largest increase is locate on road section in front of a public health care center, the large building below right.

6.2 Model Vantaa 2 – Tikkuraitti Pedestrian Area

6.2.1 Description of the model

A model of the Tikkuraitti build-up area of the 270 x 270 metres was set up. It contained in the middle an area which is settled down for recreation use. The area was a former main street, surrounding by shops, restaurants and public services serving people for recreation and day-to-day business. It succeeded to keep this role over the course of time. Nowadays the southern part of the pedestrian area contains of buildings up to 8-storeys with a mixed structure of commercial use. The northern part is dominated by residential buildings with shops and restaurants at the first floor. In between and behind the buildings there are necessary parking lots. The modeled area is presented in 3D in Figure 95.
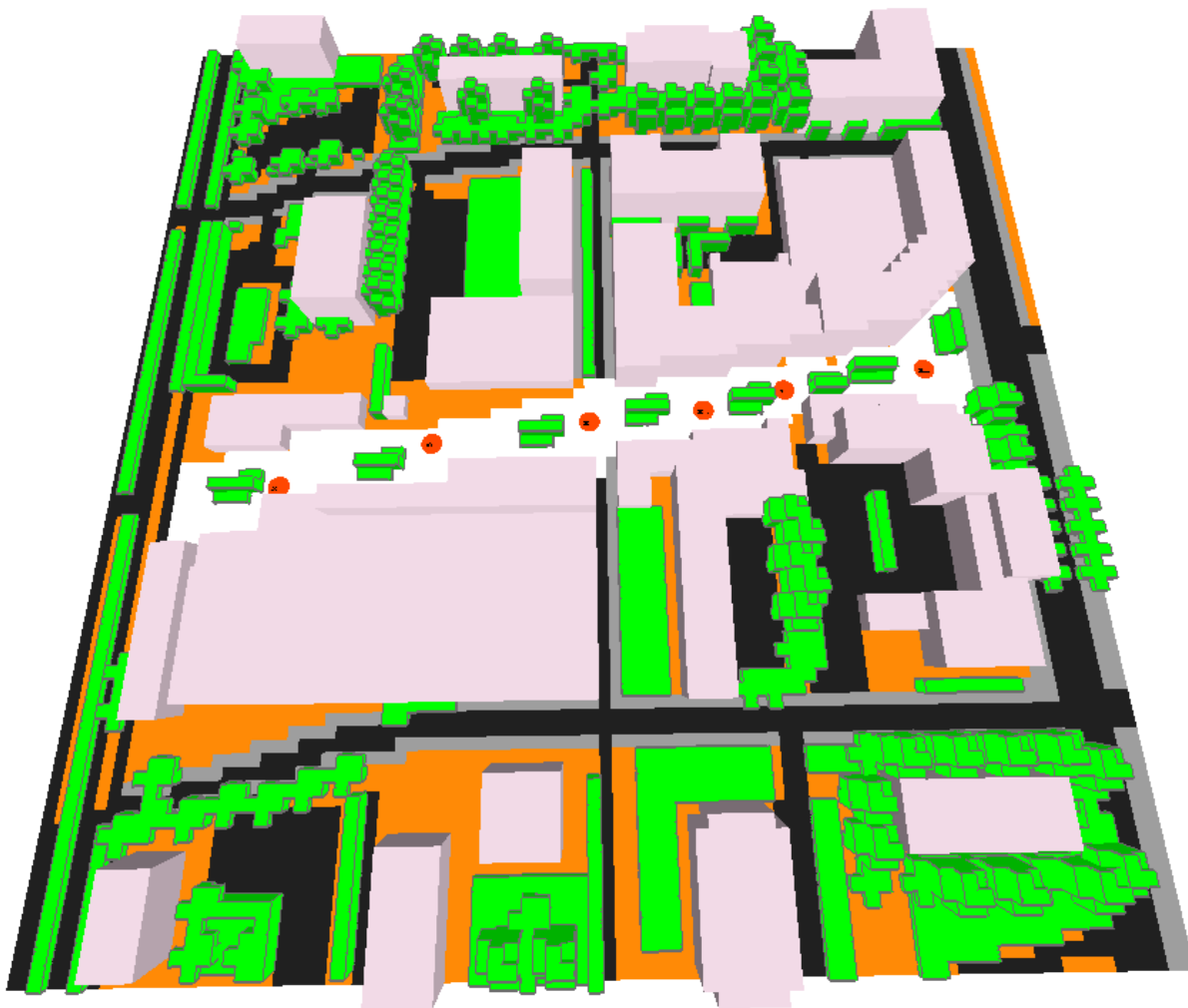
Figure 95: three-dimensional models of the Tikkuraitti pedestrian zone, black: asphalt roads, orange: loamy unsealed areas, yellow: sandy unsealed area, green: vegetation; ENVI-met setup-tool SPACE (Figure: www.envi-met.com).

The pedestrian area has length of approximately 250 meters. The surface is sealed with stone slabs. In regular intervals spots with different types of green infrastructure offer possibilities for linger and recreation.

6.2.2 Methodological approach

The methodological approach followed mostly the approach described in section 1.2.2 for the Malminiitty residential area. The difference between the Malminiitty approach and the Tikkuraitti approach is the different grid cell size of 3x3x2 meters and that the simulations were implemented in a 90x90x30 grid space. Therefore, the modeled area covers a 270x270 meters terrain. For the model Vantaa 2 a slightly different temperature and humidity input was used (Figure 96).
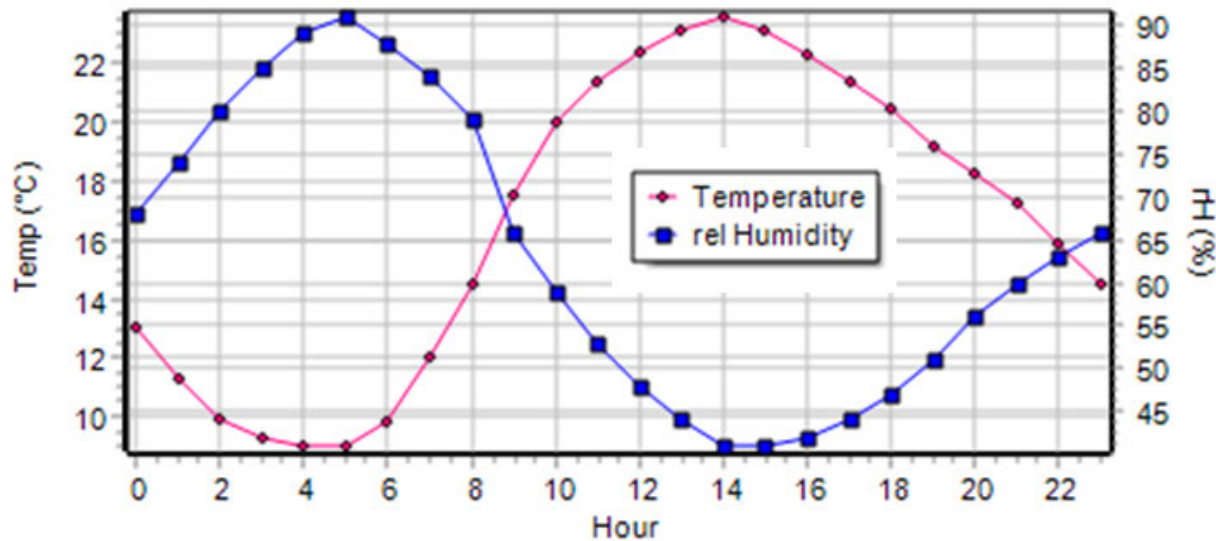
Figure 96: an idealized temperature and humidity curve for a clear-sky midsummer day in Malminiitty based on long-term observation from Helsinki-Vantaa airport, ENVI-met setup-tool ConfigWizard (source: own account, ENVI-met).

6.2.3 Model validation and verification

It turned out that there was impossible to arrange meteorological observations near-by the pedestrian area. The nearest official synoptical weather station lies at the Helsinki-Vantaa airport 6 kilometers north-west of Tikkurila. A similar equipped station like the Malminiitty observation point was located in park-like surroundings 500 meters to the south. Here the station consisting of an acoustical anemometer, sensors for air temperature and humidity and a 4-component net radiometer. The instruments were installed in 10 meters height on stand-alone mast of 20 meters. Here the data was collected in a one-second interval.

6.2.4 Modelled results and discussion

The modeled results of two runs were shown, a fully vegetated run and a run where the vegetation was completely removed. To demonstrate the influence of the solar irradiation on human thermal comfort the simulations were conducted for 12 hours starting from 7.00 o'clock AM until 7:00 o'clock PM. The results for midday air temperature simulation is shown in Figure 97. Based on the results of the air temperature simulation with and without vegetation PET was calculated within the ENVI-met software, results are shown in Figure 98. To demonstrate the differences for the two simulation runs a comparison map (simulation with vegetation minus without vegetation) is included, Figure 99. A similar map for PET (calculation with vegetation minus without vegetation) is shown in Figure 100.
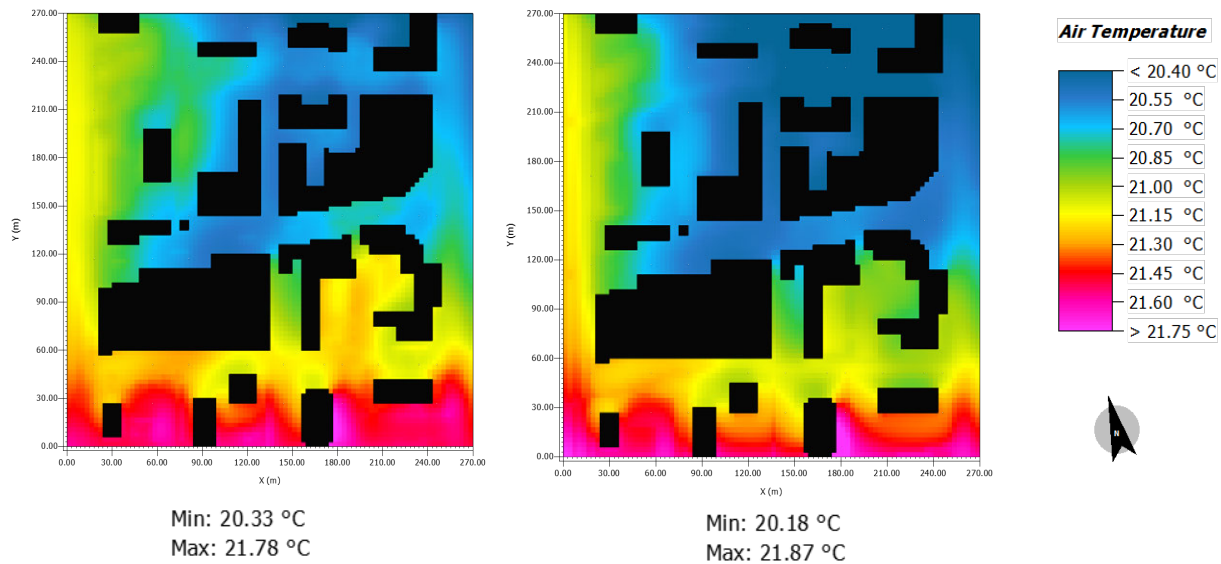
Figure 97: Tikkuraitti pedestrian zone temperature simulation, 21.06., 12:00 o'clock, inflowing wind temperature 22.4°C: left, with vegetation; right, without vegetation (source: own account).

Min: 21.80 °C
Max: 50.00 °C

Min: 22.00 °C
Max: 51.80 °C
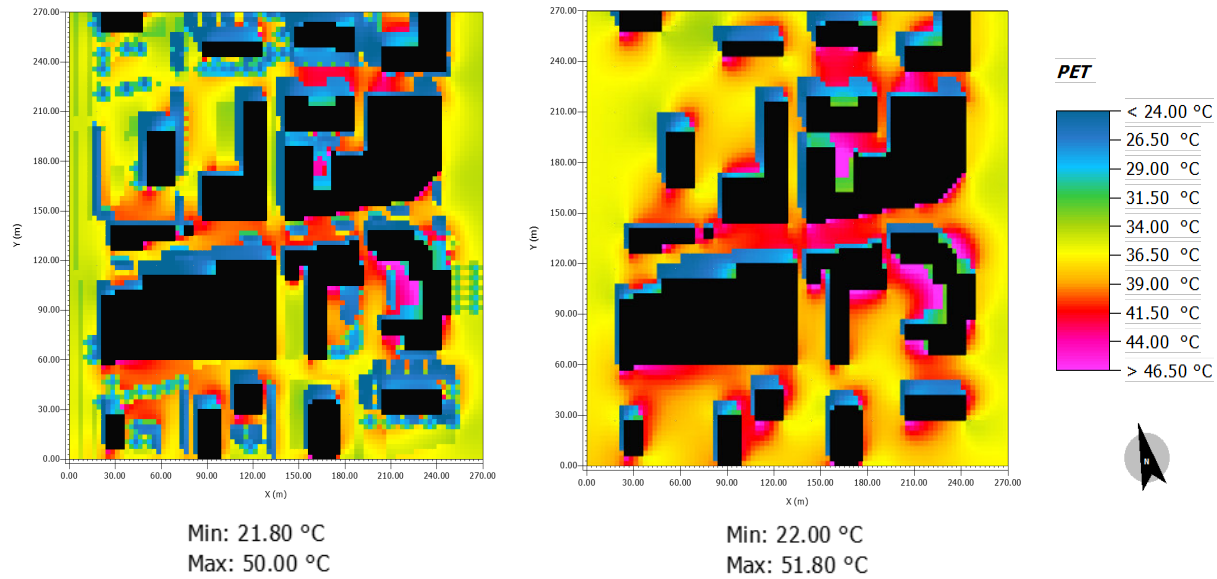
Figure 98: Tikkuraitti pedestrian area PET calculation based on simulation presented in Figure X11, 21.06., 12:00 o'clock, inflowing wind temperature 22.4°C: left, with vegetation; right, without vegetation (source: own account).
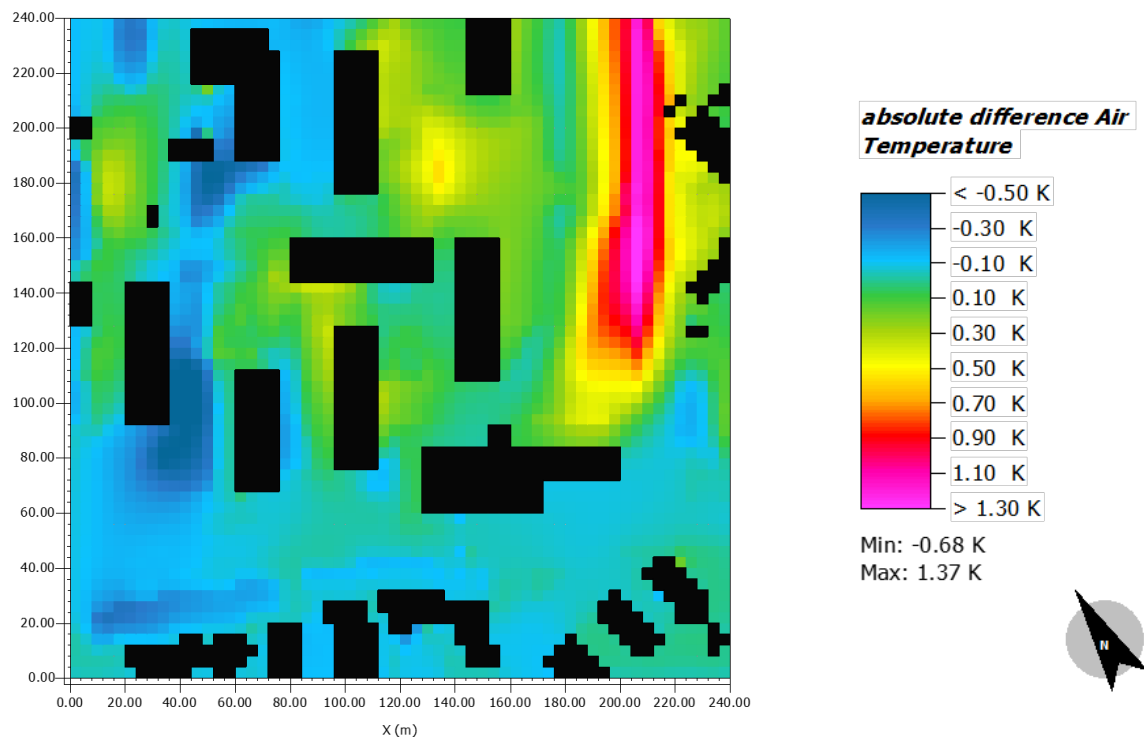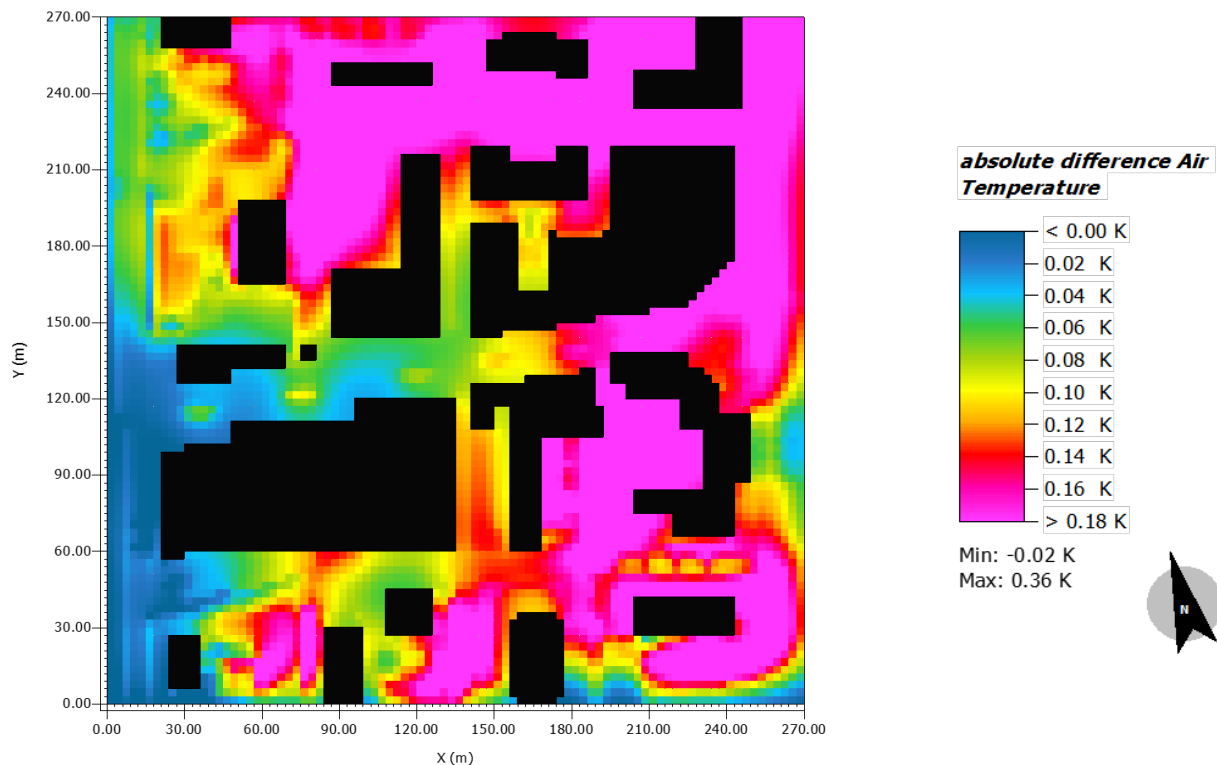

Figure 99: Tikkuraitti pedestrian zone temperature simulation, 23.06., 12:00 o'clock, inflowing wind temperature 22.4°C: absolute air temperature difference ((with vegetation) minus (without vegetation)) (source: own account).
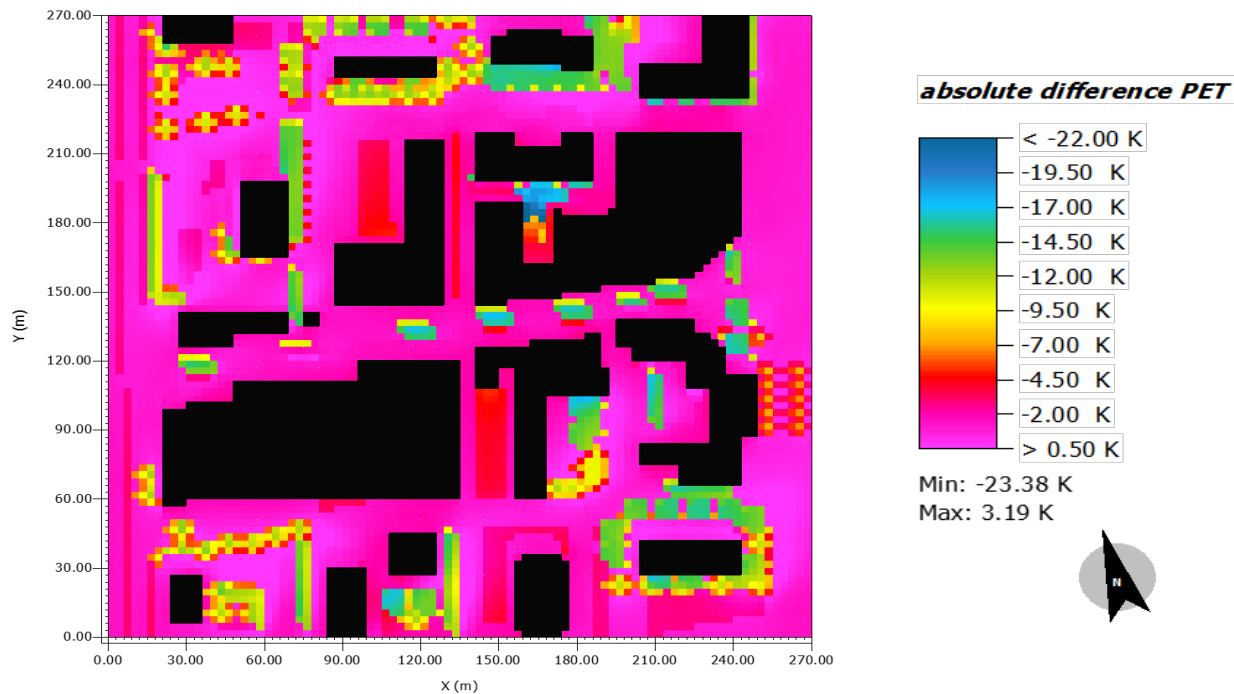
Figure 100: Tikkuraitti pedestrian area PET differences based on calculation for 21.06., 12:00 o'clock, inflowing air temperature 22.4°C: PET difference ((with vegetation) minus (without vegetation)) (source: own account).

In Vantaa, the center part of the Tikkurila administration area of about 270x270 meters was simulated and analyzed for the prevalent air temperature and the human comfort indices PET. Inside the pedestrian area Tikkuraitti the shaded areas are consistently colder than sunny location. This is also due to higher buildings south of the pedestrian area. GI in the middle of the pedestrian area reduce the thermal stress cause by the direct solar insulation during the midday hours.

The simulated area of Tikkuraitti pedestrian area consists of 8101 grid cell. In the analyzed height of 1.2 meters 2485 grid cells contain some kind of housing elements. About 993 grid cells contain vegetation with a leaf area density (LAD) below 0.5. In 10 grid cells the LAD is between 0.5 and 1. In 168 grid cells the LAD was greater than 2. The average temperature simulated for the grid cells with LAD <0.5 was 20.77°C, with LAD temperature was between 0.5 and 1 21.02°C, and with LAD greater than 2 it was equal to 21.00°C. Furthermore, solar irradiation causes an average increase of temperature of house up to 22.21°C. The overheating of the street area in the easterly part of the simulated area is due to the clear-sky condition, prevalent wind direction from south-west and the positon of the street, where the wind blows a long way over an overheated street surface.

A clear conclusion which can be derived is again the increase in PET in the simulation runs without vegetation. Here the maximum PET temperature increased from 50.0 to 51.8°C. It is to note that there is wider increase of positive temperature in easterly parts of the pedestrian area.

7 Conclusions

Cities and metropolitan areas face new challenges in adapting to the consequences of climate change and air pollution. In addition to the predicted annual mean temperature increase, the number, intensity and duration of heat waves in Europe will also increase by the end of the 21st century. The associated additional heat load will affect the health of the urban population, which is already negatively affected by the urban heat island effect. In addition, increasing air pollution, in particular from nitrogen dioxide (NO_2) and particulate matter (PM), is unhealthy for humans and is the subject of controversial debate. Inhalation of the harmful gases in combination with particulate matter can cause health effects such as cardiovascular and respiratory diseases.

Further research is needed to ensure that existing knowledge about the consequences of climate change and air pollution as well as possible adaptation measures are specifically incorporated into urban planning. In Task 6.3, model simulations were used to identify, quantify and evaluate various measures relevant to urban climate with the potential to reduce thermal pollution and air pollution. Urban-level simulations, as carried out in Task 6.3, provide an opportunity to assess the impact of different types of measures that should be tested before their application. In particular, this offers the unique opportunity to simulate and evaluate the potential effects of selected adaptation measures at both urban and neighbourhood levels. This will provide an important decision-making basis for the planning and design of strategies and measures to mitigate and adapt to climate change. However, the recommendations derived from these results can also be easily extended to other European cities.

In the following, the results achieved are evaluated and reflected with regard to their simulated effects and planning-relevant results. A presentation of the modelled results and discussion of the methodological approach were part of the preceding chapters. The effects of selected infrastructure solutions at the urban level to improve air quality and reduce UHI effects are presented for each individual city. This is due to the fact that the simulation methods and programmes as well as the investigation scales – and thus the results – differ. As reported in the Introduction section, because of the specific morphology and microclimate of each iSCAPE city, the analyses presented in this report present unique features on the one hand, but on the other hand the investigative approaches can be easily transferred to other cities in Europe, not restricting on those of the iSCAPE project.

7.1 City of Bologna

In Bologna, the evaluation of the impact of GI on UHI and AQ at the urban scale was evaluated by means of ad-hoc setup and validated simulations carried out with the ADMS dispersion model, and specifically with the ADMS-TH and ADMS-Urban models. The choice of this model type compared with other modeling approaches (such as CFD), was primarily guided by the advantage to extend the computational domain up to the urban scale, describing the use and the morphology of the local territory with appropriate parameterizations, and to decrease the computational time.

The first one, the ADMS-TH, predicts spatial variations in land use and anthropogenic heat emissions (heat from human activities), modelling the temperature and humidity perturbations as perturbations to input upwind values. ADMS-TH calculates urban air temperature and relative humidity due to changes in land use at both city and neighbourhood scale using mathematical solutions of linearized forms of heat transfer equations together with appropriate boundary conditions. It does not resolve buildings explicitly, but it treats them implicitly by increasing surface

roughness. Specifically, air temperature and humidity calculations are derived from basic meteorological input parameters (undisturbed conditions of the system) such as wind speed and direction, solar radiation, precipitation, air temperature and relative humidity. The hourly variation temperature can be modelled at a high resolution (tens of metres).

The second one is a quasi-Gaussian plume air dispersion model able to simulate a wide range of passive and buoyant releases to the atmosphere. The dispersion calculations are driven by hourly meteorological profiles of wind speed and direction, characterized through Monin-Obukhov length similarity theory. In order to accurately represent the modelled area, it is necessary to construct a comprehensive emission inventory considering all the major emission sources, to provide input meteorological data representative at the urban scale, and to set background concentrations and time varying emission factors need to be set. The ADMS-Urban model is able to take into account the dry deposition of pollutants, by setting a specific dry deposition velocity. The deposition velocity varies according to the pollutant, but also according to the target surface. Therefore, the modeling of the effects of the increase of GI in the city of Bologna was carried out comparing the results obtained with a deposition velocity typical for walls (in which case the city consists of buildings only) and trees (in which case the area of Bologna is occupied by trees for 30% of its extension.)

For the purpose of evaluating the effect of GI on UHI at urban level, after verification of the model setup by comparison of simulations with the observations at ARPAE monitoring stations, the modeling outputs in terms of simulated temperature was evaluated for two simulation scenarios in which GI was introduced firstly over one Bologna street canyon and then over the whole city centre; the results of the simulations were then compared with those obtained in the base case. The results indicated an improvement in thermal comfort extending over an area comprehending that of the interventions but also surrounding areas.

Similarly, the effect of trees on AQ was evaluated considering one simulation scenario where the presence of trees was increased of 30% with respect to the base case. The simulation outputs indicated an increase in deposition of 97% and 49% for NO_x and PM_{10} respectively at the urban traffic ARPAE air quality station Porta San Felice receptor located in Bologna over the area affected by the intervention. Importantly, the simulations also highlighted that the deposition pattern follows that of air pollutants concentrations, i.e. the impact of the higher deposition rates obtained in the presence of vegetation is higher where pollutants' concentrations are higher, for instance near busy and trafficked road streets. Although the increased deposition of pollutants would lead to a decrease in pollutants' concentrations, this effect could be non-linearly proportional; in addition, further modeling studies evaluating the impact of trees on factors other than deposition would be needed to draw more general and definitive conclusions on the effectiveness of trees in reducing air pollution in urban city centre.

Urban scale simulations such as those developed and carried out for this specific task offer the opportunity to evaluate the effect of various types of measures which might be of interest to test before their application. In particular, this offers the unique opportunity to evaluate the effect of such changes both at urban and at neighborhood scale. This can be extremely important in view of the planning and design of strategies for mitigation and adaptation to climate change, but also the recommendations that can be extracted by these results are easily extendable to other European cities.

Although the performance of both models and the comparison of simulations with observations provided more than satisfactory, one limitation of the current configuration for UHI modeling is the difficulty in taking into account the actual presence of trees in the real case, as a consequence it

is difficult to evaluate the effect of different types of trees and/or spatial configurations of trees in the streets.

In the case of the setup for AQ modeling, one limitation is the difficulty in modeling the trees over specific parts of the domain, since the dispersion model here utilized implements a dry deposition scheme through a parameterization involving the same deposition velocity all over the entire simulation domain.

7.2 City of Bottrop

ENVI-met is a dynamic numerical model, which exclusively calculates atmospheric flow processes on the basis of real climate data, whereby regional climatic processes can be reliably considered. The more detailed the resolution of the climate model is, the more complex is the calculation of atmospheric processes. However, climatological input values of global models are used for the simulations of regional models. Accordingly, these model results represent an important foundation for the representation of microclimatological processes in urban scenarios. The reproduction of real surfaces and atmospheric conditions in simulation models just approximates a given real environment. The missing representation of small-scaled conditions by grid cells causes inaccuracies in the modelling of atmospheric processes. The resulting solution proposals regarding the development of a finer resolution remains a technical challenge. Despite these limitations, model simulations serve as reliable projection of meteorological changes in the course of climate change on a global and regional level as well as its impacts on the urban fabric. In this context, it is particularly important to take changes of the land-use patterns into account. On this evidence basis of a parallel modelling of climatic and societal changes, objectives for climate protection and adaptation can be derived (Greiving et al 2018). The associated increase of the heat stress in the city is a crucial societal problem that need to be tackled by politics and urban planning. Accordingly, the adaptation strategies, anticipated in terms of an ex-ante assessment of their effects by the model simulations, provide decisive solutions for the reduction of thermal health risks in urban areas.

For the City of Bottrop, ENVI-met was processed for four selected investigation areas to simulate the actual urban climate (baseline scenario) and various reasonable planning alternatives (vegetation structures/street trees, roof greening or building position/building variety).

Regarding heat stress, the results of the models Bottrop 1 and 2 in particular show that road trees have a positive impact in small areas - this refers both to the air temperature and to the PET value, which is also influenced by wind speed and the evaporation processes of the vegetation/trees. In the surrounding area of the trees, however, there may also be a slight increase in the perceived temperature due to the changed wind conditions. These effects can also be achieved by small or even mobile trees, but to a much lesser extent. In general, rows of trees parallel to the wind should be planted by trees with leafless trunks. This would reduce the direct heat load without noticeably worsening the ventilation.

In the model Bottrop 2, no small-scaled positive effects of green roofs on the bioclimatic conditions were proven. However, large-scaled green roofs would have stronger positive effects on the urban climate by increasing the formation of fresh air. However, it can be assumed that these effects would only have measurable results if many roofs are greened across the entire area of investigation. The effects on the indoor climate of buildings (insulation by green roofs) were not investigated here.

The examined planning alternatives in terms of urban design options in the models Bottrop 3 and 4 have a partially clear effect on the bio climate, nut no general statements can be made here. Each building variant must be examined in detail. The simulated effects are mainly based on changed shading and wind conditions. For example, a block perimeter development can contribute to a channeling of the wind and to an increase in the wind speed, which may have a positive effect on the bio climate. The model runs show that building shading in combination with relatively high wind speeds leads to a better bioclimatic situation.

In order to increase the validity of the model results, a more detailed modelling of the environment should be pursued (e.g. by including information on surface materials, surface colors, building materials, different tree species, the complete vegetation). Due to the flat topography of the city of Bottrop, it was relatively insignificant for the models, but a reference to the topographical features in the form of Digital Elevation Models would have been indispensable for more mountainous urban areas. In order to provide reliable results for planning practice, the different scenarios should be calculated with different meteorological input data. In particular, the wind direction and wind speed have a significant influence on the results.

For model Bottrop 1, a distribution of air pollution (for NO_X) was simulated in addition to climatic analyses. However, these results and in particular the methodological approach are not valid enough for reliable statements. This applies in particular to the available traffic data, which cannot differentiate between the emissions of the various modes of transport. Furthermore, a daily distribution of the traffic load cannot be derived accurately enough and thus cannot be adequately mapped in the model.

To conclude, micro-scaled modelling enables the City of Bottrop to simulate and compare the potential effects of reasonable planning alternatives and identify tailor-made adaptation measures to climate change and mitigating heat stress and air pollution control. This requires an ex-ante assessment of significant environmental effects of the given planning alternatives on climatic and air-related conditions in accordance to Art. 5 § 1 of the Strategic Environmental Directive. On this sound evidence basis, a land-use plan can be approved by the responsible city assembly (see Del. 5.3). However, the selection of planning alternatives calls for an iterative process where modellers and representatives of a city planning department collaborate with each other which is the basic idea of the living lab approach.

7.3 City of Dublin

This study develops spatial land use regression (LUR) models by considering a nonlinear weighted support vector regression (W-SVR) equations to model the spatial variation of PM_{10} concentrations. Daily observed PM_{10} concentration from 13 stations data along with a set of spatial and meteorological variable data were considered to develop the LUR model. As the concentration of PM_{10} in Dublin were found to be higher in colder season when compared to the warmer season, two separate LUR models were developed and were used to predict the daily average PM_{10} concentration at different locations in the study area. Based on the developed model it has been identified that the maximum expected pollution in Dublin during colder season is 24.5 $\mu g/m^3$ and that for the warmer season is 17.39 $\mu g/m^3$, which is considerably lower that the permissible limit of 40 $\mu g/m^3$ as per European Union legislation requirement. Due to the low concentration in Dublin, installation of low boundary walls (LBWs) as passive control structure at city scale is not deemed necessary for the study area.

7.4 City of Guildford

Similar to what done in Bologna, in Guildford an integrated modelling approach has been used to simulate the effect of GI on urban air quality and urban heat temperature perturbations for the year 2015 (section 5.1.2 and 5.2.2). The Gaussian plume model based operational model ADMS-urban (4.1, Cambridge Environmental Research Consultants, UK), which simulate spatio-temporal air pollutant concentration levels from different sources under given meteorological conditions, is selected to estimate the air quality. Likewise, ADMS-*Temperature and Humidity Module* is selected to estimate the urban heat island formation (UHI). The input traffic data in Guildford are obtained from the Department for Transport (DfT), UK which operates ~130 traffic counters around Guildford. Meteorological variables such as wind velocity and direction, temperature, relative humidity, and cloud cover are required to solve the transport equations in the ADMS-Urban model. Similarly, surface properties such as albedo, surface resistance to evaporation, thermal admittance, surface roughness and normalised building volume were obtained from land cover data for UHI simulations. The hourly data for those variables were obtained for the year 2015 from a weather station located in South Farnborough (latitude = 51:28N longitude = 00:77W, and altitude = 65 metres above mean sea level). High resolution (25 m for air quality and 10 m for UHI simulations) land cover map, terrain data, road geometry have been taken from different source to develop model. The amount of pollutants deposited were estimated based on their deposition velocities and levels of concentration over GI surface. Consecutively, the anthropogenic emissions from buildings (Cambridge Environmental Research Consultants Ltd, 2018) and roads were calculated with respect to the CO_2 emissions obtained as a heat concentration parameter by considering the heat dispersion similar to pollutants dispersion using Gaussian plume dispersion model. The modelled concentration has good agreement with concentration measured by Guildford borough council and DEFRA modelled background data. The difference in air pollutant concentrations due to presence of GI provide evident that increasing urban GI has air quality benefits through a combination of deposition and dispersion effects. To maximise this benefit, the GI should be located as close as possible to the air pollutant source (e.g. roadsides), since the deposition rates increase proportionally to the concentrations of air pollutants. Also, the UHI simulations results portray the necessity of GI's, since the temperature perturbations had reached up to a higher value of 0.8⁰C along the roadways in a proposed scenario without GI's, which is a noteworthy difference in temperature (Chen, 2013; Giridharan and Emmanuel, 2018) depicting the necessity of GI's in reducing the urban air temperature.

To assess the impact of GI on urban air quality and urban heat, two scenarios (i) air quality and urban heat without presence of GI and (ii) air quality and urban heat with presence of GI were developed for Guildford city. The conclusion based on the results obtained through developed scenario are below:

The positive impact of urban GI has been observed in terms of reduced air pollutant concentration levels due to pollutant removal by dry deposition process. These reductions in pollutant concentration levels are not only over GI surface but also found in downward wind direction. The amount of removal is mainly dependent upon percent GI cover and pollutant deposition velocities in urban areas. The deposition velocity of air pollutants is influenced by GI characteristic, meteorological condition and type of pollutant. For instance, PM_{10} removal is higher for coniferous trees than broadleaf trees (Tallis et al., 2011). Although, Guildford has good percentage of GI cover compared to megacity but still there were some hotspots where air quality had breached the annual limits. According to DEFRA (2017), there were 52 roads that had exceeded the annual

mean limit (40 μg/m^3) for NO$_2$ in 2015. Since these high air pollutant concentrations occur in certain places due to highly localized reasons and will need site specific solution to reduce air pollutant exposure to public lives within vicinity. For an instance, Abhijith and Kumar (2019) demonstrated in their field experiment that roadside hedges could help to reduce air pollutant exposure up to 63% depending on the type of air pollutant. The temperature perturbations in the presence of GI's had reduced the temperature to 0.8^{0}C along the roadways, since the vegetation reduces the temperature faster due to the evapotranspiration process compared to urban structures.

The above developed scenarios allow to estimate the amount of air pollutants remove by urban GI in Guildford city and simulate the annual hourly mean concentration levels of different pollutants (NO$_x$, PM$_{10}$ and PM$_{2.5}$) at high spatial resolution in year 2015. Additionally, the simulations carried out for UHI formation were evident of the positive impact of GI's in reducing the temperature in urban areas. In recent years, urban GI planning has been acknowledged as one of potential passive methods to reduce air pollution and surface temperature of urban infrastructures. They can also bring economic, social and environmental benefits to the communities. Furthermore, the modelling approach demonstrated a simulation tool to access the effect of different GI planting schemes on urban air quality and urban heat. Apart from their maintenance cost, there are many factors linked with urban GI such as production of biogenic volatile organic compounds which can lead to photochemical ozone formation, pollen production and damage to property that need to be addressed in decision-making process.

The high-resolution spatial air quality maps could help local authorities to evaluate the air quality and urban heat in Guildford and point out possible local hotspots for them. Furthermore, roadside trees may have negative affect on the local air quality especially in street canyons (Vos et al., 2013) but trees in urban parks or urban backyard could help to reduce city-average air quality (Tiwary et al., 2009). However, the presence of GI's irrespective of the place and their features, it aids in decreasing the urban temperature. Moreover, GI's pollutant removal efficiencies vary with type of air pollutant and GI characteristic. Therefore, the optimum potential can be harvested by strategically planting of new GI in urban areas because there are only limited places available for increasing GI density in developed urban areas.

Currently, in the absence of high-resolution spatial field experiment for validation data, the study outputs have been compared with 1 km^2 DEFRA modelled data. However, the annual hourly average air quality has been simulated with certain assumptions such as no wet deposition, annual hourly average surface resistance, and annual average daily traffic. Also, due to the lack of field experiments for validating the study outputs, no validation was carried out for Guidlford, but the meteorological data were used to analyse the perturbations in temperature. In addition, the accuracy of study outputs can be increased through more detailed and high resolution spatial temporal input data such as land cover data, meteorological data and traffic emissions, but this will result in very high computational time and output data. Many times, these high-resolution input data are not readily available. For instance, daily distribution of traffic load and fleet compositions for each road in study domain are not available. Furthermore, the sensitivity of the different species is also not considered in the modelling approach due to limitation of available data. Although, the modelling approach presented here has capability to assess the potential benefit of change in GI type, traffic conditions, land cover type and GI species on urban air quality.

7.5 City of Vantaa

The City area of Vantaa has been the second urban area beside the City of Bottrop where the ENVI-met V4 simulation software was utilized. For an initial idea using ENVI-met see the description in the section of 7.2., City of Bottrop. ENVI-met in Vantaa was based on the request to perform simulation with a mature software with a low threshold for use.

Generally speaking, the urban heat island phenomenon and air quality issues caused by road traffic play nation-wide a secondary role. However, demographic development and climate change inter alia put pressure on anticipatory urban planning and here in more particularly the implementation of green infrastructure. Therefore, the conducted ENVI-met simulations focus on the influences of GI in two mature city areas where the city growth locally had reached its final state and future development of climate change and the possible increase of road traffic might have a negative impact on human well beings. The geographical location of the city of Vantaa at the edge of the humid continental climate (Dfb, after Köppen, Kottek et al., 2006) causes a substantial year-to-year and season-to-season variability in climate condition where extremes of high and low temperatures, high precipitation in liquid (rain) and solid (snow) form will still occur.

The two models developed for the city of Vantaa in the Malminiitty residential area and the Tikkuraitti pedestrian area tried to cope with the first climate extremes, the rising air temperature. The physiologically equivalent temperature (PET) has been used to describe the human thermal conditions. However, it must be explained that the PET scale is international recognized, but the response to the scale given in Table 1 differs regarding regional human thermal perceptions.

For each model a baseline scenario presents the status quo where the environmental conditions were pictured as realistic as possible. In a second scenario the GI was removed. A fast naturally development of GI seems to be unrealistic. Due to the harsh climatic condition In Finland the naturally development of GI is slow. Therefore, changes in GI will gradually introduce changes in thermal condition. Such development is difficult to simulate. Green roofs and walls are very sparsely introduced into Finnish city development. In reality there are no green roofs in the described model areas at all.

Another noticeable result of the simulations is the impact of shading on the thermal condition caused by GI and buildings. As mentioned the LAD is generally should be set to be low in simulations to assume that the shading under trees produce a different light climate. Deciduous trees in climate zones with extensive growing seasons have denser treetops with more leaves and branches. Besides the shading also evaporation is consequently different from climates with greater LAD. The cooling impact of trees in Finland should be less perceptible than in simulations for areas with greater LAD.

The two simulation runs conducted with the ENVI-met simulation software for the Malminiitty residential area and the Tikkuraitti show clearly that vegetation and shading in Vantaa can reduce the influence of direct solar insulation and therefore reduce the urban heat island effect outside of buildings. Buildings themselves warm-up in a different way due to their construction materials. The air temperature analysis and the PET calculations were conducted for heights where humans stay. Therefore, it was not possible to conclude about thermal indoor condition.

The ENVI-met software was capable to demonstrate the thermal condition of certain areas. The software is originally developed for climatic condition in mid-latitude areas like Central Europe. The use of the software in other climatic regions like Finland is still demanding a very detail and justified set-up model input parameters.

Nevertheless, the ENVI-met software was capable to demonstrate the thermal condition of certain areas. The software is originally developed for climatic condition in mid-latitude areas like Central Europe. The use of the software in other climatic regions like Finland is still demanding a very detail and justified set-up model input parameters. Fortunately, several new ENVI-met software development steps enable to expand the use of simulations all over the year. For example, a tree calendar allows to implement trees as shading factors and wind-impending obstacles outside the actual growing season.

8 References / Bibliography

Abhijith, K. V., Kumar, P., Gallagher, J., McNabola, A., Baldauf, R., Pilla, F., Broderick, B., Di Sabatino, S., and Pulvirenti, B., 2017. Air pollution abatement performances of green infrastructure in open road and built-up street canyon environments – A review. Atmos. Environ. 162, 71–86.

Abhijith, K.V., and Kumar, P., 2019. Field investigations for evaluating green infrastructure effects on air quality in open-road conditions. Atmos. Environ. 201, 132–147.

ADMS-Urban Temperature and Humidity, A supplement to the ADMS-Urban User Guide, 2018, CERC, 3 King's Parade, Cambridge, http://www.cerc.co.uk/environmental-software/assets/data/doc_userguides/CERC_ADMS-Urban_Temperature_and_Humidity_User_Guide.pdf

Aguilera, I., Sunyer, J., Fernández-Patier, R., Hoek, G., Aguirre-Alfaro, A., Meliefste, K., Bomboi-Mingarro, M.T., Nieuwenhuijsen, M.J., Herce-Garraleta, D. and Brunekreef, B., 2007. Estimation of outdoor NOx, NO2, and BTEX exposure in a cohort of pregnant women using land use regression modeling. Environmental science & technology, 42(3), pp.815-821.

Alam, M.S. and McNabola, A., 2015. Exploring the modeling of spatiotemporal variations in ambient air pollution within the land use regression framework: Estimation of PM10 concentrations on a daily basis. Journal of the Air & Waste Management Association, 65(5), pp.628-640.

Baldauf, M., 2019. Local time stepping for a mass-consistent and time-split advection scheme. Q. J. R. Meteorol. Soc. 145, 337–346.

Barnes, M.J., Brade, T.K., MacKenzie, A.R., Whyatt, J.D., Carruthers, D.J., Stocker, J., Cai, X., Hewitt, C.N., 2014. Spatially-varying surface roughness and ground-level air quality in an operational dispersion model. Environ. Pollut. 185, 44–51.

Basu, B. and Srinivas, V.V., 2014. Regional flood frequency analysis using kernel-based fuzzy clustering approach. Water Resources Research, 50(4), pp.3295-3316.

Basu, B., Alam, M.S., Ghosh, B., Gill, L. and McNabola, A., 2019. Augmenting limited background monitoring data for improved performance in land use regression modeling: using support vector regression and mobile monitoring. Atmospheric Environment.

Battis, U.; Moench, C.; Uechtritz, M.; Mattes C. and von der Groeben, C., 2015. Gutachterliche Stellungnahme zur Umsetzung der UVP-Änderungsrichtlinie im Baugesetzbuch. Erstattet im Auftrag des Bundesinstituts für Bau-, Stadt- und Raumforschung (BBSR).

Bengtsson, L. et al., 2017. The HARMONIE-AROME Model Configuration in the ALADIN-HIRLAM NWP System. In: Monthly Weather Review 145 (2017), pp. 1919–1935.

Bernard, S. and Kazmin, A. 2018. Dirty air: how India became the most polluted country on earth. In: Financial Times 11.12.2018. Access via database, online available. https://ig.ft.com/india-pollution/ (access 14.12.2018)

Bottalico, F., Chirici, G., Giannetti, F., De Marco, A., Nocentini, S., Paoletti, E., Salbitano, F., Sanesi, G., Serenelli, C., Travaglini, D., 2016. Air pollution removal by green infrastructures and urban forests in the city of Florence. Agric. Agric. Sci. Procedia 8, 243–251.

Brauer, M., Hoek, G., van Vliet, P., Meliefste, K., Fischer, P., Gehring, U., Heinrich, J., Cyrys, J., Bellander, T., Lewne, M. and Brunekreef, B., 2003. Estimating long-term average particulate air pollution concentrations: application of traffic indicators and geographic information systems. Epidemiology, 14(2), pp.228-239.

Brauer, M., Lencar, C., Tamburic, L., Koehoorn, M., Demers, P. and Karr, C., 2008. A cohort study of traffic-related air pollution impacts on birth outcomes. Environmental health perspectives, 116(5), p.680.

Briggs, D.J., de Hoogh, C., Gulliver, J., Wills, J., Elliott, P., Kingham, S. and Smallbone, K., 2000. A regression-based method for mapping traffic-related air pollution: application and testing in four contrasting urban environments. Science of the Total Environment, 253(1-3), pp.151-167.

Brunekreef, B. and Holgate, S.T., 2002. Air pollution and health. The lancet, 360(9341), pp.1233-1242.

Bruse, M., and ENVI-met Team, 2011: ENVI-met version 3.1 BETA V (incl. LEONARDO 3.75) Latest Build: 04-Oct-2010, http://www.envi-met.com/

Bruse, M., 2004. ENVI-met 3.0: updated model overview. University of Bochum. Retrieved from: www.envi-met.com

Buccolieri, R., Gromke, C., Di Sabatino, S., & Ruck, B., 2009. Aerodynamic effects of trees on pollutant concentrations in street canyons. Science of the Total Environment, 407, 5247-5246.

Camuffo, D., and Bernardi, A., 1982. An observational study of the heat fluxes and their relationships with the net radiation, Boundary-Layer Meteorology, 23(3), 359-368.

Carruthers, D J Weng, W S. 1992. "The Effects of Changes in Surface Resistance on Temperature and Humidity Fields and Fluxes of Sensible and Latent Heat." Boundary-Layer Meterology 60 (1982): 185–99.

Carruthers, D.J., Edmunds, H.A., Lester, A.E., McHugh, C.A., & Singles, R.J., 2000. Use and validation of ADMS-Urban in contrasting urban and industrial locations. International Journal of Environment and Pollution, 14, 363-374.

CERC, 2011. ADMS-Urban User Guide. Version 3.1. Cambridge, UK, 324 pp., http://www.cerc.co.uk/environmental-software/assets/data/doc_userguides/CERC_ADMS-Urban4.1.1_User_Guide.pdf. Accessed 16 Jan 2019.

CERC, 2016. ADMS 5 Atmospheric Dispersion Modeling System User Guide Version 5.2. Cambridge, UK, 446 pp, Available online at: http://www.cerc.co.uk/environmental-software/assets/data/doc_userguides/CERC_ADMS_5_2_User_Guide.pdf. Accessed 20 Feb 2019

CERC, 2018: ADMS-Urban Temperature and Humidity, A supplement to the ADMS-Urban User Guide, Version 4.1 CERC, 3 King's Parade, Cambridge. Available online: http://www.cerc.co.uk/environmental-software/assets/data/doc_userguides/CERC_ADMS-Urban_Temperature_and_Humidity_User_Guide.pdf (access 14.12.2018)

Cesaroni, G., Badaloni, C., Porta, D., Forastiere, F. and Perucci, C.A., 2008. Comparison between several indices of exposure to traffic-related air pollution and their respiratory health impact in adults. Occupational and environmental medicine.

Chen, Chi-feng. 2013. Performance Evaluation and Development Strategies for Green Roofs in Taiwan: A Review. Ecological Engineering 52: 51–58. https://doi.org/10.1016/j.ecoleng.2012.12.083.

Clark, N.A., Demers, P.A., Karr, C.J., Koehoorn, M., Lencar, C., Tamburic, L. and Brauer, M., 2010. Effect of early life exposure to air pollution on development of childhood asthma. Environmental health perspectives, 118(2), p.284.

David R.Stauffer and Nelson L.Seaman, 1989. Use of Four-Dimensional Data Assimilation in a Limited-Area Mesoscale Model. Part I: Experiments with Synoptic-Scale Data. Am. Meteorol. Soc. 118, 1250–1277.

Davies, C., 1977. QUARTERLY METEOROLOGICAL Updating prediction models by dynamical relaxation: an examination of the technique. Q. J. R. Meteorol. Soc. 103, 225–245.

Dee, D.P., Uppala, S.M., Simmons, A.J., Berrisford, P., Poli, P., Kobayashi, S., Andrae, U., Balmaseda, M.A., Balsamo, G., Bauer, P., Bechtold, P., Beljaars, A.C.M., Berg, L. Van De, Bidlot, J., Bormann, N., Delsol, C., Dragani, R., Fuentes, M., Geer, A.J., Dee, D.P., 2011. The ERA-Interim reanalysis: configuration and performance of the data assimilation system. Q. J. R. Meteorol. Soc. 137, 553–597.

DEFRA, 2016. Emissions Factors Toolkit v7.0 User Guide.

DEFRA, 2017. Air quality plan for nitrogen dioxide (NO2) in UK (2017). Department for Environment Food and Rural Affairs.

Di Sabatino, S., Buccolieri, R., Pulvirenti, B., & Britter, R.E., 2008. Flow and pollutant dispersion in street canyons using FLUENT and ADMS-Urban. Environmental Modeling and Assessment, 13(3),369-381.

Di Sabatino, S., Leo, L.S., Cataldo, R., Britter, R.E., 2010. Costruction of digital elevation models for a southern European city and a comparative morphological analysis with respect to northern European and north American cities, Journal of Applied Meteorology and Climatology, 49, 1377-1396.

Dimakopoulou, K., Gryparis, A. and Katsouyanni, K., 2017. Using spatio-temporal land use regression models to address spatial variation in air pollution concentrations in time series studies. Air Quality, Atmosphere & Health, 10(9), pp.1139-1149.

Duniec, G., Mazur, A., 2018. Influence of parameterization of soil processes on numerical forecasts of vertical. R. Meteorol. Soc. 25, 350–356.

European Environmental Agency, 2017. Air Quality Standards. Available at https://www.eea.europa.eu/themes/air/air-quality-standards.

Fallmann, J., Forkel R., and Emeis S.. 2016. "Secondary Effects of Urban Heat Island Mitigation Measures on Air Quality." Atmospheric Environment 125: 199–211. https://doi.org/10.1016/j.atmosenv.2015.10.094.

Fanger, P.O., 1970. Thermal Comfort: Analysis and Applications in Environmental Engineering. New York: McGraw Hill.

Farhadi, H., Faizi, M., Sanaieian, H., 2019. Mitigating the urban heat island in a residential area in Tehran: Investigating the role of vegetation, materials, and orientation of buildings. Sustain. Cities Soc. 46, 101448.

Finardi, S., Silibello, C., D'Allura, A., Radice, P., 2014. Analysis of pollutant exchange between the Po Valley and the surrounding European region, Urban Climatology, 10, 682-702.

Gallagher, J., Gill., L.W., & McNabola, A., 2012. Numerical modeling of the passive control of air pollution in asymmetrical urban street canyons using refined mesh discretization schemes. Building and Environment, 56, 232-240.

Gallagher, J., Baldauf, R., Fuller, C.H., Kumar, P., Gill, L.W., McNabola, A., 2015. Passive methods for improving air quality in the built environment: A review of porous and solid barriers. Atmos. Environ. 120, 61–70.

GBC, 2016. Air quality annual status report (ASR).

Gilbert, N.L., Woodhouse, S., Stieb, D.M. and Brook, J.R., 2003. Ambient nitrogen dioxide and distance from a major highway. Science of the Total Environment, 312(1-3), pp.43-46.

Giridharan, R., Emmanuel, R., 2018. The impact of urban compactness, comfort strategies and energy consumption on tropical urban heat island intensity: A review. Sustain. Cities Soc.

Greiving, S., Arens, S., Becker, D., Fleischhauer, M., & Hurth, F. 2018: Improving the assessment of potential and actual impacts of climate change and extreme events through a parallel modelling of climatic and societal changes at different scales. Journal of Extreme Events. DOI 10.1142/S2345737618500033

Gromke, C., 2011. A vegetation modeling concept for Building and Environmental Aerodynamics wind tunnel tests and its application in pollutant dispersion studies. Environmental Pollution, 159, 2094-2099.

Hamilton, I., Stocker, J., Evans, S., Davies, M., & Carruthers, D., 2013. The impact of the London Olympic parkland on the urban heat island. Journal of Buildings Performance Simulation, 7, 2, 119-132.

Hanna, S., STRIMAITIS, D.G., CHANG, J.C., 1991. Hazard Response Modeling Uncertainty (A Quantitative Method). Volume 2. Evaluation of Commonly Used Hazardous Gas Dispersion Models.

Haykin, S. (2003), Neural Networks: A Comprehensive Foundation, pp. 842, Pearson Educ., Singapore. [Fourth Indian Reprint.].

Henderson, S.B., Beckerman, B., Jerrett, M. and Brauer, M., 2007. Application of land use regression to estimate long-term concentrations of traffic-related nitrogen oxides and fine particulate matter. Environmental science & technology, 41(7), pp.2422-2428.

Hien, Wong Nyuk, and Marcel Ignatius. 2016. "Urban Heat Island in Singapore Contributing Factors and Mitigation Solutions." Singapore.

Huang, W. and Shen, L., 2008, August. Weighted support vector regression algorithm based on data description. In Computing, Communication, Control, and Management, 2008. CCCM'08. ISECS International Colloquium on (Vol. 1, pp. 250-254). IEEE.

Huttner, S. and Bruse, M. (2009). NUMERICAL MODELING OF THE URBAN CLIMATE – A PREVIEW ON ENVI-MET 4.0, Proceedings: The seventh International Conference on Urban Climate, 29 June - 3 July 2009, Yokohama, Japan

ISO 7726. Ergonomics of the thermal environment - Instrument for measuring physical quantities. Geneva, Switzerland: International Organization for Standardization. November 1998.

Jackson, D.L., 2000. Guidance on the interpretation of the Biodiversity Broad Habitat Classification (terrestrial and freshwater types): Definitions and the relationship with other habitat classifications. Habitat.

Janhäll, S., 2015. Review on urban vegetation and particle air pollution – Deposition and dispersion. Atmos. Environ. 105, 130–137.

Jayasooriya, V.M.M., Ng, A.W.. W.M., Muthukumaran, S., Perera, B.J.C.J.C., 2017. Green infrastructure practices for improvement of urban air quality. Urban For. Urban Green. 21, 34–47.

Jeanjean, A.P.R.P.R., Monks, P.S.S., Leigh, R.J.J., 2016. Modelling the effectiveness of urban trees and grass on PM 2.5 reduction via dispersion and deposition at a city scale. Atmos. Environ. 147, 1–10.

Jerrett, M., Arain, A., Kanaroglou, P., Beckerman, B., Potoglou, D., Sahsuvaroglu, T., Morrison, J. and Giovis, C., 2005. A review and evaluation of intraurban air pollution exposure models. Journal of Exposure Science and Environmental Epidemiology, 15(2), p.185.

Jin, Hong, Peng Cui, Nyuk Hien Wong, and Marcel Ignatius. 2018. "Assessing the Effects of Urban Morphology Parameters on Microclimate in Singapore to Control the Urban Heat Island Effect." Sustainability (Switzerland) 10 (206): 1–18. https://doi.org/10.3390/su10010206.

Jylhä, K. et al. 2011. Rakennusten energialaskennan testivuosi TRY2012 ja arviot ilmastonmuutoksen vaikutuksista. In: Ilmatieteen laitos, Raportteja 6 (2011).

Karr, C.J., Demers, P.A., Koehoorn, M.W., Lencar, C.C., Tamburic, L. and Brauer, M., 2009a. Influence of ambient air pollutant sources on clinical encounters for infant bronchiolitis. American journal of respiratory and critical care medicine, 180(10), pp.995-1001.

Karr, C.J., Rudra, C.B., Miller, K.A., Gould, T.R., Larson, T., Sathyanarayana, S. and Koenig, J.Q., 2009b. Infant exposure to fine particulate matter and traffic and risk of hospitalization for RSV bronchiolitis in a region with lower ambient air pollution. Environmental research, 109(3), pp.321-327.

Karush, W., 1939. Minima of functions of several variables with inequalities as side constraints. M. Sc. Dissertation. Dept. of Mathematics, Univ. of Chicago.

King, E.A., Murphy, E., McNabola, A., 2009. Reducing pedestrian exposure to environmental pollutants: A combined noise exposure and air quality analysis approach. Transportation Research Part D: Transport and Environment, 14, 309-316.

Klasa, C., Walser, A., 2018. An evaluation of the convection-permitting ensemble COSMO-E for three contrasting precipitation events in Switzerland. Q. J. R. Meteorol. Soc. 144, 744–764.

Kolokotroni, M. and Renganathan, G., 2008. "Urban Heat Island Intensity in London: An Investigation of the Impact of Physical Characteristics on Changes in Outdoor Air Temperature during Summer." Solar Energy. https://doi.org/10.1016/j.solener.2008.05.004.

Kotharkar, Rajashree, Aparna Ramesh, and Anurag Bagade. 2018. "Urban Heat Island Studies in South Asia: A Critical Review." Urban Climate 24: 1011–26. https://doi.org/10.1016/j.uclim.2017.12.006.

Kottek, M., J. Grieser, C. Beck, B. Rudolf, and F. Rubel, 2006. World Map of the Köppen-Geiger climate classification updated. Meteorol. Z., 15, 259-263. DOI: 10.1127/0941-2948/2006/0130.

Kuhn, H.W. and Tucker, A., 1951. Nonlinear programming, In Proc. 2nd Berkeley Symposium on Mathematical Statistics and Probability (pp. 481-492), Berkeley: University of California Press. 291.

Kumar, A., Luo, J., Bennett, G.F., 1993. Statistical Evaluation of Lower Flammability Distance (LFD) Using Four Hazardous Release Models. Process Saf. Prog. 12, 1–11.

Kunz, M., Blahak, U., Handwerker, J., Schmidberger, M., Heinz, J., Mohr, S., Bedka, K.M., 2017. The severe hailstorm in southwest Germany on 28 July 2013 : characteristics , impacts and meteorological conditions. Q. J. R. Meteorol. Soc. 1–20.

Landrigan, P.J., 2017. Air pollution and health. Lancet Public Health. http://dx.doi.org/10.1016/S2468-2667(16)30023-8.

Laumbach, R., Meng, Q., Kipen, H., 2015. What can individuals do to reduce personal health risks from air pollution? J. Thorac. Dis. 7, 96–107.

Maggiotto, G., Buccolieri, R., Santo, M.A., Leo, L. S., Di Sabatino, S., 2014a. Validation of temperature-perturbation and CFD-based modelling for the prediction of the thermal urban environment: the Lecce (IT) case study. Environmental Modelling & Software, 60, 69-83.

Maggiotto, Giuseppe, Riccardo Buccolieri, Marco A. Santo, Silvana Di Sabatino, and Laura S. Leo. 2014b. "Study of the Urban Heat Island in Lecce (Italy) by Means of ADMS and ENVI-MET." International Journal of Environment and Pollution 55: 41–49. https://doi.org/10.1504/IJEP.2014.065903.

Masson, V. et al. 2013. *The SURFEX v7.2 land and ocean surface platform for coupled or offline simulation of earth surface variables and fluxes.* In: Geoscientific Model Development 6 (2013), pp. 929–960.

Matzarakis, A., Mayer, H. and Iziomon, M.G., 1999. Applications of a universal thermal index: 367 Physiologically equivalent temperature. In: International Journal of Biometeorology, 43: 76-84.

Matzarakis, Andreas et al. (2000). Estimation and Calculation of the Mean Radiant Temperature within Urban Structures. Selected papers from the Conference ICB-ICUC'99, Sydney, WCASP-50

Matzarakis, Andreas, 2013: Stadtklima vor dem Hintergrund des Klimawandels. In: Gefahrstoffe Reinhaltung der Luft 73 (2013) Nr. 3: 115-118.

McCreddin, A., Alam, M.S. and McNabola, A., 2015. Modelling personal exposure to particulate air pollution: An assessment of time-integrated activity modelling, Monte Carlo simulation & artificial neural network approaches. International journal of hygiene and environmental health, 218(1), pp.107-116.

McDonald, R.W., Griffith, R.F., Hall, D.J., 1998. An improved method for the estimation of surface roughness of obstacle arrays, Atmospheric Environment, 32(11), 1857-1864.

McNabola, A., 2010. New directions: Passive control of personal air pollution exposure from traffic emissions in urban street canyons. Atmospheric Environment, 44, 2940-2941.

Meehl, G.A., Stocker, T.F., Collins, W.D., Friedlingstein, P., Gaye, A.T., Gregory, J.M., et al., 20007. Global climate projections. In: Climate Change 2007: The physical science basis. Solomon, S., Qin, D., Manning, M., Chen, Z., Marquis, M., Averyt, K.B., et al. [eds.] Contribution

of Working Group I to the Fourth Assessment Report of the Intergovernmental Panel on Climate Change, Cambridge, UK, Cambridge University Press.

Miller, K.A., Siscovick, D.S., Sheppard, L., Shepherd, K., Sullivan, J.H., Anderson, G.L. and Kaufman, J.D., 2007. Long-term exposure to air pollution and incidence of cardiovascular events in women. New England Journal of Medicine, 356(5), pp.447-458.

Moore, D.K., Jerrett, M., Mack, W.J. and Künzli, N., 2007. A land use regression model for predicting ambient fine particulate matter across Los Angeles, CA. Journal of Environmental Monitoring, 9(3), pp.246-252.

Morgenstern, V., Zutavern, A., Cyrys, J., Brockow, I., Gehring, U., Koletzko, S., Bauer, C.P., Reinhardt, D., Wichmann, H.E. and Heinrich, J., 2006. Respiratory health and individual estimated exposure to traffic-related air pollutants in a cohort of young children. Occupational and environmental medicine, 64(1), pp.8-16.

Morgenstern, V., Zutavern, A., Cyrys, J., Brockow, I., Koletzko, S., Kramer, U., Behrendt, H., Herbarth, O., von Berg, A., Bauer, C.P. and Wichmann, H.E., 2008. Atopic diseases, allergic sensitization, and exposure to traffic-related air pollution in children. American journal of respiratory and critical care medicine, 177(12), pp.1331-1337.

Mumovic, D., Crowther, J.M., Stevanovic, Z., 2006. Integrated air quality modelling for a designated air quality management area in Glasgow. Build. Environ. 41, 1703–1712.

National Radiological Protection Board (NRPB), 2001. NRPB-322. Review of Deposition Velocity and Washout Coefficient AND Review of Flow and Dispersion in the Vicinity of Groups of Buildings. Atmospheric Dispersion Modelling Liaison Committee. Annual Report 1998/99. ISBN 0899514544

Nowak, D.J., 1994. Air Pollution Removal by Chicago's Urban Forest, in: Chicago's Urban Forest Ecosystem: Results of the Chicago Urban Forest Climate Project. PA, pp. 63–81.

OECD (Organization for Economic Cooperation and Development) 2014: The Cost of Air Pollution: Health Impacts of Road Transport. Paris: OECD Publishing.

Pope III, C.A. and Dockery, D.W., 2006. Health effects of fine particulate air pollution: lines that connect. Journal of the air & waste management association, 56(6), pp.709-742.

Pope, C.A., Thun, M.J., Namboodiri, M.M., Dockery, D.W., Evans, J.S., Speizer, F.E. and Heath, C.W., 1995. Particulate air pollution as a predictor of mortality in a prospective study of US adults. American journal of respiratory and critical care medicine, 151(3), pp.669-674.

Priyadarsini, R, and N H Wong. 2007. "An Investigation of the Urban Heat Island of Singapore." In An Investigation of the Urban Heat Island of Singapore, 191–98.

Righi, S., Lucialli, P., Pollini, E., 2009. Statistical and diagnostic evaluation of the ADMS-Urban model compared with an urban air quality monitoring network. Atmos. Environ. 43, 3850–3857.

Roth, Matthias, and Winston T.L. Chow. 2012. "A Historical Review and Assessment of Urban Heat Island Research in Singapore." Singapore Journal of Tropical Geography 33: 381–97. https://doi.org/10.1111/sjtg.12003.

Rowland, C.S., Morton, R.D., Carrasco, L., McShane, G., O'Neil, A.W., Wood, C.M., 2017. Digimap [WWW Document]. URL http://digimap.edina.ac.uk/ (accessed 12.5.17).

Ryan, P.H., LeMasters, G.K., Levin, L., Burkle, J., Biswas, P., Hu, S., Grinshpun, S. and Reponen, T., 2008. A land-use regression model for estimating microenvironmental diesel exposure given multiple addresses from birth through childhood. Science of the Total Environment, 404(1), pp.139-147.

Seinfeld, J.H., Pandis, S.N., 2006. Atmospheric Chemistry and Physics: From Air Pollution to Climate Change, Atmospheric Chemistry and Physics.

Shrestha, P., Kurtz, W., Vogel, G., Schulz, J., Sulis, M., 2018. Connection Between Root Zone Soil Moisture and Surface Energy Flux Partitioning Using Modeling , Observations , and Data Assimilation for a Temperate Grassland Site in Germany. J. Geophys. Res. Biogeosciences 123, 2389–2862.

Slama, R., Morgenstern, V., Cyrys, J., Zutavern, A., Herbarth, O., Wichmann, H.E., Heinrich, J. and LISA Study Group, 2007. Traffic-related atmospheric pollutants levels during pregnancy and offspring's term birth weight: a study relying on a land-use regression exposure model. Environmental Health Perspectives, 115(9), p.1283.

Smith, S.E., Stocker, J., Seaton, M., & Carruthers, D., 2017. Model inter-comparison and validation study of ADMS plume chemistry schemes. International Journal of Environment and Pollution, 62, 395-406.

Stadt Bottrop (2014): Machbarkeitsstudie für Klimaanpassungspotenziale im Innenstadtbereich von Bottrop (unpublished). Bottrop.

Stewart, I.D., and Oke, T.R., 2012. Local Climate Zones for urban temperature studies, Bulletin of the Americal Meteorological Society, 93(12), 1879-1900.

Stocker, J., Hood, C., Carruthers, D., & McHugh, C., 2012. ADMS-Urban: developments in modelling dispersion from the city scale to the local scale. International Journal of Environment and Pollution, 50, 308-316.

Stocker, T.F., & Raible, C.C., 2005. Climate change: water cycle shifts gear. Nature, 434, 830-833.

Stocker, T.F., Qin, D., Plattner, G.-K., Tignor, M.M.B., Allen, S.K., Boschung, J., Nauels, A., Xia, Y., Bex, V., Midgley, P.M. [Eds.], 2013. Climate Change 2013. The Physical Science Basis. Working Group I Contribution to the Fifth Assessment Report of the Intergovernmental Panel on Climate Change. Cambridge University Press, New York, NY, USA, ISBN 978-1-107-66182-0

Tallis, M., Taylor, G., Sinnett, D., Freer-Smith, P., 2011. Estimating the removal of atmospheric particulate pollution by the urban tree canopy of London, under current and future environments. Landsc. Urban Plan. 103, 129–138.

Tasker, G.D., 1980. Hydrologic regression with weighted least squares. Water Resources Research, 16(6), pp.1107-1113.

Tebaldi, C., Hayhoe, K., Arblasster, J., & Meehl, G., 2006. Going to the extremes. An intercomparison of model-simulated historical and future changes in extreme events. Climatic Change, 79, 185-211.

Thomson, D.J. 2010. "ADMS Met Input Module." UKMet Office. 2010. http://www.cerc.co.uk/environmental-software/assets/data/doc_techspec/CERC_ADMS4_P05_01.pdf.

Townsend, C.L., Maynard, R.L., 2002. Effects on health of prolonged exposure to low concentrations of carbon monoxide. Occup Environ Med, 59, 708-711.

Tiwary, A., Sinnett, D., Peachey, C., Chalabi, Z., Vardoulakis, S., Fletcher, T., Leonardi, G., Grundy, C., Azapagic, A., Hutchings, T.R., 2009. An integrated tool to assess the role of new planting in PM10 capture and the human health benefits: A case study in London. Environ. Pollut. 157, 2645–2653.

United Nations, 2018. "World Urbanization Prospects: The 2018 Revision." World Urbanization Prospects: The 2018 Revisions: The 2018 Revision. 2018.

Vapnik Vladimir N., 1995. The nature of statistical learning theory. Springer science & business media.

Vos, P.E.J., Maiheu, B., Vankerkom, J., Janssen, S., 2013. Improving local air quality in cities: To tree or not to tree? Environ. Pollut. 183, 113–122.

Wesely, M.., 2000. A review of the current status of knowledge on dry deposition. Atmos. Environ. 34, 2261–2282.

Wesely, M.L., 1989. Parameterization of surface resistances to gaseous dry deposition in regional-scale numerical models. Atmos. Environ. 23, 1293–1304.

WHO, 2018. Ambient (outdoor) air quality and health. Available online at https://www.who.int/news-room/fact-sheets/detail/ambient-(outdoor)-air-quality-and-health, last accessed 26 Feb 2019

World Meteorological Organization (WMO), 2014. WMO-No. 731Guide to Meteorological Observing and Information Distribution Systems for Aviation Weather Services. WMO-No. 731. Geneva.

Zhang, L., Brook, J. R., and Vet, R., 2003. A revised parameterization for gaseous dry deposition in air-quality models. Atmos. Chem. Phys., 3, 2067–2082.

Zhu, Y., Hinds, W.C., Kim, S. and Sioutas, C., 2002. Concentration and size distribution of ultrafine particles near a major highway. Journal of the air & waste management association, 52(9), pp.1032-1042.

Website envi-met 1: https://www.envi-met.com/citiesandhealth/ (last access on 25.02.2019)

Website envi-met 2: https://envi-met.info/doku.php?id=intro:modelconcept (last access on 25.02.2019)

Website ordnancesurvey (OpenData): https://www.ordnancesurvey.co.uk/opendatadownload/products.html (last access on 25.02.2019)

Annex - Additional maps from ENVI-met for the models of the city of Bottrop
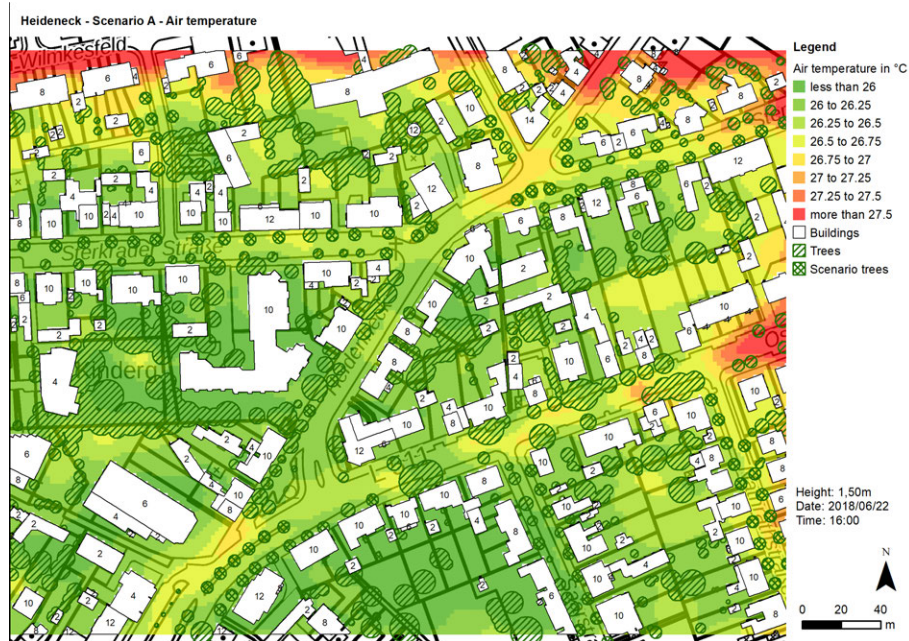

Figure 101: Model Bottrop 1 (Heideneck): Scenario A - ENVI-met calculated air temperature (source: own account, data: City of Bottrop).

Figure 102: Model Bottrop 1 (Heideneck): Scenario A - ENVI-met calculated PET values (source: own account, data: City of Bottrop).
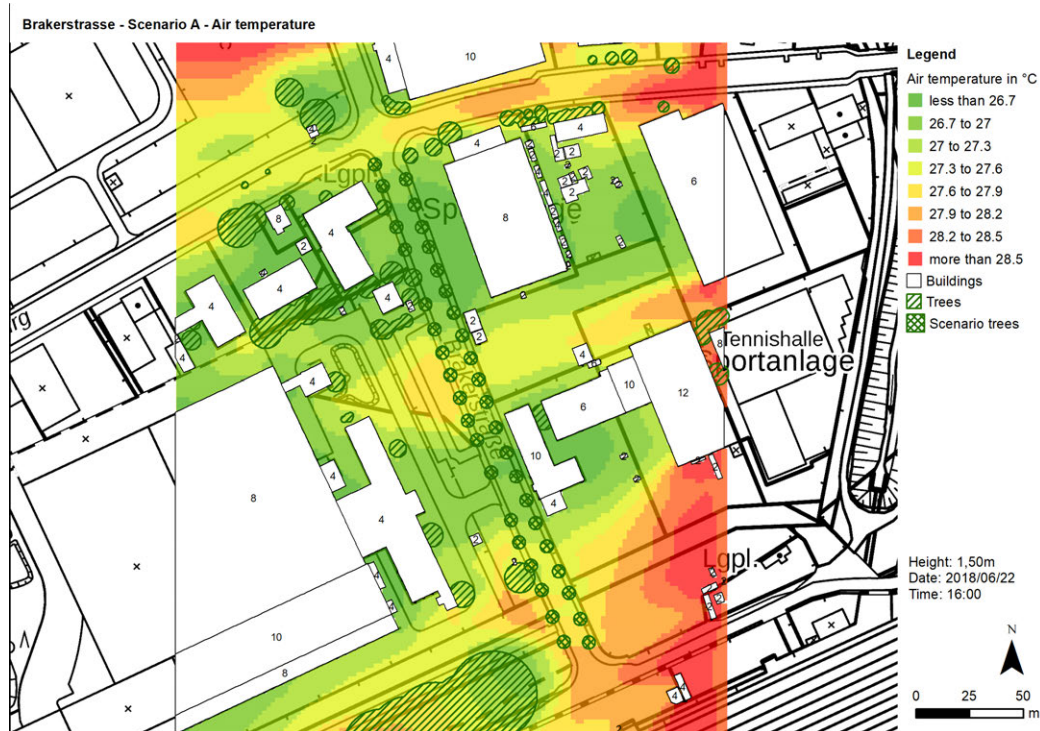
Figure 103: Model Bottrop 2 (Brakerstraße): Scenario A - ENVI-met calculated air temperature (source: own account, data: City of Bottrop).

Figure 104: Model Bottrop 2 (Brakerstraße): Scenario A - ENVI-met calculated PET values (source: own account, data: City of Bottrop).
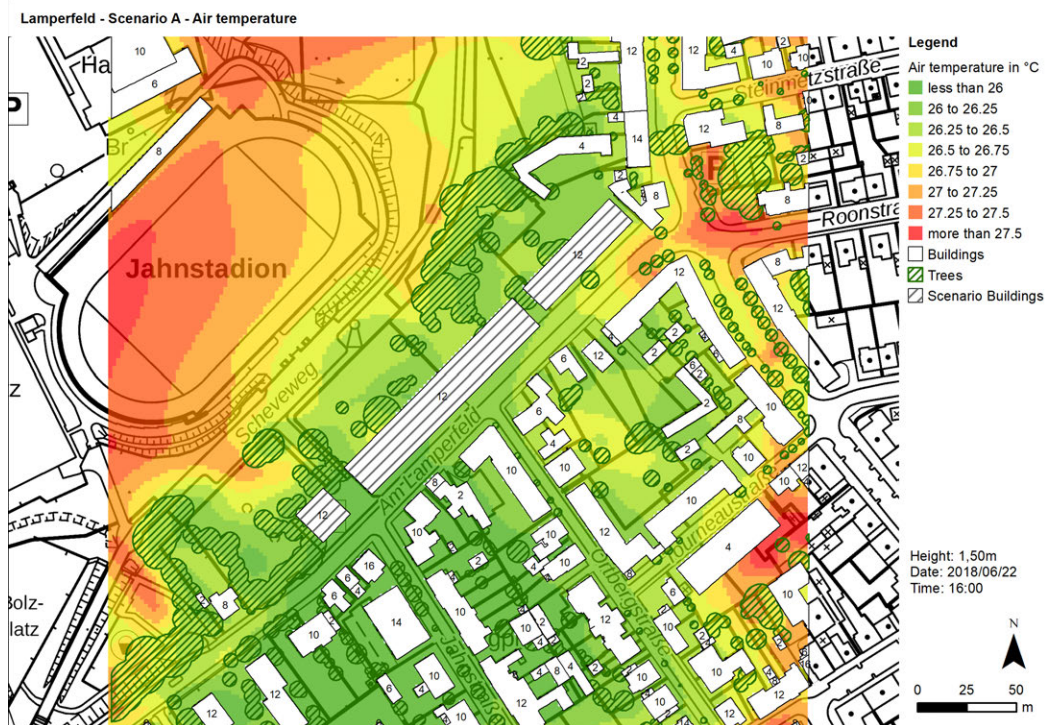
Figure 105: Model Bottrop 2 (Brakerstraße): Scenario B - ENVI-met calculated air temperature (source: own account, data: City of Bottrop).

Figure 106: Model Bottrop 2 (Brakerstraße): Scenario B - ENVI-met calculated PET values (source: own account, data: City of Bottrop).

Figure 107: Model Bottrop 3 (Am Lamperfeld): Scenario A - ENVI-met calculated air temperature (source: own account, data: City of Bottrop).
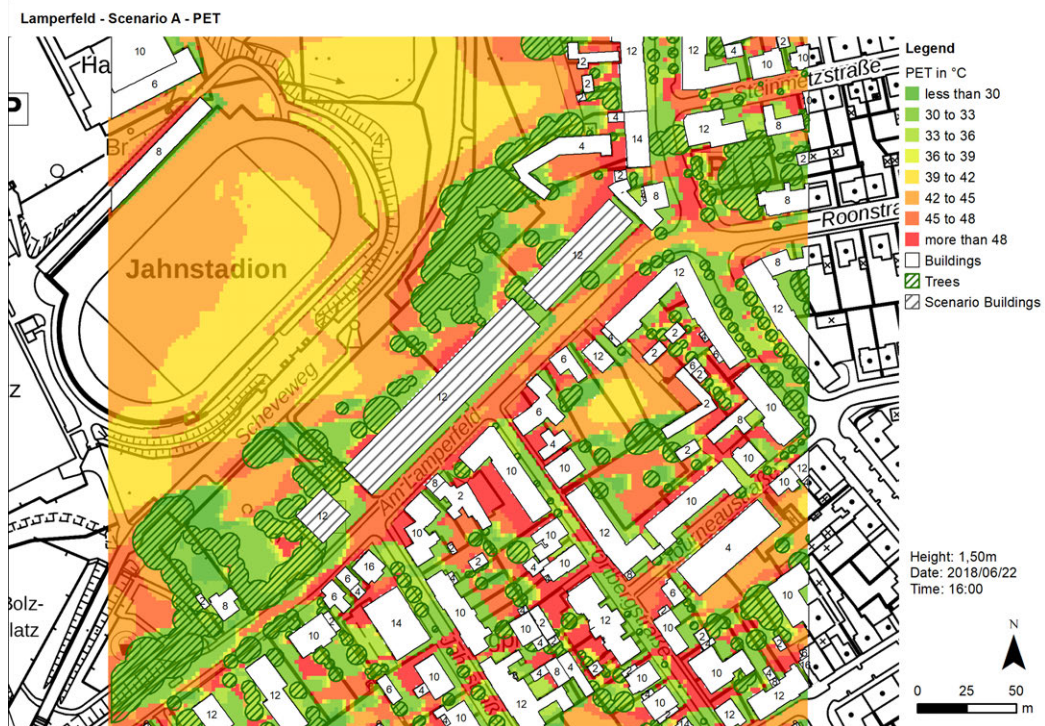

Figure 108: Model Bottrop 3 (Am Lamperfeld): Scenario A - ENVI-met calculated PET values (source: own account, data: City of Bottrop).
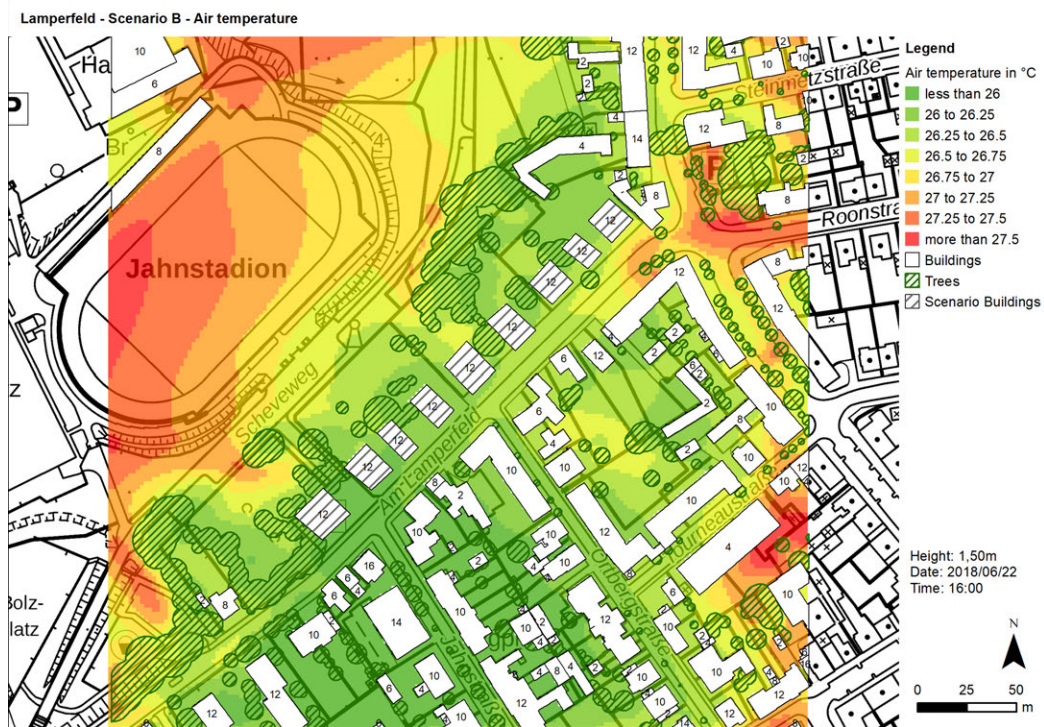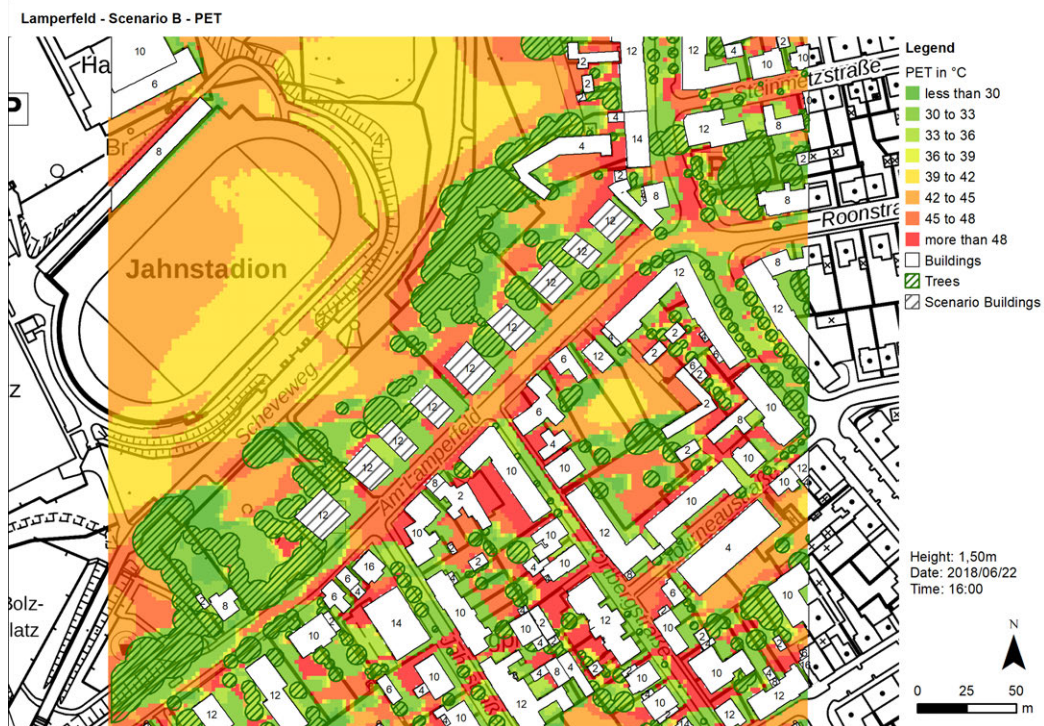
Figure 109: Model Bottrop 3 (Am Lamperfeld): Scenario B - ENVI-met calculated air temperature (source: own account, data: City of Bottrop).

Figure 110: Model Bottrop 3 (Am Lamperfeld): Scenario B - ENVI-met calculated PET values (source: own account, data: City of Bottrop).
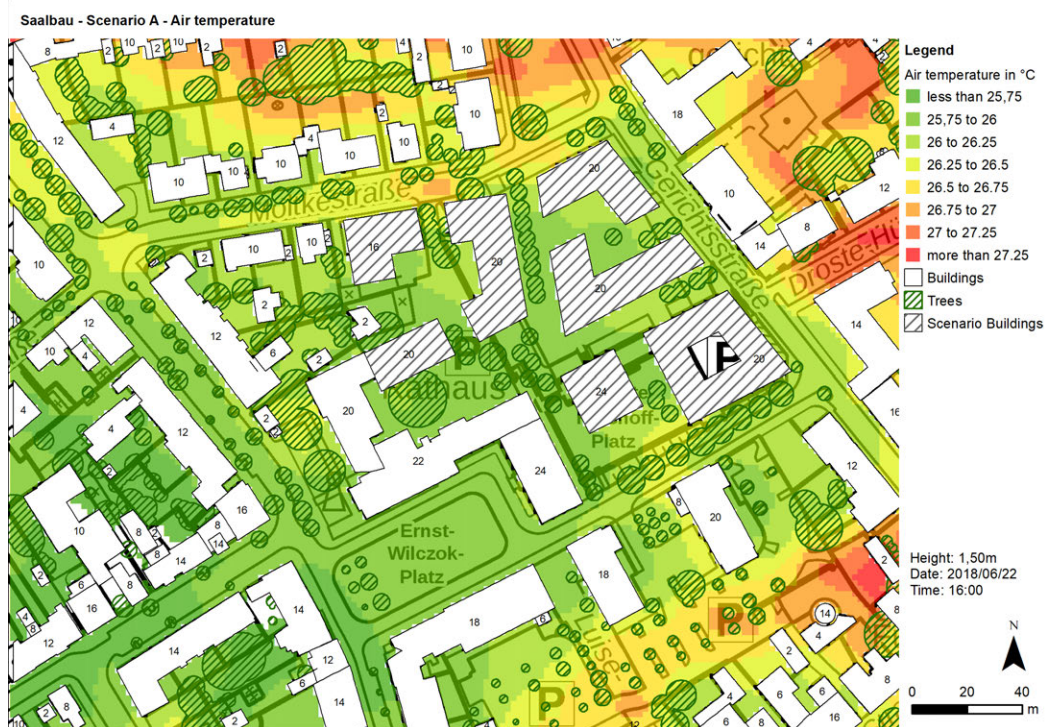
Figure 111: Model Bottrop 4 (Saalbau): Scenario A - ENVI-met calculated air temperature (source: own account, data: City of Bottrop).
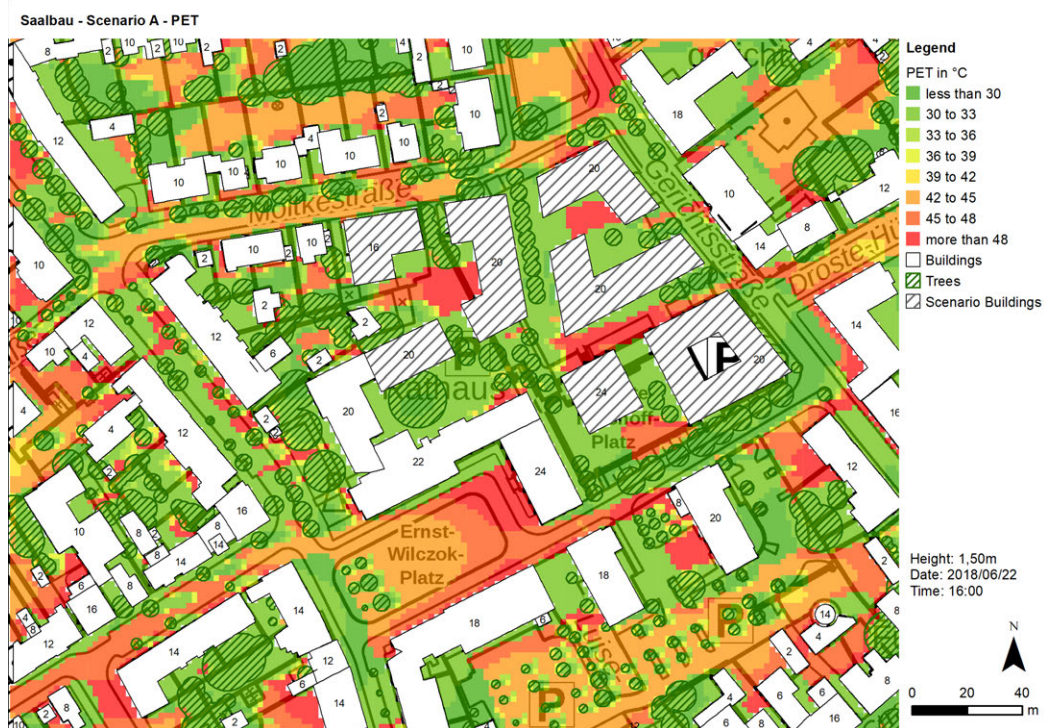

Figure 112: Model Bottrop 4 (Saalbau): Scenario A - ENVI-met calculated PET values (source: own account, data: City of Bottrop).